

DOWNSTREAM CHANGES IN RIVER MORPHOLOGY AS A RESULT OF DAM DEVELOPMENTS

By

Julia S. BECK



Thesis presented in partial fulfilment of the requirements for the degree of Master of
Science in Engineering at the University of Stellenbosch

Thesis Supervisor: Prof. G.R. Basson

Stellenbosch

December 2001

Declaration

I, the undersigned, hereby declare that the work contained in this thesis is my own original work and I have not previously in its entirety or in part submitted it at any university for a degree.

Signature:

Date:

Summary

A dam can have a significant impact on the downstream river morphology by altering both the flow regime and the sediment load. The effect of a dam is dependent on factors such as the storage capacity relative to the mean annual runoff (MAR), the operation of the reservoir and the sediment yield of the catchment. Changes in the river morphology include the degradation and coarsening of the riverbed, generally closer to the dam, and aggradation further downstream where the sediment delivered by tributaries cannot be carried through because of the reduced sediment transport capacity of the river. The impact of a dam can stretch over several hundreds of kilometres.

The main objective of this thesis was to gain a better understanding of the impacts that dams can have on the downstream river morphology. This was done by developing equations that can describe the channel geometry, investigating the effect of the presence of clay and silt on the sediment transport behaviour of sediments, as well as detailed evaluation of simulations carried out with a one-dimensional mathematical river model (MIKE 11).

The calibrated regime equations were found to be comparable to other internationally developed regime equations and to be suitable for natural rivers. It was found, however, that these regime equations are not applicable to rivers downstream of dams that have highly unnatural release patterns. Further research is needed in this regard.

By investigating the effect of cohesive sediments on the sediment transport behaviour of mixed sediments it was found that as little as 7% clay and silt in the bed could affect their sediment transport characteristics. A methodology was also developed by which the critical conditions for mass erosion of cohesive sediments can be described in terms of the applied stream power. Sediment transport equations were calibrated and verified in terms of the unit input stream power for fine and non-cohesive

sediments. The sediment transport equation for fine sediments was implemented in MIKE 11.

The simulations over a 40 km reach of the Pongola River downstream of Pongolapoort Dam, have shown that even when a large demand is placed on the stored water, and most of the smaller floods are therefore absorbed by the dam, the downstream impact can still be considerable, with as much as 5 m deep erosion in places. The sediment loads are generally reduced (by as much as 35%), but the effective catchment area downstream of the dam has been reduced by as much as 90%, indicating that substantial erosion had to have taken place in the river. Coarsening of the riverbed was also observed during the simulations.

Opsomming

'n Dam kan 'n aansienlike impak hê op die riviermorfologie stroomaf daarvan, deurdat dit beide die vloei en sedimentlading drasties kan verander. Die effek van 'n dam hang van verskeie faktore af, soos die opgaarkapasiteit in vergelyking met die gemiddelde jaarlikse afloop (GJA), die bestuur van die dam en die sedimentlewering van die opvanggebied. Veranderinge in die riviermorfologie behels die degradering van die rivierbed, sowel as die uitspoel van fyn materiaal uit die rivierbed, veral nader aan die dam. Deponering vind verder stroomaf van die dam plaas, waar die sediment wat deur die sytakke ingevoer word nie deurgevoer kan word nie, weens die verlaagde sedimentdravermoë van die rivier. Sodoende kan rivierlope oor honderde kilometers deur 'n dam beïnvloed word.

Die hoofdoel van die tesis was om meer insig te verkry oor die impak wat damme op die stroomaf riviermorfologie kan hê. Derhalwe is vergelykings ontwikkel wat die riviermorfologie kan beskryf. Die effek van die teenwoordigheid van klei en slik op die sedimentvervoer-eienskappe is ondersoek, en gedetailleerde ontledings is met 'n een-dimensionele wiskundige riviermodel (MIKE 11) is gedoen.

Daar is bevind dat die regime-formules goed vergelyk met ander internasionaal-ontwikkelde formules en dat hulle geskik is vir toepassing op natuurlike riviere. Daar is egter gevind dat die formules nie geskik is vir riviere wat stroomaf lê van damme wat hoogs onnatuurlike loslatings het nie. Verdere navorsing is op hierdie gebied nodig.

Ondersoek na die effek wat klei en slik op die sedimentdravermoë het, het getoon dat slegs 7% klei en slik in die rivierbed die sedimentvervoer-eienskappe van mengsels van fyn en growwe materiaal kan beïnvloed. 'n Metode is ontwikkel waarmee die kritiese toestande vir massa-erosie van kohesiewe sediment beskryf kan word in terme van die aangewende stroomdrywing teen die bed. 'n Sedimentvervoer-vergelyking in terme van die eenheids-insetstroomdrywing vir fyn en nie-kohesiewe sedimente is

gekalibreer en geverifieer. Die nuwe sedimentvervoer-vergelyking vir fyn sedimente is gebruik in die MIKE 11 simulاسies.

Hierdie simulاسies oor 'n 40 km loop van die Pongolarivier stroomaf van Pongolapoort Dam, het getoon dat selfs as daar 'n groot aanvraag op 'n dam se water geplaas word, en gevolglik meeste van die kleiner vloede deur die dam geabsorbeer word, die impak van die dam nogs steeds aansienlik kan wees, met soveel as 5 m diep uitskuring in plekke. Die sedimentladings het gewoonlik verminder (met soveel as 35%), maar die diep effektiewe opvanggebiedarea stroomaf van die dam het met meer as 90% verminder, wat daarop dui dat daar aansienlike erodering in die rivier plaasgevind het. Die simulاسies het ook getoon dat die hoeveelheid fyn materiaal in die rivierbed verminder het.

Acknowledgements

I would like to express my gratitude to the following persons:

- Prof. GR Basson for his guidance and patience with endless questions.
- Mr N Combrinck, Mr CJ Brink and Mr B Marais for their help with the laboratory set-up, tests and analysis of samples.
- Mrs F Sibanyoni and Mrs M Erasmus, DWAF, for providing data.
- The Department of Water Affairs and Forestry (DWAF) for the opportunity to do field work at Pongolapoort Dam.
- The Water Research Commission (WRC) for sponsorship of this project.
- Julie and Rodney for their faith in me.
- My parents and sisters for their support. Thank you for always being there for me when I needed you.

Table of Contents

| | |
|--|-------------|
| Declaration | i |
| Summary | ii |
| Opsomming | iv |
| Acknowledgements | vi |
| Table of Contents | vii |
| List of Figures | x |
| List of Tables | xiii |
| List of Symbols | xiv |
| <hr/> | |
| 1. INTRODUCTION | 1-1 |
| 1.1 Aims | 1-3 |
| 1.2 Methodology | 1-3 |
| 2. DOWNSTREAM IMPACTS OF DAM DEVELOPMENTS | 2-1 |
| 2.1 Changes in Discharge | 2-4 |
| 2.2 Changes in Sediment Load | 2-5 |
| 2.3 Changes in Channel Depth | 2-6 |
| 2.4 Changes in Channel Width | 2-8 |
| 2.5 Changes in Bed Material Size | 2-10 |
| 2.6 Changes in Slope and Channel Pattern | 2-13 |
| 2.7 Changes in Vegetation | 2-15 |
| 2.8 Affected Distance | 2-16 |
| 3. RIVER CHANNEL MORPHOLOGY | 3-1 |
| 3.1 Dominant Discharge | 3-2 |
| 3.2 Existing Regime Equations | 3-4 |
| 3.2.1 <i>Width Equations</i> | 3-5 |
| 3.2.2 <i>Depth Equations</i> | 3-7 |
| 3.2.3 <i>Slope Equations</i> | 3-9 |
| 3.3 Proposed Regime Equations for South African Conditions | 3-11 |

| | | |
|-----------|---|------------|
| 3.3.1 | <i>Theory</i> | 3-11 |
| 3.3.2 | <i>Calibration of New Regime Equations</i> | 3-13 |
| 3.3.2.1 | Data Set | 3-13 |
| 3.3.2.2 | Calibration | 3-16 |
| 3.3.2.3 | Comparison and Verification | 3-20 |
| 3.4 | Minimization of Stream Power | 3-23 |
| 3.4.1 | <i>Theory and Application</i> | 3-24 |
| 3.4.2 | <i>Discussion</i> | 3-25 |
| 3.5 | Channel Patterns | 3-27 |
| 3.5.1 | <i>Theory and Background</i> | 3-27 |
| 3.5.2 | <i>Development of Discharge-Slope Relationship for South African Rivers</i> | 3-29 |
| 3.6 | Applications | 3-31 |
| 4. | SEDIMENT TRANSPORT | 4-1 |
| 4.1 | Cohesive Sediment Transport Processes | 4-1 |
| 4.1.1 | <i>Sand and Clay Mixtures</i> | 4-2 |
| 4.1.2 | <i>Erosion</i> | 4-4 |
| 4.1.2.1 | Surface Erosion | 4-4 |
| 4.1.2.2 | Mass Erosion | 4-5 |
| 4.2 | Equilibrium Sediment Transport | 4-7 |
| 4.2.1 | <i>Stream Power Concept</i> | 4-7 |
| 4.3 | Laboratory Flume Studies | 4-12 |
| 4.3.1 | <i>Equipment</i> | 4-13 |
| 4.3.2 | <i>Laboratory Procedure</i> | 4-16 |
| 4.4 | Analysis of Results | 4-21 |
| 4.4.1 | <i>Critical Conditions for Mass Erosion</i> | 4-24 |
| 4.4.2 | <i>Evaluation and Calibration of Sediment Transport Equations for Fine and Non-Cohesive Sediments</i> | 4-29 |
| 4.4.2.1 | Calibration | 4-30 |
| 4.4.2.2 | Comparison | 4-34 |
| 4.4.2.3 | Verification | 4-36 |

| | |
|--|------------|
| 5. NUMERICAL MODELLING OF THE RIVER MORPHOLOGY DOWNSTREAM OF DAMS | 5-1 |
| 5.1 Mathematical Model | 5-1 |
| 5.1.1 <i>Hydrodynamic Module</i> | 5-2 |
| 5.1.2 <i>Advection-Dispersion Module</i> | 5-2 |
| 5.1.3 <i>Non-Cohesive Sediment Transport Module</i> | 5-3 |
| 5.2 Case Study | 5-4 |
| 5.2.1 <i>Model Input</i> | 5-9 |
| 5.3 Discussion of Simulation Results | 5-13 |
| | |
| 6. CONCLUSIONS AND RECOMMENDATIONS | 6-1 |
| 6.1 Conclusions | 6-1 |
| 6.2 Recommendations for Further Research | 6-3 |
| | |
| 7. REFERENCES | 7-1 |

Appendix A

Appendix B

Appendix C

List of Figures

| Figure | Description | Page |
|------------|--|------|
| Fig 2.1 | Cumulative storage capacity of dams worldwide (dams > 15 m) (White, 2000) | 2-3 |
| Fig 2.2 | Cumulative storage capacity of dams in South Africa | 2-3 |
| Fig 2.2.1 | Suspended sediment loads at successive downstream stations before and after the closure of Canton Dam on the North Canadian River, USA (Williams and Wolman, 1984) | 2-6 |
| Fig 2.3.1. | Variation of bed degradation downstream of Glen Canyon Dam, USA, nine years after closure of the dam | 2-7 |
| Fig 2.4.1 | Changes in channel width of the Pongola River between 1956 and 1996 downstream of Pongolapoort Dam, South Africa (positions of tributaries indicated) | 2-10 |
| Fig 2.5.1 | Variation of d_{50} downstream of Parker Dam, USA (Williams and Wolman, 1984) | 2-11 |
| Fig 2.5.2 | Variation of d_{50} downstream of Pongolapoort Dam, South Africa | 2-12 |
| Fig 2.5.3 | Variation of d_{50} downstream of Sanmenxia Dam, China, with different modes of operation (Chien, 1985) | 2-13 |
| Fig 2.6.1 | Changes in slope of the Colorado River below Glen Canyon Dam, USA (Williams and Wolman, 1984) | 2-14 |
| Fig 3.3.1 | Cross-sectional levels | 3-15 |
| Fig 3.3.2 | Calibration of South African regime width equation | 3-18 |
| Fig 3.3.3 | Calibration of South African regime depth equation | 3-19 |
| Fig 3.3.4 | Comparison of existing and new width equations | 3-22 |
| Fig 3.3.5 | Comparison of existing and new depth equations | 3-22 |
| Fig 3.4.1 | Flow chart showing major steps of calculation (Chang, 1979) | 3-26 |
| Fig 3.5.1 | Threshold line separating meandering and braided rivers | 3-30 |
| Fig 4.1.1 | Mechanism for initiation of motion (adapted from Panagiotopoulos <i>et al.</i> , 1997) | 4-3 |
| Fig 4.1.2 | Correlation between applied stream power and shear strength, % clay and consolidation pressure (Basson and Rooseboom, 1996) | 4-6 |
| Fig 4.3.1 | Layout of laboratory system | 4-13 |

| | | |
|------------|--|------|
| Fig 4.3.2 | VERIFLUX flow meter and converter | 4-14 |
| Fig 4.3.3 | Particle size distribution curves | 4-15 |
| Fig 4.3.4 | TROXLER moisture-density gauge | 4-16 |
| Fig 4.4.1 | Irregular bedforms after the flume was drained (20% clay and silt contents) | 4-21 |
| Fig 4.4.2 | Bedforms developed during runs made with 7% clay and silt content (fine deposited layer developed after runs were stopped) | 4-22 |
| Fig 4.4.3 | Layers of sediments developed during runs with 7% clay and silt content | 4-23 |
| Fig 4.4.4 | Correlation between applied stream power and fine particle content | 4-23 |
| Fig 4.4.5 | Correlation between critical shear stress and fine particle content | 4-25 |
| Fig 4.4.6 | Correlation between applied stream power and fine particle content (mass erosion only) | 4-26 |
| Fig 4.4.7 | Correlation between applied stream power and dry density | 4-27 |
| Fig 4.4.8 | Correlation between applied stream power and shear strength | 4-27 |
| Fig 4.4.9 | Observed versus calculated critical applied stream power for mass erosion | 4-29 |
| Fig 4.4.10 | Correlation between dimensionless unit stream power and concentration for both cohesive and non-cohesive sediments | 4-31 |
| Fig 4.4.11 | Calibration of sediment transport equation for both cohesive and non-cohesive sediments | 4-31 |
| Fig 4.4.12 | Calibration of sediment transport equation for cohesive sediments | 4-32 |
| Fig 4.4.13 | Calibration of sediment transport equation for non-cohesive sediments | 4-33 |
| Fig 4.4.14 | Comparison between sediment transport equation for cohesive and non-cohesive sediments and Yang's relationship | 4-35 |
| Fig 4.4.15 | Comparison between sediment transport equation for non-cohesive sediments and Yang's relationship | 4-35 |
| Fig 4.4.16 | Comparison between sediment transport equation for cohesive sediments and Basson and Rooseboom's relationship | 4-36 |
| Fig 4.4.17 | Verification of sediment transport equation for non-cohesive | 4-38 |

| | | |
|------------|--|------|
| | sediments with independent flume data | |
| Fig 4.4.18 | Verification of sediment transport equation for non-cohesive sediments with independent river data | 4-38 |
| Fig 5.2.1 | Pongola River directly below Pongolapoort Dam (app. 400 m ³ /s discharge) | 5-4 |
| Fig 5.2.2 | Pongola River map | 5-5 |
| Fig 5.2.3 | Natural 10-year flow sequence | 5-7 |
| Fig 5.2.4 | 10-year flow sequence with 2MAR reservoir and 16% MAR demand (2MAR) | 5-7 |
| Fig 5.2.5 | 10-year flow sequence with 2MAR reservoir and 60% MAR demand (2MAR60) | 5-8 |
| Fig 5.2.6 | 10-year flow sequence with 1MAR reservoir and 45% MAR demand (1MAR45) | 5-8 |
| Fig 5.2.7 | Pongola River reach modelled (with chainages shown in brackets) | 5-10 |
| Fig 5.2.8 | Sediment input over 10-year period | 5-13 |
| Fig 5.3.1 | Simulated bed levels | 5-14 |
| Fig 5.3.2 | Simulated sediment fractions – natural conditions | 5-15 |
| Fig 5.3.3 | Simulated sediment fractions – 2MAR reservoir | 5-17 |
| Fig 5.3.4 | Simulated sediment fractions – 2MAR60 reservoir | 5-18 |
| Fig 5.3.5 | Simulated sediment fractions – 1MAR45 reservoir | 5-18 |

Table 5.1

Table 5.2

Table 5.3

Table 5.4

Table 5.5

List of Tables

| Table | Description | Page |
|--------------|---|-------------|
| Table 3.2.1 | Summary of width equations (adapted from Wargadalam, 1993) | 3-6 |
| Table 3.2.2 | Summary of depth equations (adapted from Wargadalam, 1993) | 3-8 |
| Table 3.2.3 | Summary of slope equations (adapted from Wargadalam, 1993) | 3-10 |
| Table 3.3.1 | Variability of channel parameters | 3-17 |
| Table 3.3.2 | Results of regression analysis | 3-17 |
| Table 3.3.3 | Accuracy of new width relationships | 3-19 |
| Table 3.3.4 | Accuracy of new depth relationships | 3-19 |
| Table 3.3.5 | Ranges of exponents | 3-21 |
| Table 3.3.6 | Accuracy ranges of width relationships (independent river data) | 3-23 |
| Table 3.3.7 | Accuracy ranges of depth relationships (independent river data) | 3-23 |
| Table 3.6.1 | River channel geometry | 3-32 |
| Table 4.3.1 | Sediment types | 4-15 |
| Table 4.3.2 | Particle size ranges | 4-20 |
| Table 4.4.1 | Variation of absolute roughness with % clay and silt, and d_{50} | 4-25 |
| Table 4.4.2 | Accuracy ranges of sediment transport equations | 4-34 |
| Table 4.4.3 | Accuracy ranges of sediment transport equation for cohesive and non-cohesive sediments (independent data) | 4-37 |
| Table 4.4.4 | Accuracy ranges of sediment transport equation for non-cohesive sediments (independent data) | 4-37 |
| Table 5.2.1 | Pongola River flood peaks – natural | 5-5 |
| Table 5.2.2 | Pongolapoort Dam – catchment characteristics | 5-6 |
| Table 5.2.3 | Sediment fractions of bed sediment | 5-12 |
| Table 5.3.1 | Simulated sediment loads at km 35 | 5-16 |
| Table 6.1 | Impacts and causes | 6-1 |

List of Symbols

| Symbol | Description |
|-------------------------------------|--|
| $\frac{dv}{dy}$ | Velocity gradient (s^{-1}) |
| $\left(\tau \frac{dv}{dy}\right)_0$ | Applied stream power at the bed (W/m) |
| $\rho g Q S$ | Total input stream power (W/m) |
| α | Exponent of regime equation |
| β | Exponent of regime equation |
| γ | Exponent of regime equation |
| ρ | Specific density of water (kg/m^3) |
| κ | Von Kármán coefficient |
| ν | Kinematic viscosity (m^2/s) |
| γ | Specific weight of clear water (N/m^3) |
| τ | Bed shear stress (Pa) |
| ρ_d | Dry density of sediment (kg/m^3) |
| ρ_m | Specific density of sediment laden flow (kg/m^3) |
| γ_m | Specific weight of sediment-laden flow (N/m^3) |
| ν_m | Kinematic viscosity of sediment-laden flow (m^2/s) |
| ρ_s | Specific density of sediment (kg/m^3) |
| γ_s | Specific weight of sediment (N/m^3) |
| τ_v | Vane shear strength (kPa) |
| $\frac{vS}{w}, \frac{v_{cr}S}{w}$ | Dimensionless unit stream power and critical unit stream power |
| A | Cross-sectional area (m^2) |
| A | Reading for VERIFLUX converter (A) |
| A | Cross-sectional area of return pipe (m^2) |
| a | Coefficient of regime equations |
| B | Top width (m) |
| B | Reading for VERIFLUX converter (m/s) |
| b | Coefficient of regime equations |

| | |
|--------------------|---|
| b | River bed width (m) |
| C | Sediment concentration (mg/l or %) |
| c | Coefficient of regime equations |
| C_b | Regression coefficient |
| C_d | Regression coefficient |
| C_t | Total sediment concentration (mg/l or %) |
| C_v | Suspended sediment concentration (mg/l or %) |
| d | Sediment particle size (mm or m) |
| D | Flow depth (m) |
| d_s | Sediment size (m) |
| d_{50} | Median particle diameter (mm or m) |
| d_{84}, d_{90} | Sediment size for which 84% and 90%, respectively, of the material is finer (mm or m) |
| Fr | Froude number |
| F_s | Side factor in <i>Blench</i> regime equation |
| g | Gravitational acceleration (m/s^2) |
| h_1, h_2 | Flow depths at successive reference points 1 and 2 (m) |
| k_1, k_3 | Coefficient of regime equations |
| k_s | Absolute roughness (m) |
| L | Distance between successive reference points (m) |
| L | Total length of reach (m) |
| L_i | Distance between successive cross-sections (m) |
| m | Parameter in exponents of <i>Julien and Wargadalam</i> regime equations |
| P | Wetted perimeter (m) |
| p_i | Proportion of sediments in particle size range i |
| P | Percentage clay or clay and silt |
| Q | Flow rate (m^3/s) |
| Q_2, Q_5, Q_{10} | Flood peak with recurrence interval of 2, 5, 10, 20 and 50 years, |
| Q_{20}, Q_{50} | respectively (m^3/s) |
| Q_s | Sediment discharge (m^3/s) |
| R | Hydraulic radius (m) |
| S | Slope |
| s | Specific gravity of sediment |

| | |
|---------------|--|
| S_i | Bed slope between 2 successive cross-sections |
| S_o | Bed slope |
| S_w | Water surface slope |
| t | Time (h) |
| T | Temperature ($^{\circ}\text{C}$) |
| U_* | Shear velocity (m/s) |
| v | Flow velocity (m/s) |
| v_1, v_2 | Mean flow velocities at successive reference points 1 and 2 (m/s) |
| v_p | Flow velocity in return pipe (m/s) |
| vS, vS_{cr} | Unit stream power and critical unit stream power (m/s) |
| w | Particle settling velocity (m/s) |
| w_i | Sediment particle settling velocity of fraction i (m/s) |
| w_m | Particle settling velocity in sediment-laden flow (m/s) |
| w_s | Settling velocity of suspended sediments (m/s) |
| X | Longitudinal distance (m) |
| Y | Potential energy per unit weight above a certain datum (m) |
| z | Side slope of trapezoidal channel shape |
| z_1, z_2 | Elevation above arbitrary datum at successive reference points 1 and 2 (m) |

1. Introduction

The construction of a dam can drastically alter the flow regime and sediment load of the river downstream by altering flood peaks and durations, as well as by trapping large quantities of sediment. The imposed changes in flows can lead to riverbed degradation directly downstream, as a result of very low sediment loads, as well as narrowing of river channels due to decreased transporting capacities further downstream. The increasing number and size of dams built during recent decades has drawn more attention to the impacts that dams can have, so much so that the World Commission on Dams (WCD, 2000a) has completed a worldwide study on dams. In South Africa there have also been some studies focusing on the impacts of river developments on a river system such as interbasin transfer schemes (Rowntree *et al.*, 2000). It has, however, become clear that there are still some issues to be addressed in order to gain a better understanding of the changes in the downstream river morphology that may occur as a result of dam developments.

When attempting to analyse the impacts of dams on the downstream river morphology, two fundamental questions have to be answered:

1. What sort of changes are to be expected, e.g. will the river become deeper or shallower and by how much?
2. How do these changes come about, e.g. does the river become deeper because of a lack of released sediments, or narrower due to reduced flood peaks?

In order to answer these two questions the first step will have to be to determine the factors that influence the channel morphology and the aspects of the river morphology that are likely to change. A study of existing literature should offer some answers in that respect since numerous studies have dealt with these aspects.

This does, however, not resolve the question of the magnitude or direction of the changes that are to be expected. What is necessary is to be able to describe the channel geometry in terms of the factors that are likely to have a significant effect.

For natural rivers so-called regime equations, which were either empirically or theoretically derived, were used in the past to describe the river channel geometry. It will have to be determined whether these equations can be applied to impacted rivers.

An important aspect of all the regime equations has always been the determination of the so-called dominant or effective discharge, responsible for maintaining or forming the river channel. The determination of the dominant or effective discharge is not only important for the regime equations but also plays a vital role in determining a controlled flow regime that will maintain a river in its natural or desired state. For South African conditions this aspect still needs consideration even though other researchers are also working on providing answers in that regard, e.g. Dollar *et al.* (2000).

Once these matters have been dealt with, the second part of the problem will have to be addressed. The sediment transport characteristics of the downstream river channel play a vital role in this regard. Generally speaking degradation of the riverbed takes place close to the dam whereas further downstream aggradation is more common, since sediments are supplied by the tributaries, which cannot all be transported because of the lower sediment transport capacities due to the reduced flood peaks. The material that thus becomes deposited may consist of both coarse and fine fractions, including cohesive sediments. Fine materials, consisting of clay and silt fractions, display distinctly different erosion and deposition patterns to non-cohesive sediments, due to the fact that the erosion resistance of fine particles is governed to a large degree by physical and chemical forces. While the entrainment and transport of non-cohesive sediments can already be described adequately, the entrainment and transport of clay and silt, as well as mixtures of cohesive and non-cohesive sediments has not been investigated adequately. Knowledge of the behaviour of fine sediments may also be useful for sediment flushing from reservoirs, since the reservoir deposits usually contain high percentages of clay and silt.

The materials found in the downstream river channel are not the only factors that determine why a river will change as it does. Other key factors are the flows released

from the reservoir as well as the amount of sediment supplied by the incremental downstream catchment. The regime equations mentioned above may give an indication of the magnitude and direction that changes in the river morphology may take, but they cannot describe whether a river has changed in response to lower flood peaks or longer flow durations. One way in which to accurately determine the effect of a sequence of events is through numerical modelling. A model should take into consideration the effect of fine materials, changes in cross-sectional shape or slope along a river section and also the variability of flows. In this way the long-term impacts of dams can be studied.

1.1 Aims

The overall aim of the thesis is to investigate the impacts of dam developments on the downstream river morphology, specifically:

- The assessment of the changes in the downstream river morphology as a result of different dam development scenarios.
- The development of methods for predicting the downstream river channel geometry for South African conditions.
- An investigation into the effects of clay and silt on the sediment transport behaviour of sediments.

1.2 Methodology

This study consisted of the following components:

1. An overview of literature on the impacts of dams on downstream river morphology in South Africa and the rest of the world (**Chapter 2**).
2. Existing regime equations as well as other tools that can be employed to determine the resulting equilibrium river channel geometry are reviewed and

2. regime equations for South African conditions are developed (**Chapter 3**). The concept of a dominant discharge is also explored.
3. The differences in behaviour between cohesive and non-cohesive sediments are investigated with the aid of flume studies and sediment transport equations are calibrated for fine and non-cohesive sediments (**Chapter 4**).
4. A one-dimensional hydrodynamic and morphological numerical model (MIKE 11) is utilized to investigate the impacts of dams by analysing several scenarios (**Chapter 5**) such as:
 - natural conditions,
 - and various reservoir capacities and water yields.

2. Downstream Impacts of Dam Developments

Kariba Reservoir on the Zambezi River, Zimbabwe/Zambia, has a surface area of about 5500 km² at full supply level and Gariep Reservoir on the Orange River, South Africa, has a full supply capacity of 5950 million m³. Considering the large sizes of these and most of the other dams built during the past 100 years, it is not surprising that they have major impacts on the rivers downstream. However, it is not only due to the large reservoirs that changes in the rivers can be observed, but even small structures can disturb an otherwise stable river. A river compensates for the imposed changes due to a dam by adjusting to a new quasi-stable form.

The closure of a dam has an immediate impact on the downstream river channel by changing the natural water discharge and sediment load. The magnitude of this impact depends on various factors:

- **Storage capacity of the impoundment:**

Reservoirs with large storage capacities relative to the mean annual runoff (MAR), typically absorb most of the smaller floods, attenuate larger floods and trap most of the sediments that enter the reservoir (Chien, 1985). Tarbela Reservoir on the River Indus, Pakistan, has a relatively small storage in comparison to flood volume, and thus has little impact on floods with return periods greater than 10 years. Lake Nasser behind the High Aswan Dam on the other hand has such a large storage capacity in relation to the flood volume that even the largest floods are partially absorbed (Acreman, 2000).

- **Operational procedure of the dam:**

Typically dams are built for one of the following reasons: storage, hydropower, irrigation or flood detention. Many dams are also built for multiple purposes. The impacts of each type of operation are different. While a storage reservoir may release almost no water unless its storage capacity has been exceeded, a hydropower dam may release a relatively constant high flow for certain times of the day.

- **Bed materials:**
Coarser bed materials like cobbles and boulders and even gravel reduce the degradation below a dam to some degree, whereas sand bed rivers are more susceptible to degradation or erosion.
- **Outlet structures:**
If a dam has the necessary outlet structures, sediment can be released from a reservoir, through sluicing incoming sediments or flushing deposited sediments. The effect of the released sediment on the river channel of course depends on the operation of the outlet works.
- **Sediment load:**
A dam will have a much greater impact on a river with a high natural sediment load than on a river with a low natural sediment load, because the former will experience a much greater reduction in sediment load than the latter. Also the sediments supplied by tributaries downstream of a dam can have a major effect on a river in that the flow can become oversaturated if the sediment transport capacity of the river is reduced.

There was a dramatic increase in the number and size of the dams being built after the Second World War, peaking during the 1970's worldwide (**Figure 2.1**). In South Africa the trend was similar (**Figure 2.2**, data obtained from the Department of Water Affairs and Forestry). This increase in both size and capacity of reservoirs has made the impacts of dams even more obvious. Numerous studies have been carried out that describe both the impacts and their causes, like Williams and Wolman (1984), Chien (1985), and Hadley and Emmett (1998). The primary impacts are the attenuation of flood peaks and the trapping of sediments in reservoirs, leading to changes in channel cross-section, bed particle size, channel pattern and roughness.

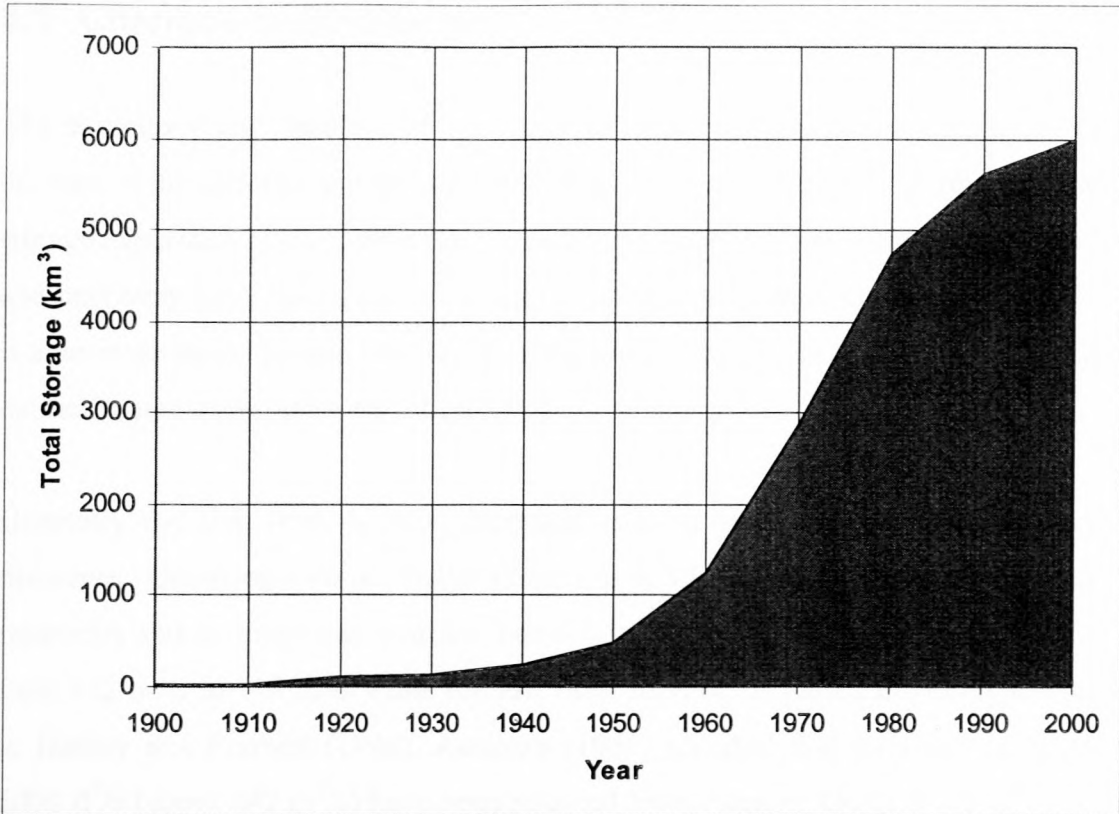


Figure 2.1: Cumulative storage capacity of dams worldwide (dams > 15 m) (White, 2000)

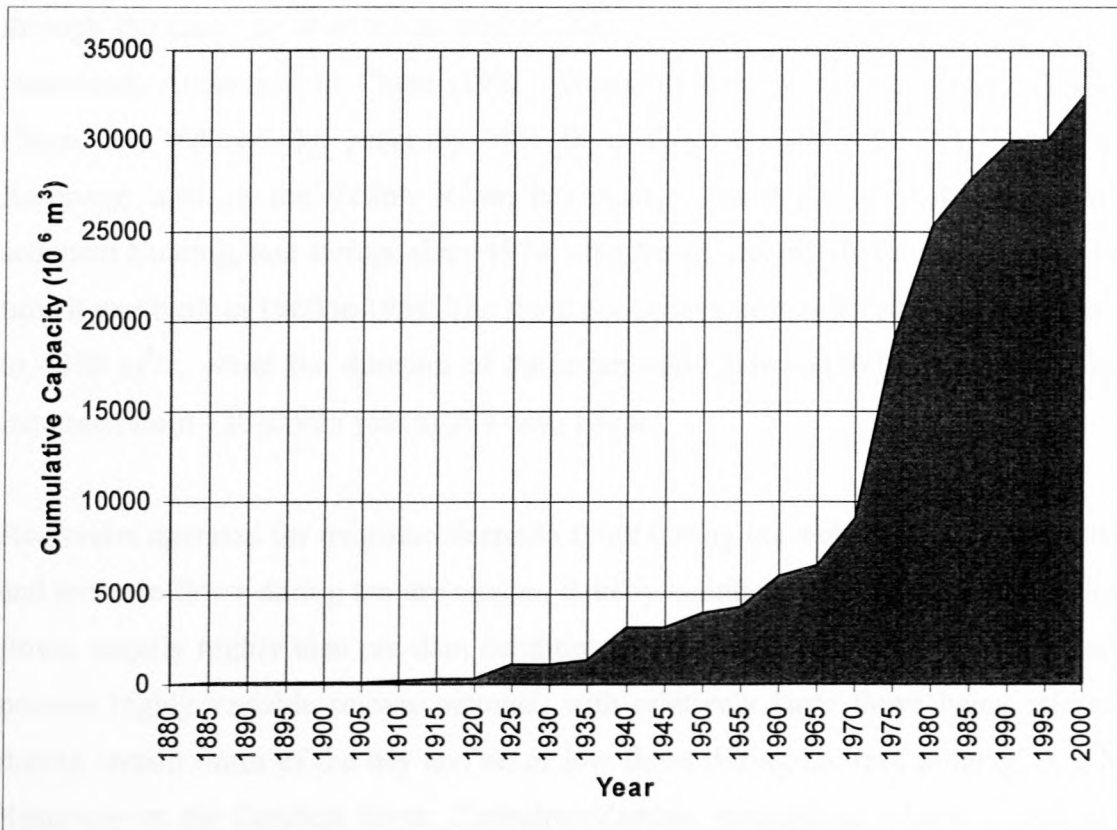


Figure 2.2: Cumulative storage capacity of dams in South Africa

2.1 Changes in Discharge

The magnitude and duration of the flows released vary from one dam to another, because of the different purposes for which dams are built. Due to the relatively large storage capacities of most reservoirs, floods are either absorbed or at least attenuated and only very large floods move through a reservoir relatively unchanged. The result is a decrease in the natural variability of streamflow, as is the case below Gariiep Dam on the Orange River, RSA (WCD, 2000b).

Generally the low flow duration increases and the magnitude of the flood peaks decreases. Gunnison Gorge on the Gunnison River, USA, is downstream of four reservoirs and an interbasin transfer. The 1:10-year flood peak has decreased by 53% from 422 m³/s to 198 m³/s while the low flow duration increased threefold according to Hadley and Emmett (1998). Andrews (1986) reported that no flows larger than 5000 ft³/s (about 142 m³/s) have been released from Flaming Gorge Reservoir on the Green River, USA, while the mean annual flow has not changed.

In flood detention reservoirs the low and medium flows are usually allowed to pass through the reservoir with no or limited damming, but the larger floods are greatly attenuated. According to Chien (1985), Guanting Reservoir on the Yellow River, China, has reduced the peaks by 78% from 3700 m³/s to 800 m³/s. Sanmenxia Reservoir, also on the Yellow River, has been operated for flood detention, with sediment sluicing, and storage since 1974, after being used solely for storage from the time it was built in 1960 to 1964. The flood peaks have been reduced from 12400 m³/s to 4870 m³/s, while the duration of the mean daily flows (1000 – 3000 m³/s) has increased from 130 days a year to 204 days a year.

Reservoirs operated for irrigation decrease flows during the wet season to store water, and increase flows during the dry season, thereby maintaining relatively constant low flows, usually higher than pre-dam conditions. Hydropower dams on the other hand possess highly variable release patterns, with relatively large flows being released during certain times of the day and no or low flows during the rest, although Kariba Reservoir on the Zambezi River, Zimbabwe/Zambia, manages to release a minimum flow of 283 m³/s (SI and CESDC, 2000), which is rather the exception.

2.2 Changes in Sediment Load

Together with the reduction in flood peaks a drastic decrease in the sediment volumes released from a reservoir is experienced, unless the dam is equipped to sluice or flush sediments through the reservoir. Williams and Wolman (1984) reported that the trap efficiency of large reservoirs is commonly greater than 99% in the USA.

Glen Canyon Reservoir on the Colorado River, USA, has reduced the average annual suspended sediment load by 87% from 126 million tons/a to 17 million tons/a (Williams and Wolman, 1984). The downstream station at which the measurements were taken is 150 km away from the dam, which shows that the dam's influence extends far downstream. The impact of a dam on the sediment load however decreases with distance from the dam, as can be seen downstream of Canton Dam on the North Canadian River, USA (**Figure 2.2.1**). The control station included in the figure indicates that the upstream sediment load has remained unchanged, whereas the downstream reach has experienced a considerable reduction in sediment load. Also below Flaming Gorge Dam on the Green River, USA, tributaries have replenished the sediment supply within 68 miles downstream according to Andrews (1986).

Not only are sediments trapped in a reservoir, but the transport capacity in the downstream channel also decreases due to the attenuated flood peaks and is diminished by coarsening of the bed and flatter bed slopes associated with bed degradation. Downstream of Danjankou Dam on the Han River, China, the sediment concentration at flows of 3000 m³/s was reduced by 60.4% (Chien, 1985) and downstream of the High Aswan Dam on the Nile, the suspended sediment concentration typically measured during August decreased from 3500 mg/ℓ to 100 mg/ℓ (Schumm and Galay, 1994).

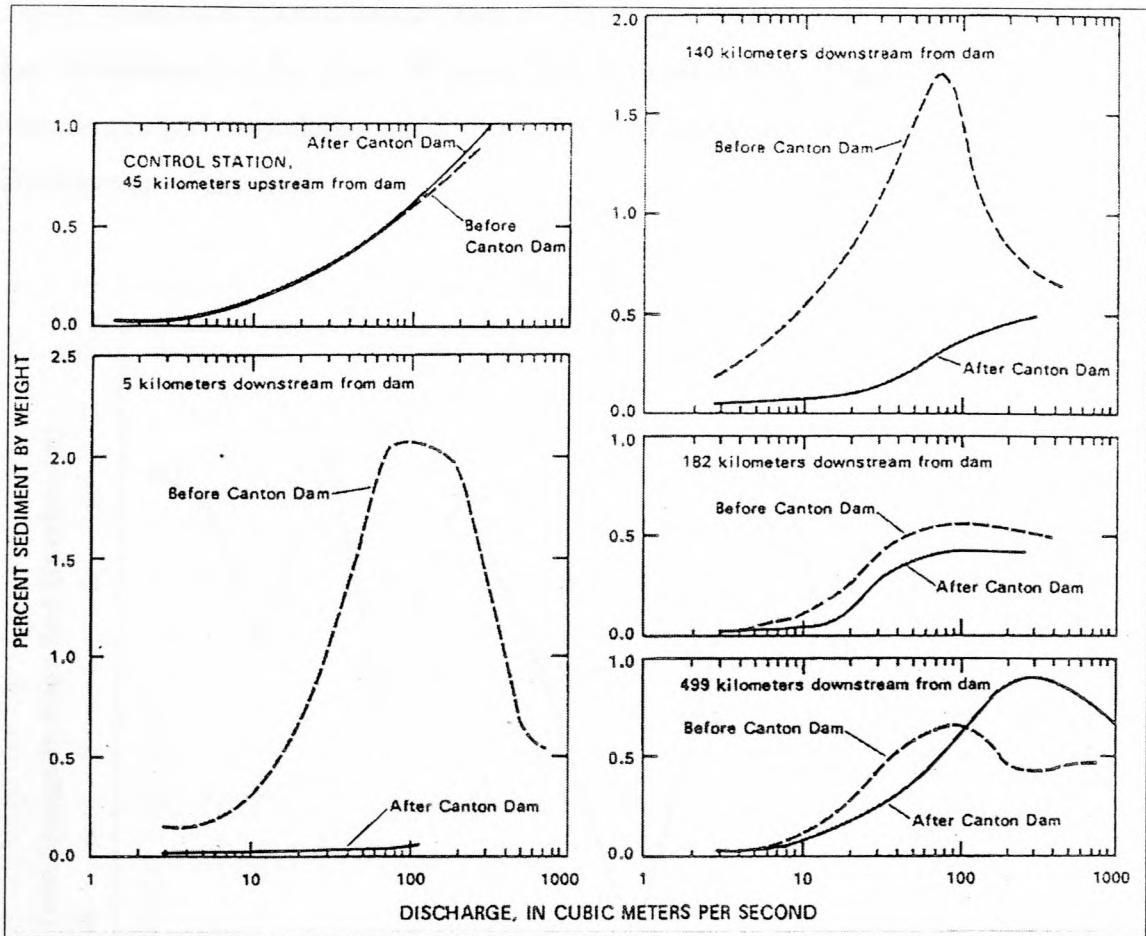


Figure 2.2.1: Suspended sediment loads at successive downstream stations before and after the closure of Canton Dam on the North Canadian River, USA (Williams and Wolman, 1984)

2.3 Changes in Channel Depth

The changes in flow regime and sediment load have a dramatic effect on the channel morphology, since these are two of the controlling factors. Due to the large amounts of clear water released from most reservoirs the most common response of the river channel downstream is degradation. After the completion of Sanmenxia Dam, the average bed degradation was between 0.6 m and 1.3 m during the first four years of storage operation (Chien, 1985). Williams and Wolman (1984) reported much greater impacts below Hoover Dam on the Colorado River, USA, where the maximum degradation 13 years after the completion of the dam was 7.5 m. In most cases the maximum degradation will occur directly below or near the dam, which is the case at the High Aswan Dam with a maximum degradation of 0.7 m (Schumm and Galay,

1994), whereas at Glen Canyon Dam a 7.25 m bed level lowering was measured 16 km downstream of the dam (Williams and Wolman, 1984). **Figure 2.3.1** shows the variation in bed degradation, nine years after the completion of the dam, with distance downstream of the dam.

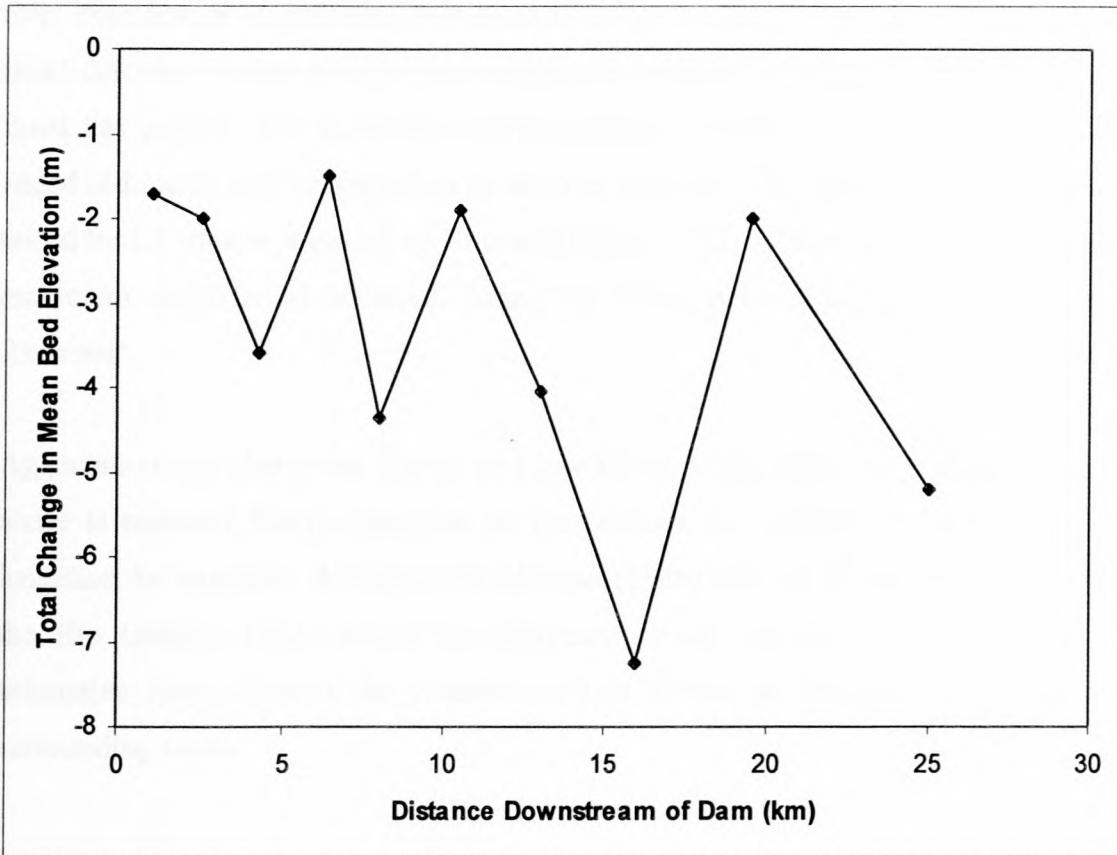


Figure 2.3.1: Variation of bed degradation downstream of Glen Canyon Dam, USA, nine years after closure of the dam

The amount of degradation will depend on local controls such as bedrock or the development of an armour layer. Armouring occurs when fine materials in the bed are eroded, leaving the coarser fractions behind. These create a protective layer that limits erosion of the underlying particles. Likewise flattening of the channel slope will decrease the flow competence, which will control degradation.

Rutherford (2000) reported some scour below Keepit Dam on Dumaresq Creek, Australia, but generally scour below dams has been limited in Australia either by the exposure of bedrock or by armouring, which occurred below Glenbawn Dam, Hunter River, and Eildon Dam on the Goulburn River. Another reason for the limited amount

of erosion below Australian dams is the naturally low sediment yield of the rivers, so that channels may already be adjusted to low sediment transport rates (Rutherford, 2000).

On the other hand when a certain amount of sediment is released from a reservoir the river experiences aggradation. Naodehai Dam on the Liu River, China, was built for flood detention where most of the sediment is released with the lower flows after a flood has passed. The sediment carrying capacity of the flows is exceeded by the added sediments and thus deposits in the river channel. This resulted in the bed being raised by 1.5 m over a period of 10 years (Chien, 1985). Chien also reported that the maximum aggradation occurred during the flood detention phase of Sanmenxia Reservoir.

Aggradation can also occur due to very low flows, which take place when very little water is released from a reservoir or the releases are depleted by extractions for irrigation for example. Williams and Wolman (1984) cite the Elephant Butte Dam on the Rio Grande, USA, where the decreased flows and sediment contributed by tributaries have allowed the riverbed to rise almost to the same height as the surrounding lands.

2.4 Changes in Channel Width

Unlike the changes in channel depth, which are generally dependent on the discharge, sediment load and sediment characteristics as well as local bed controls, the changes in width are also a function of the bank materials and vegetation. Cohesive banks retard erosion to some degree and an increase in vegetation adds to the stability of the banks as well as trapping of sediments. Reduced sediment loads and longer flow durations on the other hand result in widening of the channel, especially when accompanied by an increase in depth, which leads to bank undercutting and subsequent bank collapse (Williams and Wolman, 1984).

Generally a river channel widens when the channel experiences regular dry and wet periods, characteristic of hydropower dams. This could be a result of bank instability due to alternate wetting and drying of the riverbanks. Garrison Dam on the Missouri River, USA, was built for flood control and hydropower in 1953. After 23 years the maximum width increase was 625 m (from 525 m to 1150 m) 47 km downstream of the dam. In contrast a river can become narrower when it carries only low flows for long periods. During this time vegetation can encroach onto the river channel. The low flows rarely manage to reach the flood plains and even then are not competent enough to remove the established vegetation. This effectively reduces the channel width. Channel widening has been reported by Rutherford (2000) for several rivers in Australia including the Upper Murray and Swampy Plains Rivers. The channel widening is a result of consistent regulated releases that increase the duration of the near-bankfull flows.

Channel contraction usually occurs on rivers where the flows are low or are cut off completely for most of the time. Jemez Canyon on the Jemez River, USA, was built for flood and sediment control and as a result 1.6 km downstream of the dam the channel width was reduced by 250 m from 270 m to only 20 m (Williams and Wolman, 1984). Parangana Dam on the Mersey River, Australia, diverts the water and as a result the sediment delivered from the tributaries accumulates in the channel and native vegetation encroaches on the river channel. Rutherford (2000) also reported channel narrowing below several other dams in Australia, including Windamere Dam, on the Cudgegong River, and Jindabyne Dam on the Snowy River. Channel contraction can also be seen below Manapouri Lake on the Waiau River, New Zealand (Brierly and Fitchett, 2000). The Manapouri Power Scheme reduced the mean flow by 75%, resulting in a decrease in channel width from 250 m to 175 m.

The two examples from Garrison Dam and Jemez Canyon also show that the maximum change does not occur directly below a dam. In fact there seems to be no trend in the magnitude of the change in width downstream of dams.

Pongolapoort Dam on the Pongola River was used as a case study for this study, and the changes in width were determined from contour maps compiled before the dam was built in 1973, and 1:15 000 aerial photographs from 1996. Of the 158 sections

analysed 90% have narrowed and only 10% have widened. **Figure 2.4.1** shows the difference in the widths. On average the Pongola River has narrowed by 35% over the 80 km analysed. From the figure it can also be seen that the greatest changes have taken place close to the dam, with a 50% reduction in width over the first 20 km. The width has remained almost unchanged at a section close to the Lubambo tributary.

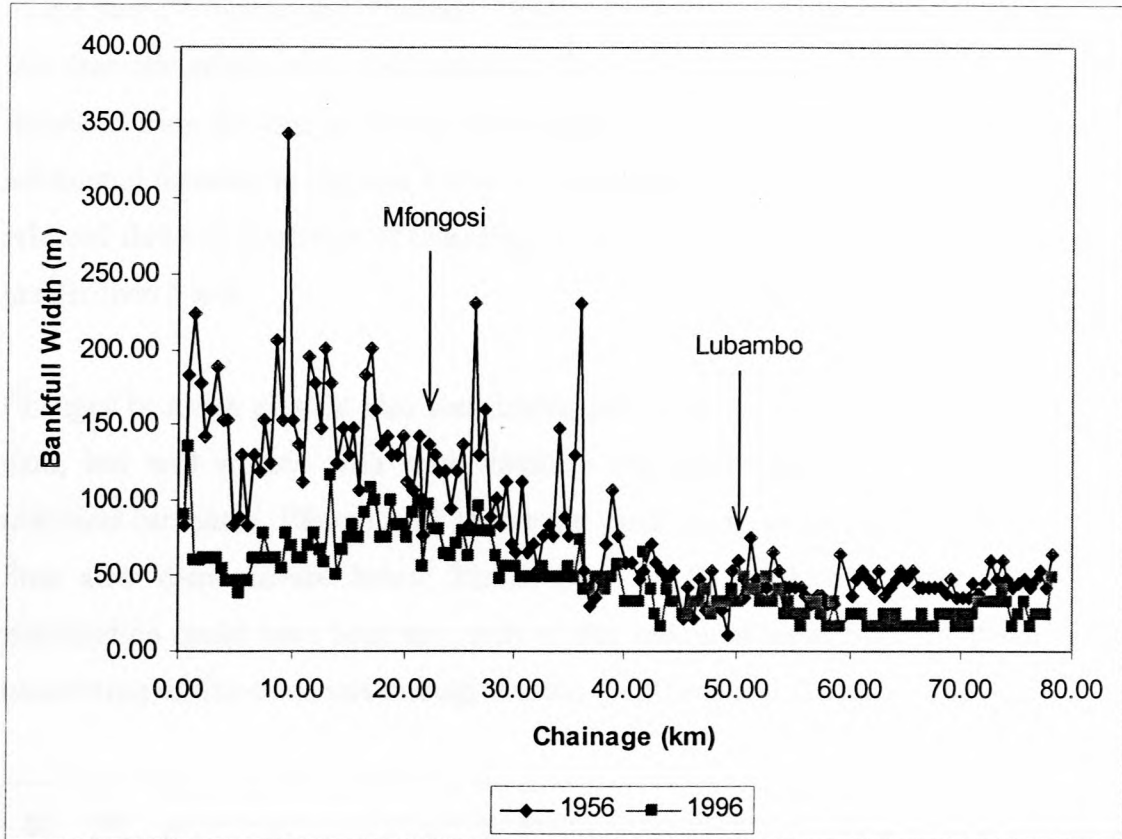


Figure 2.4.1: Changes in channel width of the Pongola River between 1956 and 1996 downstream of Pongolapoort Dam, South Africa (position of tributaries indicated)

2.5 Changes in Bed Material Size

Due to the decrease in magnitude and frequency of the high flows caused by a reservoir, the released flows are unable to transport the same amount and size of particles as before the dam was built. On the other hand the water released from a reservoir is usually clear and the flows are therefore able to entrain fine materials from the riverbed, while the coarser fractions in the bed are left behind. The relatively clear water releases can also be responsible for removing complete surface layers

from the riverbed if they are composed of finer materials and thereby expose coarser layers.

Downstream of Hoover Dam on the Colorado River, USA, the median bed-particle diameter (d_{50}) increased from 0.2 mm to about 80 mm within seven years after closure of the dam (Williams and Wolman, 1984). Guanting Reservoir has had a similar but less dramatic effect on the bed material of the river. The median particle diameter d_{50} increased from 0.4 mm to about 7 mm (Chien, 1985). In the case of Hoover Dam the substantial increase in d_{50} was a result of the exposure of a layer of gravel, while the released flows downstream of Guanting Dam were not large enough to transport sizes greater than 5 mm.

Changes in mean particle size start taking place immediately after completion of a dam, but will reduce with time, because the availability of transportable finer materials decreases. **Figure 2.5.1** shows the variation in mean particle diameter with time after dam closure below Parker Dam on the Colorado River, USA. The stabilization could have been the result of fine sediment input from tributaries or the uncovering of fine materials through erosion (Williams and Wolman, 1984).

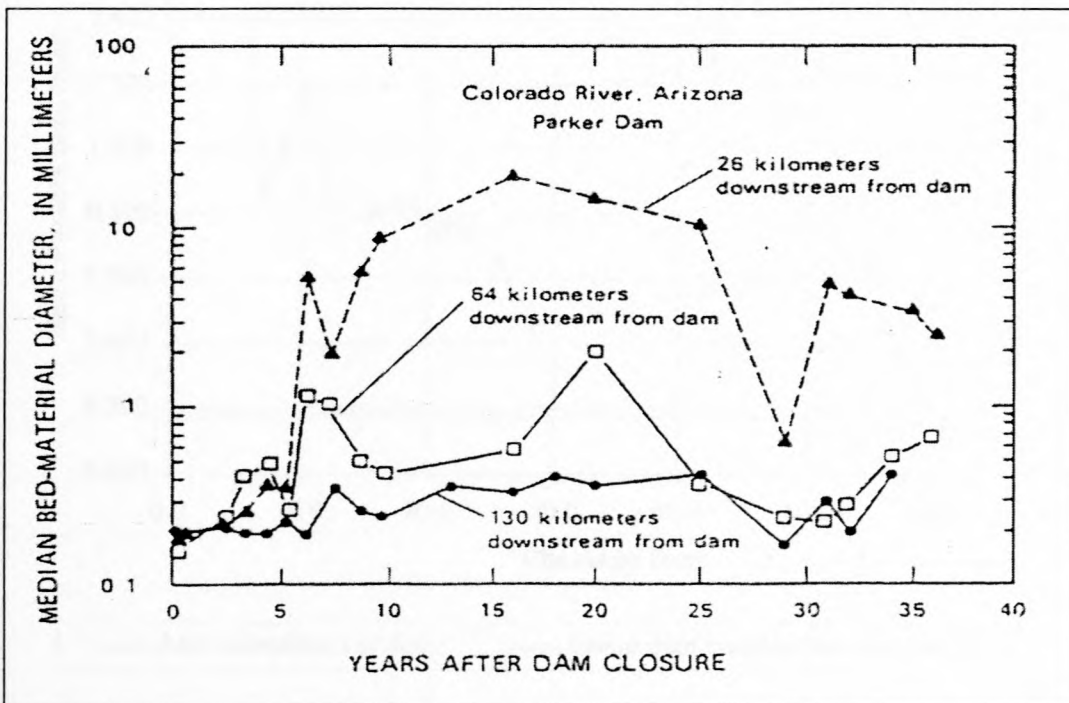


Figure 2.5.1: Variation of d_{50} downstream of Parker Dam, USA (Williams and Wolman, 1984)

The coarsening of the bed decreases with distance from a dam. This could be because further downstream tributaries again supply a certain amount of finer sediments, which could be deposited in the river channel. Another reason could be the decrease in bed degradation, which means that the likelihood of uncovering coarser materials is lower. **Figure 2.5.2** shows this trend for Pongolapoort Dam, where d_{50} decreases from 1.7 mm to 0.17 mm over a distance of 60 km. Particle sizes were even bigger nearer the dam, with exposed bedrock at the dam. The mean particle diameter of 0.18 mm before the dam was built was estimated from particle size distributions of samples taken upstream of the dam (DWAF, 1985), such as that shown in **Figure 2.5.2**. As mentioned above, Sanmenxia Reservoir has had different modes of operation and the effect on the mean particle diameter is shown in **Figure 2.5.3**. During the flood detention phases muddy water was released after the floods had passed through the reservoir, whereas clear water was released during the storage periods. The reversal in trend was immediate, and the mean particle diameter remained relatively constant between 1964 and 1972.

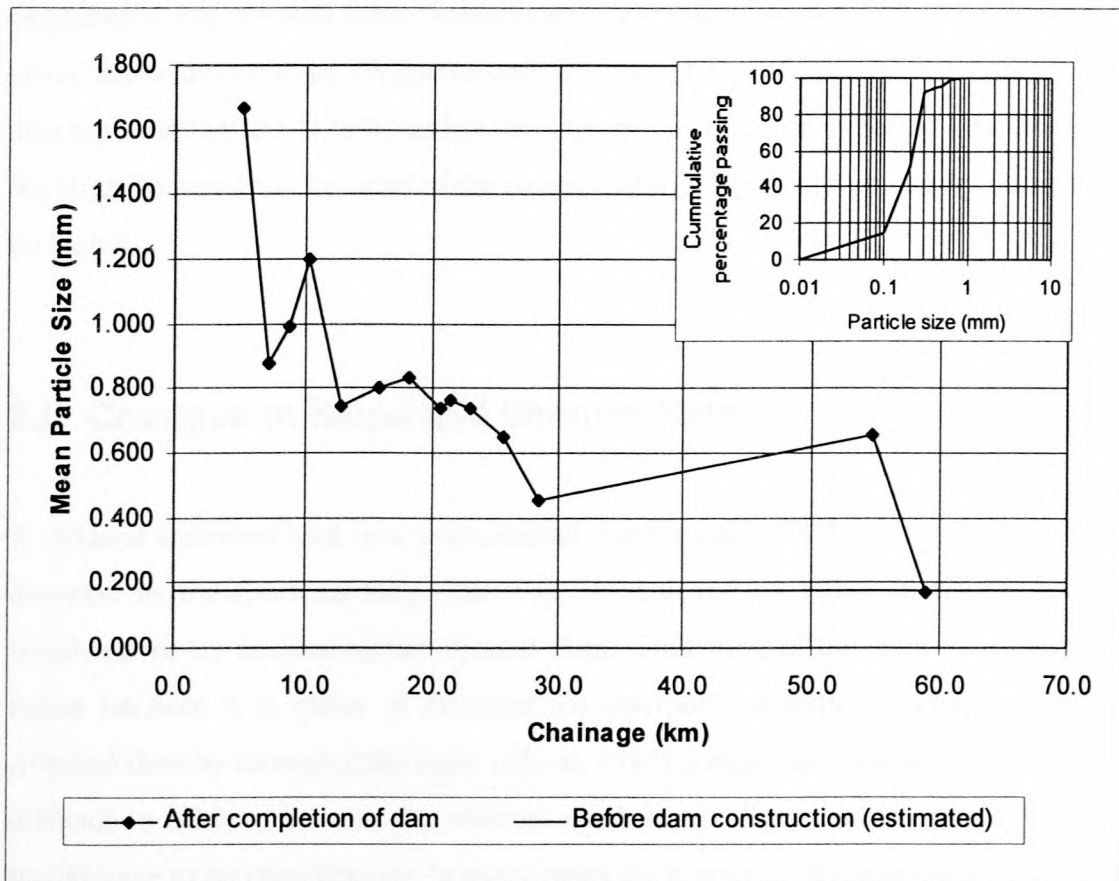


Figure 2.5.2: Variation of d_{50} downstream of Pongolapoort Dam, South Africa

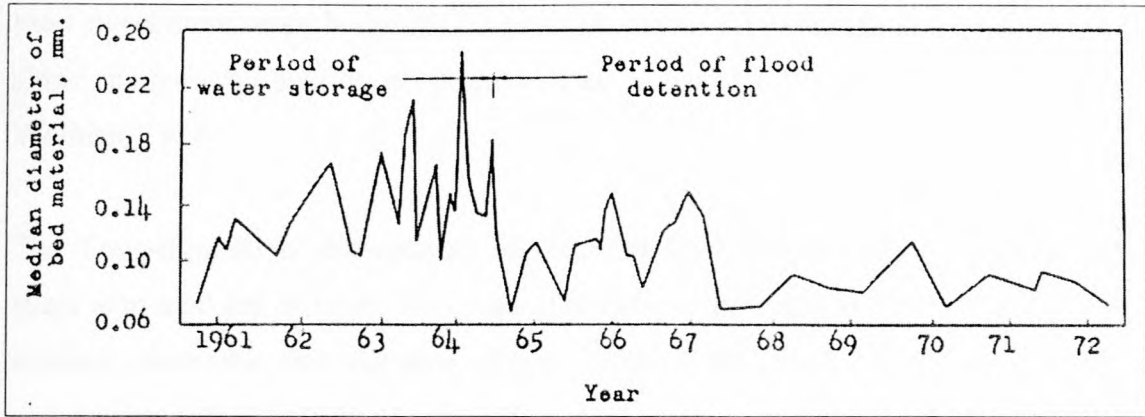


Figure 2.5.3: Variation of d_{50} downstream of Sanmenxia Dam, China, with different modes of operation (Chien, 1985)

Coarsening of the bed leads to an increase in roughness and a subsequent decrease in the transport capacity of the river. Chien (1985) reported that an increase in the mean particle diameter from 0.1 mm to 0.13 mm could reduce the transport capacity by 65%. Development of an armour layer is also important, because it controls degradation. On the Red River downstream of Dennison Dam, USA, 30 to 50% gravel cover limits degradation (Williams and Wolman, 1984). Schumm and Galay (1994) also reported that the Nile River has not degraded as much as expected downstream of the High Aswan Dam because of the coarse material being introduced by wadis along its length.

2.6 Changes in Slope and Channel Pattern

A reduced sediment load in a river channel downstream of a dam is associated with a decrease in transport capacity. This can be achieved by either increasing the bed roughness or by decreasing the channel slope. Flattening of the slope is usually only minor because it is easier to decrease the transport capacity by coarsening of the riverbed than by changing the slope (Chien, 1985). Large adjustments of the slope are difficult to achieve because the affected reach is usually very long and degradation would have to be considerable. In many cases the degree of degradation is also limited by the presence of bedrock, which is generally present below dam walls. In many cases there might therefore be no noticeable change in slope over a long reach, but on

most rivers there could be small changes over shorter distances. On the other hand bed slope changes can also occur as a result of an increase in sinuosity (Williams and Wolman, 1984).

The Yong-ding River downstream of Guanting Dam shows virtually no change in slope over a 60 km distance. Six years after closure the bed was lowered by the same distance over the full distance (Chien, 1985). The same trend was observed downstream of the High Aswan Dam (Schumm and Galay, 1994), unlike the Colorado River below Glen Canyon Dam where the slope has decreased slightly within three years after the dam was built, and after that increased considerably as shown in Figure 2.6.1.

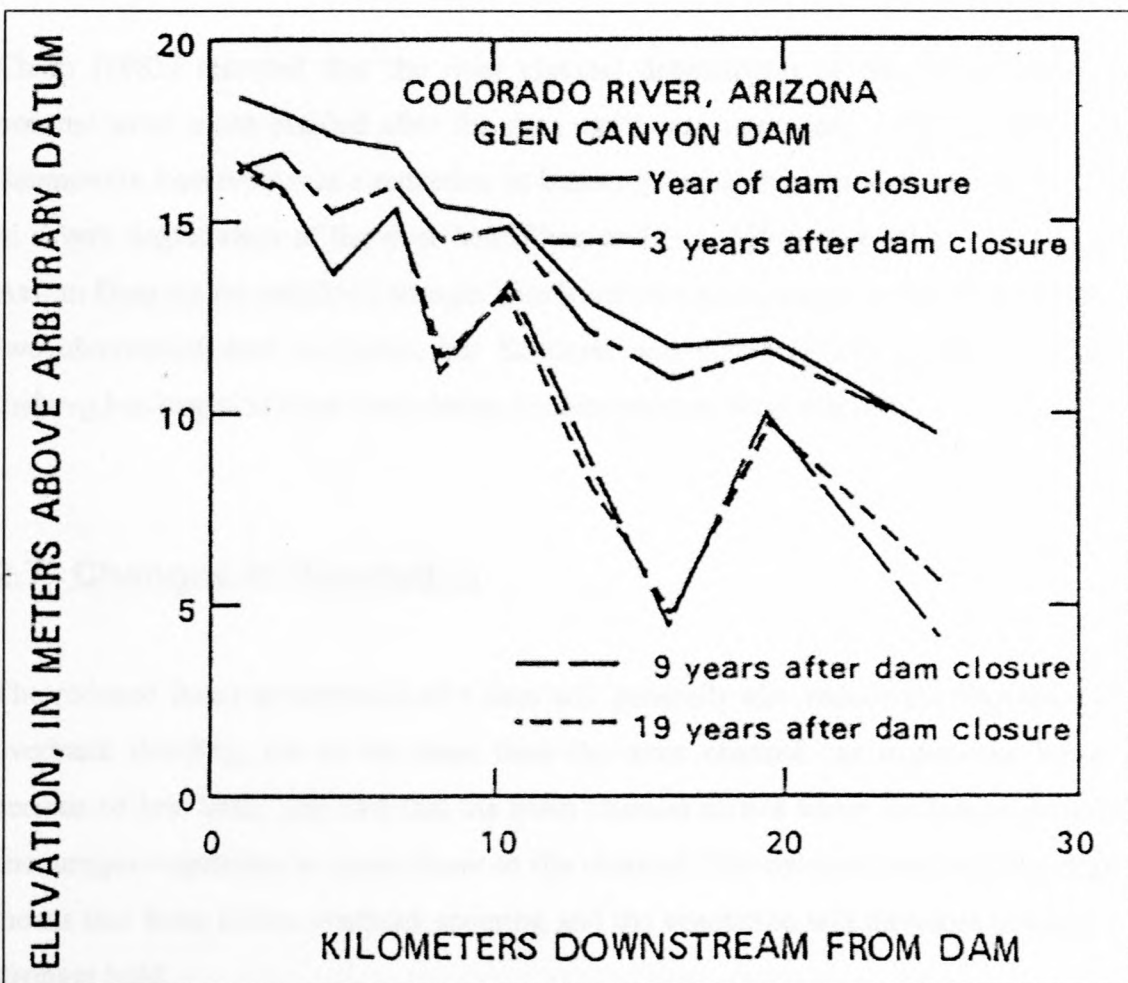


Figure 2.6.1: Changes in slope of the Colorado River below Glen Canyon Dam, USA (Williams and Wolman, 1984)

Since the bed profile downstream of a dam is dependent on factors like variations in bed material, water discharge, local controls and tributary contributions, the changes in slope along a certain reach are generally highly variable. This variability is evident downstream of Fort Randall Dam, Missouri River, where aggradation, degradation and no change occurred from one cross-section to another (Williams and Wolman, 1984).

A change in slope can be accompanied by a change in channel pattern. Leopold and Wolman (1957) have pointed out that the kind of channel pattern, which a river follows, depends amongst others on the channel slope. Braided rivers generally occur on steeper slopes than meandering rivers. As the river may adjust its slope in response to the construction of a dam, there may occur a corresponding change from braided to meandering or vice versa.

Chien (1985) reported that the river channel downstream of Naodehai Dam has become even more braided after the dam came into operation, while the effect of Sanmenxia Reservoir was a reduction in braiding during the impoundment phase due to severe degradation of the river bed (Zhou and Pan, 1994). The effect of the High Aswan Dam on the relatively straight Nile River has not occurred as rapidly as for the two abovementioned examples, but Schumm and Galay (1994) reported that the thalweg has begun to show meandering tendencies over short reaches.

2.7 Changes in Vegetation

The reduced flows downstream of a dam will generally also reduce the frequency of overbank flooding, but at the same time the main channel can experience longer periods of low flows. The fact that the main channel carries water for longer periods encourages vegetation to grow closer to the channel. The reduced overbank flooding means that there is less overbank scouring and the vegetation will therefore develop a stronger hold.

The increased vegetation can block part of the river channel and thereby reduce the flow area and also trap sediments, which leads to aggradation of the bed. The vegetation can also increase bank stability due to the binding and protective effects of the vegetation (Williams and Wolman, 1984).

According to Schumm and Galay (1994) the bank erosion of the Nile River has in part been controlled by the growth of natural vegetation. The same was reported by Hadley and Emmett (1998) for Bear Creek, USA, downstream of Bear Creek Lake. The width increased only by 0.5 m over a period of 15 years, which they accredited to the growth of woody vegetation.

The increase in vegetation on the banks and floodplains leads to an increase in hydraulic roughness. This can result in higher flood levels.

2.8 Affected Distance

The river reach affected by a dam increases with time, until the river has adjusted to the new flow and sediment regime. The length of the reach affected by a dam depends on several factors. The location and number of major tributaries has a significant effect, as they are essential in replenishing both the sediment and water discharge, and the type of material they transport is also important. Andrews (1986) has reported for the Green River below Flaming Gorge Dam that tributaries have replenished the sediment supply within 68 miles (about 109 km).

Downstream base-level controls such as another reservoir or a weir can stop the progression of erosion, as can a reduction in transport capacity (either by a reduction in the slope or through coarsening of the bed material). All of these factors make it difficult to predict the exact extent of the affected reach.

Chien (1985) attempted to describe the process of degradation below a dam. The clear water released from the dam picks up sediment from the channel until the incoming load becomes equal to the sediment transporting capacity of the flow and the flow

becomes saturated. This is called the point of concentration recovery and at the beginning of reservoir operation this also represents the point to which degradation progresses. After some time has elapsed, the bed material becomes coarser upstream of the point of concentration recovery, which means the transported sediment becomes coarser and the load becomes less than the transport capacity. On the other hand the coarsening of the bed material also results in a considerable reduction in the transport capacity of the flow. The result is that the point of concentration recovery actually moves towards the dam with time. However below the point of concentration recovery enough fine material still exists and the transporting capacity of the flow is larger than the incoming load. This results in further erosion and coarsening downstream. If the flow conditions remain unchanged the whole process will continue, causing degradation to extend far downstream of the dam. Chien however did not account for the effect of tributaries or downstream controls.

The length of the degraded reach below Hoover Dam was 120 km long, 13 years after closure, and there was no indication that the reach had stopped lengthening (Williams and Wolman, 1984). Below Sanmenxia Dam the affected distance was even longer at 480 km, as reported by Chien (1985). This is partly due to the fact that there are no major tributaries on the Yellow River below Sanmenxia Dam and it is feared that the whole river course of over 800 km could degrade over time.

3. River Channel Morphology

A natural river is never completely stable because of the natural variability of the factors that control the morphology especially the water discharge and sediment load. Even though the variability can be great, as is the case in the semi-arid climate of South Africa, a river will strive to attain a state of dynamic or quasi-equilibrium, by changing its cross-section, slope and even channel pattern to obtain optimal transport of water and sediments. Such a river is said to be in regime, meaning that it has obtained a long-term stable configuration, with only minor adjustments. Major changes tend to only occur as a result of significant events like a 1:100-year flood or the construction of a dam.

In order to analyse the effects that a dam can have on the downstream river channel, it is important to be able to describe the stable river morphology. There are two approaches to describing the hydraulic geometry of alluvial rivers: the empirical approach and the theoretical or analytical approach. The empirical approach attempts to derive relationships from available data and is thus dependent on the quality of the data. The theoretical or analytical approach relies on fundamental hydraulic processes like flow resistance and sediment transport, where the identification of the dominant processes is very important. A first attempt is generally the development of empirical regime equations that provide at least an indication of the direction of the changes. Regime equations based on hydraulic processes occur in very much the same format as the empirical equations, with the same input variables. The one difference is that the theoretical/analytical regime equations are generally applicable to a wider range of conditions. Another way of describing the channel geometry is through some form of extremal hypothesis, e.g. the minimization of stream power approach by Chang (1979, 1988).

A river has at least three degrees of freedom in its width, depth and slope, while Chang (1979) added the channel pattern to the list. The velocity is not regarded as a degree of freedom because it is determinable from the discharge and channel geometry. The factors that control or influence these variables are the water discharge, sediment load, and bed and bank materials. The water and sediment discharge are by

far the most dominant factors also as a result of their great variability. The bed and bank materials remain relatively unchanged under stable conditions, and generally only change as a result of a change in water and sediment discharge. This is also why dams have such far-reaching impacts on a river, because they disturb the flows and sediment load to such a high degree.

3.1 Dominant Discharge

The water discharge is by far the most important parameter responsible for the geometrical shape of a channel and it is obvious that identifying the correct discharge is of utmost importance. Although a whole range of flows normally shapes a river, there is a general consensus that one steady flow rate, the dominant discharge, should produce the same channel dimensions as a sequence of events. This channel-forming discharge can be defined as either the flow rate that determines particular channel parameters or that cumulatively transports the most sediment.

Many researchers have equated the dominant discharge with the bankfull discharge. Bankfull discharge is the flow rate that just fills the channel to the tops of the banks, corresponding to the condition of incipient flooding. Ackers (1988) argued that sediment transport would decrease once the flow goes overbank, because of an increase in overall resistance and reduction in erosive tendencies of the flow, while Ackers and Charlton (1970) found that the bankfull discharge works best for describing sinuosity and meander wavelength. Carling (1988) reasoned that at bankfull level the resistance to flow is a minimum and the sediment transport rate a maximum. The dominant discharge has also been linked to a recurrence interval of approximately 1-2 years by several researchers (Harvey, 1969), but most of these studies actually established a much wider range for bankfull flow recurrence intervals between 1 and 10 years.

There are several problems regarding the use of bankfull discharge as the dominant discharge. The biggest is that there exist numerous definitions of the bankfull level, as Williams (1978) pointed out. These include either the elevation of certain benches or

the active floodplain, the lower boundary of perennial vegetation or the elevation at which the width/depth ratio becomes a minimum. The determination of the discharge corresponding to the bankfull elevation presents an additional problem. The most common ways of determining this discharge are by means of a rating curve, hydraulic geometry or flow equations. Considering all the different approaches it is not surprising that by comparing the various methods, Williams (1978) obtained a wide range of results, in most cases varying by more than 100%. He also observed that obtaining a bankfull discharge at one cross-section is questionable since it can be radically different a few meters upstream or downstream.

In regions with highly variable runoff the bankfull discharge may not represent the dominant discharge because the water rarely flows at bankfull for long periods of time. The assumptions of a return period of 1 – 2 years also does not hold true in drier climates, because these floods are not nearly large enough to shape a channel extensively. On the other hand large floods have the capacity to reshape the channel geometry, but they occur too infrequently to have a lasting effect and the river changes back to a more stable channel. Wolman and Miller (1960) observed that the greater the variability in runoff, the larger the percentage of sediment carried by infrequent floods, which means the dominant discharge is bound to have a longer recurrence interval than 1 - 2 years. Osterkamp and Hedman (1979) studied ephemeral rivers and found that their widths are more indicative of more unusual discharges than the mean discharge. They related the channel width of ephemeral streams to the 1:10-year flood. Clark and Davies (1988) also found that the dominant discharge had an average return period of 10 years.

For the bankfull discharge to actually occur at bankfull level, means that the river channel must have already adjusted to accommodate that flow, because as soon as the flow regime changes the frequency of the former bankfull discharge will either increase or decrease depending on the changes in regime. This means that the former bankfull discharge will not have the same effects as before and that a different “bankfull” discharge with a different magnitude will emerge. If this is smaller than the original bankfull discharge, the channel will be too big and the “bankfull” discharge will actually not fill the channel to the top of the banks. On the other hand if the flows should increase in magnitude the “bankfull” discharge will actually flow over the

banks. The river channel will adjust to the changed flow regime and it will thus take a while before the “bankfull” discharge will actually flow at bankfull level, and only then will it have reached its full effectiveness. Considering that the bankfull discharge has been related to the dominant discharge, because of the extraordinary conditions at bankfull level, i.e. maximum sediment transport rate, the bankfull discharge is a misleading concept in the formation of a river channel’s geometry, while it might be more likely to maintain a river channel once it has adjusted to a new flow regime.

When establishing mathematical or analytical tools describing the changes in channel geometry after the construction of a dam, it might be more correct to use a discharge that can actually be predicted with accuracy. Although it is difficult to link the dominant discharge to a specific recurrence interval, it seems that for a region like South Africa the river channels are formed by discharges that occur rather infrequently, with a recurrence interval between 5 and 20 years.

3.2 Existing Regime Equations

Regime equations have been used to describe river channel geometry for over a century, starting with the first attempts by Kennedy for irrigation canals in 1895. Further attempts were made by Lacey and Blench on straight canals, both having incorporated factors relating to sediment transport. Leopold and Maddock were among the first to develop regime equations for straight alluvial rivers. Later attempts were made to extend the equations to gravel-bed rivers, as well as to meandering rivers.

These regime equations were all empirically derived. The problem with the empirical regime equations is that they are only applicable to the range of conditions for which they were derived. Analytically or theoretically derived regime equations on the other hand are applicable to a wide range of conditions. Nonetheless it is important to correctly identify the dominant processes involved in the formation of a stable channel geometry. Since these processes are rather complex, it is mostly necessary to

simplify the equations by deriving coefficients empirically, leading to semi-theoretical or semi-analytical regime equations.

3.2.1 Width Equations

The width generally shows the greatest adjustment after a change in flow regime, and some of the regime equations that have been derived are summarised in **Table 3.2.1**, which shows that most equations are expressed only in terms of discharge. This is because the water discharge is by far the most important factor influencing the channel geometry. From the summarised equations the following qualitative observation can be made regarding the effects of changing input variables on the channel width. A plus or minus exponent denotes an increase or decrease in the variable considered.

$$Q^{+/-} \rightarrow B^{+/-}$$

$$d^{+/-} \rightarrow B^{-/+}$$

$$C^{+/-} \rightarrow B^{+/-}$$

$$S^{+/-} \rightarrow B^{-/+}$$

with Q = discharge

B = channel top width

d = particle size

C = sediment concentration

S = channel slope

An increase in discharge will thus lead to an increase in width due to its increased erosive tendency, while an increase in the particle size leads to a decrease in channel width because coarser particles are more difficult to erode. Usually the change in particle size is related to the change in discharge, so both will change together. The coarsening of the bed material may thus be a way for the river to counteract the effect of the increasing discharge.

Table 3.2.1: Summary of width equations (adapted from Wargadalam, 1993)

| Author | Equation | Units | Remarks |
|----------------------------|---|-------|--|
| Lacey (1930) | $P = 2.667 Q^{0.5}$ | ft | Bankfull discharge, sand-silt canals |
| Blench (1957) | $B = b Q^{0.5} d^{0.25}$ | ft | Bankfull discharge, sand-silt canals, $d = d_{50}$ (mm), $b = \sqrt{(1.9(1 + 0.012C)/F_s)}$ |
| Leopold & Maddock (1953) | $B = a Q^{0.5}$ | ft | Bankfull discharge, alluvial rivers, a varies for individual streams |
| Henderson (1963) | $B = 0.93 Q^{0.46} d^{-0.15}$ | ft | Design discharge, narrow channels, $d = d_{50}$ |
| Kellerhals (1967) | $B = 1.8 Q^{0.5}$ | ft | Dominant discharge, gravel-bed rivers |
| Chitale (1966) | $P = 2.187 Q^{0.523}$ | ft | Sand-silt canals |
| Bray (1982) | $B = 2.38 Q^{0.527}$ | ft | 1:2-year discharge, gravel-bed rivers |
| Bray (1982) | $B = 2.08 Q^{0.528} d^{-0.07}$ | ft | 1:2-year discharge, $d = d_{50}$, gravel-bed rivers |
| Hey & Thorne (1986) | $B = k_l Q^{0.5}$ | m | Bankfull discharge, gravel-bed rivers, $k_l = f(\text{bank vegetation})$ |
| Nouh (1988) | $B = 28.30 (Q_{50}/Q)^{0.83} + 0.018 (1 + d)^{0.93} C^{1.25}$ | m | Mean annual discharge, $d = d_{50}$, ephemeral channels (arid zone) |
| Julien & Wargadalam (1995) | $B = 0.512 Q^\alpha d_s^\beta S^\gamma$ | m | Dominant discharge, $\alpha = (2 + 4m)/(5 + 6m)$, $\beta = -4m/(5 + 6m)$, $\gamma = (-2m - 1)/(5 + 6m)$, $m = 1/\ln(12.2D/d_s)$ |

Considering that the exponent of discharge in the width equations is generally close to 0.5 and thereby almost twice as large as the particle size exponent, which is usually less than -0.2 , the effect of a change in discharge will outweigh a change in particle size.

Most of the variables under consideration will not change in isolation, but rather in response to, or together with another variable. An increase in discharge, which causes channel widening, is generally accompanied by a decrease in slope. Thus a decrease in slope can be associated with an increase in width. The same principle applies to an increase in sediment concentration, which is a consequence of an increase in discharge. A widening of the river channel can therefore be expected when the sediment concentration increases in this way.

3.2.2 Depth Equations

The depth is generally the first to change when the natural flows of a river are altered. The magnitude of this change is not as considerable as that of the width, because the depth can be controlled to a much larger degree by armouring or the exposure of bedrock.

A summary of some depth equations is provided in **Table 3.2.2**. The same variables that determine the width also describe the depth. Although the discharge is still the most important factor, more equations describe the depth in terms of discharge and particle size, meaning that the particle diameter has a greater effect on the depth than the width. From the summarised equations the following observation can be made regarding the effects of changing input variables on the channel depth.

$$Q^{+/-} \rightarrow D^{+/-}$$

$$d^{+/-} \rightarrow D^{-/+}$$

$$C^{+/-} \rightarrow D^{-/+}$$

$$S^{+/-} \rightarrow D^{-/+}$$

with D = channel depth

Table 3.2.2: Summary of depth equations (adapted from Wargadalam, 1993)

| Author | Equation | Units | Remarks |
|----------------------------|--|-------|---|
| Lacey (1930) | $R = 0.405 Q^{0.333} d^{-0.167}$ | ft | Bankfull discharge, sand-silt canals |
| Blench (1969) | $D = c Q^{0.333} d^{-0.333}$ | ft | Bankfull discharge, sand-silt canals, $d = d_{50}$ (mm), $c = [F_s / (1.9(1 + 0.012C))]^{0.333}$ |
| Leopold & Maddock (1953) | $D = b Q^{0.3}$ | ft | Bankfull discharge, ephemeral streams, b varies for individual streams |
| Henderson (1963) | $R = 0.12 Q^{0.46} d^{-0.15}$ | ft | Design discharge, narrow channels, $d = d_{50}$ |
| Kellerhals (1967) | $D = 0.166 Q^{0.4} k_s^{-0.12}$ | ft | Dominant discharge, gravel-bed rivers, $k_s = d_{90}$ |
| Chitale (1966) | $R = 0.486 Q^{0.341}$ | ft | Sand-silt canals |
| Bray (1982) | $D = 0.266 Q^{0.333}$ | ft | 1:2-year discharge, gravel-bed rivers |
| Bray (1982) | $D = 0.256 Q^{0.331} d^{-0.025}$ | ft | 1:2-year discharge, $d = d_{50}$, gravel-bed rivers |
| Hey & Thorne (1986) | $D = 0.22 Q^{0.37} d^{-0.11}$ $R = k_3 Q^{0.41} Q_s^{0.02} d^{-0.14}$ | m | Bankfull discharge, $d = d_{50}$, gravel-bed rivers, $k_3 = f(\text{bank vegetation})$ |
| Nouh (1988) | $R = 1.29 (Q_{50}/Q)^{0.65} -$ $0.01 (1 + d)^{0.98} C^{0.46}$ | m | Mean annual discharge, $d = d_{50}$, ephemeral channels (arid zone) |
| Julien & Wargadalam (1995) | $D = 0.2 Q^\alpha d_s^\beta S^\gamma$ | m | Dominant discharge, $\alpha = 2/(5 + 6m)$, $\beta = 6m/(5 + 6m)$, $\gamma = -1/(5 + 6m)$, $m = 1/\ln(12.2D/d_s)$ |

Much the same patterns can be observed here as those that were encountered for the width equations. A deeper channel can occur as a result of an increased discharge, coarser bed material or a decrease in channel slope. The one difference is that a river channel becomes deeper with a decrease in sediment concentration. A decreasing sediment concentration signifies that the transport capacity of the flow is not fully utilised and more sediment will be picked up from the bed, leading to a deeper river channel.

3.2.3 Slope Equations

Apart from changes in width and depth an alluvial river can also change its slope in response to an altered flow regime. A change in channel slope can have far reaching consequences as it can be accompanied by a change in channel pattern, but it usually takes much longer for an appreciable change in slope to become evident, which means that changes in channel pattern may take even longer to occur.

Table 3.2.3 gives an overview of some slope equations. As with the width and depth, discharge and particle size are the two dominant variables that determine the slope. Generally however the slope equations have very poor correlation coefficients.

$$Q^{+/-} \rightarrow S^{-/+}$$

$$d^{+/-} \rightarrow S^{+/-}$$

$$Q_s^{+/-} \rightarrow S^{+/-}$$

with Q_s = sediment load

As mentioned before, the relationship between discharge and channel slope is such that as the discharge decreases the slope becomes steeper, which also follows from the slope equations in **Table 3.2.3**. This occurs because the transport capacity of the river channel decreases as the discharge is reduced and the increase in channel slope is a measure to increase the transport capacity again.

| Author | Equation | Units | Remarks |
|----------------------------|--|-------|---|
| Lacey (1930) | $S = 0.00118 Q^{-0.167} d^{0.833}$ | ft | Bankfull discharge, sand-silt canals |
| Leopold & Maddock (1953) | $S = a Q^{-0.95}$ | ft | Bankfull discharge, ephemeral streams, a varies for individual streams |
| Henderson (1963) | $S = 0.44 Q^{-0.46} d^{1.15}$ | ft | Design discharge, narrow channels, $d = d_{50}$ |
| Kellerhals (1967) | $S = 0.12 Q^{-0.4} k_s^{-0.92}$ | ft | Dominant discharge, $k_s = d_{90}$ |
| Chitale (1966) | $S = 0.0005 Q^{-0.165}$ | ft | Sand-silt canals |
| Bray (1982) | $S = 0.0354 Q^{-0.342}$ | ft | 1:2-year discharge, gravel-bed rivers |
| Bray (1982) | $S = 0.0965 Q^{-0.334} d^{0.586}$ | ft | 1:2-year discharge, $d = d_{50}$, gravel-bed rivers |
| Hey & Thorne (1986) | $S = 0.087 Q^{-0.43} Q_s^{0.1} d_{50}^{-0.09} d_{84}^{0.84}$ | m | Bankfull discharge, gravel-bed rivers, |
| Nouh (1988) | $S = 18.25 (Q_{50}/Q)^{-0.35} - 0.88 (1+d)^{1.13} C^{0.36}$ | m | Mean annual discharge, $d = d_{50}$, ephemeral channels (arid zone) |
| Julien & Wargadalam (1995) | $S = 12.4 Q^\alpha d_s^\beta S^\gamma$ | m | Dominant discharge, $\alpha = -1/(3 + 2m)$, $\beta = 5/(4 + 6m)$, $\gamma = (5 + 6m)/(4 + 6m)$, $m = 1/\ln(12.2D/d_s)$ |

Table 3.2.3: Summary of slope equations (adapted from Wargadalam, 1993)

The particle size d on the other hand is directly proportional to the slope. This probably is due to the fact that on steeper slopes the transport capacity increases and most of the finer material is washed away. Judging by the magnitude of the particle size exponent, d also plays a much greater role in determining the slope than the depth or width. Although in this case it is more likely that the slope determines the particle size, whereas the depth and width are definitely influenced by the particle size.

The reason for the poor correlation coefficients of most slope equations may be that the slope takes so much time to adjust to the altered flows and that it may only change over short distances. The measured field slopes might therefore not be equilibrium slopes, making it incorrect to use them in calibration or verification processes.

3.3 Proposed Regime Equations for South African Conditions

In this chapter an attempt is made to develop a set of regime equations much like those listed in **Chapter 3.2** for South African rivers.

3.3.1 Theory

The concept of stream power has been used in one way or another to describe various aspects of a river's morphology. Bagnold (1966) introduced the concept of stream power to the study of sediment transport. The unit stream power approach was used by Yang (1973) to explain the behaviour of meandering rivers as well as sediment transport. He argued that the suspended sediment concentration C is related to the unit stream power vS and particle settling velocity w :

$$C \propto \frac{vS}{w} \dots\dots\dots 3.3.1$$

where vS/w is the dimensionless unit input stream power.

Integrating the unit stream power over the cross-sectional area of the channel gives the total input stream power per unit channel length $\rho g Q S$, which is proportional to the total sediment load Q_s .

$$Q_s \propto \frac{\rho g Q S}{w} \dots\dots\dots 3.3.2$$

Apart from the water discharge the sediment load is one of the major factors determining the channel geometry, and it therefore follows that the channel geometry, i.e. width B and depth D , should be determined by the total stream power. This means:

$$B = f(Q, S, w) \dots\dots\dots 3.3.3$$

$$D = f(Q, S, w) \dots\dots\dots 3.3.4$$

Since the settling velocity w is a function of the median particle diameter d_{50} , it follows that

$$B = f(Q, S, d_{50}) \dots\dots\dots 3.3.5$$

$$D = f(Q, S, d_{50}) \dots\dots\dots 3.3.6$$

From **Tables 3.2.1** and **3.2.2** it can be seen that the general form of the regime equations is basically the same regardless of the approach followed to establish these. For example Bray's (1982) equations are purely empirical and in the form:

$$B = C_b Q^\alpha d_{50}^\beta \dots\dots\dots 3.3.7$$

$$D = C_d Q^\alpha d_{50}^\beta \dots\dots\dots 3.3.8$$

Julien and Wargadalam (1995) on the other hand used the following four fundamental relationships to derive hydraulic geometry equations:

1. Flow rate
2. Resistance to flow
3. Particle mobility
4. Secondary flow

To simplify the established equations for practical applications, some coefficients had to be empirically determined, leading to the semi-theoretical equations in **Tables 3.2.1** and **3.2.2**.

The basic forms of the regime equations, describing the downstream channel morphology, developed in this study are therefore:

$$B = C_b Q^\alpha S^\beta d_{50}^\gamma \dots\dots\dots 3.3.9$$

$$D = C_d Q^\alpha S^\beta d_{50}^\gamma \dots\dots\dots 3.3.10$$

The calibration of these two equations is discussed in the following section.

3.3.2 Calibration of New Regime Equations

3.3.2.1 Data Set

For the calibration of the channel geometry equations, data from a large number of South African rivers were utilised. The data were in the form of cross-sectional surveys taken by the Department of Water Affairs and Forestry (DWAF) at 59 sites where dams were to be built. Some of these sites were on the same river, but since a river is never the same over its entire length, the sites were used as if they represented a different river. For each site five consecutive cross-sections were chosen, typically between 250 m and 2 km apart depending on the size of the proposed dam, and a representative slope *S* was determined from topographical maps of various scales for that reach, by weighing the slopes between cross-sections according to the respective distance between cross-sections.

$$S = \frac{\sum_i (S_i * L_i)}{L} \dots\dots\dots 3.3.11$$

where S_i = slope between two successive cross-sections

L_i = distance between successive cross-sections

L = total length of the reach

In addition to the cross-sectional surveys, peak discharges of return periods between 2 and 200 years (DWAF, 1998), as well as other catchment data (i.e. sediment yield, particle size) were available for the sites (see **Appendix A1**). The particle sizes could not be determined from field data because dams have had an impact on the river reaches under consideration, and any field data taken at this stage would not reflect natural conditions. The particle sizes were therefore determined from the erodibility index of the sediment yield map of Southern Africa (Rooseboom, 1992). For each catchment the proportions of low, medium and high erodibility were determined and particle sizes representing coarse, medium and fine sediments, associated with each erodibility index. A representative particle size was thus determined.

With the use of computer software the width B , hydraulic radius R , wetted perimeter P and cross-sectional area A were determined at various levels for every cross-section. Using the Chezy resistance equation, the channel slope S and assuming an absolute roughness k_s of 1 m, which was estimated to be representative of field conditions for alluvial rivers during floods (Le Grange, 1994), the discharge corresponding to each level was calculated:

$$Q = 18 \log \left(\frac{12R}{k_s} \right) \sqrt{RS} A \dots\dots\dots 3.3.12$$

For the 1:2-, 1:5-, 1:10- and 1:20-year peak discharge the following hydraulic parameters were determined: top width, average depth, hydraulic radius and velocity. The peak discharges with return periods greater than 20 years were not used because these probably do not occur frequently enough to determine the equilibrium channel

morphology. They might be able to radically change the channel morphology, but the channel will not remain in that form for long. The smaller floods that occur more frequently will modify the changes brought about by the larger floods.

Of the 295 cross-sections that were originally selected, some 50 cross-sections, depending on the return period, were discarded for the following reasons:

- Above a certain level the cross-sections exhibit one or two secondary channels besides the main channel (**Figure 3.3.1**). Below level A there is no problem and the cross-section can be used for the analysis. Above level A however the problem is that it isn't known whether the water first fills the main channel and then overflows into the side channels (level C), or if at some point upstream the river temporarily splits into two channels and the water therefore runs in both of these channels at that particular cross-section (level B). The two scenarios are hydraulically very different. Therefore all the data for a cross-section was discarded once the water level rose above level A. However once the water level rose above level D the data were again included because at that stage the water flows in a single channel again.
- Data were also discarded for cross-sections where the water just reached the stage where it overflows onto the floodplain. The floodplain is a different system from the river channel, and our interest lies in the river channel geometry.

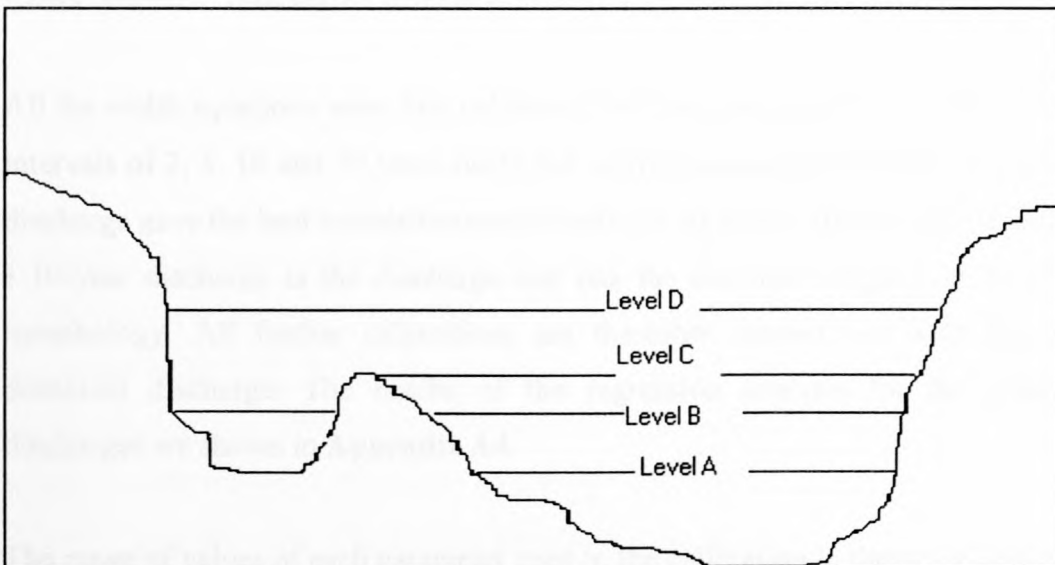


Figure 3.3.1: Cross-sectional levels

The results from the remaining cross-sections for each reach were used to determine an average width, depth, hydraulic radius and velocity for that reach, leaving 59 data sets to work with for each of the four peak discharges.

3.3.2.2 Calibration

In order to calibrate **Equations 3.3.9** and **3.3.10** all the pertinent values were first log-transformed and the coefficients and exponents derived by linear regression analysis. All the regression values were then de-transformed to obtain the final calibrated equations. In addition to **Equations 3.3.9** and **3.3.10** the following relationships were also tested to determine the relative importance of each of the three independent parameters (water discharge Q , channel slope S and particle size represented by d_{50}):

$$B = C_b Q^\alpha \dots\dots\dots 3.3.13$$

$$B = C_b Q^\alpha S^\beta \dots\dots\dots 3.3.14$$

$$B = C_b Q^\alpha S^\beta d_{50}^\gamma \dots\dots\dots 3.3.9$$

$$D = C_d Q^\alpha \dots\dots\dots 3.3.15$$

$$D = C_d Q^\alpha S^\beta \dots\dots\dots 3.3.16$$

$$D = C_d Q^\alpha S^\beta d_{50}^\gamma \dots\dots\dots 3.3.10$$

where B (m), D (m), Q (m^3/s), S (m/m), d_{50} (m)

All the width equations were first calibrated for four peak discharges with recurrence intervals of 2, 5, 10 and 20 years using the corresponding top widths. The 1:10-year discharge gave the best correlation coefficients for all cases. This would mean that the 1:10-year discharge is the discharge that has the dominant impact on the channel morphology. All further calibrations are therefore carried out with Q_{10} as the dominant discharge. The results of the regression analysis for the other peak discharges are shown in **Appendix A4**.

The range of values of each parameter used in the calibration is shown in **Table 3.3.1**, while the results of the regression analysis are shown in **Table 3.3.2**.

Table 3.3.1: Variability of channel parameters

| Parameter | Range |
|--|-------------------|
| Discharge Q_{10} (m ³ /s) | 68 – 5200 |
| Width B (m) | 22 – 351 |
| Average Depth D (m) | 0.51 – 5.90 |
| Hydraulic Radius R (m) | 0.49 – 6.40 |
| Slope S | 0.00015 – 0.07198 |
| d_{50} (mm) | 0.005 – 0.5 |

Table 3.3.2: Results of regression analysis

| Dependent Variable | Equation | C_b/C_d | α | β | γ | r^2 |
|--------------------|----------|-----------|----------|---------|----------|-------|
| B | 3.3.13 | 4.417 | 0.485 | - | - | 0.51 |
| B | 3.3.14 | 2.488 | 0.357 | -0.230 | - | 0.66 |
| B | 3.3.9 | 4.034 | 0.365 | -0.228 | 0.053 | 0.67 |
| D | 3.3.15 | 0.125 | 0.462 | - | - | 0.72 |
| D | 3.3.16 | 0.085 | 0.377 | -0.153 | - | 0.82 |
| D | 3.3.10 | 0.071 | 0.374 | -0.154 | -0.020 | 0.82 |

The new regime equations are thus:

$$B = 4.034Q_{10}^{0.365} S^{-0.228} d_{50}^{0.053} \dots\dots\dots 3.3.17$$

$$D = 0.071Q_{10}^{0.374} S^{-0.154} d_{50}^{-0.02} \dots\dots\dots 3.3.18$$

It should be remembered that **Equations 3.3.17** and **3.3.18** only predict the average width and depth, whereas these two variables can vary considerably from one section to another on a river. For the rivers under consideration, it was found that on average the widths could be 30% larger or smaller than the average width over a certain river reach. This means that a river with an average width of 100 m is likely to be between 70 and 130 m wide. For the depths a slightly smaller variation of 20% was found.

From **Table 3.3.2** it can be seen that all the depth equations have better correlation coefficients than the width equations. This is probably due to the fact that not all the factors influencing the width are included in the analysis. Although the water discharge is the major controlling factor for widths, bank material and type and amount of vegetation on the banks also determine the width. The depth on the other hand seems to be more adequately related to the three chosen parameters. The correlations of **Equations 3.3.9** and **3.3.10** are shown in **Figures 3.3.2** and **3.3.3**. The lowest correlation coefficients for both the depth and width relationships occur when the discharge is the only independent variable. Looking at the results of the regression analysis for **Equation 3.3.13** however, it can be seen that the exponent is very close to 0.5, which is in agreement with traditional regime relationships. The inclusion of the channel slope improves the relationship, while the inclusion of the particle size has very little impact on the correlation as well as on the exponents. The magnitude of the exponents gives an indication of the relative importance of the three independent variables. As already mentioned the discharge is the most influential parameter and the channel slope is also relatively important, but the particle size seems to have very little effect on both the width and depth.

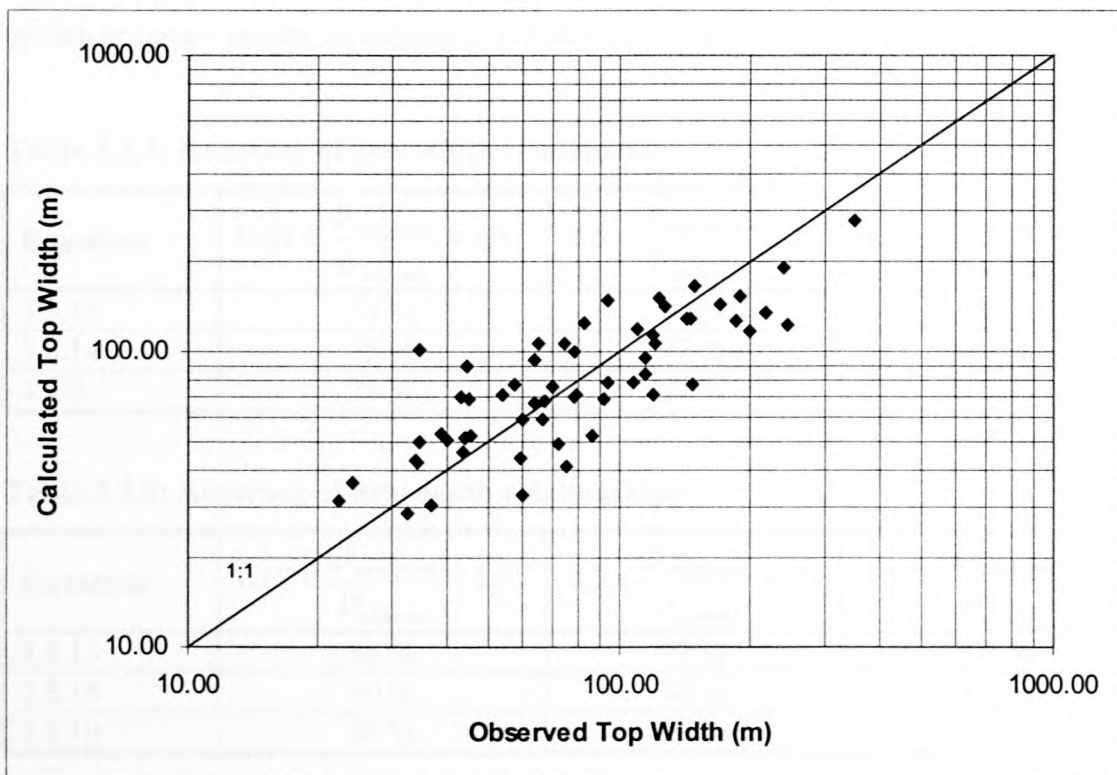


Figure 3.3.2: Calibration of South African regime width equation

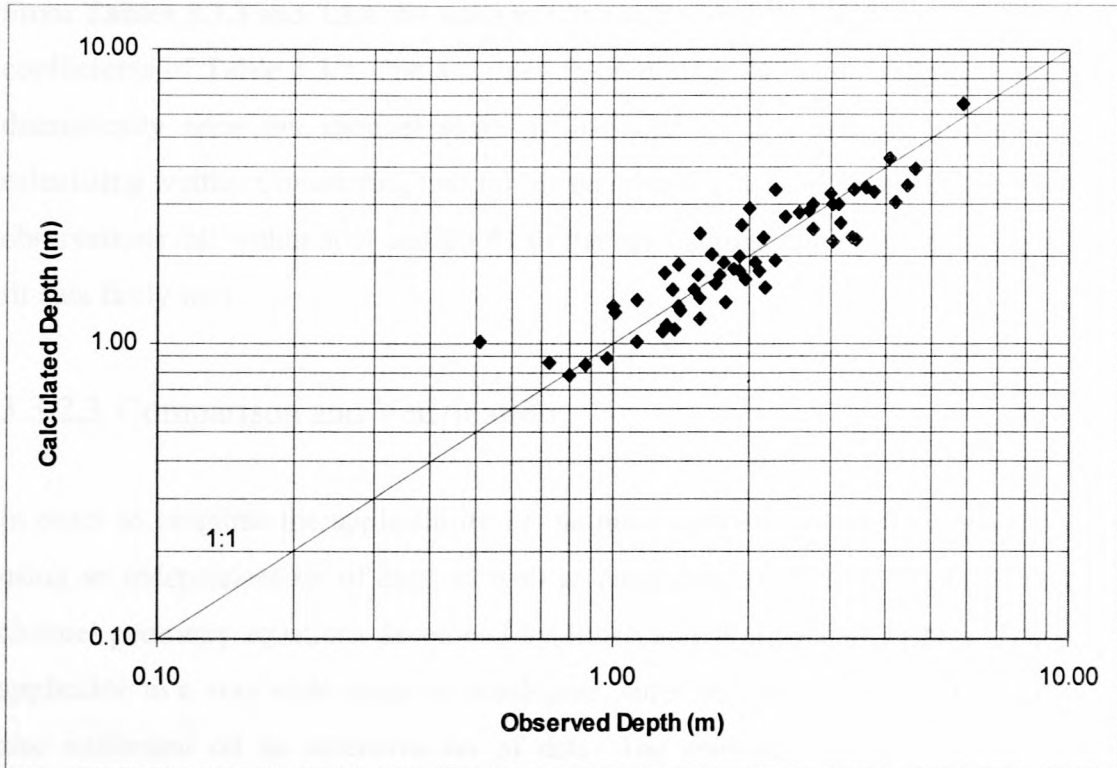


Figure 3.3.3: Calibration of South African regime depth equation

In addition to the correlation coefficient it is sometimes useful to express the accuracy of the relationships in terms of their ability to predict the width and depth within certain accuracy ranges, as indicated in **Tables 3.3.3** and **3.3.4**.

Table 3.3.3: Accuracy of new width relationships

| Equation | $0.67 < \frac{B_{calculated}}{B_{observed}} < 1.5$ | $0.5 < \frac{B_{calculated}}{B_{observed}} < 2$ | $0.33 < \frac{B_{calculated}}{B_{observed}} < 3$ |
|----------|--|---|--|
| 3.3.13 | 57 % | 92 % | 98 % |
| 3.3.14 | 75 % | 97 % | 100 % |
| 3.3.9 | 75 % | 97 % | 100 % |

Table 3.3.4: Accuracy of new depth relationships

| Equation | $0.67 < \frac{D_{calculated}}{D_{observed}} < 1.5$ | $0.5 < \frac{D_{calculated}}{D_{observed}} < 2$ | $0.33 < \frac{D_{calculated}}{D_{observed}} < 3$ |
|----------|--|---|--|
| 3.3.15 | 85 % | 97 % | 100 % |
| 3.3.16 | 90 % | 98 % | 100 % |
| 3.3.10 | 90 % | 98 % | 100 % |

From **Tables 3.3.3** and **3.3.4** the same trends can be observed as from the correlation coefficients of **Table 3.3.2**. The accuracy in predicting the width and depth improve dramatically once the channel slope is included in the analysis, especially for calculating widths. Considering that for all except one equation, more than 95% of the observations fall within 50% and 200% of the calculations, the new regime equations fit data fairly well.

3.3.2.3 Comparison and Verification

In order to establish the applicability of the new regime equations they are verified using an independent set of data, as well as comparing them to the semi-theoretical channel geometry equations developed by Julien and Wargadalam (1995). These are applicable to a very wide range of conditions, since they are theoretically based and also calibrated on an extensive set of data. The semi-theoretical relations are as follows:

$$B = 1.33Q^{(2+4m)/(5+6m)} d_{50}^{-4m/(5+6m)} S^{-(1+2m)/(5+6m)} \dots\dots\dots 3.3.19$$

$$D = 0.2Q^{2/(5+6m)} d_{50}^{6m/(5+6m)} S^{-1/(5+6m)} \dots\dots\dots 3.3.20$$

where $m = \frac{1}{\ln\left(\frac{12.2D}{d_{50}}\right)} \dots\dots\dots 3.3.21$

The same data set used for the calibration of the new regime equations is first used to determine the exponents of **Equations 3.3.19** and **3.3.20**, then both widths and depths are determined from these equations and the results are compared to the original data as well as values computed from **Equations 3.3.17** and **3.3.18**.

The first point that became obvious was that the exponents of **Equations 3.3.19** and **3.3.20** vary very little for this particular data set. The ranges of coefficients are shown in **Table 3.3.5**, with α , β and γ indicating the exponent of discharge, particle size and slope, respectively, for the width and depth equations.

Table 3.3.5: Ranges of exponents

| | | α | β | γ |
|-------|---------|----------|---------|----------|
| Width | Minimum | 0.419 | -0.072 | -0.214 |
| | Maximum | 0.429 | -0.047 | -0.209 |
| | Average | 0.423 | -0.057 | -0.211 |
| Depth | Minimum | 0.357 | 0.07 | -0.214 |
| | Maximum | 0.372 | 0.107 | -0.181 |
| | Average | 0.366 | 0.086 | -0.211 |

Using the average values does not compromise the accuracy of the equations, but it makes it easier to compare the equations with the newly developed South African regime equations. Substituting the average coefficients into **Equations 3.3.19** and **3.3.20** yields the following:

$$B = 1.33Q^{0.423} d_{50}^{-0.057} S^{-0.211} \dots\dots\dots 3.3.22$$

$$D = 0.2Q^{0.366} d_{50}^{0.086} S^{-0.211} \dots\dots\dots 3.3.23$$

These two equations are very similar to the regime equations developed in this study and the computed values are very close as shown in **Figure 3.3.4** and **3.3.5**, although **Equations 3.3.22** and **3.3.23** seem to overestimate both the width and depth slightly. The fact that the semi-theoretical channel geometry equations by Julien and Wargadalam (1995) and the new regime equations of this study produce very similar results and also have similar accuracy ranges, give **Equations 3.3.17** and **3.3.18** a sound basis.

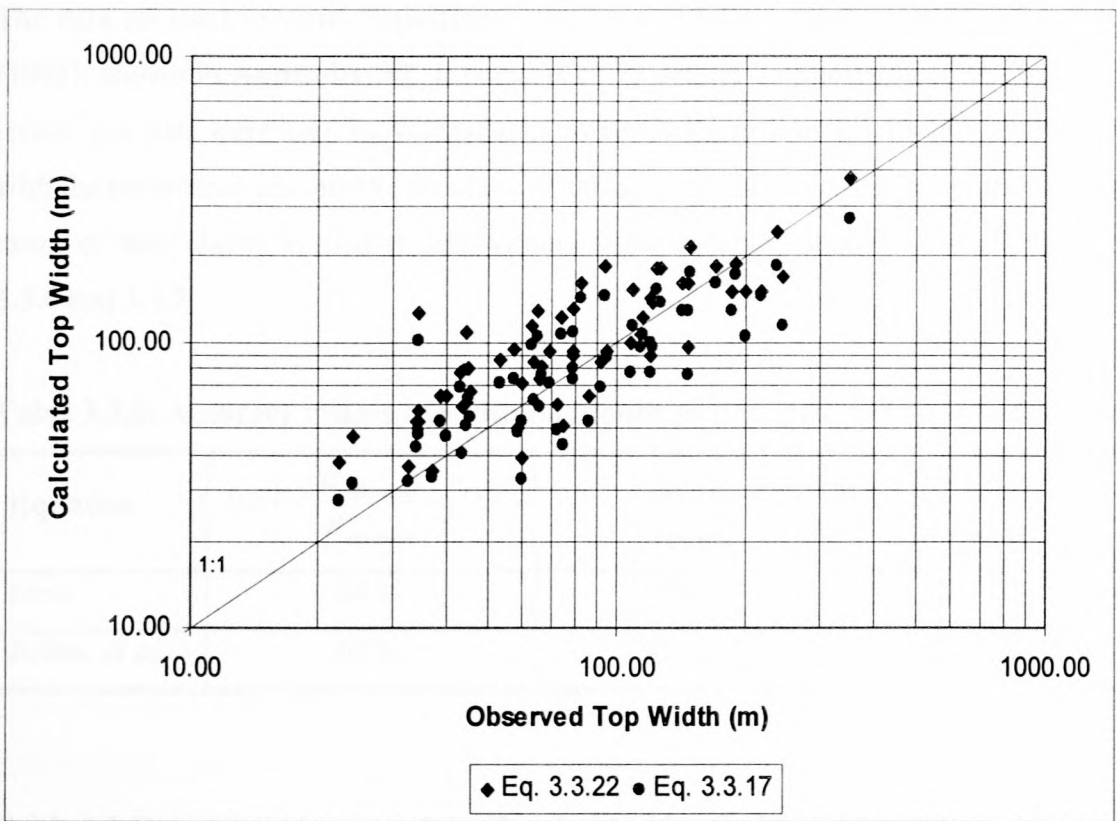


Figure 3.3.4: Comparison of existing and new width equations

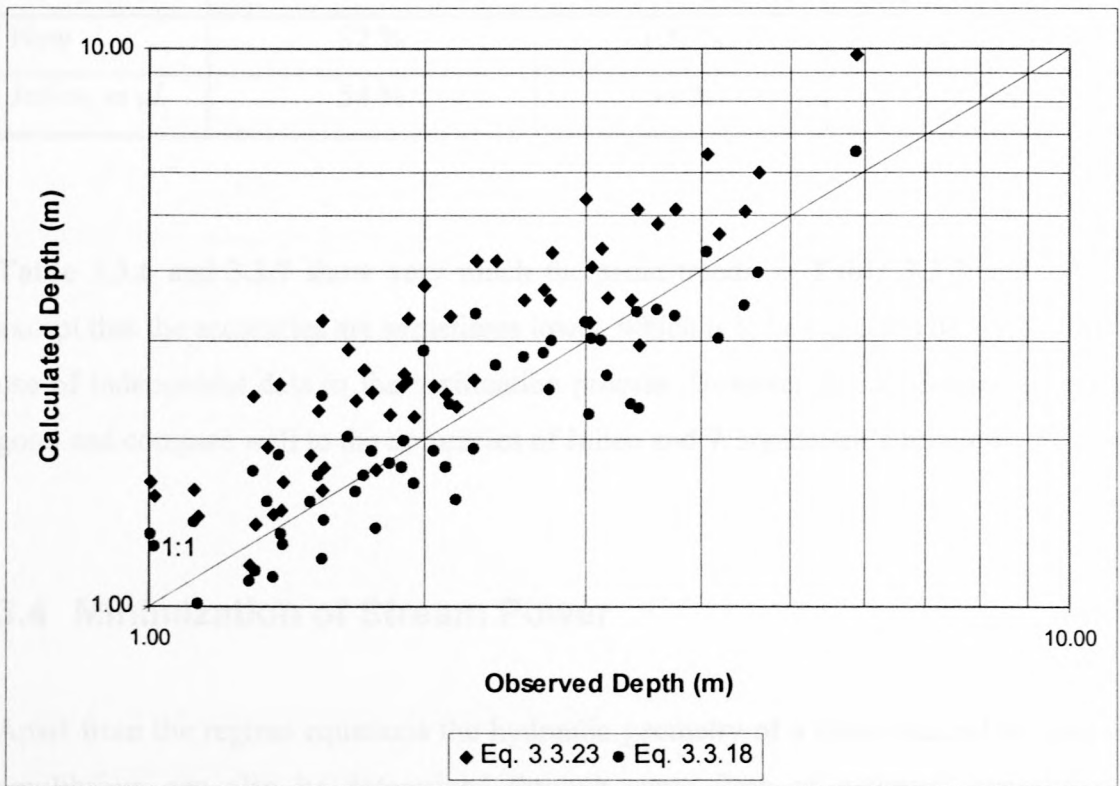


Figure 3.3.5: Comparison of existing and new depth equations

The data set used to verify **Equations 3.3.17** and **3.3.18** is taken from Wargadalam (1993), shown in **Appendix A2**. It consists of 28 sets of data from various sand bed rivers. The data were used by Wargadalam to verify **Equations 3.3.19** and **3.3.20**. As with the calibration process the accuracy of the new regime equations are expressed in terms of their ability to predict data within certain accuracy ranges, shown in **Table 3.3.6** and **3.3.7**.

Table 3.3.6: Accuracy ranges of width relationships (independent river data)

| Equation | $0.67 < \frac{B_{calculated}}{B_{observed}} < 1.5$ | $0.5 < \frac{B_{calculated}}{B_{observed}} < 2$ | $0.33 < \frac{B_{calculated}}{B_{observed}} < 3$ |
|-----------------------|--|---|--|
| New | 64 % | 79 % | 96 % |
| Julien, <i>et al.</i> | 61 % | 89 % | 100 % |

Table 3.3.7: Accuracy ranges of depth relationships (independent river data)

| Equation | $0.67 < \frac{D_{calculated}}{D_{observed}} < 1.5$ | $0.5 < \frac{D_{calculated}}{D_{observed}} < 2$ | $0.33 < \frac{D_{calculated}}{D_{observed}} < 3$ |
|-----------------------|--|---|--|
| New | 82 % | 100 % | 100 % |
| Julien, <i>et al.</i> | 54 % | 93 % | 100 % |

Table 3.3.6 and **3.3.7** show very much the same trends as **Table 3.3.3** and **3.3.4**, except that the accuracies are sometimes lower, which is to be expected because of the use of independent data in the verification process. However the accuracies are still good and compare well to the accuracies of Julien and Wargadalam's relations.

3.4 Minimization of Stream Power

Apart from the regime equations the hydraulic geometry of a river channel in quasi-equilibrium can also be determined through some form of extremal hypothesis, involving the maximization or minimization of one parameter. This hypothesis

usually forms part of a set of equations, with the others being the sediment transport capacity and flow resistance.

3.4.1 Theory and Application

Given a flow resistance equation and a sediment discharge equation, Chang (1979) proposed the hypothesis of minimum stream power as the third required relation. He stated that an alluvial channel with a given water discharge Q and sediment load Q_s will establish its width, depth and slope such that the stream power is a minimum. The input stream power per unit channel length is given by $\rho g Q S$. Since Q is a given parameter, minimum $\rho g Q S$ means minimum channel slope S . This concept of minimum stream power is similar to the concept of minimum unit stream power proposed by Yang (1973), which also implies maximum sediment transport.

Chang (1988) used the flow resistance formula by Lacey and the DuBoys bed load formula in conjunction with the minimization of stream power to develop a design procedure for stable alluvial canals, approximating the channel shape as a trapezoid with bank slope z . He also stated that the procedure is not limited to Lacey's and DuBoys' formulas, but that both can be replaced by any other valid formulas. In this study Chezy's flow resistance formula (3.4.1) is used as well as Engelund and Hansen's total load formula (3.4.2).

$$v = 18 \log \left(\frac{12R}{k_s} \right) \sqrt{RS} \dots\dots\dots 3.4.1$$

$$Q_s = \frac{v^2}{20gDS} \sqrt{\frac{(\rho_s - \rho)gd^3}{\rho}} \left(\frac{\rho DS}{(\rho_s - \rho)d} \right)^{5/2} \dots\dots\dots 3.4.2$$

where Q_s = the total sediment discharge (m^3/s)

v = flow velocity (m/s)

D = flow depth (m)

S = slope

ρ_s, ρ = sediment and water density, respectively (kg/m^3)

d = sediment particle size (m)

The basic procedure is outlined below as well as in **Figure 3.4.1** (Chang, 1988):

- Select a set of independent variables Q, Q_s, d, z as input variables.
- Assume a set of incremental widths B and for each width assume a depth D . Compute the slope from the sediment transport formula and the velocity from the flow resistance formula. In order to calculate the slope it is more convenient to rewrite Engelund and Hansen's transport formula to express the slope in terms of the specified variables, and also incorporate the resistance equation since the transport formula is also defined in terms of the velocity.

$$S = \left(\frac{20Q_s d \sqrt{g} (\rho_s - \rho)^2}{R^{5/2} \rho^2 \left(18 \log \left(\frac{12R}{k_s} \right) \right)^2} \right)^{2/5} \dots\dots\dots 3.4.3$$

Calculate the discharge and compare it to the input discharge. Change the depth and repeat the procedure until the input discharge and the calculated discharge are equal, then go to the next width.

- The stable width and depth correspond to the minimum slope computed.

3.4.2 Discussion

Chang (1988), using the procedure set out above, explained the variation of stream power expenditure with channel width as follows. The stream power $\rho g Q S$ or slope S attains a minimum under certain counteractive forces. Starting with a large width, where the bank effect is small the channel slope decreases with decreasing width because the flow is more concentrated in a smaller channel and therefore the transport efficiency increases. This means that Q and Q_s are transported at lower power expenditure. The surface areas of the channel banks contribute relatively little to bed

load transport so that when the channel width decreases so does the effective (bottom) width for bed load transport, meaning that the bank effect increases. Consequently the channel slope has to become steeper at some point to transport the given discharge and sediment load, and the power expenditure increases. When the two opposing forces are balanced the channel attains a stable width when the channel slope is a minimum.

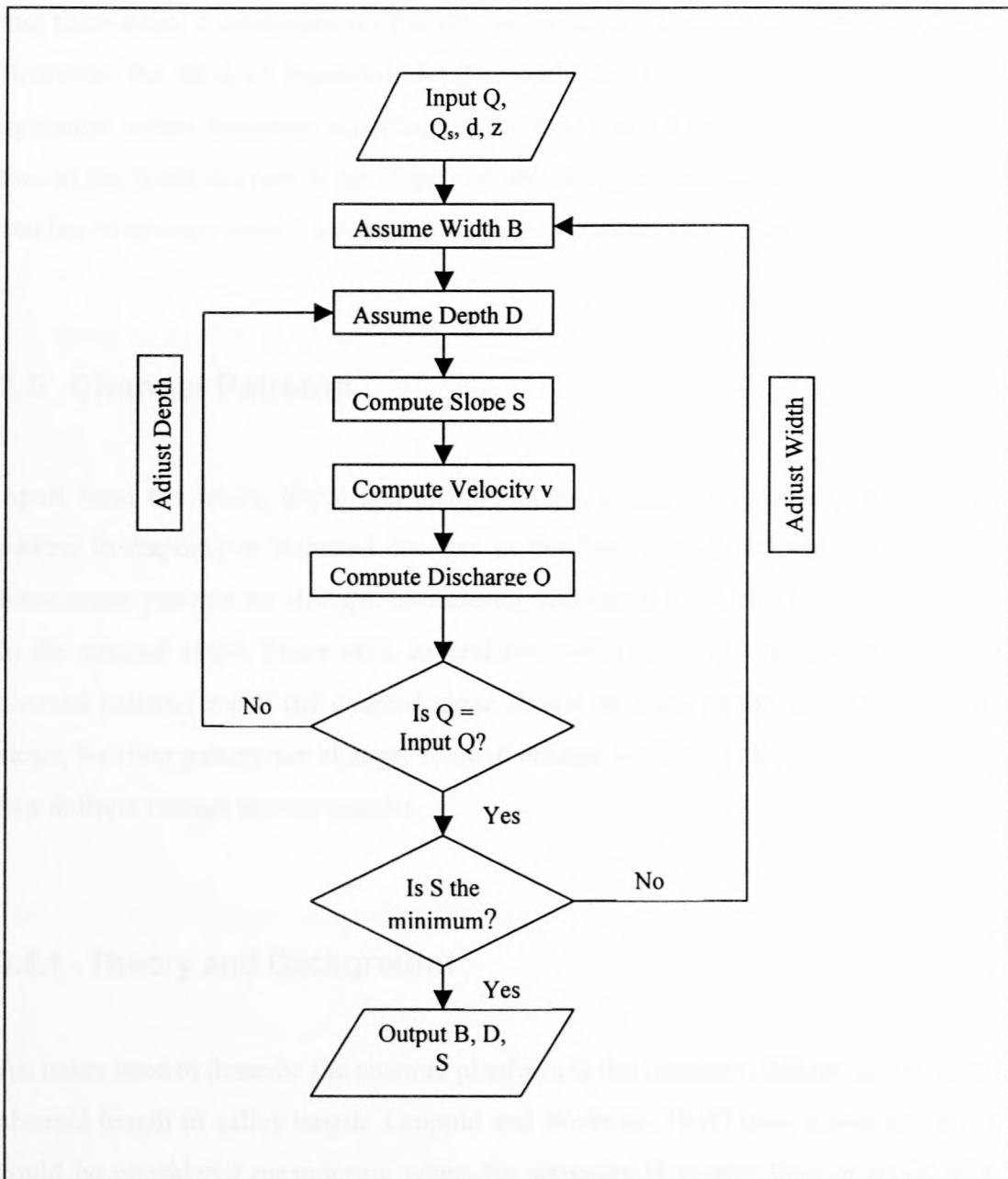


Figure 3.4.1: Flow chart showing major steps of calculation (Chang, 1979)

Chang (1988) and Brandt (1998) have successfully applied the procedure outlined in **Section 3.4.1**, both using Lacey's resistance formula and DuBoys' bed load formula. In this study Engelund and Hansen's transport formula was used, but this did not produce a minimum slope. The problem can be explained by looking at the variables used in **Equation 3.4.4**. Given Q_s , d , ρ_s , ρ and k_s , the only remaining variable is the hydraulic radius R . It was found that starting with a large width and decreasing the width in steps would result in an increase in the hydraulic radius. This could mean that there exists a combination of width and depth for which the slope is a minimum. However, the form of **Equation 3.4.3** is such that as the width decreases and the hydraulic radius increases accordingly, the slope will always decrease. This means that as the width decreases the slope can only decrease accordingly. This shows that one has to be very careful when deciding which transport formulas to use.

3.5 Channel Patterns

Apart from the width, depth and channel slope, a river can also adjust its channel pattern in response to imposed changes in the flow regime and sediment load. The three major patterns are straight, meandering and braided, which are very much linked to the channel slope. There exist several thresholds or discontinuities between these channel patterns and if the channel slope should be close to the critical or threshold slope, the river pattern can change. A small change in channel slope can therefore lead to a definite change in river pattern.

3.5.1 Theory and Background

An index used to describe the channel planform is the sinuosity, defined as the ratio of channel length to valley length. Leopold and Wolman (1957) have stated that a reach could be considered meandering when the sinuosity is greater than or equal to 1.5. The value is arbitrary, but they argued that a sinuosity of 1.5 indicates a truly meandering river. Chang (1988) as well as other researchers have adopted that value.

The channel patterns and their relationships with the channel slope can therefore be identified as follows:

- Truly straight rivers (sinuosity < 1.1), rarely occurring in nature and are usually artificially maintained.
- Straight rivers (sinuosity < 1.5) generally occur on flat slopes with small width/depth ratios and low velocities. Although a river may have a relatively straight alignment the thalweg usually has a distinct meandering pattern.
- On steeper slopes the river becomes meandering (sinuosity > 1.5) and the width/depth ratio increases, as does the velocity.
- On even steeper slopes the sinuosity generally decreases and the river becomes braided, in conjunction with an even higher width/depth ratio.

Several researchers have identified thresholds between different channel patterns, but they differ somewhat from one study to another, which is a result of the different data sets being used as well as the difference in the definitions of the various channel patterns.

The discharge-slope relation developed by Leopold and Wolman (1957) separates meandering and steeper braided streams:

$$S = 0.0125Q^{-0.44} \dots\dots\dots 3.5.1$$

where Q is the bankfull discharge in m³/s.

The following meandering-braided threshold has been developed by Begin (cited in Carson, 1984):

$$S = 0.0016Q^{-0.33} \dots\dots\dots 3.5.2$$

Carson (1984) pointed out the importance of including the sediment particle size in the relationship, since streams with gravel beds must plot higher on a Q-S diagram than sand bed rivers, simply because it requires more power to transport gravel than

sand. Henderson (cited in Chang, 1988) obtained the following equation for gravel-bed rivers:

$$S = 0.0002d_{50}^{1.15} Q^{-0.46} \dots\dots\dots 3.5.3$$

3.5.2 Development of a Discharge - Slope Relationship for South African Rivers

As mentioned in Section 3.5.1 a small change in channel slope can result in a major change in channel pattern, and it is therefore useful to establish a discharge-slope relationship applicable to South African rivers.

The same set of rivers used for the calibration of the South African regime equations in **Section 3.3** were used to determine the Q-S relationship. Sinuosities for each river were determined from 1:50 000 topographical maps (see **Appendix A3**). Each section was chosen to be representative of the river reach under consideration, by disregarding for instances reaches that were obviously prevented from developing normally either by natural controls such as rock formations or manmade controls. The sinuosities were then plotted (as labels) together with the corresponding 1:10-year discharges and slopes as shown in **Figure 3.5.1**.

The fact that a meandering river is defined as having a sinuosity of greater than 1.5 is mentioned in **Section 3.5.1** and braided rivers generally occur on slopes steeper than those of meandering rivers. The position of the threshold separating meandering and braided rivers would therefore be expected to be found in the upper region of **Figure 3.5.1** where the sinuosities start decreasing. The data in **Figure 3.5.1** indicate that braided rivers are separated from meandering channels by a line described by the following equation:

$$S = 0.159Q_{10}^{-0.557} \dots\dots\dots 3.5.4$$

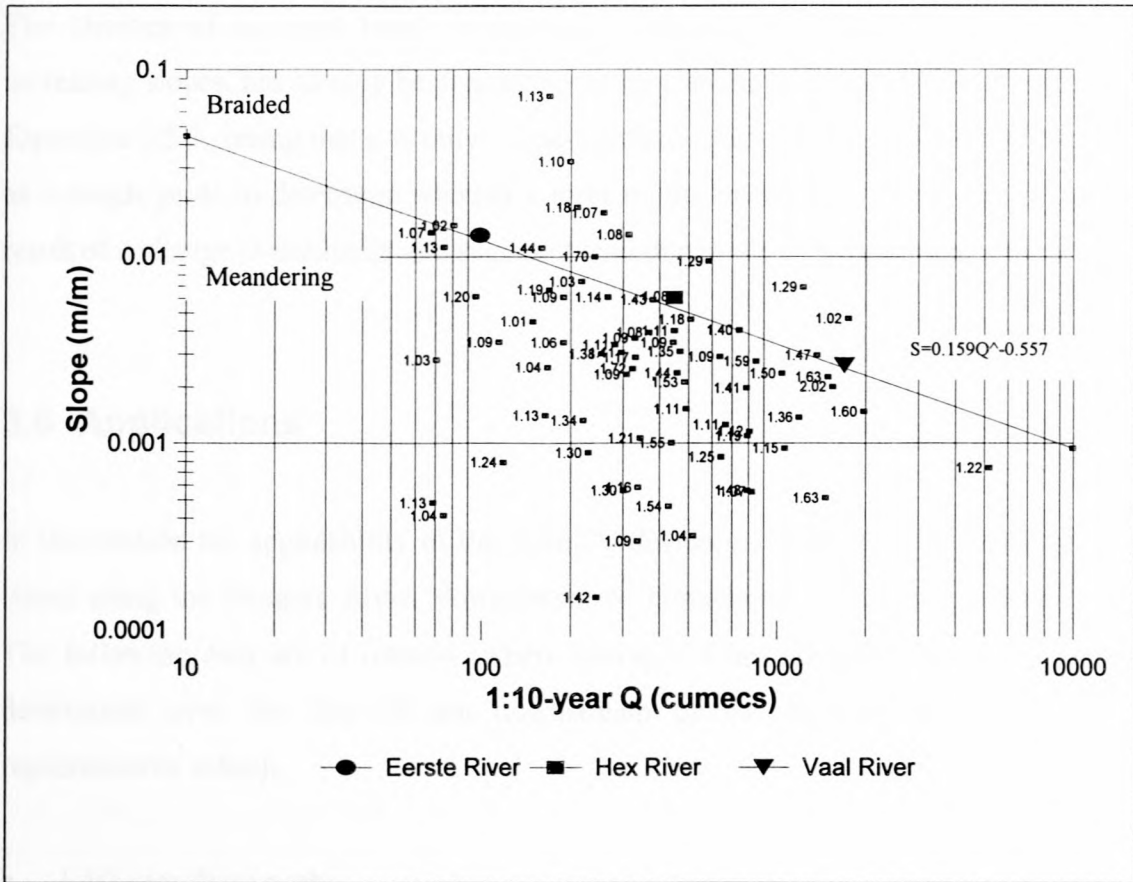


Figure 3.5.1: Threshold line separating meandering and braided rivers

The Eerste River, Hex River and Vaal River data are all shown in **Figure 3.5.1**. All three rivers have braided reaches and plot just above the threshold line.

Several observations can be made from **Figure 3.5.1**:

1. There is only a weak trend of increasing sinuosity with increasing slope for meandering rivers, which makes it impossible to determine a threshold between straight and meandering rivers.
2. No trend could be found for increasing width/depth ratios with increasing slopes or that coarser grained particles plot at higher Q-S combinations than finer particles.
3. There is no indication of different thresholds for different particle sizes as suggested by Carson (1984), but this could be because the particles sizes of the data analysed, all fall into the range of fine to medium sand. The effect of the particles size might only become obvious when a wider range of particle sizes is investigated.

The absence of any real trend of increasing sinuosity or width/depth ratio with increasing slopes, has already been pointed out by Carson (1984) amongst others, and **Equation 3.5.3**, seeing that it is only a best-fit relationship, should really only be used as a rough guide to determine whether a river might change its channel pattern as a result of a change in discharge and sediment load due to the construction of a dam.

3.6 Applications

In this section the applicability of the methods developed in the previous sections is tested using the Pongola River, downstream of Pongolapoort Dam, as an example. The following data are of interest (where average values are mentioned they were determined over the first 20 km downstream of the dam in order to get a representative value):

- 1:10-year flood peak:

Both flood peaks (before and after the dam was built) were determined through statistical methods with data obtained from DWAF. The flood peak determined for the period after the dams was built, was however based on a rather short record of only 16 years.

- Median particle size:

The median particle size for the period before the dam was built was estimated from particle size distribution curves of samples taken upstream of the dam (Kovacs *et al.*, 1985). For the period after the dam was built the average median particle size was determined from samples taken during flood releases at Pongolapoort during 2000.

- Channel slope:

The channel slope before the dam was built was determined from topographical maps and the slope does not seem to have changed appreciably.

- Top width and mean depth:

The width and depth of the river before the dam was built were obtained from surveys by DWAF. For the period after the dam was built the average width was determined from aerial photographs taken in 1996. Only one depth could however be obtained for the period after the dam was built, which was determined from a surveyed cross-section 2 km below the dam (DWAF). The widths before and after the dam's construction are listed in **Appendix C2**.

The 1:10-year flood changed from 1877 m³/s to 759 m³/s when the dam was built and the median particle size changed from 0.19 mm to 1 mm. The channel geometry of the natural river, the impacted river and the predicted values for both are summarised in **Table 3.6.1**. The ranges given in the table give an indication of the natural variability of both the width and depth, as pointed out in **Section 3.3.2.2**.

Table 3.6.1: River channel geometry

| | Natural | | |
|---------------|------------------|--|--|
| | Observed | Calculated (equ. 3.3.17/18) | Calculated (equ. 3.3.22/23) |
| Average width | 148 m | 176 m | 207 m |
| Range (width) | 83 – 343 m | 123 - 229 m | 145 – 269 m |
| Average depth | 4.6 m | 3.8 m | 6.0 m |
| Range (depth) | 3.7 – 5.5 m | 3 – 4.6 m | 4.8 – 7.2 m |
| Slope | 0.0015 | - | - |
| | After Dam | | |
| | Observed | Calculated (equ. 3.3.17/18) | Calculated (equ. 3.3.22/23) |
| Average width | 71 m | 139 m | 129 m |
| Range (width) | 39 – 135 m | 97 – 181 m | 90 – 168 m |
| Average depth | 4.7 m | 2.7 m | 4.9 m |
| Range (depth) | - | 2.2 – 3.2 m | 3.9 – 5.9 m |
| Slope | 0.0015 | - | - |

From the changes in both slope and discharge the channel pattern can also be predicted. From **Figure 3.5.1** it can be seen that the Q-S combinations of both the natural river as well as the altered river will plot below the threshold line, correctly indicating a meandering pattern. Since the Q-S combination of the river after the dam was built plots lower on the chart than the original combination, it is highly unlikely that the river pattern will change drastically except for a slight reduction in sinuosity.

From the **Table 3.6.1** it can be seen that the predicted values for the natural river differ only by about 17% for the regime equations developed in this study, whereas the predicted widths for the altered river differ considerably. The rather small widths observed from aerial photos 23 years after the dam was built could be a result of an almost constant release of $5 \text{ m}^3/\text{s}$ from the dam in recent years. The constant releases could have created favourable conditions for vegetation, which could have encroached onto the river channel thereby reducing the channel width. The Domoina flood of 1984 with a peak inflow of $13\,000 \text{ m}^3/\text{s}$, was almost completely absorbed by the dam, which was almost empty when the flood reached the dam. This means that the river reach below the dam has not experienced any large floods since the dam was built. This could also have contributed to the fact that the river channel has narrowed to such a degree.

The statistical methods used to determine the 1:10-year discharge for the post-dam period might not be applicable here, since the 1:10-year discharge is not very different from the 1:20-year discharge, which is $800 \text{ m}^3/\text{s}$. What has not been considered is the duration of the discharges. Whereas a 1:10-year flood would have maybe lasted one or two days naturally, the releases from the dam occurred over one week or longer, with a very different effect from a duration of only one day. The 1:10-year discharge seems to have lost its meaning in this case.

Evidently the methods available for predicting a stable channel geometry are not very precise because they do not take into consideration all the factors that determine the channel geometry. Considering however that it is almost impossible to account for all these factors and often very little information is available, the methods outlined in this chapter are still very valuable for natural rivers. In the case of a river affected by a dam these regime equations may be useful if the releases from the dam do not differ

drastically from the natural flow pattern. The regime equations with the 1:10-year discharge as dominant discharge are, however, not applicable to rivers where the flow pattern has drastically changed. In order to determine the morphological changes a river undergoes when affected by a dam, more detailed analyses are necessary.

especially if the dam has drastically altered the flow regime. The analysis should take aspects than just the 1:10-year discharge regime, which is the dominant discharge. In determining the channel geometry, although the cross-sections are important, the longitudinal profile is an important aspect. The sediment transport characteristics of the river, i.e. cohesive or non-cohesive, silt or clay content, etc., should also be taken into account, as they have a large effect on the river morphology. The sediment transport characteristics should be taken into consideration, except for the sediment size, which is not dealt with in the first two aspects mentioned above. The sediment transport characteristics of non-cohesive sediment transport has been researched extensively, but there is still a need to gain more knowledge of the initiation of motion and the sediment transport of cohesive sediments. The erosion and deposition of cohesive sediments is significantly different from those of non-cohesive sediments, and the presence of a small percentage of clay or silt in the material can drastically alter the transport characteristics of the sediment (Panagiotopoulos *et al.*, 1997). Many studies have shown that the fraction of cohesive material, and a dam can cause the erosion to decrease, resulting in a lowering of the flood peaks, which are not able to transport or excavate sediment from downstream tributaries, causing deposition of even fine sediments.

The theory of critical conditions for the entrainment of cohesive sediments has been investigated in detail in this chapter. A cohesive sediment transport theory has been developed, calibrated and verified with laboratory and field data.

4.1 Cohesive Sediment Transport Processes

Cohesive sediments are essentially mixtures containing silt and clay that possess various degrees of cohesion. The particles are small enough so that the surface physical-chemical forces become much more important than their weight, which is the determining factor in the erosion of non-cohesive sediments (Partinides, 1971).

4. Sediment Transport

It was shown in **Section 3.6** that regime equations alone are not adequate for the prediction of the changes in channel morphology after a dam has been built, especially if the dam has drastically altered the flow in the river. The fact is that other aspects than just the 1:10-year discharge, channel slope and particle size, play a role in determining the channel geometry, although they certainly are some of the most important aspects. The sediment transport capacity of a river, the type of sediment in a river, i.e. cohesive or non-cohesive, sediment grading and riparian vegetation all may have a large effect on the river morphology. The regime equations do not take these factors into consideration, except for the sediment size, which makes it necessary to deal with the first two aspects mentioned above in more detail. While the theory of non-cohesive sediment transport has been researched extensively, it is necessary to gain more knowledge of the initiation of motion and the sediment transport of cohesive sediments. The erosion and deposition of cohesive sediments differ significantly from those of non-cohesive sediments, and the presence of even small percentages of clay or silt in the riverbed can drastically alter the transport behaviour of the sediment (Panagiotopoulos *et al.*, 1997). Many sand-bed rivers contain some fraction of cohesive material, and a dam can cause that fraction to increase through lowering of the flood peaks, which are not able to transport the incoming sediments from downstream tributaries, causing deposition of even fine sediments.

The theory of critical conditions for the entrainment of cohesive sediments is investigated in detail in this chapter. A cohesive sediment transport theory is also developed, calibrated and verified with laboratory and field data.

4.1 Cohesive Sediment Transport Processes

Cohesive sediments are essentially mixtures containing silt and clay that possess various degrees of cohesion. The particles are small enough so that the surface physical-chemical forces become much more important than their weight, which is the determining factor in the erosion of non-cohesive sediments (Partheniades, 1971).

Depending on the physical and chemical properties of the water and the composition of the fine sediments the net effect of the interparticle forces can be repulsion or attraction, where the fine particles tend to cling to each other and to form flocs. These flocs or aggregates have much greater sizes and settling velocities than the individual particles. The growth of these aggregates is determined by the concentration, physical-chemical properties of the water-sediment mixture, as well as the flow conditions. At some stage, generally at concentrations greater than 10 000 mg/ℓ (Mehta *et al.*, 1989), the aggregates will become too big and will start to hinder each other and the settling velocity decreases rapidly. However, flocculation will probably not occur during turbulent flow and sediment transport conditions experienced in South Africa (Basson and Rooseboom, 1996) and therefore settling velocities for individual particles were used in this study. The behaviour of cohesive sediments can also be modified by the properties of the fluid (temperature, salinity) or the clay properties themselves (clay type, organic content).

4.1.1 Sand and Clay Mixtures

The presence of clay in the sediment in the bed can dramatically alter the behaviour of the sediment, depending mainly on the amount of clay present. Approximately 5 – 10% of clay minerals, by dry weight, are considered sufficient to control the soil properties (Panagiotopoulos *et al.*, 1997). With increasing clay content the sediment deposits become more plastic and swelling, shrinkage and compressibility increase. The result is that the resistance to erosion generally increases as the clay content increases, although some researchers have found that the resistance to erosion can increase with increasing sand content (Panagiotopoulos *et al.*, 1997).

Panagiotopoulos *et al.* (1997) have carried out experiments to determine the influence of clay on the erosion threshold of sand beds. They found that with clay contents less than approximately 11%, the increase in the critical threshold conditions with increasing clay content is smaller than for clay contents larger than 11%, and that the sediment mixtures with high clay contents are more difficult to erode. These observations prove again that clay contents of about 10% are enough to limit sediment

erosion. Panagiotopoulos *et al.* (1997) have argued that at clay contents less than 10% the sand particles are still close enough to be in contact with each other and so pivoting is the main mechanism for the initiation of sediment motion (**Figure 4.1.1**). At higher clay contents, however, the clay particles fill the voids between the sand particles, which are no longer in contact with each other. The pivoting mechanism is not the dominant mechanism any longer, but the erosion is instead controlled by the resistance of the clay fraction.

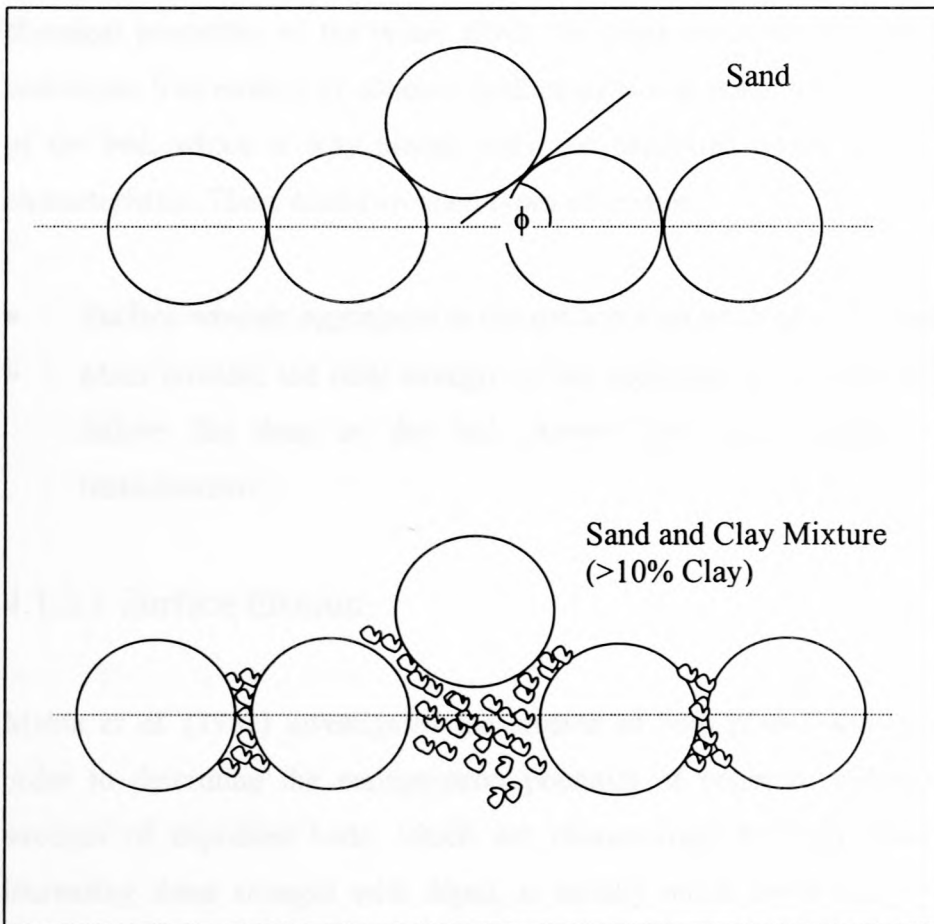


Figure 4.1.1: Mechanism for initiation of motion (adapted from Panagiotopoulos *et al.*, 1997)

Experiments carried out by Torfs *et al.* (1994) have shown results very similar to those of Panagiotopoulos *et al.* (1997), although they also observed a transition zone between cohesive and non-cohesive behaviour. Sediment mixtures with less than 7% fines (clay and silt) behaved as non-cohesive sediments, forming ripples and dunes. The fine particles were washed out from the top layer leaving the sand behind. Sediments with higher contents of fines behaved as cohesive sediments. No bedforms

were observed and very high shear stresses were needed to start erosion. For fines contents ranging between 7 and 13%, a transitional behaviour pattern was observed, exhibiting irregular bedforms.

4.1.2 Erosion

The amount and type of clay minerals, the clay properties and the physical and chemical properties of the water affect the shear stress required to erode cohesive sediments. The erosion of cohesive sediments is also dependent on the shear strength of the bed, which is why placed beds and deposited beds have different erosion characteristics. There exist two main types of erosion:

- Surface erosion: aggregates in the surface layer are broken up and entrained.
- Mass erosion: the bulk strength of the sediment is exceeded and the plane of failure lies deep in the bed. Above that plane resuspension is almost instantaneous.

4.1.2.1 Surface Erosion

Mehta *et al.* (1982) investigated the erosion of both placed and deposited beds in order to determine the resuspension potential of cohesive sediments. The shear strength of deposited beds, which are characterised by high water contents and increasing shear strength with depth, is usually much lower than for placed beds. Placed beds have a much more uniform variation of shear strength with depth and also lower water contents. The rate of surface erosion of these beds becomes nearly constant with time unlike the rate of erosion of deposited beds, which tends to become zero after a while. Parchure and Mehta (1985) have argued that in the latter case the eroded bed has reached a layer with critical shear strength equal to the applied bed shear stress. Partheniades and Paaswell (1970) reported that the ratio of strengths of the remoulded to the deposited bed was about 100:1. However, the minimum scouring shear stress was about the same for both beds. They concluded that the shear strength is not the only factor governing erosion.

4.1.2.2 Mass Erosion

Although many researchers have investigated the erosion of cohesive materials, because of the complexity of the problem many arbitrary and subjective criteria were established (Kamphuis and Hall, 1983). The critical shear stresses obtained from these studies vary greatly, with results ranging between 11.5 – 72 Pa for one study. The large variation is a result of experimental error, variation in experimental procedure, simplistic interpretation of sediment properties, and the use of different criteria for defining the onset of erosion. Kamphuis and Hall (1983) found that the critical shear stress is dependent on the amount and type of clay, water content, pH and temperature of the fluid, and the chemical composition of the pore fluid and eroding fluid.

Kamphuis and Hall (1983) conducted experiments to determine the onset of erosion of consolidated clays, investigating the effect of different consolidation pressures and clay contents. They found a linear relationship between critical shear stress and compressive strength as well as vane shear strength. The resistance to erosion increases with increasing clay content and consolidation pressure.

Basson and Rooseboom (1996) have argued that a more appropriate approach would be to use the applied stream power at the bed $\left(\tau \frac{dv}{dy}\right)_0$ instead of the critical shear stress at the bed to describe the critical conditions for erosion. It also takes the effect of increasing or decreasing roughness into account through the inclusion of the variable k_s :

$$\left(\tau \frac{dv}{dy}\right)_0 = \frac{30 \rho g D S \sqrt{g D S}}{\kappa \kappa_s} \dots\dots\dots 4.1.1$$

with ρ = density

D = flow depth

S = slope

κ = Von Kármán coefficient

k_s = absolute roughness

$$\frac{dv}{dy} = \text{velocity gradient}$$

$$\tau = \text{bed shear stress}$$

They assumed $\kappa = 0.4$ and $k_s = d_{50}$ (not enough data were given by Kamphuis and Hall to calculate k_s), and derived a relationship between the critical applied stream power and vane shear strength, % clay and consolidation pressure, shown in **Figure 4.1.2**. The correlation coefficient so obtained was 0.91, which is good. The assumption of $k_s = d_{50}$ is however not entirely correct, which became evident during laboratory test performed for this study, as is described later in the chapter.

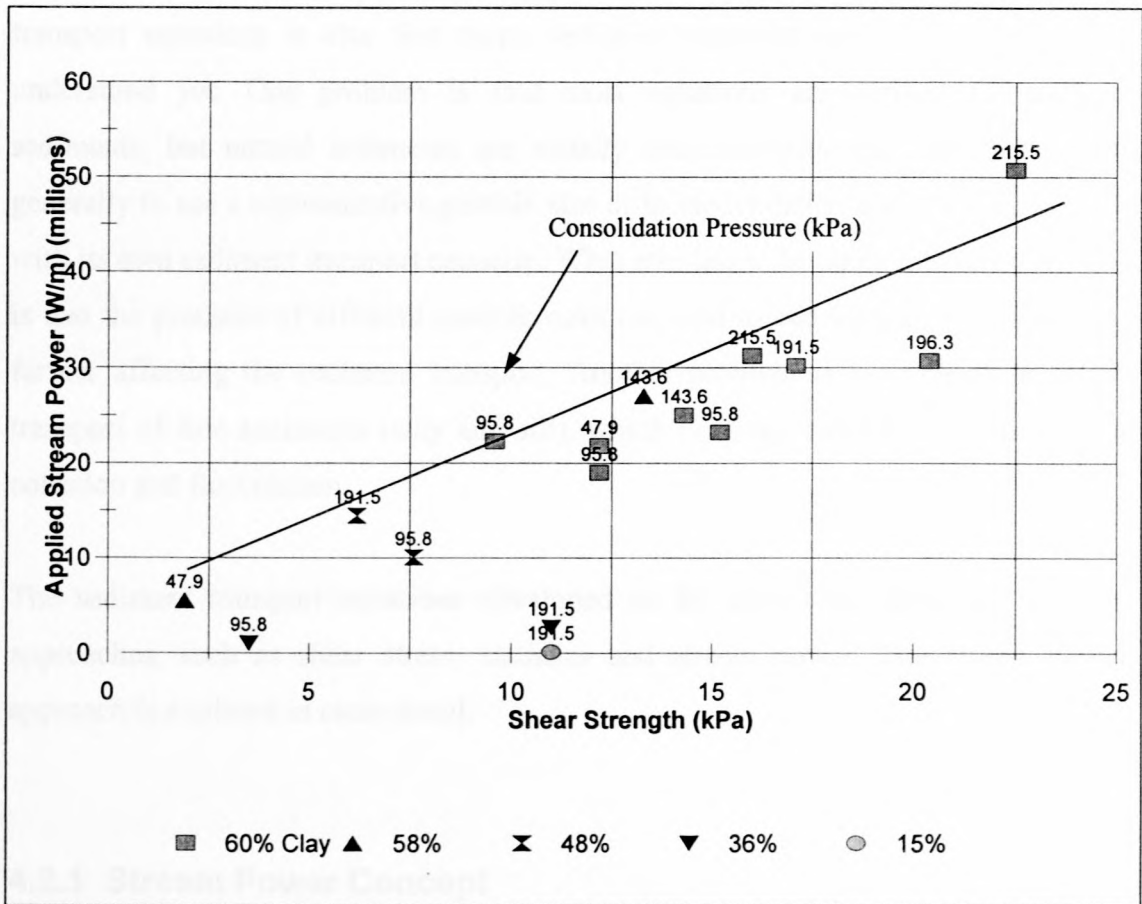


Figure 4.1.2: Correlation between applied stream power and shear strength, % clay and consolidation pressure. (Basson and Rooseboom, 1996)

4.2 Equilibrium Sediment Transport

Sediments can be transported in a river as suspended load and/or bed load. The bed load is that part of the load that is moving on or near the bed, whereas the suspended load consists of particles usually finer than those found in the bed. Of the vast amount of sediment transport equations developed there are those that predict bed load, suspended load or the total load, i.e. the bedload and suspended load combined. Because of the complexity of the sediment transport processes, the sediment transport rate cannot be predicted following a purely theoretical approach. The sediment transport equations have all needed to be calibrated using either laboratory or field data, or both. This means that most equations will only yield accurate results within certain ranges or for certain conditions. The problem with the accuracy of most transport equations is also that many sediment transport processes are not fully understood yet. One problem is that most equations are derived for uniform sediments, but natural sediments are usually non-homogeneous. The approach is generally to use a representative particle size or to model different particle sizes, each with its own sediment transport capacity. What also has to be taken into consideration is that the presence of different particle sizes can lead to bed armouring and sorting, further affecting the sediment transport. Another problem is the prediction of the transport of fine sediments (clay and silt), which is complicated by aspects such as cohesion and flocculation.

The sediment transport equations developed so far have been based on different approaches, such as shear stress, statistics and stream power. The stream power approach is explored in more detail.

4.2.1 Stream Power Concept

The concept of stream power has been used in various forms to determine the sediment transport, such as Bagnold (1966) and Yang (1972).

Bagnold used the stream power per unit area to relate the rate of energy dissipation used in transporting sediment particles to the sediment transport capacity, with two separate components for bedload and suspended load.

Yang (1972) defined the unit stream power as the rate of potential energy expenditure per unit weight of water:

$$\frac{dY}{dt} = \frac{dX}{dt} \frac{dY}{DX} = vS \dots\dots\dots 4.2.1$$

where Y = Potential energy per unit weight above a certain datum

X = longitudinal distance

t = time

vS = unit stream power

Yang argued that since the sediment transport is related to the strength of the turbulent flow conditions, the rate of total sediment transport rate or concentration should be directly related to the unit stream power. The basic form of Yang's unit stream power equation is:

$$\log(C_t) = \alpha + \beta \log(vS - vS_{cr}) \dots\dots\dots 4.2.2$$

where C_t = total sediment concentration in ppm

α, β = coefficients

vS_{cr} = critical unit stream power

Yang found that both α and β are dependent on the water depth and that β is also dependent on the particle size. In 1973 Yang sought to improve on **Equation 4.2.2** through dimensional analysis. He found the following:

$$C_t = \Phi \left(\frac{vS}{w} - \frac{v_{cr}S}{w}, \frac{U_*}{w}, \frac{wd}{v} \right) \dots\dots\dots 4.2.3$$

where w = particle settling velocity

$$U_* = \text{shear velocity} = \sqrt{gDS}$$

ν = kinematic viscosity

d = particle size

The basic form of **Equation 4.2.3** is very similar to **Equation 4.2.2**:

$$\log(C_t) = \alpha + \beta \log\left(\frac{\nu S}{w} - \frac{\nu_{cr} S}{w}\right) \dots\dots\dots 4.2.4$$

where α, β = coefficients

$$\frac{\nu S}{w}, \frac{\nu_{cr} S}{w} = \text{dimensionless unit stream power and critical unit stream power, respectively}$$

When the concentrations are more than 100 ppm the dimensionless critical unit stream power is relatively small in relation to the value of the unit stream power and the $\left(\frac{\nu_{cr} S}{w}\right)$ term can be excluded (Yang and Molinas, 1982).

$$\log(C_t) = \alpha + \beta \log\left(\frac{\nu S}{w}\right) \dots\dots\dots 4.2.5$$

Based on laboratory and field measurements the coefficients α and β were determined through regression analysis. Yang's sediment transport equation for sand, including the critical unit stream power term, is as follows:

$$\begin{aligned} \log(C_t) = & 5.435 - 0.286 \log\left(\frac{wd}{\nu}\right) - 0.457 \log\left(\frac{U_*}{w}\right) \\ & + \left(1.799 - 0.409 \log\left(\frac{wd}{\nu}\right) - 0.314 \log\left(\frac{U_*}{w}\right)\right) \log\left(\frac{\nu S}{w} - \frac{\nu_{cr} S}{w}\right) \dots\dots\dots 4.2.6 \end{aligned}$$

For concentrations of more than 100 ppm the incipient motion criterion does not play a significant role and the following equation can be used:

$$\log(C_i) = 5.165 - 0.153 \log\left(\frac{wd}{\nu}\right) - 0.297 \log\left(\frac{U_*}{w}\right) + \left(1.780 - 0.360 \log\left(\frac{wd}{\nu}\right) - 0.480 \log\left(\frac{U_*}{w}\right)\right) \log\left(\frac{\nu S}{w}\right) \dots\dots\dots 4.2.7$$

The dimensionless critical average flow velocity can be computed as follows (Yang, 1973):

$$\frac{v_{cr}}{w} = \frac{2.5}{\log\left(\frac{U_* d}{\nu}\right) - 0.06} + 0.66; \quad 1.2 < \frac{U_* d}{\nu} < 70 \dots\dots\dots 4.2.8$$

$$\frac{v_{cr}}{w} = 2.05; \quad 70 \leq \frac{U_* d}{\nu} \dots\dots\dots 4.2.9$$

Yang *et al.* (1996) modified **Equation 4.2.5** for use in sediment-laden flows with high concentrations of fine materials. The modifications included the particle settling velocity, viscosity and relative specific weight, with the coefficients being unchanged. The modified formula is as follows:

$$\log(C_i) = 5.165 - 0.153 \log\left(\frac{w_m d}{\nu_m}\right) - 0.297 \log\left(\frac{U_*}{w_m}\right) + \left(1.780 - 0.360 \log\left(\frac{w_m d}{\nu_m}\right) - 0.480 \log\left(\frac{U_*}{w_m}\right)\right) \log\left(\frac{\gamma_m}{\gamma_s - \gamma_m} \frac{\nu S}{w_m}\right) \dots\dots\dots 4.2.10$$

with:

$$w_m = w(1 - C_v)^{7.0} \dots\dots\dots 4.2.11$$

$$\nu_m = \frac{\rho}{\rho_m} e^{5.06 C_v} \dots\dots\dots 4.2.12$$

$$\rho_m = \rho + (\rho_s - \rho)C_v \dots\dots\dots 4.2.13$$

where w , w_m = particle settling velocity in clear water and sediment-laden flow, respectively

ν_m = kinematic viscosity of sediment-laden flow

ρ , ρ_m , ρ_s = specific density of clear water, sediment-laden flow and sediment, respectively

γ , γ_m , γ_s = specific weight of clear water, sediment-laden flow and sediment, respectively

C_v = suspended sediment concentration by volume

Equations 4.2.10 to 4.2.12 are however only applicable to the Yellow River, China with hyper-concentrations. For any other river with high concentrations of fine sediments these equations will have to be recalibrated.

Basson and Rooseboom (1996) argued that the applied stream power would be a more appropriate basis for determining the sediment transport, as the applied stream power is determined by basic hydraulic variables. They have developed a sediment transport equation that is based on the applied stream power $\left(\tau \frac{dv}{dy} \right)$, which has been calibrated extensively with laboratory and river data:

$$C = \left(\left(\frac{\rho}{\rho_s - \rho} \right) (gDS)^{1.5} \right)^{1.969} (0.4k_s)^{-1.146} w^{-3.286} \left(\frac{k_s}{D} \right)^{0.856} \left(\frac{w}{0.4\sqrt{gDS}} \right)^{2.560} \dots\dots\dots 4.2.14$$

where C is the sediment concentration in % (by weight).

Besides **Equation 4.2.14** Basson and Rooseboom have also developed a sediment transport equation for implementation in a numerical model based on the unit input stream power approach:

$$\log(C_t) = 4.31 + 0.343 \log \left(\frac{vS}{w} \right) \dots\dots\dots 4.2.15$$

where C_i = sediment concentration in ppm

Equation 4.2.15 has been calibrated with data from a large number of South African reservoirs for flood flushing and storage operations, which means that it has been calibrated with fine sediment fractions. **Equation 4.2.15** may however not be applicable to rivers because it has been calibrated on reservoir data, which are obtained under non-uniform flow conditions, unlike river or laboratory data.

Equations 4.2.6 and **4.2.7**, as well as **Equation 4.2.14** give excellent results for a wide range of particle sizes; however, they do not extend to finer particles in the clay and silt range. Yang's attempt to modify his original transport equation for sediment-laden flow with high concentrations of fine materials is only partially successful, since his equation is only applicable to the Yellow River and also dependent on the suspended sediment concentration. **Equation 4.2.9** gives the total sediment concentration, i.e. bedload and suspended load combined, but before the equation can be used the suspended sediment concentration must be known. In very few cases is it known how much sediment is carried in a river at a given flow rate. This makes **Equation 4.2.9** difficult to apply, even when calibrated for different rivers. But the unit input stream power concept is still one of the best approaches to describe sediment transport because it can be theoretically derived and it is dimensionally homogeneous. The unit input stream power approach will therefore be used to develop a sediment transport equation, in the form of **Equation 4.2.5**, for fine sediments.

4.3 Laboratory Flume Studies

The objective of the experiments was to obtain hydraulic and sediment data on non-cohesive and cohesive sediments at equilibrium, as well as mixtures of cohesive and non-cohesive sediments, to determine the effect of fine sediment on the hydraulic and sediment transport characteristics. The data obtained were used to describe critical conditions for mass erosion of cohesive sediments, as well as to calibrate a sediment transport equation for fine sediments.

4.3.1 Equipment

The experiments were carried out in the Hydraulics Laboratory at the University of Stellenbosch in a recirculating flume (0.6 m wide, 1.5 m deep and 17 m long) and return pipe (\varnothing 150 mm) system as shown in **Figure 4.3.1**. The flow rate could be varied from 0 to 100 ℓ/s by adjusting both the variable speed pump and the two valves. The slope of the flume was adjustable and baffles were placed at the entrance of the flume to ensure energy dissipation and a uniform flow rate at the entrance. The sampling point for suspended sediments was located on the return pipe to ensure that sediment and water were completely mixed.

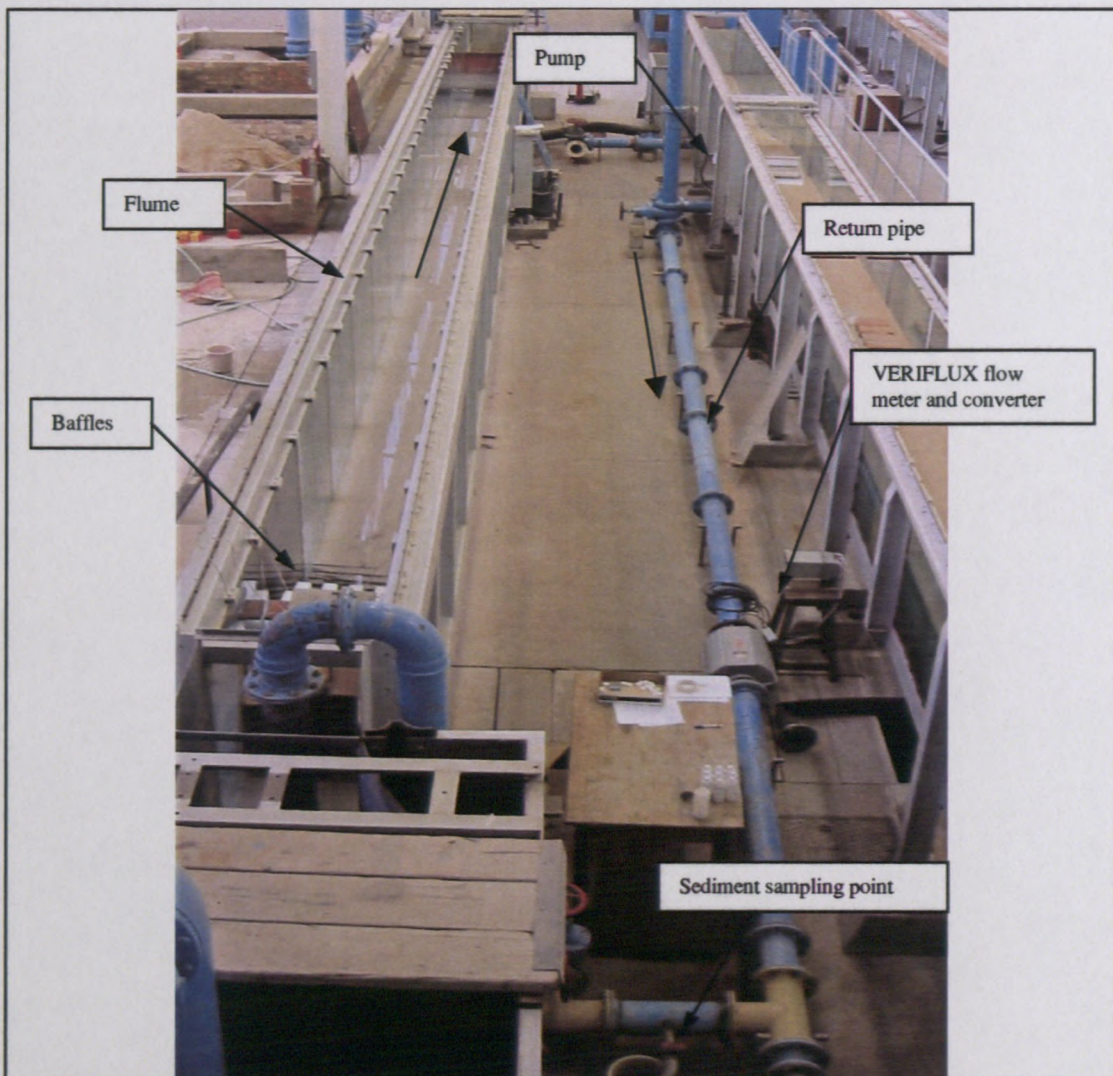


Figure 4.3.1: Layout of laboratory system

Velocities were determined with the use of an electromagnetic VERIFLUX VAC 0.075 kW flow meter installed on the return pipe. Readings were taken with the aid of the VERIFLUX Series 2-2 Converter (**Figure 4.3.2**). The velocities are determined as follows:

$$v_p = \frac{A \cdot B}{10} \dots\dots\dots 4.3.1$$

where A, B = readings from the converter

v_p = velocity in return pipe (m/s)

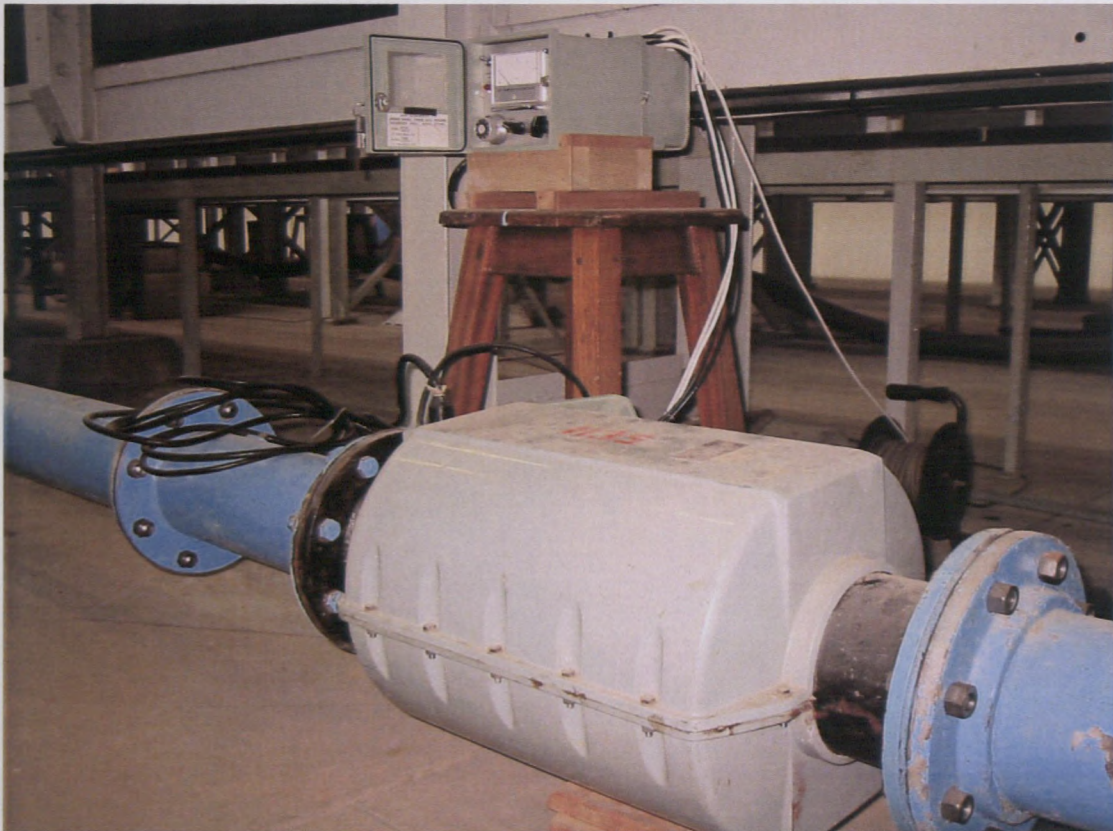
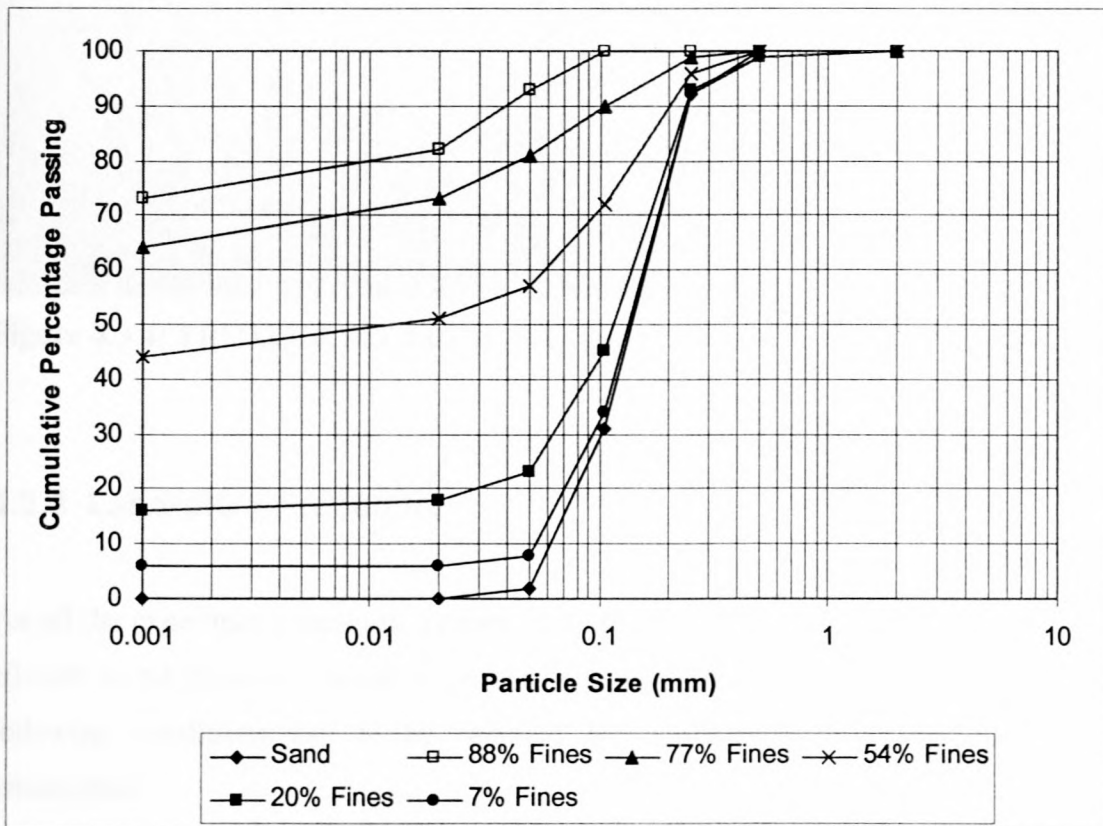


Figure 4.3.2: VERIFLUX flow meter and converter

The types of sediments that were used, are summarized in **Table 4.3.1**, and the gradings shown in **Figure 4.3.3**. The cohesive - non-cohesive mixtures were obtained by combining certain percentages (by weight) of sand and clay. The following fine contents (< 0.03 mm) were aimed at: 10%, 20%, 60% and 80%, but the actual mixtures are shown in **Table 4.3.1**.

Table 4.3.1: Sediment types

| Sediment Type | Median Particle Diameter (mm) |
|----------------------|-------------------------------|
| Sand | 0.12 |
| Clay: 88% Fines | < 0.001 |
| Mixture 1: 77% Fines | < 0.001 |
| Mixture 2: 54% Fines | 0.017 |
| Mixture 3: 20% Fines | 0.105 |
| Mixture 4: 7% Fines | 0.11 |

**Figure 4.3.3: Particle size distribution curves**

The shear strength of the sediment was determined through the use of the vane shear test. The densities were determined with the aid of a TROXLER moisture-density gauge (Model 3411-B), shown in **Figure 4.3.4**, after draining the water from the flume. Density measurements were performed by utilizing a radioactive source and gamma ray detectors.



Figure 4.3.4: TROXLER moisture-density gauge

4.3.2 Laboratory Procedure

For all the experiments the basic procedure was to recirculate a given water-sediment mixture in the flume at a preset slope until equilibrium conditions were reached. The following conditions had to be satisfied for equilibrium to be considered as established:

- Sand: the average water surface slope and the bed slope were found to have remained constant and parallel, and the bed configuration was consistent throughout the test section, both with respect to time.
- Clay and clay/sand mixtures: the average energy slope remained constant with respect to time, and the suspended-sediment concentration was observed to be constant.

The different procedures for the different sediments were as follows:

1. Sand

The slope of the flume was adjusted to 1:500, and the sand was allowed to reach its equilibrium bed slope. A 150 mm layer of dry sand was then placed in the flume by hand, levelled as best as possible and clear water was slowly added without disturbing the sediment. The runs were started at a low flow rate and measurements were taken at various time intervals until equilibrium was reached. For the first seven runs the flow rate was increased each time, with the bed forms changing from ripples in run 1 up to antidunes in runs 6 and 7. Run 8 was added to obtain more data in the dunes range. The time it took each run to be completed varied from 2.5 to 18 hours, depending on the bed configuration. Runs 6 and 7 took the least time because of the high rates of erosion.

2. Clay and sand/clay mixtures:

The slope of the flume was adjusted to 1:20 000 and a 170 mm layer of dry pottery clay was placed in the flume by hand, levelled as best as possible and clear water was added without disturbing the clay too much. The clay was then left to consolidate for four days, and then the water was pumped at a high flow rate so that most of the clay could erode, after which the clay was allowed to deposit again whilst the water was still flowing. The clay was again allowed to consolidate for four days under saturated conditions and then the runs were again started at a very low flow rate. The same measurements were taken as for the sand, except at shorter time intervals, as each run only took 2 to 3 hours. After equilibrium was reached the flow rate was immediately increased for the next run, allowing for three to four runs each day. The pump was not allowed to run throughout the night and to ensure continuity throughout all runs, the flow rate was raised in steps to the desired flow rate at the start of the second and following days, to make sure that the same conditions were present as at the end of the previous day. The experiments ended when the erosion changed from surface to mass erosion. Mass erosion was defined as that stage at which the bed started to exhibit noticeable scouring throughout the whole test section

For the mixtures, about two-thirds of the clay was removed from the flume and certain amounts of sand were added and mixed by hand. The mixtures were then left

to consolidate for four days under water and the same procedures were followed as for the clay alone. In order to compare all the runs, more or less the same flow depths and flow rates were used for each mixture, and the runs with the same flow rate and flow depth given the same numbers. In **Appendix B1/2** the runs with the same numbers for the mixtures and the clay are therefore directly comparable. Because the data obtained for the first few runs of each experiment varied very little, it was decided to leave out some of the lower flow rates and to add higher flow rates for the mixtures containing larger amounts of sand.

The following data were determined for all sediments:

- Average water surface slope S_w
- Average bed slope S_o
- Average depth of flow D
- Water discharge Q
- Suspended-sediment concentrations C
- Water temperature T
- Particle size distribution of sediment
- Particle settling velocity w

The water surface and bed level were measured at 1 m intervals along a 10 m test section, which was chosen to exclude all entrance and exit influences. The flow depth was determined from the difference between the water surface and bed levels, and the discharge was obtained from the velocity meter, which had been installed in the pipe:

$$Q = Av_p \dots\dots\dots 4.3.2$$

where Q = discharge

v_p = velocity in return pipe

A = cross-sectional area of pipe

Suspended-sediment samples were taken at the start and end of each run and the temperatures were recorded to the nearest half degree Centigrade. The particle size

distributions were determined from samples taken from the bed before and after each experiment to determine any changes in bed material.

From the measured data the following variables were computed:

- Average energy slope S_f :

The energy slope was determined from the energy equation:

$$z_1 + h_1 + \frac{v_1^2}{2g} - z_2 - h_2 - \frac{v_2^2}{2g} = h_f \dots\dots\dots 4.3.3$$

$$S_f = \frac{h_f}{L} \dots\dots\dots 4.3.4$$

where z_1, z_2 = elevation above arbitrary datum

h_1, h_2 = flow depths

v_1, v_2 = mean flow velocities

h_f = friction losses between sections 1 and 2

L = distance between points 1 and 2

- Mean velocity v :

The mean velocity was determined from the observed values of discharge Q , depth D and width B of flume by means of the continuity equation:

$$v = \frac{Q}{DB} \dots\dots\dots 4.3.5$$

- Shear stress at bed τ :

The shear stress at the bed was calculated as follows:

$$\tau = \rho g D S \dots\dots\dots 4.3.6$$

- Froude number Fr :

The Froude number was calculated from the formula:

$$Fr = \frac{v}{\sqrt{gD}} \dots\dots\dots 4.3.7$$

- Absolute roughness k_s :

The resistance factor was determined from Chezy's resistance formula:

$$k_s = \frac{12D}{10 \frac{v}{18\sqrt{DS}}} \dots\dots\dots 4.3.8$$

- Particle settling velocity w :

The settling velocity was calculated from the following two equations:

For $d < 0.1$ mm (Stokes range): $w = \frac{1}{18} \frac{(\rho_s - \rho)gd^2}{\nu\rho} \dots\dots\dots 4.3.9$

For $0.1 < d < 1$ mm (Zanke, 1977): $w = 10 \frac{\nu}{d} \left(\sqrt{1 + \frac{0.01(s-1)gd^3}{\nu^2}} - 1 \right) \dots\dots\dots 4.3.10$

Since non-uniform sediments were used for some of the experiments the effective settling velocities were calculated as the summation of the settling velocities for certain particles sizes w_i (Table 4.3.2) according to their proportion p_i in the sediment grading curve:

$$w = \sum p_i w_i \dots\dots\dots 4.3.11$$

Table 4.3.2: Particle size ranges

| Particle Size Range (mm) |
|--------------------------|
| 2 – 0.5 |
| 0.5 – 0.25 |
| 0.25 – 0.106 |
| 0.106 – 0.05 |
| 0.05 – 0.02 |
| 0.02 – 0.002 |
| < 0.002 |

4.4 Analysis of Results

The laboratory results (**Appendix B1- B3**) show that as the clay content decreased the sediment did not exhibit any non-cohesive behaviour until the fines content was only 20%. At that point some irregular bedforms appeared towards the end of that series of runs (**Figure 4.4.1**). These took a few hours to develop throughout the flume, whereas the bedforms of the sand alone developed almost immediately throughout the test section. During the tests done on the sediment with 7% fine content, larger dunes and ripples appeared (**Figure 4.4.2**). These sometimes did not develop throughout the whole test section, and generally took more than a day to stabilize. At the end of this set of runs the bed also did not display scouring as experienced during the tests with higher fine contents, with a rough uneven surface, but rather a smooth flat bed developed, as evident during the transitional phase of the experiments on the sand alone.



Figure 4.4.1: Irregular bedforms after the flume was drained (20% clay and silt contents)

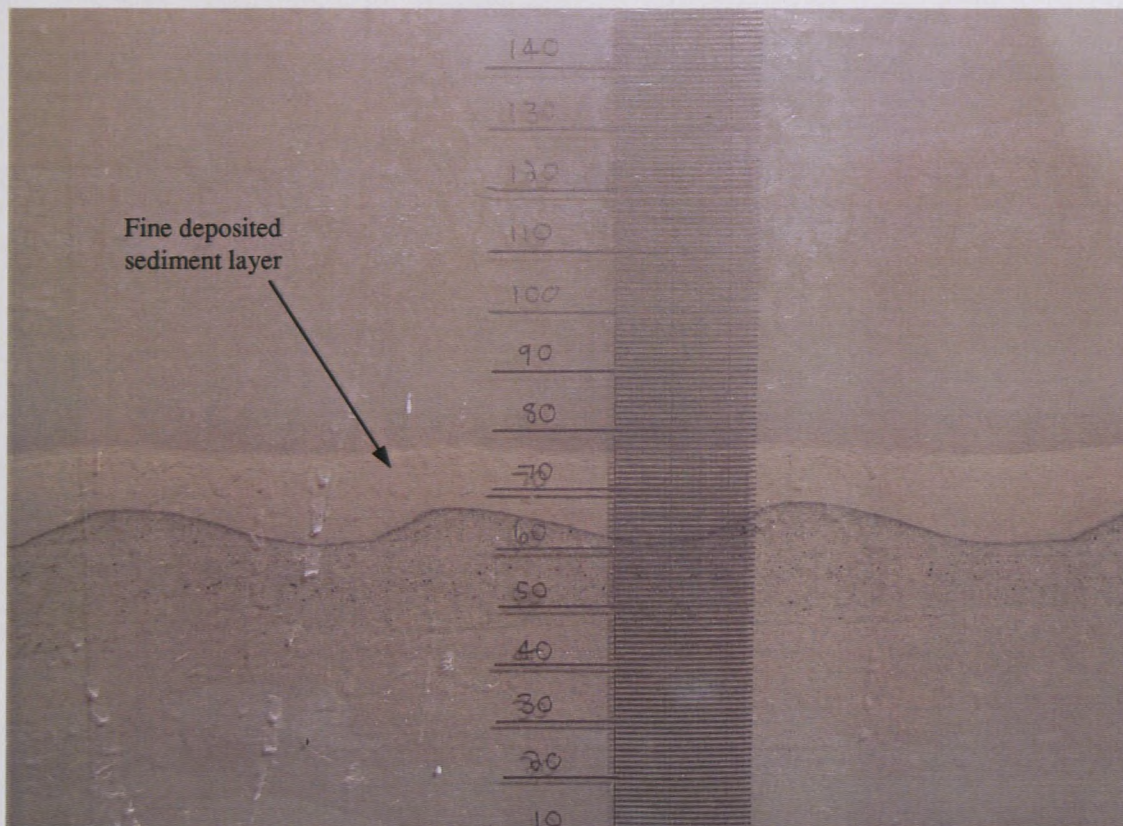


Figure 4.4.2: Bedforms developed during runs made with 7% clay and silt content (fine deposited layer developed after runs were stopped)

The bedforms that developed with 7 and 20% fines content seemed to develop on top of the original mixed layer (**Figure 4.4.3**). There was a noticeable difference in the composition of the bedforms and the lower mixed layer, in that the bedforms seemed to be entirely made up of sand. This together with the fact that the suspended sediments were made up almost entirely of fine materials means that instead of transporting the same fractions of particle sizes as present in the bed, the finer sediments were washed out and only a small fraction of the coarser material was transported. The sediment transport of graded sediment therefore seems to be based on the sediment transport capacity of each fraction.

The fact that fines contents of 7% and greater can dominate the erosion behaviour of sediments can also be seen from **Figure 4.4.4**, which shows the correlation between applied stream power and clay content. The points represent the series of runs made for each of the six sediments.

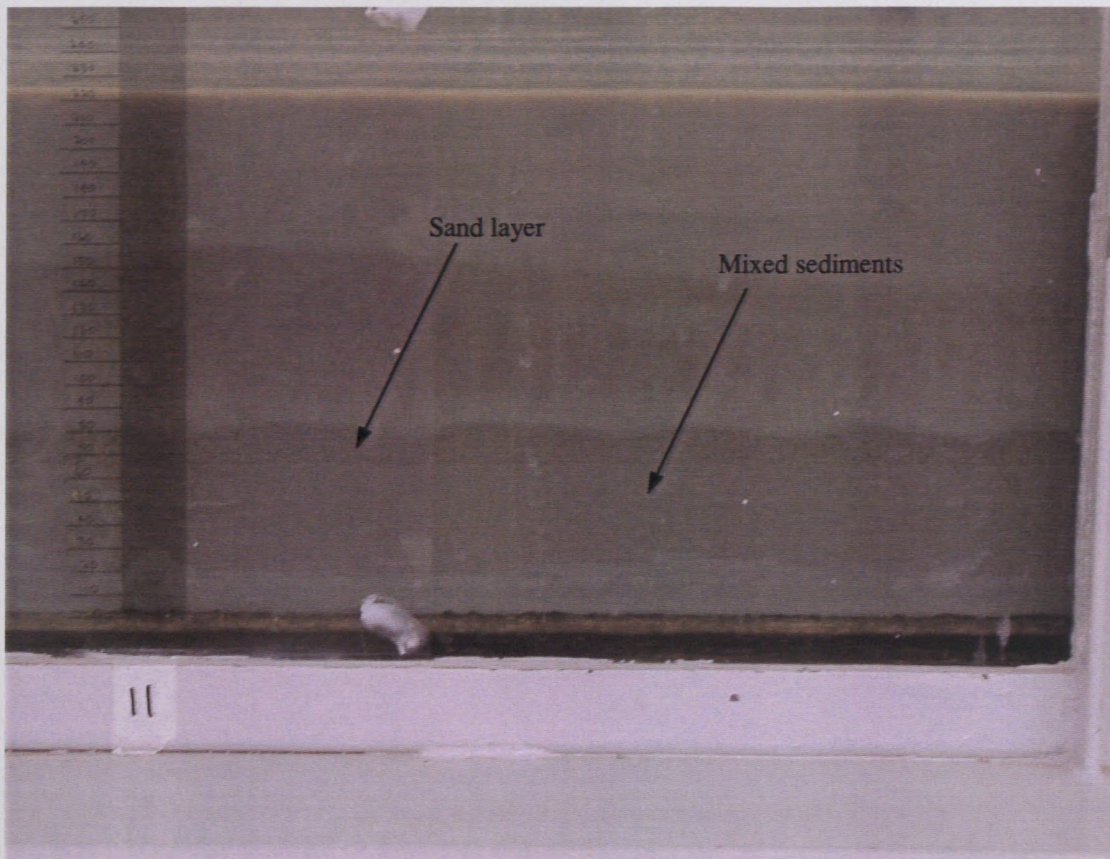


Figure 4.4.3: Layers of sediment developed during runs with 7% clay and silt content

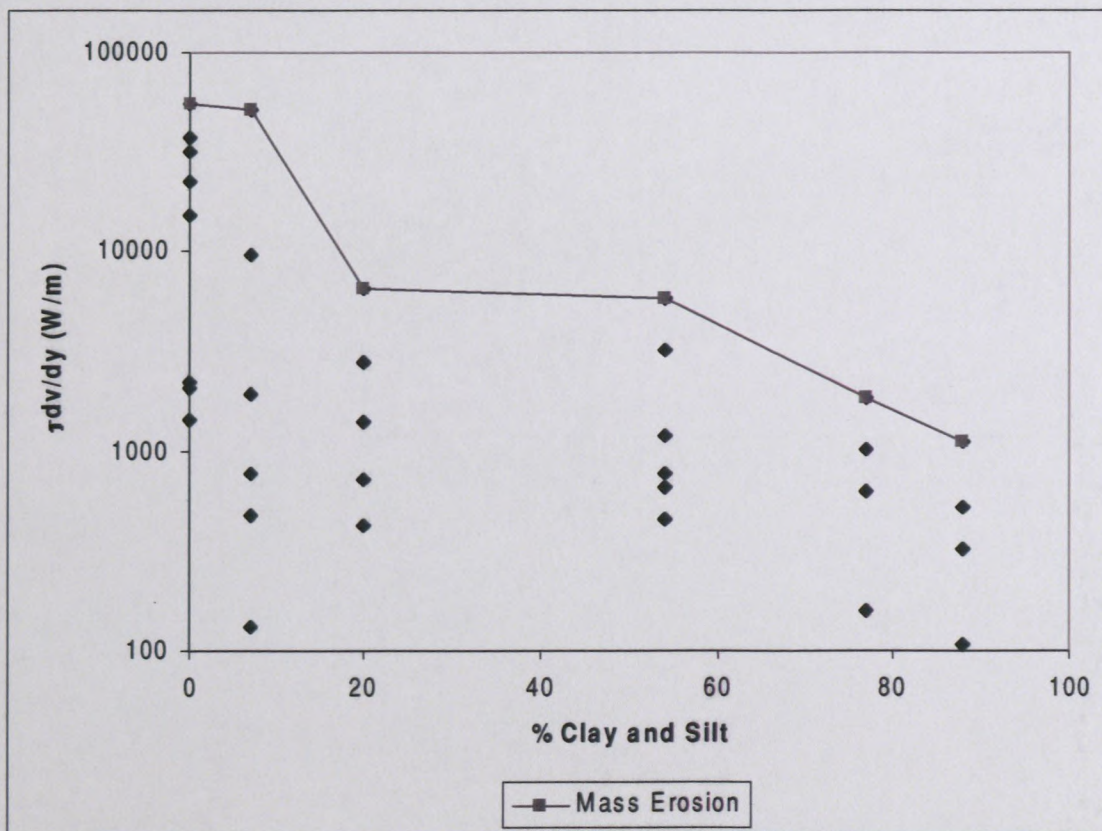


Figure 4.4.4: Correlation between applied stream power and fine particle content

To be able to compare the mass erosion states of the various sediments, an equivalent state had to be defined for the non-cohesive sediments. Since relatively large amounts of sediments are transported and there is an almost immediate change to a smooth flat bed for the transition phase of non-cohesive sediments, this state was chosen. The solid line in **Figure 4.4.4** connects the points indicating mass erosion. There appear to be two points of change, which divide the graph into three regions. The first occurs with between 7 and 20% fines content, which is where the clay and silt start dominating the erosion pattern of the sediments. The second change occurs between 54 and 77% clay and silt. This could be a point where there is enough sand present to affect the erosion through armouring.

4.4.1 Critical Conditions for Mass Erosion

Kamphuis and Hall (1983) and Torfs *et al.* (1994) amongst others have defined the critical conditions for erosion of cohesive sediments in terms of the critical shear stress or critical velocity. **Figure 4.4.5** however shows that the critical shear stress ρgDS may not be a clear indicator for mass erosion. Generally the critical shear stress τ_{cr} increases with increasing clay content, which is true for up to 54% clay content, after which the critical shear stress decreases dramatically. This could be due to the fact that the critical shear stress is highly susceptible to even small changes in both depth and slope. During the experiments the slope was difficult to determine accurately because it was so small and also because of water surface fluctuations.

The fact that the critical shear stress is only dependent on the depth and slope is one of the reasons to consider the use of the applied stream power $\left(\tau \frac{dv}{dy} \right)_0$ at the bed to describe the critical conditions for erosion.

$$\left(\tau \frac{dv}{dy} \right)_0 = \frac{30 \rho gDS \sqrt{gDS}}{\kappa \kappa_s} \dots\dots\dots 4.1.1$$

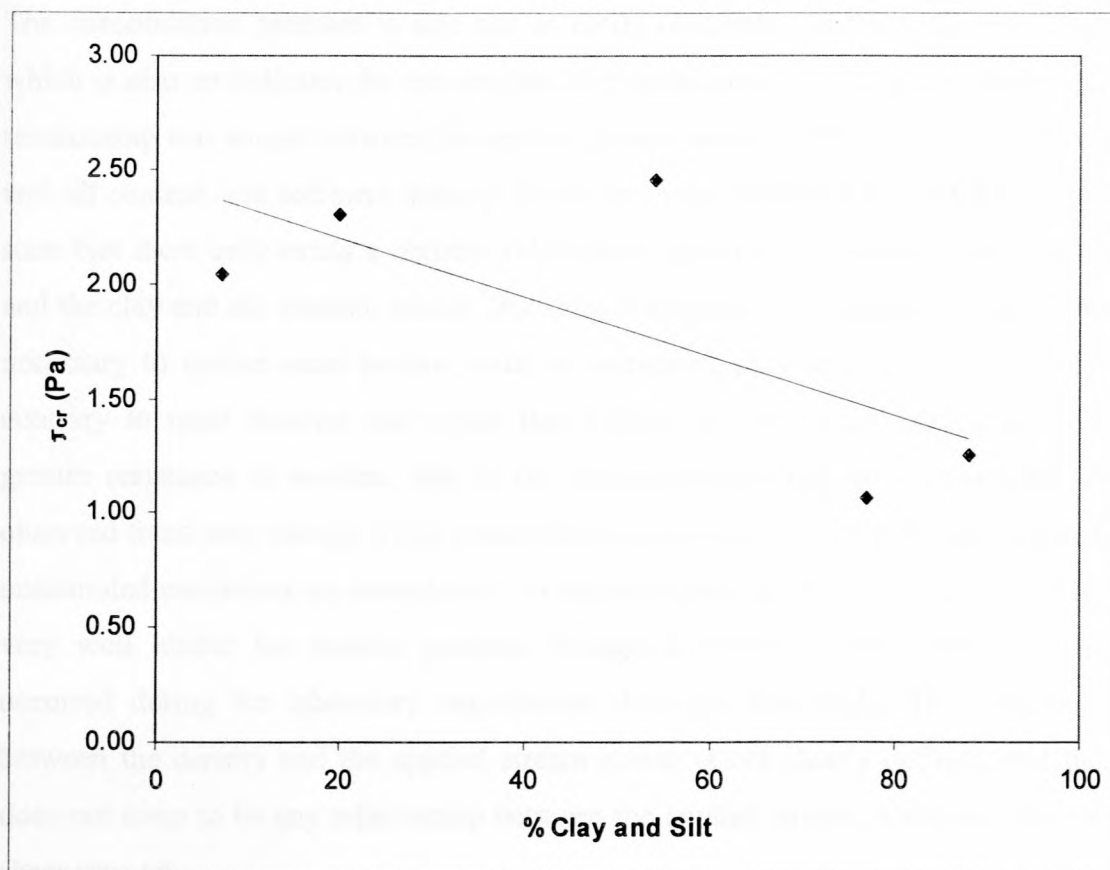


Figure 4.4.5: Correlation between critical shear stress and fine particle content

The applied stream power takes into consideration the effect of roughness, which is an important parameter in sediment transport (Basson and Rooseboom, 1996).

Basson and Rooseboom (1996) have used Kamphuis and Hall's data to develop a relationship between the applied stream power and the shear strength, % clay and consolidation pressure. They assumed $k_s = d_{50}$, since k_s could not be determined from the Kamphuis and Hall data. The roughness values determined from the flume experiments are however much greater than the mean particle size, especially when the fine particle contents were substantial (Table 4.4.1).

Table 4.4.1: Variation of absolute roughness with % clay and silt, and d_{50}

| k_s (m) | d_{50} (mm) | % Clay and silt |
|-----------|---------------|-----------------|
| 0.003 | < 0.001 | 88 |
| 0.0014 | < 0.001 | 77 |
| 0.0016 | 0.017 | 54 |
| 0.0013 | 0.105 | 20 |
| 0.0001 | 0.11 | 7 |

The consolidation pressure is also not as easily obtainable as the sediment density, which is also an indicator for the amount of consolidation. In this study, therefore, a relationship was sought between the applied stream power and the shear strength, clay and silt content, and sediment density. However, from **Figures 4.4.6 to 4.4.8** it can be seen that there only exists a definite relationship between the applied stream power and the clay and silt content, which illustrates a decrease in the applied stream power necessary to induce mass erosion with an increasing clay and silt content. This is contrary to most theories that argue that higher fine material contents will offer greater resistance to erosion, due to the cohesive properties of the particles. The observed trend may change when consolidation and drying of the cohesive bed under unsaturated conditions are considered. On the other hand greater amounts of sand may very well hinder the erosion process through armouring, which seems to have occurred during the laboratory experiments done for this study. The relationship between the density and the applied stream power is not clearly defined, and there does not seem to be any relationship between the applied stream power and the vane shear strength.

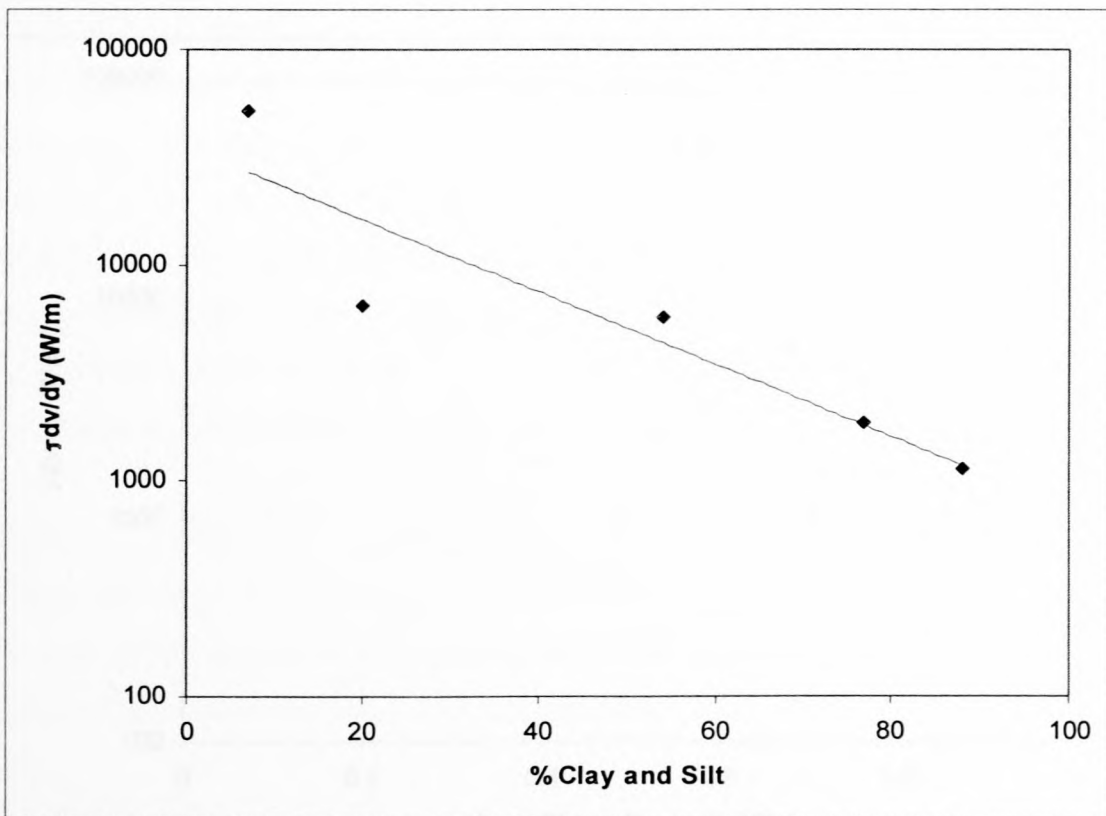


Figure 4.4.6: Correlation between applied stream power and fine particle content (mass erosion only)

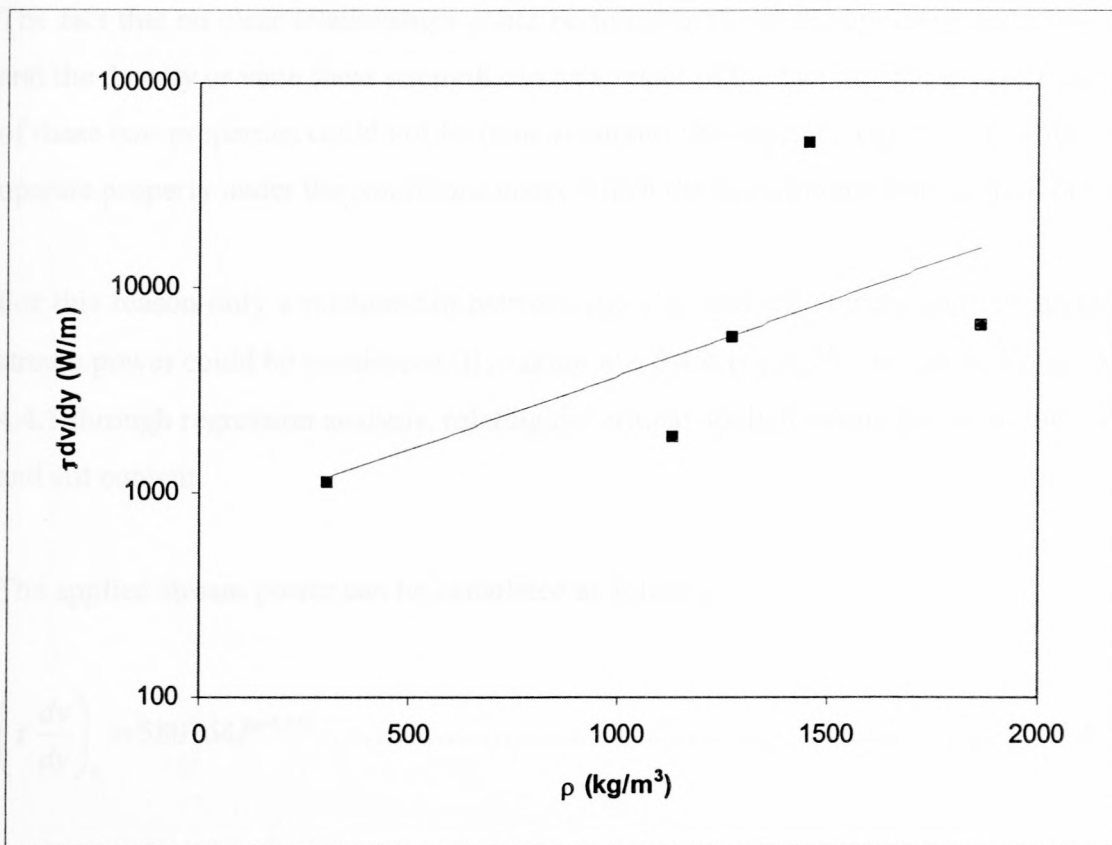


Figure 4.4.7: Correlation between applied stream power and dry density

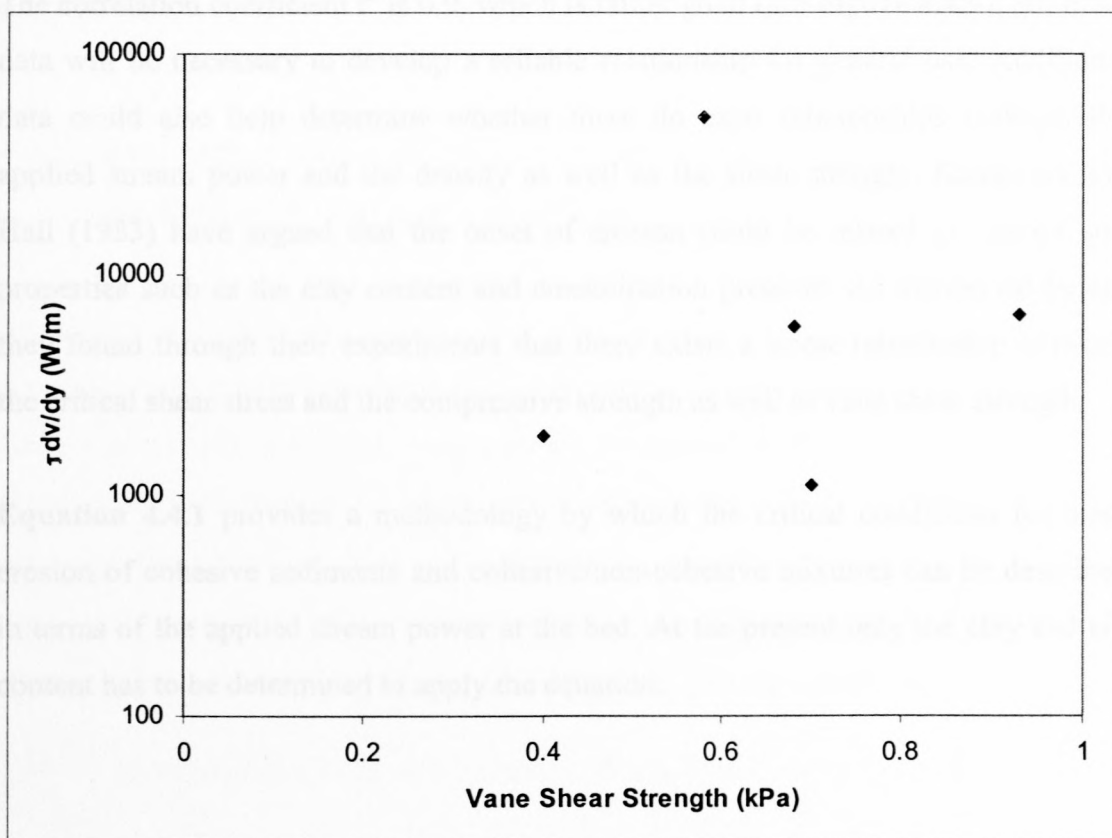


Figure 4.4.8: Correlation between applied stream power and shear strength

The fact that no clear relationships could be found between the applied stream power and the density or vane shear strength can be a result of the fact that the measurements of these two properties could not be done accurately because the equipment could not operate properly under the conditions under which the experiments were carried out.

For this reason only a relationship between the clay and silt content and the applied stream power could be considered. By taking $\kappa = 0.4$ it is possible to derive **Equation 4.4.1** through regression analysis, relating the critical applied stream power to the clay and silt content.

The applied stream power can be calculated as follows:

$$\left(\tau \frac{dv}{dy} \right)_0 = 580764P^{-1.313} \dots\dots\dots 4.4.1$$

where P = percentage clay and silt

The correlation coefficient r^2 is 0.9, which is rather good (see **Figure 4.4.9**), but more data will be necessary to develop a reliable relationship for general use. Additional data could also help determine whether there do exist relationships between the applied stream power and the density as well as the shear strength. Kamphuis and Hall (1983) have argued that the onset of erosion could be related to various soil properties such as the clay content and consolidation pressure. As mentioned before they found through their experiments that there exists a linear relationship between the critical shear stress and the compressive strength as well as vane shear strength.

Equation 4.4.1 provides a methodology by which the critical conditions for mass erosion of cohesive sediments and cohesive/non-cohesive mixtures can be described in terms of the applied stream power at the bed. At the present only the clay and silt content has to be determined to apply the equation.

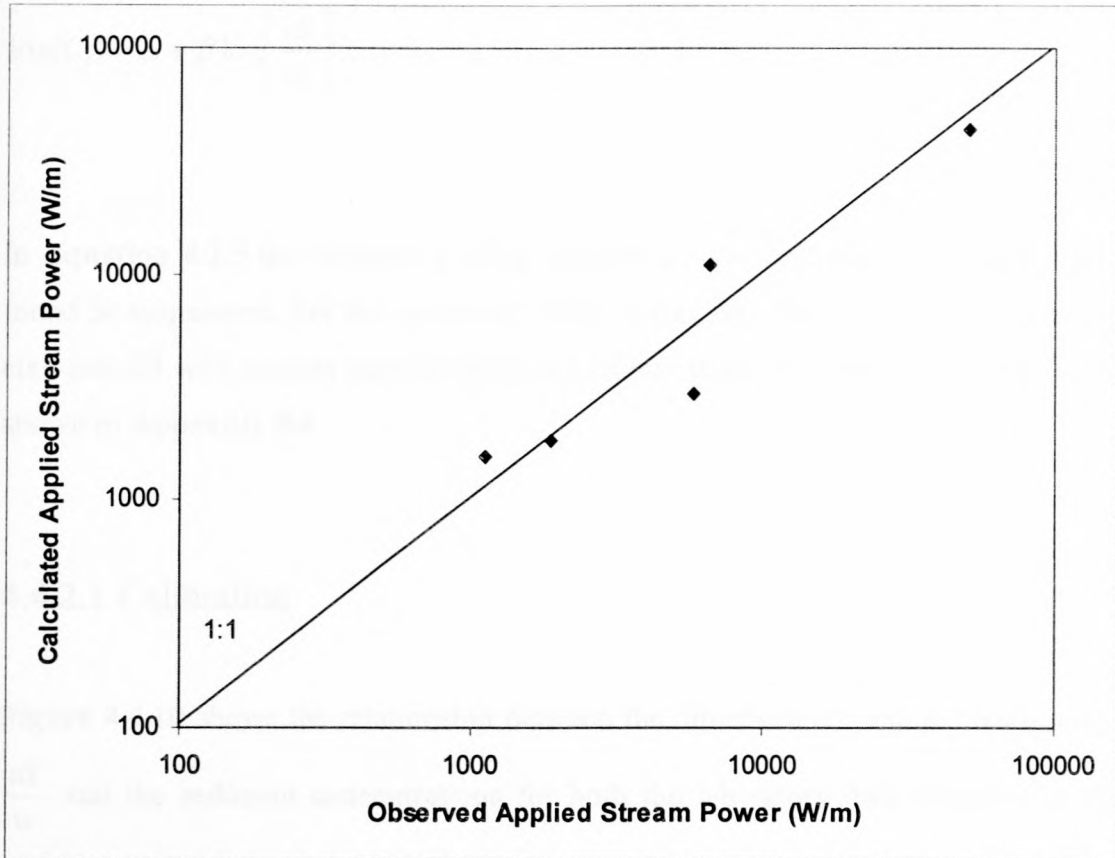


Figure 4.4.9: Observed versus calculated critical applied stream power for mass erosion

4.4.2 Evaluation and Calibration of Sediment Transport Equations for Fine and Non-Cohesive Sediments

In addition to the data obtained from the experiments, data sets from other researchers were also used for the calibration and verification process. One data set, compiled by Guy *et al.* (1966), was used to supplement the limited sand data that was obtained during this study because the experiments were mostly done on cohesive sediments. From the data set of Guy *et al.* only the data for concentrations greater than 100 mg/ℓ were used, because all of the concentrations obtained during laboratory experiments done in this study were also greater than 100 mg/ℓ, and the critical unit stream power $\left(\frac{v_{cr} S}{w}\right)$ is negligible (Yang and Molinas, 1982). The data of Guy *et al.* and the

laboratory data were used to calibrated the following sediment transport relationship:

$$\log(C_t) = \alpha + \beta \log\left(\frac{vS}{w_s}\right) \dots\dots\dots 4.2.5$$

In **Equation 4.2.5** the effective settling velocity w_s was determined for the particles found in suspension. For the sediment mixtures this was found to be predominantly clay and silt with median particle diameters of less than 0.001 mm. The gradings are shown in **Appendix B4**.

4.4.2.1 Calibration

Figure 4.4.10 shows the relationship between the dimensionless input stream power $\frac{vS}{w}$ and the sediment concentrations for both the laboratory data obtained in this study as well as data from Guy *et al.*, which represents a data set of 305 observations. The calibrated sediment transport equation has a correlation coefficient of 0.75 and is shown in **Figure 4.4.11**:

$$\log(C_t) = 4.472 + 0.978 \log\left(\frac{vS}{w_s}\right) \dots\dots\dots 4.4.2$$

with C_t = suspended sediment concentrations (mg/ℓ)

In **Figure 4.4.11** it can be seen that the data lie in two slightly different regions, with the data associated with clay and silt situated slightly lower on the graph and at a different slope. This would explain the relatively low correlation coefficient. The divergence occurs because of the difference in the particle sizes that are in suspension. For the sediments containing at least 7% clay and silt, most of the suspended sediments were found to be predominantly clay and silt, whereas for sediments with less than 7% fine particles most of the suspended sediment was sand. It would therefore be more accurate to separate the data associated with clay and silt, and to calibrate two sediment transport equations.

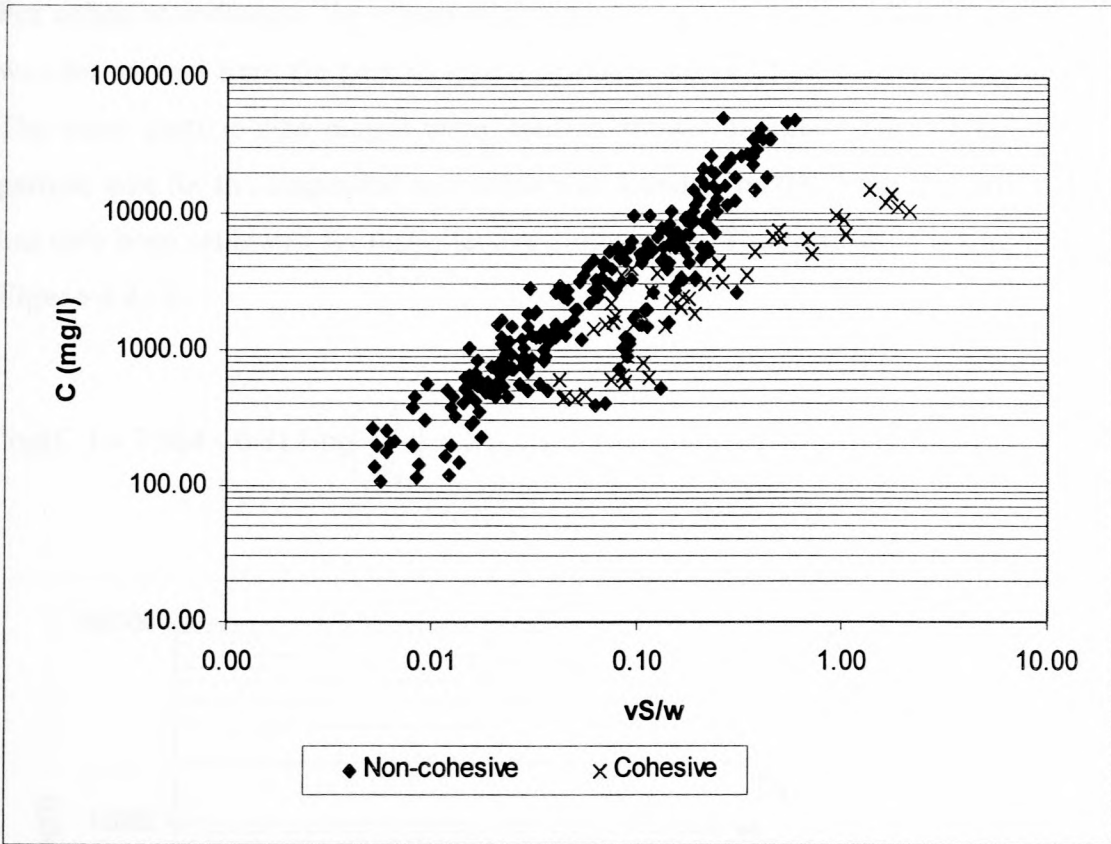


Figure 4.4.10: Correlation between dimensionless unit stream power and concentration for both cohesive and non-cohesive sediments

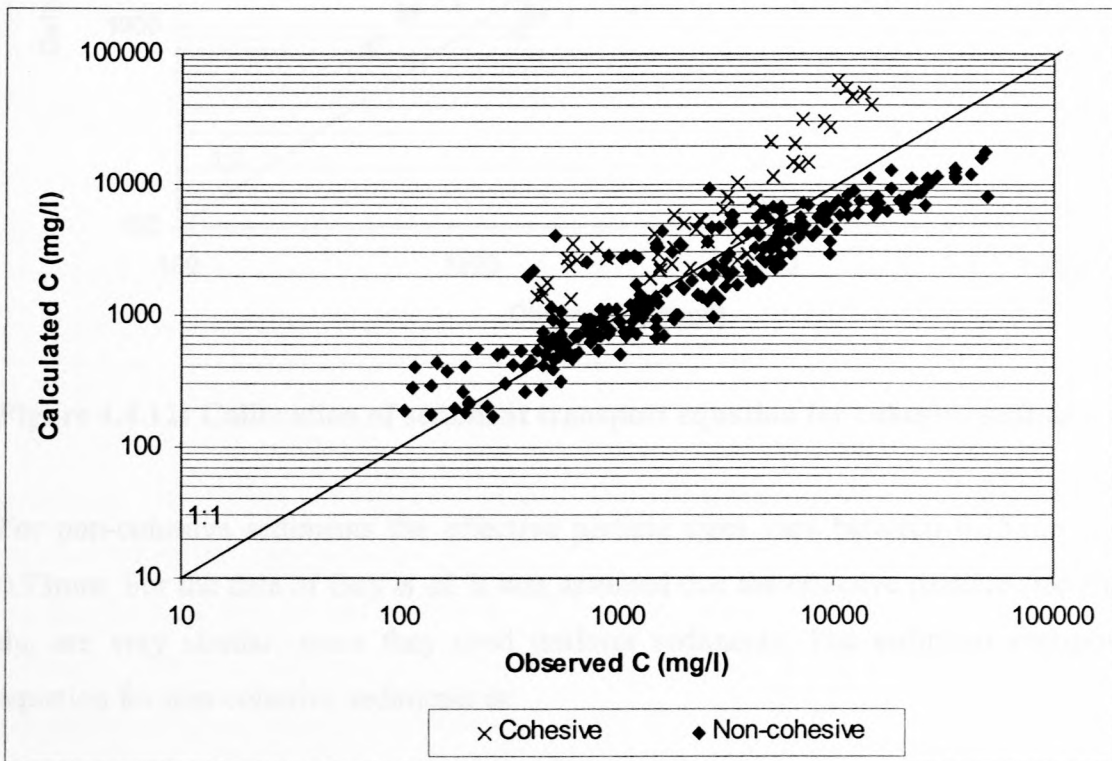


Figure 4.4.11: Calibration of sediment transport equation for both cohesive and non-cohesive sediments

For cohesive sediments the effective settling velocity of the materials in suspension was determined from the particle size distribution curve of the suspended sediments. The same particle size ranges were used as shown in **Table 4.3.2**. The effective particle size for the suspended sediments was found to be 0.025mm. **Equation 4.4.3** has only been calibrated for that effective particle size. The correlation is illustrated in **Figure 4.4.12**.

$$\log(C_t) = 3.964 + 0.812 \log\left(\frac{vS}{w_s}\right) \dots\dots\dots 4.4.3$$

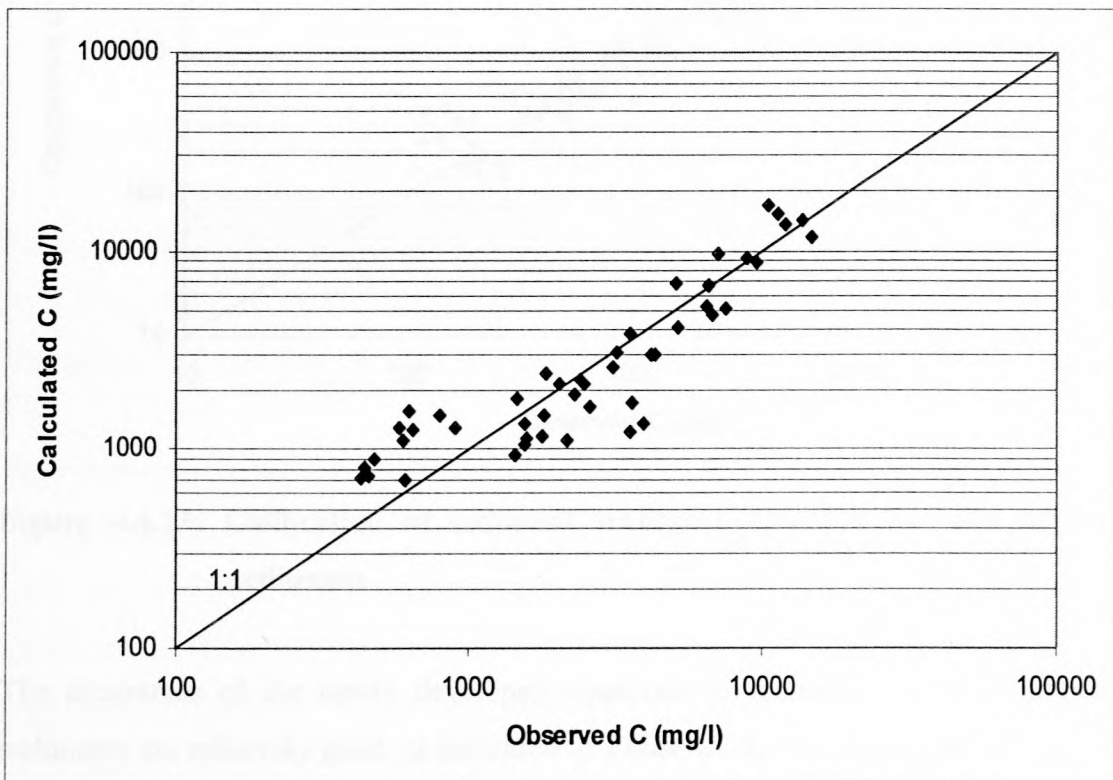


Figure 4.4.12: Calibration of sediment transport equation for cohesive sediments

For non-cohesive sediments the effective particle sizes vary between 0.15mm and 0.93mm. For the data of Guy *et al.* it was assumed that the effective particle size and d_{50} are very similar, since they used uniform sediments. The sediment transport equation for non-cohesive sediments is:

$$\log(C_t) = 4.765 + 1.160 \log\left(\frac{vS}{w_s}\right) \dots\dots\dots 4.4.4$$

The calibrated function is illustrated in **Figure 4.4.13**. With correlation coefficients of 0.81 and 0.86, respectively, the two equations show a significant improvement over **Equation 4.4.2**. All three sediment transport equations can be used for non-uniform sediment transport.

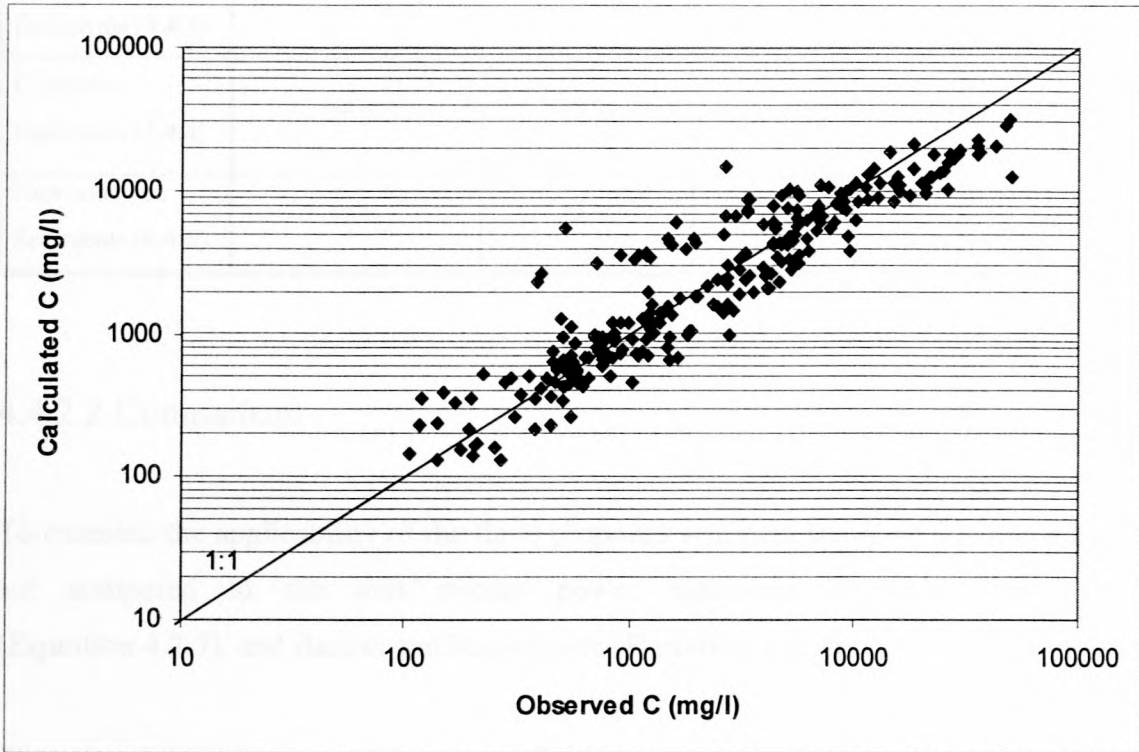


Figure 4.4.13: Calibration of sediment transport equation for non-cohesive sediments

The accuracies of the newly developed equations for cohesive and non-cohesive sediments are relatively good, as indicated in **Table 4.4.2**, with more than 80% of the predicted values varying by no more than a factor of 2. The sediment transport equation for both cohesive and non-cohesive sediments combined has a lower accuracy. The reason for this can be seen in **Figure 4.4.11** where **Equation 4.4.2** overestimates the concentrations for the cohesive sediments. A reason for this could be that the data used for the calibration of **Equation 4.4.2** are predominantly for non-cohesive sediment, and that the cohesive sediment data have very little impact on the magnitude of the calibration coefficients.

Table 4.4.2: Accuracy ranges of sediment transport equations

| Data | $0.67 < \frac{C_{calc}}{C_{obs}} < 1.5$ | $0.5 < \frac{C_{calc}}{C_{obs}} < 2$ | $0.33 < \frac{C_{calc}}{C_{obs}} < 3$ | No. of Observations |
|---|---|--------------------------------------|---------------------------------------|---------------------|
| Cohesive and Non-cohesive Sediments (4.4.3) | 46 % | 67 % | 89 % | 305 |
| Cohesive Sediments (4.4.4) | 64 % | 89 % | 100 % | 47 |
| Non-cohesive Sediments (4.4.5) | 59 % | 84 % | 95 % | 258 |

4.4.2.2 Comparison

To examine the applicability of the three proposed sediment transport equations they are compared to the unit stream power equations developed by Yang (Equation 4.2.7), and Basson and Rooseboom (Equation 4.2.15).

The comparison between the new sediment transport equation (4.4.2) for both cohesive and non-cohesive sediments, and Yang's sediment transport equation is presented in Figure 4.4.14, which shows that both equations give much the same results with similar accuracy ranges. Even better results can be found when Yang's relationship is compared to the new sediment transport equation for non-cohesive sediments alone (Figure 4.4.15). In Figure 4.4.16 the comparison between Basson and Rooseboom's unit stream power equation and the new cohesive sediment transport equation is shown, but Equation 4.2.15 for the most part predicts much higher concentrations than were observed, which could be due to the fact that the equation has been calibrated with reservoir data and non-uniform flow conditions.

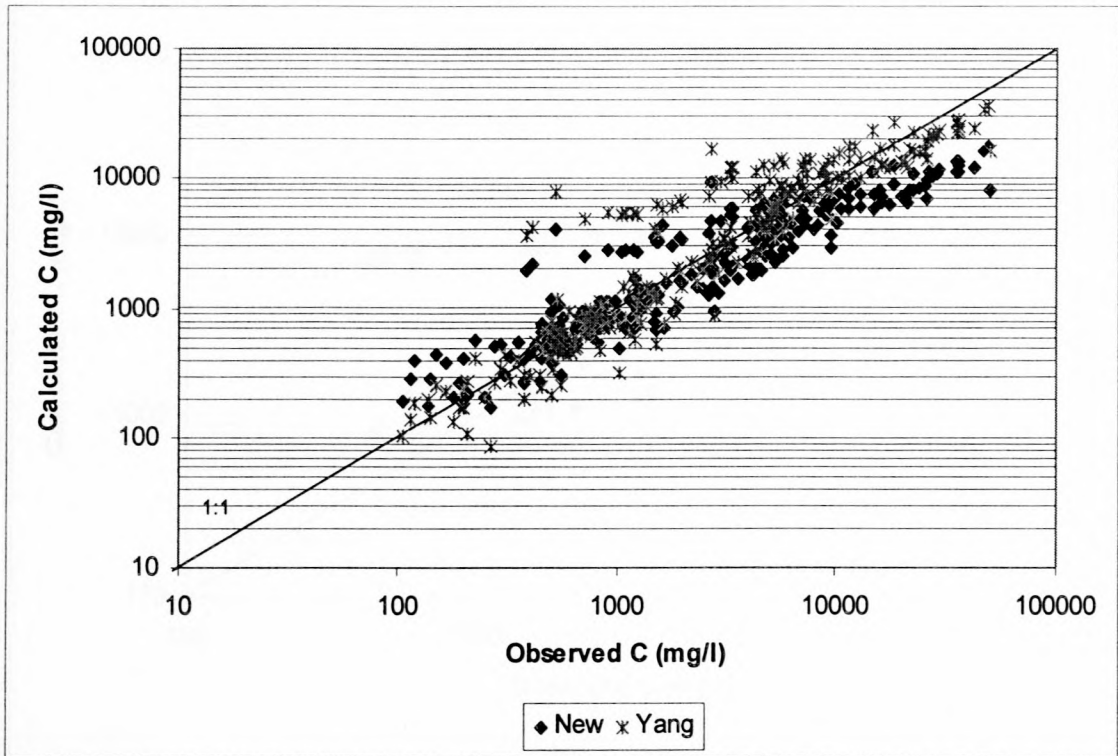


Figure 4.4.14: Comparison between sediment transport equation for cohesive and non-cohesive sediments and Yang's relationship

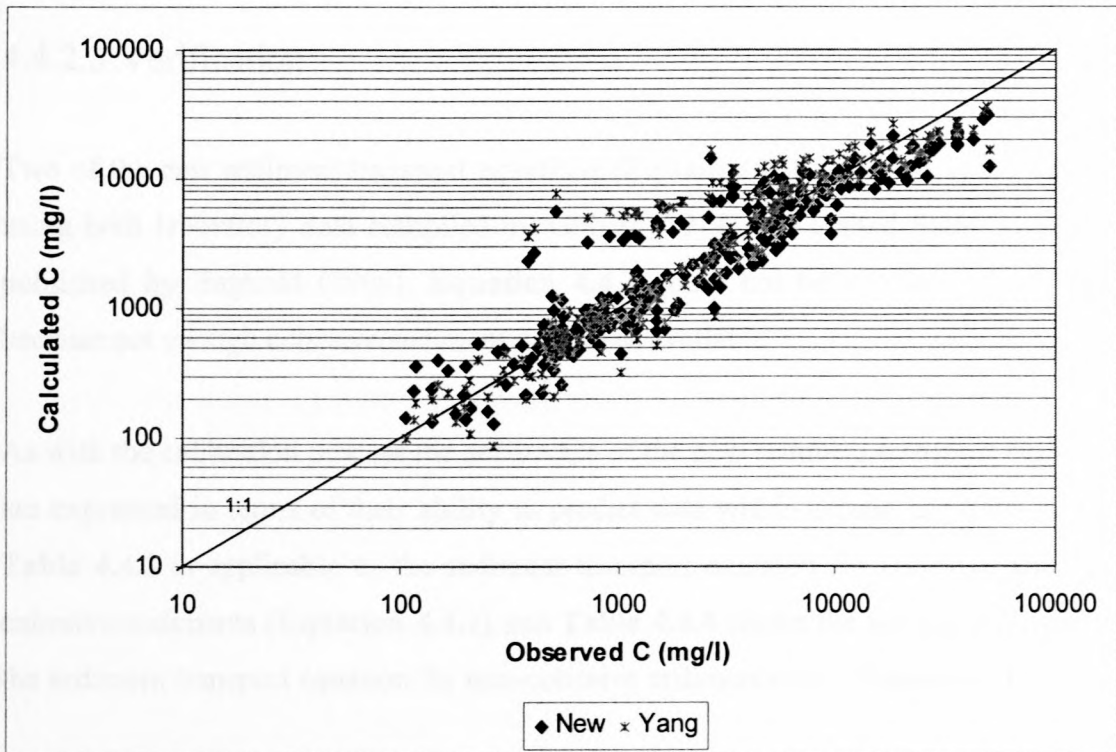


Figure 4.4.15: Comparison between sediment transport equation for non-cohesive sediments and Yang's relationship

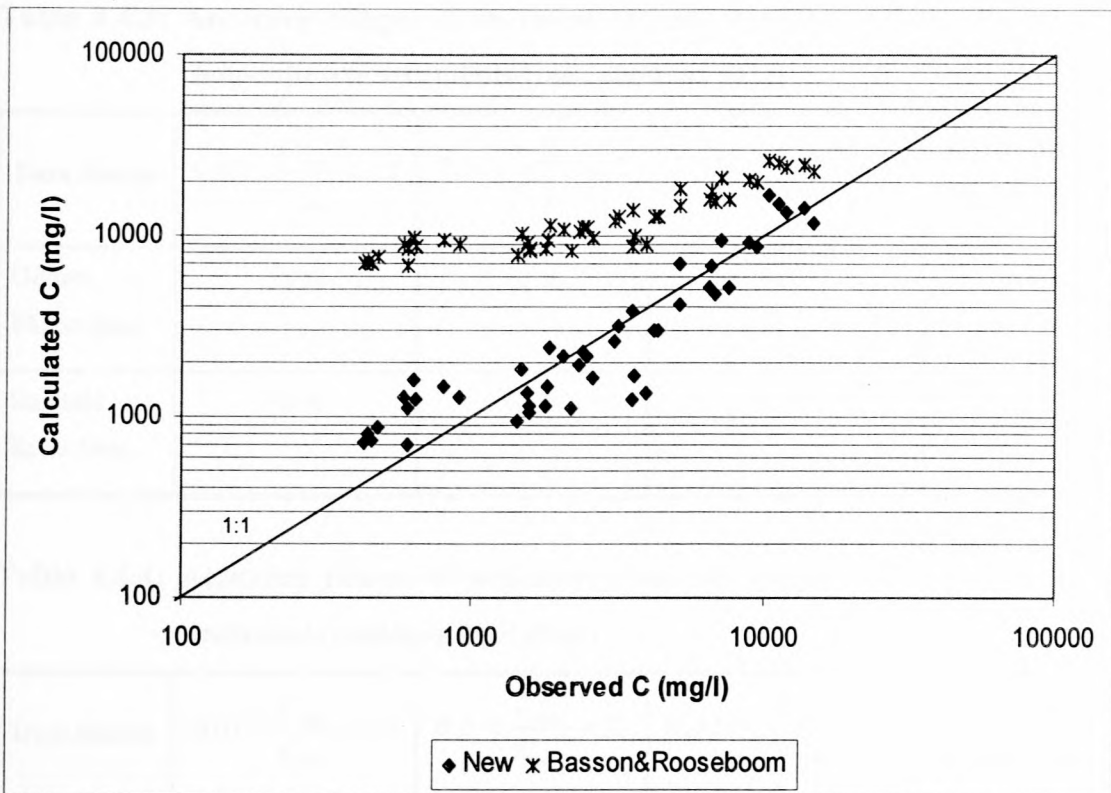


Figure 4.4.16: Comparison between sediment transport equation for cohesive sediments and Basson & Rooseboom's relationship

4.4.2.3 Verification

Two of the new sediment transport equations (**Equation 4.4.2** and **4.4.4**) are verified using both laboratory data compiled by Gilbert (1914) and United States river data published by Bagnold (1966). **Equation 4.4.3** could not be verified at this stage because not enough cohesive sediment data were available.

As with the calibration process the accuracies of the new sediment transport equations are expressed in terms of their ability to predict data within certain accuracy ranges. **Table 4.4.3** is applicable to the sediment transport equation for cohesive and non-cohesive sediments (**Equation 4.4.2**) and **Table 4.4.4** shows the accuracy ranges for the sediment transport equation for non-cohesive sediments only (**Equation 4.4.4**).

Table 4.4.3: Accuracy ranges of sediment transport equation for cohesive and non-cohesive sediments (independent data)

| Data Source | $0.67 < \frac{C_{calc}}{C_{obs}} < 1.5$ | $0.5 < \frac{C_{calc}}{C_{obs}} < 2$ | $0.33 < \frac{C_{calc}}{C_{obs}} < 3$ | No. of Observations |
|--------------------|---|--------------------------------------|---------------------------------------|---------------------|
| Gilbert Flume Data | 28 % | 61 % | 94 % | 615 |
| Bagnold River Data | 38 % | 62 % | 83 % | 122 |

Table 4.4.4: Accuracy ranges of sediment transport equation for non-cohesive sediments (independent data)

| Data Source | $0.67 < \frac{C_{calc}}{C_{obs}} < 1.5$ | $0.5 < \frac{C_{calc}}{C_{obs}} < 2$ | $0.33 < \frac{C_{calc}}{C_{obs}} < 3$ | No. of Observations |
|--------------------|---|--------------------------------------|---------------------------------------|---------------------|
| Gilbert Flume Data | 57 % | 89 % | 100 % | 615 |
| Bagnold River Data | 45 % | 80 % | 95 % | 122 |

Table 4.4.4 shows that the accuracy of Equation 4.4.4 is very good, since the accuracy ranges for the independent flume data are even better than for the data used in the calibration process. This can also be seen in Figure 4.4.17, as all the data lie in a very narrow band. Equation 4.4.4 even predicts river data fairly well with 80% of the predicted values varying by no more than a factor of 2, although the scatter is much greater than for laboratory data (Figure 4.4.18). The sediment transport equation for both cohesive and non-cohesive sediments shows slightly lower accuracies, which is to be expected considering that the correlation coefficient is only 0.75.

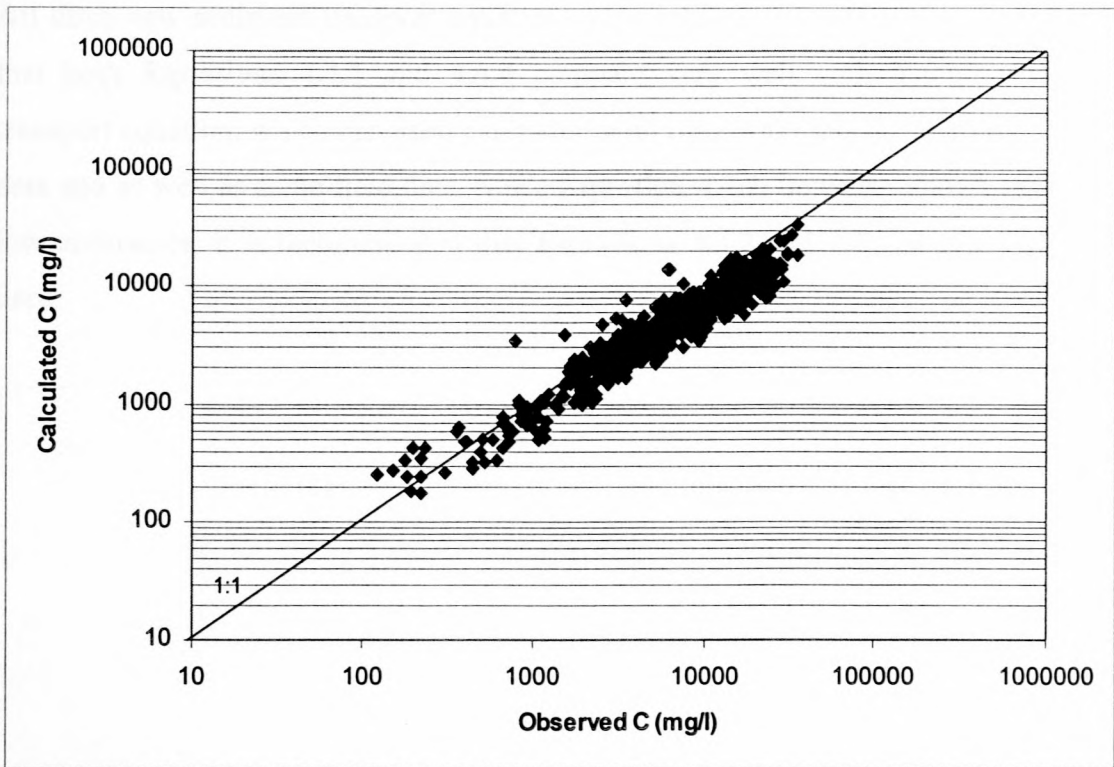


Figure 4.4.17: Verification of sediment transport equation for non-cohesive sediments with independent flume data

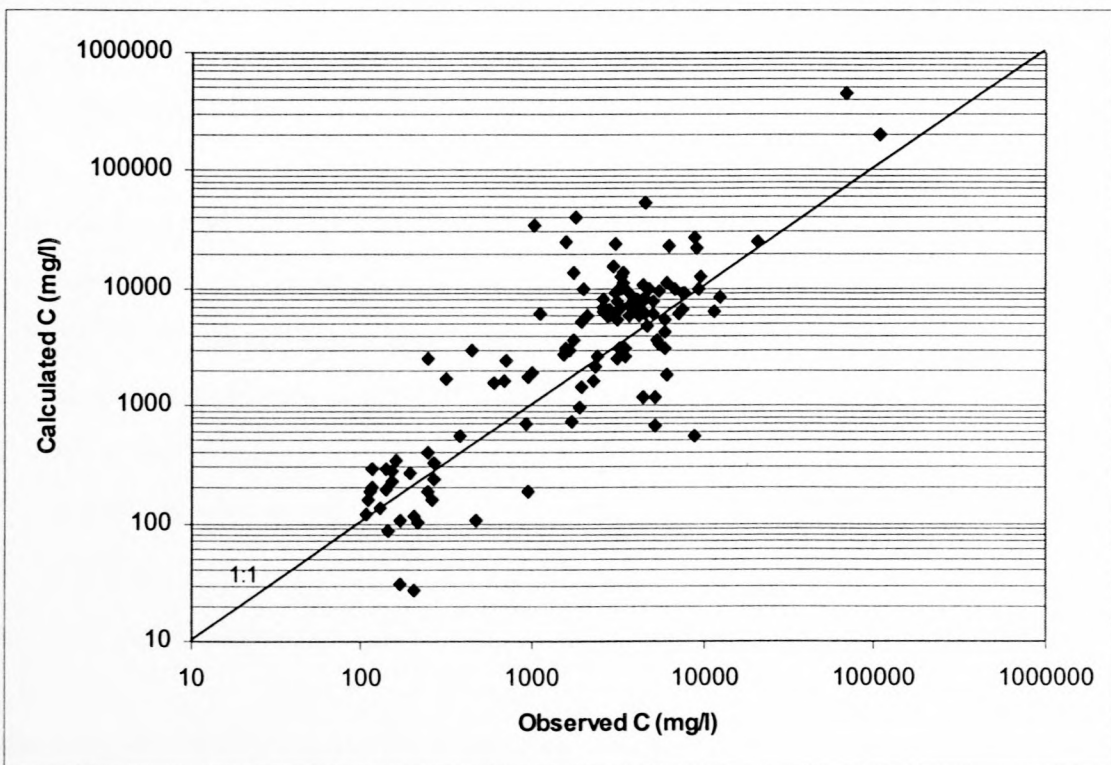


Figure 4.4.18: Verification of sediment transport equation for non-cohesive sediments with independent river data

All three new sediment transport equations give relatively good results, considering that both **Equations 4.4.2** and **4.4.4** compare very well with Yang's sediment transport equation, which has been calibrated with over 1000 sets of laboratory flume data and as well as some field data. Since **Equation 4.4.2**, however, shows relatively low accuracies, it is recommended that **Equations 4.4.3** and **4.4.4** should rather be used.

In Chapter 3, this is because the regression analysis showed that the effect of increasing or decreasing turbidity on the sediment transport rate is increased riparian vegetation and the effect of increasing or decreasing bed material or suspended sediment. Factors such as the effect of the effects of smaller flows, the difference in roughness between the flood plain and the effect of fine sediment are not included in the model.

The 1D mathematical model HEC-11 was used to simulate the flow and sediment transport in the post-dam river morphology of the Fongda River downstream of the Dam. The theory developed in Chapter 4 was implemented in the model.

5.1 Mathematical Model

The model used for the simulation is the one-dimensional (1D) model developed by the Danish Hydraulic Institute (DHI) for the simulation of sediment transport and water quality in rivers, estuaries and coastal waters. The model comprises several components, of which only the first two are used in this project:

- River modelling
- NAM – rainfall-runoff
- Flood forecast
- Unit hydrographs

The river-modelling component consists of several modules of which the following three were used in this project:

- Hydrodynamic (HD)

5. Numerical Modelling of the River Morphology Downstream of Dams

Chapter 3 has shown that regime equations alone are not adequate in determining the changes in river morphology that are due to the construction of a dam. As pointed out in **Chapter 3**, this is because the regime equations do not take into consideration the effect of increasing or decreasing durations of certain flood peaks, the significance of increased riparian vegetation and the effect of presence of clay and silt in either the bed material or suspended sediment. Factors such as the duration of certain flows, the effects of smaller flows, the difference in roughness between the river channel and the flood plain and the effect of fine sediments can be dealt with by a mathematical model.

The 1D mathematical model MIKE 11 was used to simulate both the natural as well as the post-dam river morphology of the Pongola River downstream of Pongolapoort Dam. The theory developed in **Chapter 4** was implemented in the model.

5.1 Mathematical Model

The model used for the simulations is the one-dimensional model MIKE 11, developed by the Danish Hydraulics Institute (DHI) for the simulation of flows, sediment transport and water quality in rivers, estuaries and similar water bodies. The model comprises several components, of which only the first was used:

- River modelling
- NAM – rainfall-runoff
- Flood forecast
- Unit hydrograph

The river-modelling component consists of several modules of which the following three were used in this project:

- Hydrodynamic (HD)

- Advection-dispersion (AD)
- Non-cohesive sediment transport and morphology (NST)

The overview given here is a short summary of the general descriptions of aspects of the MIKE 11 modelling system, as given in the MIKE 11 Reference Manual (DHI, 1992).

5.1.1 Hydrodynamic Module

The MIKE 11 hydrodynamic (HD) module is an implicit, finite difference model for the computation of unsteady flows in rivers and reservoirs, based on the St Venant equations representing conservation of mass and momentum. The model can describe both subcritical as well as supercritical flow conditions, and modules are incorporated that describe flow past hydraulic structures. The model can be applied to looped networks and quasi two-dimensional flow simulation on flood plains. The HD module provides three different flow descriptions:

- The dynamic wave approach, which uses the full momentum equation.
- The diffuse wave approach, which only models the bed friction, gravity forces and the hydrostatic gradient terms of the momentum equation.
- The kinematic wave approach, where the flow is calculated on the assumption of a balance between the friction and gravity forces. Backwater effects cannot be simulated.

5.1.2 Advection-Dispersion Module

The advection-dispersion (AD) module is based on the one-dimensional equation of the conservation of mass of a dissolved suspended material, i.e. the advection-dispersion equation. The module requires the output from the hydrodynamic module in terms of discharges and water levels. The advection-dispersion equation is solved numerically using the implicit finite difference scheme. Part of the AD module is the cohesive sediment transport (CST) module, which uses the AD module to describe the

transport of suspended cohesive sediments, because unlike non-cohesive sediment transport, the cohesive sediment transport cannot be described by local parameters only. The erosion and deposition of cohesive sediments is modelled as a source/sink term in the advection-dispersion equation.

The unit input stream power equation was implemented in the MIKE 11 model for the transport of fine sediments (Basson and Rooseboom, 1996) by using user-defined parameters A and B :

$$\log(C) = A + B \log\left(\frac{vS}{w}\right) \dots\dots\dots 4.2.5$$

The parameters have been determined in **Chapter 4**: $A = 3.964$ and $B = 0.812$.

5.1.3 Non-Cohesive Sediment Transport Module

The non-cohesive sediment transport (NST) module can be run in two modes: explicit and morphological. In the explicit mode output is required from the HD module, but no feedback occurs from the NST module to the HD module. In the morphological mode sediment transport is calculated together with the HD module and feedback is given from the NST module to the HD module. The results are in the form of bed level changes, sediment transport rates and bed resistance. The morphological model updates either the whole cross-section or only a part of it (generally the part representing the river channel).

Traditional sediment transport equations such as Ackers and White, and Engelund and Hansen are incorporated in the MIKE 11 model for non-cohesive sediment transport. All of these can be run with a single representative particle size or a number of particle sizes.

5.2 Case Study

Pongolapoort Dam was completed in 1973 on the Pongola River (**Figure 5.2.1**) and is located in northern Kwazulu-Natal close to the Swaziland border. The Pongola River floodplain below the dam flows through the Makatini Flats, with numerous pans, before reaching the border to Mozambique (**Figure 5.2.2**). The reservoir is one of the largest in South Africa with a full supply capacity of 2445 million m³ (app. 2 MAR). The dam was built mainly for irrigation, storage and domestic use, but the most water is actually used for artificial flood releases (sometimes more than 300 million m³/a). The reach of the Pongola River downstream of the dam is steeper (typical slope is about 0.001) for about 40 km than the terrain further downstream. Most of the pans are also situated downstream of the 40 km mark. For the purpose of this thesis only the first 40 km was modelled. Some of the natural flood peaks are summarised in **Table 5.2.1**.



**Figure 5.2.1: Pongola River directly below Pongolapoort Dam
(app. 400 m³/s discharge)**

Table 5.2.1: Pongola River flood peaks – natural

| Recurrence interval (years) | Flood peak (m ³ /s) |
|-----------------------------|--------------------------------|
| 2 | 765 |
| 5 | 1367 |
| 10 | 1877 |
| 20 | 4640 |
| 50 | 10451 |
| 100 | 11158 |



Figure 5.2.2: Pongola River map

The Pongola River has been selected for a case study because:

- Relatively long flow records are available both upstream and downstream of the dam.
- Detailed surveys of the river and the flood plains before the dam was built were undertaken.
- Aerial photographs from 1996 are available.

Since the dam was built releases from the reservoir have been strongly controlled with flood peaks of between 300 and 800 m³/s being released once or twice a year. For the purpose of this thesis the controlled releases were not modelled. The characteristics of Pongolapoort Reservoir, such as the storage-area relationship, were used to set up a reservoir balance to determine an outflow sequence that is more representative of normal reservoir operations without artificial flood releases. The reservoir basin characteristics such as rainfall and evaporation were obtained from WR90 (Midgley *et al.*, 1990), also shown in **Table 5.2.2**. The inflow sequence (daily values) and the daily irrigation demand were obtained from gauging stations from the Department of Water Affairs and Forestry (DWAFF). The gauging station from which the inflow sequence was obtained was situated upstream of the dam, but this station had the longest record available (39 years). Using the cumulative discharge curve over that period as a reference, a 10-year representative period was chosen (1950 – 1960). In the 10-year period some of the data were missing and the total usable data amounted to about nine years, however, the period under consideration will still be called a 10-year period. The extra demand placed on the water stored in the reservoir for two of the scenarios was obtained from the storage-draft-frequency curves of WR90. Three 10-year outflow sequences were thus determined, as shown in **Figures 5.2.3 to 5.2.6**, of which parts were used as input to the model.

Table 5.2.2: Pongolapoort Dam - catchment characteristics

| | |
|--|--------|
| MAP (mm) | 581 |
| MAE (mm) | 1500 |
| MAR (10 ⁶ m ³) | 1160 |
| Upstream gauging station (7081 km ²) | W4H002 |
| Irrigation gauging station | W4H014 |
| Catchment area (km ²) | 7831 |
| Hydro zone | Q |

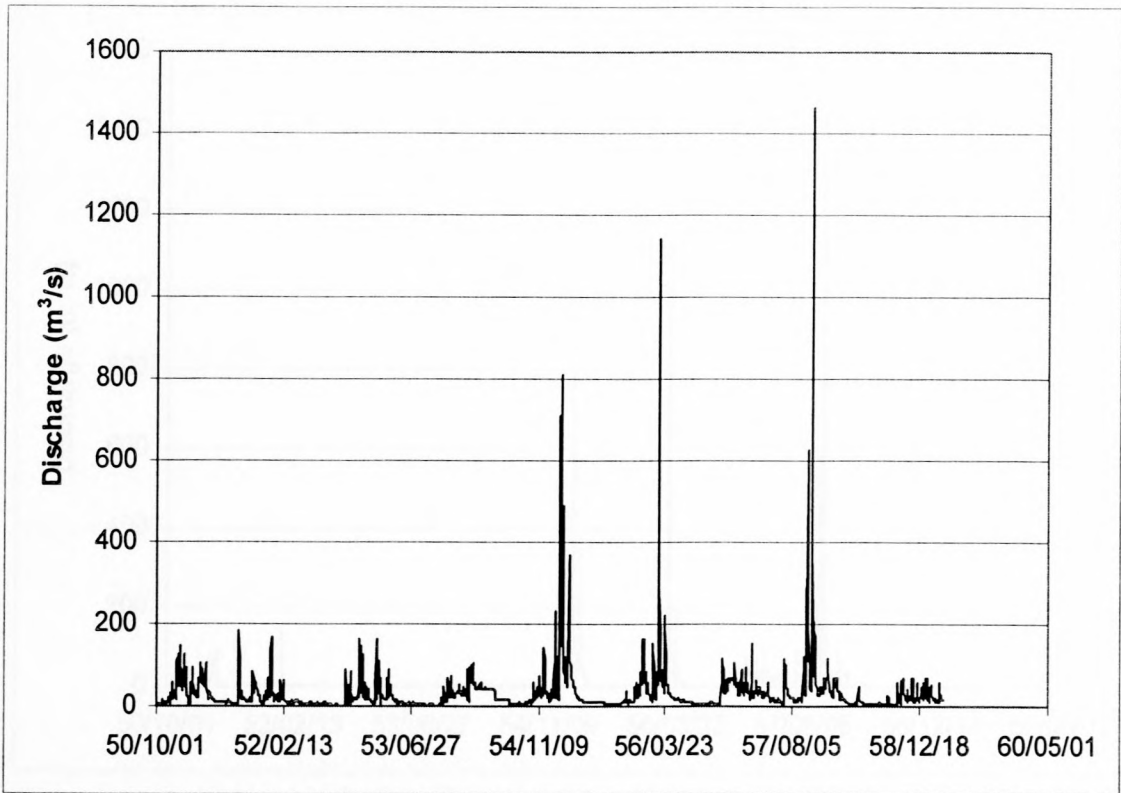


Figure 5.2.3: Natural 10-year flow sequence



Figure 5.2.4: 10-year flow sequence with 2MAR reservoir and 16% MAR demand (2MAR)

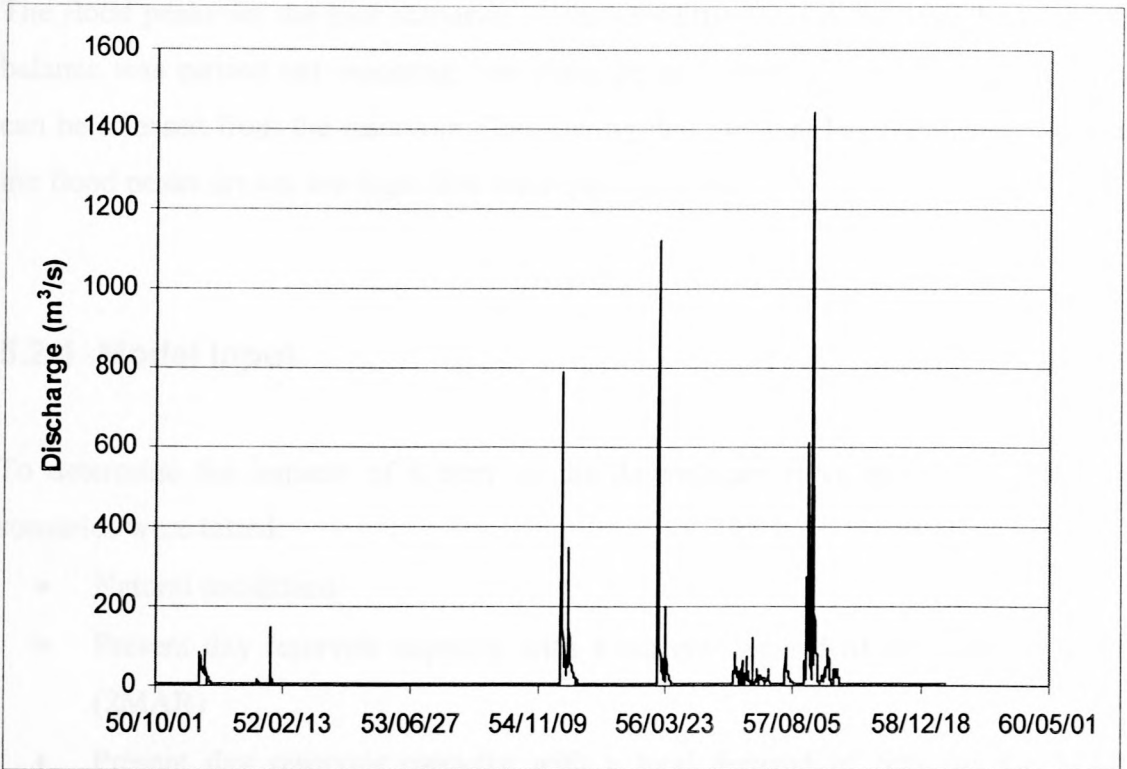


Figure 5.2.5: 10-year flow sequence with 2MAR reservoir and 60% MAR demand (2MAR60)

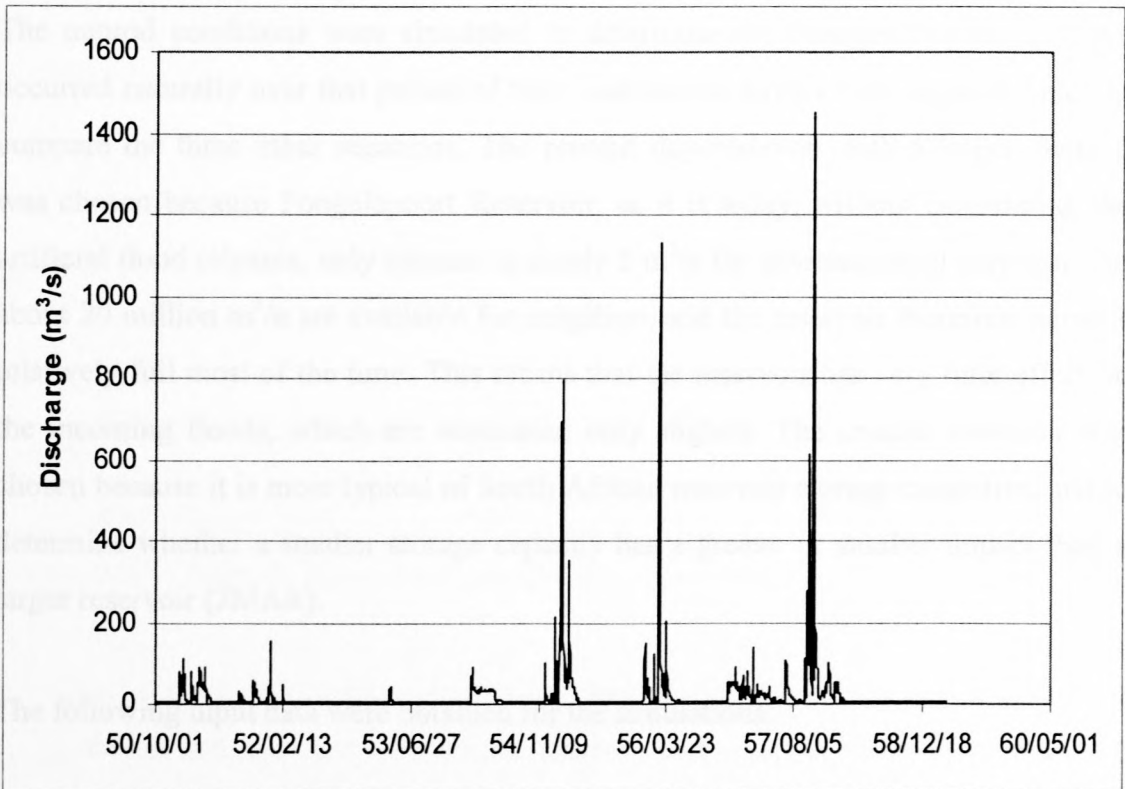


Figure 5.2.6: 10-year flow sequence with 1MAR reservoir and 45% MAR demand (1MAR45)

The flood peaks for the four scenarios differ very little. This is because the reservoir balance was carried out assuming that there are no restrictions on how much water can be released from the reservoir. Considering that the dam has floodgates and that the flood peaks are not too high, this assumption is valid.

5.2.1 Model Input

To determine the impacts of a dam on the downstream river reach the following scenarios were tested:

- Natural conditions
- Present day reservoir capacity with a current demand of 16% of the MAR (2MAR)
- Present day reservoir capacity with a total demand of 60% of the MAR (2MAR60)
- 1MAR reservoir capacity with a total demand of 45% of the MAR (1MAR45)

The natural conditions were simulated to determine the changes that would have occurred naturally over that period of time, and also to have a basis against which to compare the three other scenarios. The present day reservoir with a larger demand was chosen because Pongolapoort Reservoir, as it is today, without considering the artificial flood releases, only releases a steady $5 \text{ m}^3/\text{s}$ for environmental purposes and about 20 million m^3/a are available for irrigation, and the reservoir therefore remains relatively full most of the time. This means that the reservoir has very little effect on the incoming floods, which are attenuated only slightly. The smaller reservoir was chosen because it is more typical of South African reservoir storage capacities, and to determine whether a smaller storage capacity has a greater or smaller impact than a larger reservoir (2MAR).

The following input data were obtained for the simulations:

- Cross-sections: 80 cross-sections of the Pongola River downstream of the dam were obtained from topographical maps (1933 and 1957) for the 40 km reach

(shown in **Figure 5.2.7**). Typically the distance between sections is 500 m. **Appendix C1** contains the whole set of cross-sections.

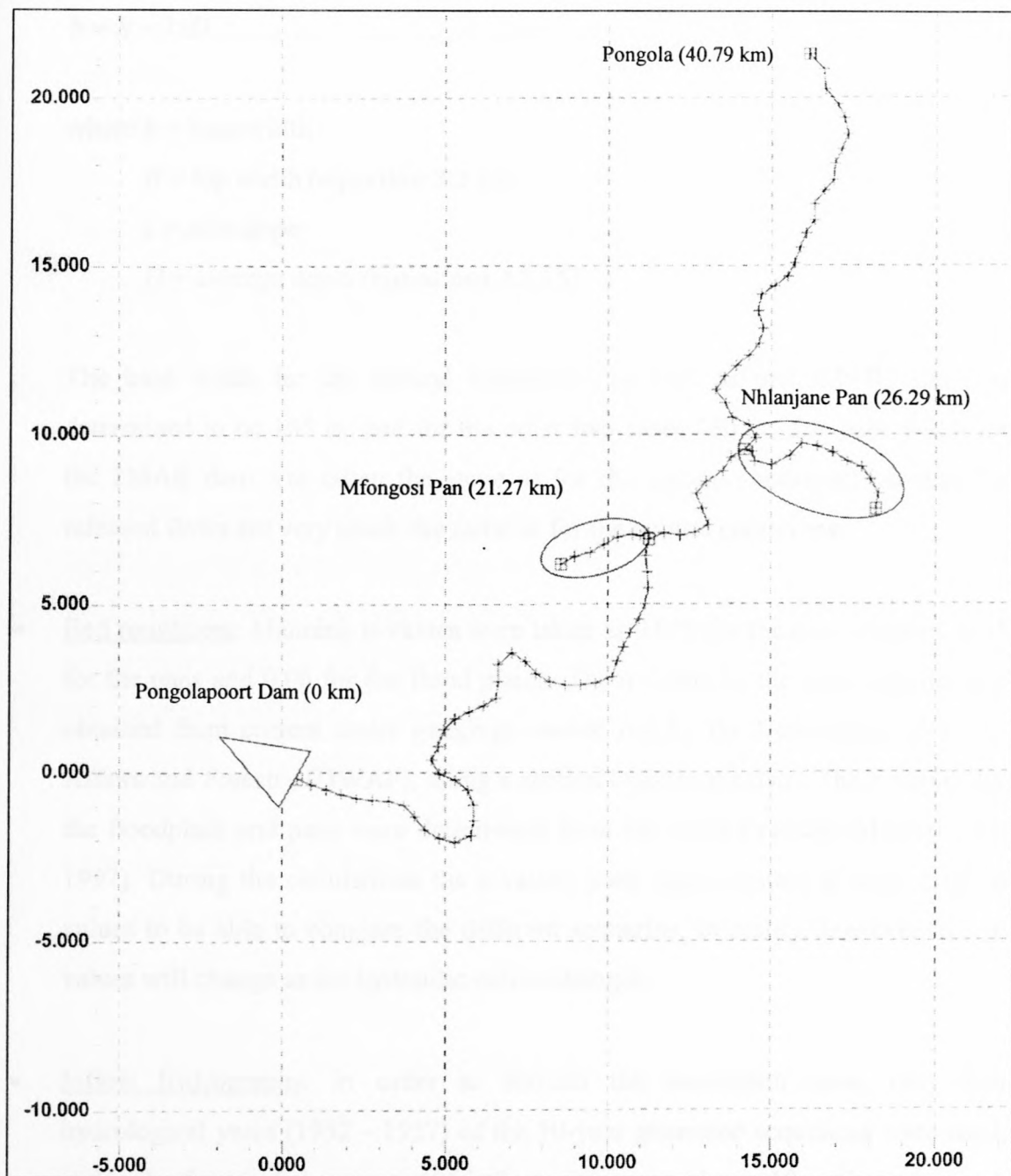


Figure 5.2.7: Pongola River reach modelled (with chainages shown in brackets)

- Cross-section deformation: During erosion and deposition it is assumed that the cross-section will have a trapezoidal shape with a constant base width, side slope of 1:2 and a varying depth. This means that the same basic cross-sectional shape remains, but will be lowered or elevated depending on whether the riverbed

undergoes erosion or deposition. The base width was derived with the aid of the regime equations developed in **Chapter 3**.

$$b = B - 2zD \dots\dots\dots 5.3.1$$

where b = base width

B = top width (**equation 3.3.13**)

z = side slope

D = average depth (**equations 3.3.15**)

The base width for the natural conditions, as well as the 2MAR dam was determined to be 165 m, and for the other two cases 130 m. The base width for the 2MAR dam was taken the same as for the natural conditions because the released flows are very much the same as for the natural conditions.

- **Bed roughness:** Manning n -values were taken as 0.039 for the river channel, 0.05 for the pans and 0.06 for the flood plains. The n -value for the river channel was obtained from current meter gaugings carried out by the Department of Water Affairs and Forestry (DWAF), along a section close to the dam. The n -values for the floodplain and pans were determined from the Road Drainage Manual (DT, 1997). During the simulations the n -values were kept constant at their original values to be able to compare the different scenarios. In reality, however, the n -values will change as the hydraulic radius changes.
- **Inflow hydrographs:** in order to shorten the simulation time, only five hydrological years (1952 – 1957) of the 10-year generated sequences were used, and only flows of the generated inflow sequences above $10 \text{ m}^3/\text{s}$ were used, because flows smaller than $10 \text{ m}^3/\text{s}$ will probably have very little influence on the sediment transport and morphology. For flood peaks greater than $500 \text{ m}^3/\text{s}$ primary data was used instead of daily flow data because the differences between the daily values and the actual flood peak were quite significant in some instances, and a flood peak of $1500 \text{ m}^3/\text{s}$ has a very different sediment transport capacity than a $1000 \text{ m}^3/\text{s}$ flood peak.

- Sediment fractions in the bed: only two sediment fractions were used. Fraction 2, with a diameter of 0.24 mm, was estimated from particle size distribution curves of samples taken upstream of the dam (Kovacs *et al.*, 1985) where 0.24 mm was found to be the effective particle size. Fraction 1 was added to represent fine sediments, with an effective particle size of 0.035 mm. The fractions and their respective proportion of the bed material are shown in **Table 5.2.3**.

Table 5.2.3: Sediment fractions of bed sediment

| Fraction | Particle size (mm) | Percentage of sediment size in fraction |
|----------|--------------------|---|
| 1 | 0.035 | 5 |
| 2 | 0.24 | 95 |

- Sediment load: for the natural conditions a sediment input sequence was generated for two sediment fractions with particle sizes of 0.24 mm and 0.035 mm respectively. Comparing suspended sediment concentrations taken on the Pongola River to calculated sediment concentrations (Engelund and Hansen's sediment transport formula) for 0.24 mm, it was determined that about 60% of the suspended sediment concentrations had to be made up of material finer than the 0.24 mm. A sequence of suspended sediment concentrations was determined by means of a sediment load-discharge rating curve for the natural inflow hydrograph and 60% assigned to a particle size of 0.035 mm and 40% assigned to the coarser particle size of 0.24 mm. The total sediment input is shown in **Figure 5.2.8**.
- Storage areas: two pans (Mfongosi and Nhlanjane) are connected with the river on the 40 km reach under consideration. The effect of the pans was modelled by assigning storage areas at certain elevations for each of the pans shown in **Appendix C3** (DWA, 1987). In this way the volume of water stored in the pans could be accounted for. The MIKE 11 model is capable of simulating the flow over a weir, which would be more correct in the case of a pan, where the water level in the river channel has to rise above a point before spilling into the pans, but this caused instabilities in the program due to sediment build-up at the weir.

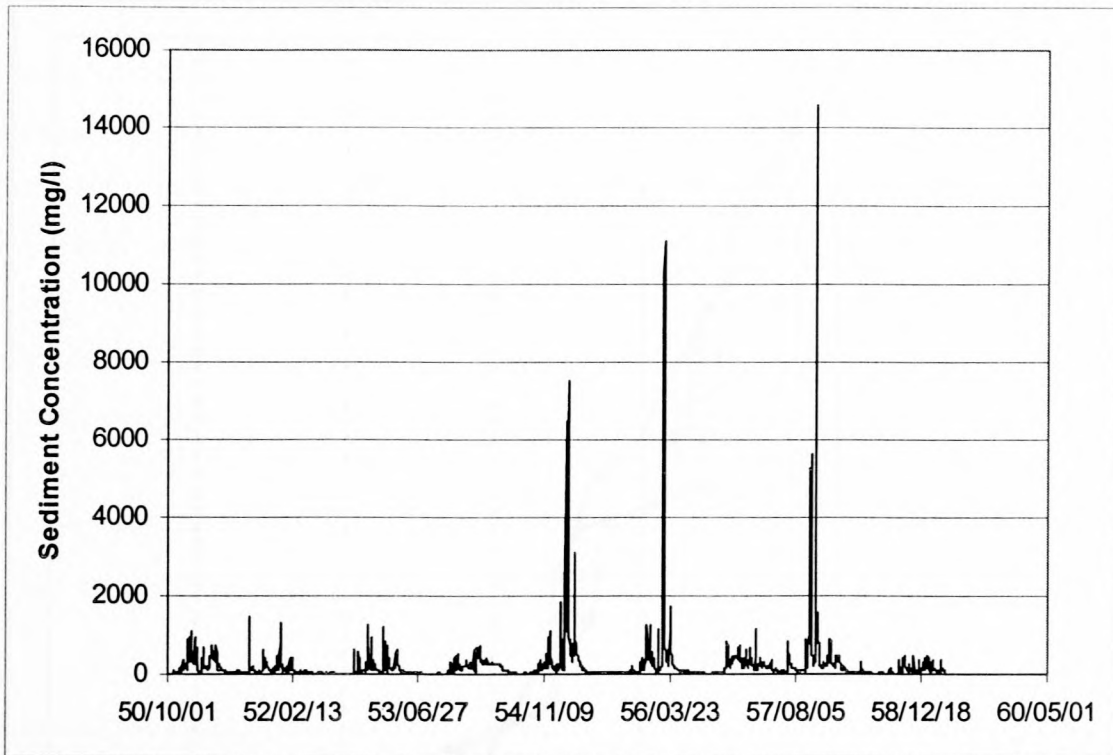


Figure 5.2.8: Sediment input over 10-year period

- Q-h boundary: at the downstream end of the river reach under consideration a Q-h boundary was set up relating the elevation above mean sea level to the discharge. The characteristics of the cross-section at km 40.79 were taken and the discharge calculated with Chezy's flow resistance formula (3.3.12).
- Cohesive sediments: for cohesive sediment the critical shear stresses for erosion and deposition had to be specified. The values are $\tau_c = 10$ Pa for deposition and $\tau_c = 12$ Pa for mass erosion.

5.3 Discussion of Simulation Results

The natural conditions were simulated to determine whether the assumptions that have been made, such as the adopted sediment fractions, are accurate and also to have a basis against which to compare the different dam scenarios. From **Figure 5.3.1** it can be seen that the bed level has changed somewhat. In some places erosion took place, most noticeably between km's 20 and 27.

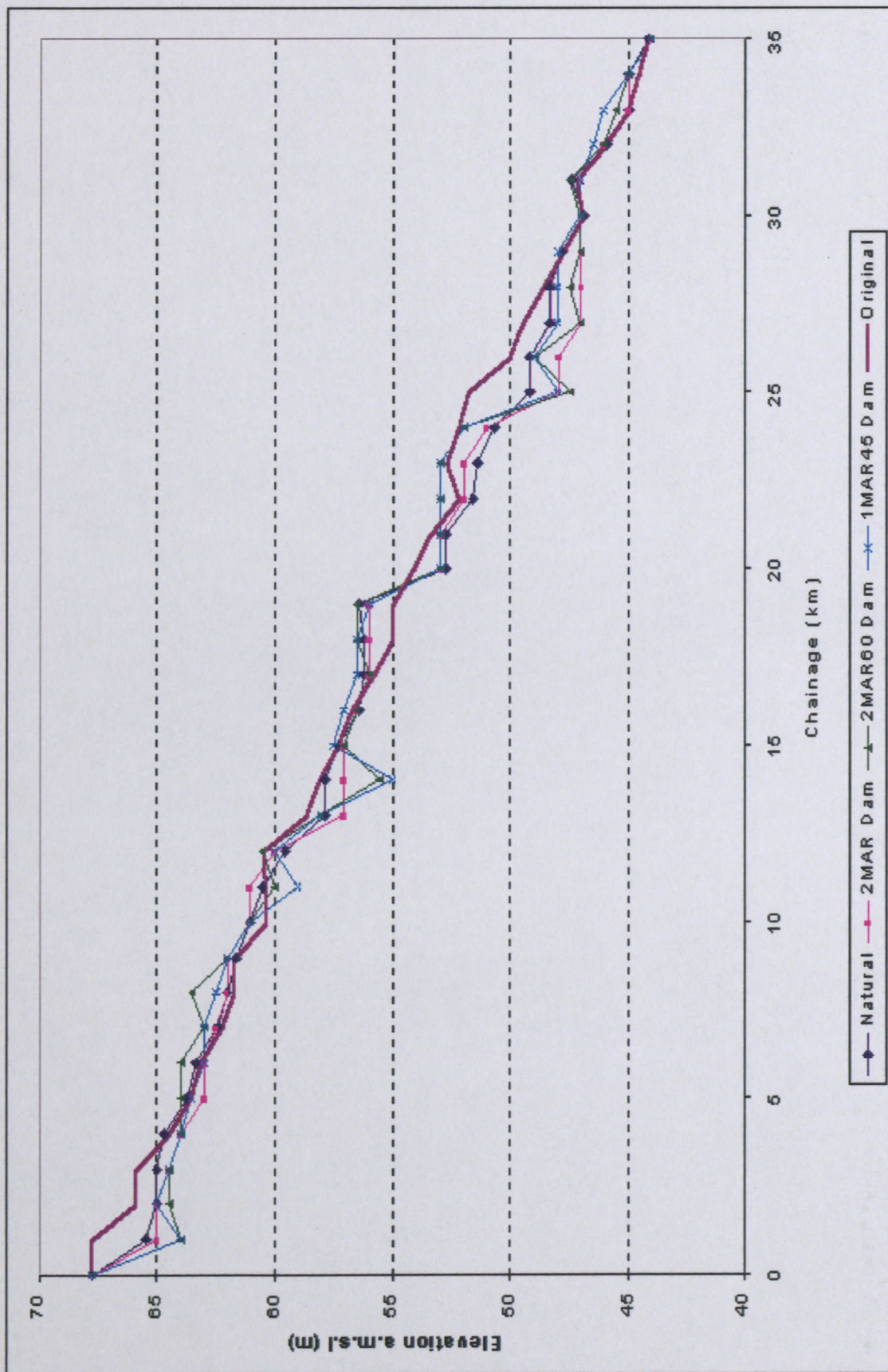


Figure 5.3.1: Simulated bed levels

This could be a result of sudden changes in cross-section or local slope changes, which could have resulted in higher velocities in that reach. Another reason could be that the effect of tributaries has not been taken into consideration. A tributary enters the Mfongosi Pan (km 21.27) and could have supplied sediments that could have prevented the erosion that occurs below that point. It has to be remembered, however, that **Figure 5.3.1** only shows the final bed levels at the end of the simulations. During the simulations there was actually a built-up of sediments at lower flows, which were subsequently removed by the larger floods. Just before the end of the simulation time a small flood moved through the system, which could have caused some of the erosion seen in **Figure 5.3.1**. The overall effect, however, was that the general bed slope has flattened to some degree.

From **Figure 5.3.2** it can be seen that the bed material has become somewhat finer, with the fine fraction (0.035 mm) increasing slightly from 5 to 8%, and the coarser fraction (0.24 mm) changing from 95 to 92%.

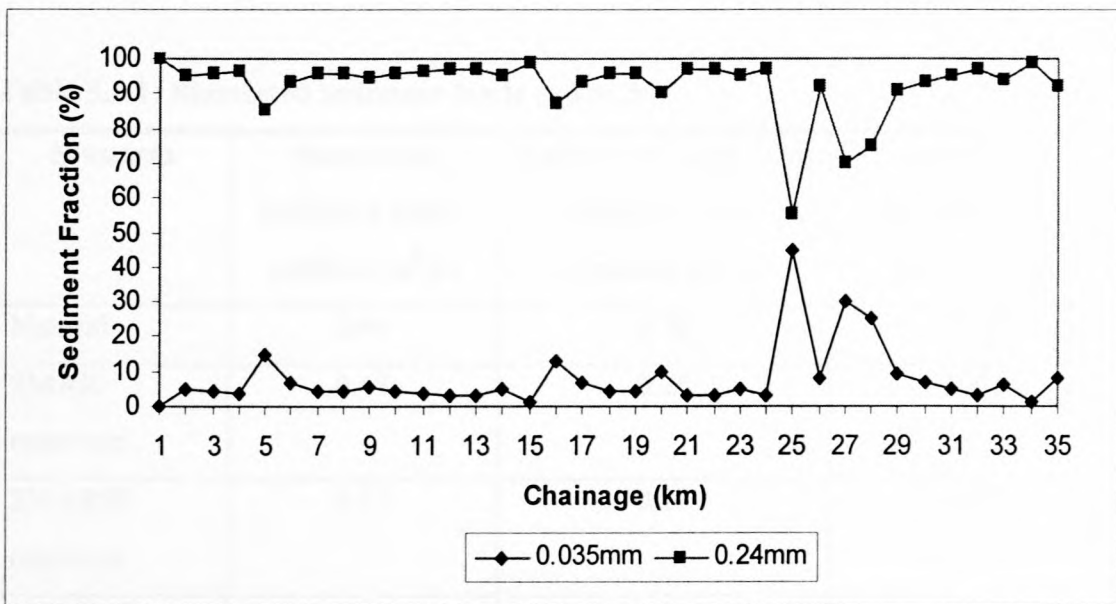


Figure 5.3.2: Simulated sediment fractions – natural conditions

The simulated sediment load (taken at km 35 to avoid the influence of the Q-h boundary at km 40) over the 5-year time period is 0.46 million m³/a, which corresponds to a simulated long-term sediment yield of 119 ton/km².a, which is very close to the average sediment yield determined from observed records (Rooseboom, 1992) of 133 ton/km².a, and to the sediment input upstream. There is therefore a

balance between the incoming and outgoing sediment. This, together with the fact that there were relatively little changes in the bed level and in the sediment fractions, means that the assumptions that have been made are relatively accurate.

The long-term sediment yield was determined by obtaining a sediment load-discharge rating curve from the five years of simulated data and applying that rating curve to the 39 years of observed flow data from which the inflow hydrographs were also determined. Not all the simulated data was used for this rating curve. During the first few months of the simulation time there were relatively high sediment transport rates, because of the initially large amounts of erosion taking place. After a while, however, the sediment transport rates became lower and more stable. Therefore the sediment load-discharge rating curve was fitted through the band of data lying lowest on the graphs. The results are summarised in **Table 5.3.1**. The sediment yields of the three dam development scenarios were calculated, based on the effective catchment area downstream of the dam, i.e. 680 km².

Table 5.3.1: Simulated sediment loads at km 35

| Scenario | Simulated sediment load ¹ (million m ³ /a) | Calculated long-term sediment load ² (million m ³ /a) | Long-term sediment yield ² (ton/km ² .a) |
|------------------|---|--|---|
| Natural | 0.46 | 0.38 | 119 |
| 2MAR reservoir | 0.48 | 0.28 | 1091 |
| 2MAR60 reservoir | 0.37 | 0.27 | 1052 |
| 1MAR45 reservoir | 0.31 | 0.29 | 1130 |

¹ Based on 5-year simulation time

² Based on 39 years of observed flow data

The 2MAR reservoir without any additional demand had by far the greatest impact of all three reservoir scenarios. This was to be expected since the incoming flows are released from the reservoir almost unchanged, but the reservoir holds all the sediment

back. The bed sediment has become slightly coarser with the fine sediment fraction decreasing to 4%. This might not seem like much, but by comparing **Figures 5.3.3 to 5.3.5**, it can be seen that the fine sediment fraction with the 2MAR reservoir has never risen above 13% at any point, whereas for the other reservoirs the fine fraction has risen to as much as 34%.

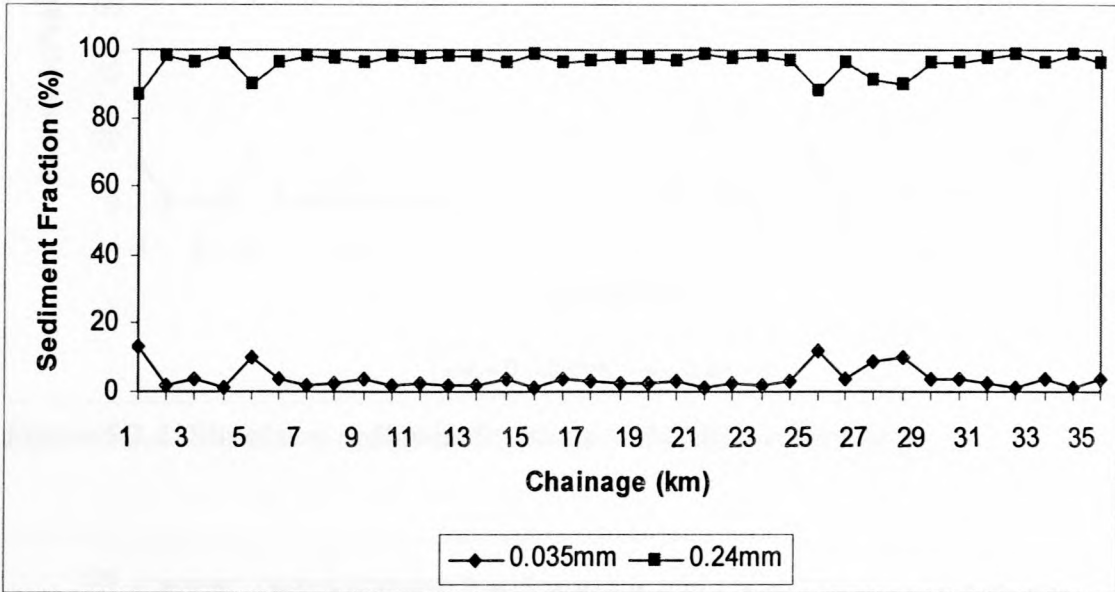


Figure 5.3.3: Simulated sediment fractions – 2MAR reservoir

The overall bed level has not changed much in comparison with the natural conditions, except for some erosion below km 25. However, the simulated sediment load has actually increased in comparison with the natural conditions to 0.48 million m^3/a . In the long-term the situation appears to be slightly improved, with a sediment load that is lower than the natural long-term value by about 26%. Considering, however, that there is no sediment input at the upstream boundary, as in the case of the natural conditions, and no tributary contributions, all of the sediment had to come from the river alone. This means that quite a large amount of scouring must have taken place.

The other two reservoirs (2MAR60 and 1MAR45) had less of an impact, due to the fact that either reservoir absorbs most of the smaller flows. The results obtained for the two are very similar, which is not surprising, considering that the flow sequences are very similar. The 2MAR60 and 1MAR45 reservoirs have both shown slightly deeper scouring in places, but at the same time the river reach has also shown more

aggradation in other places. This could be as a result of the smaller base width that was assumed for these two scenarios.

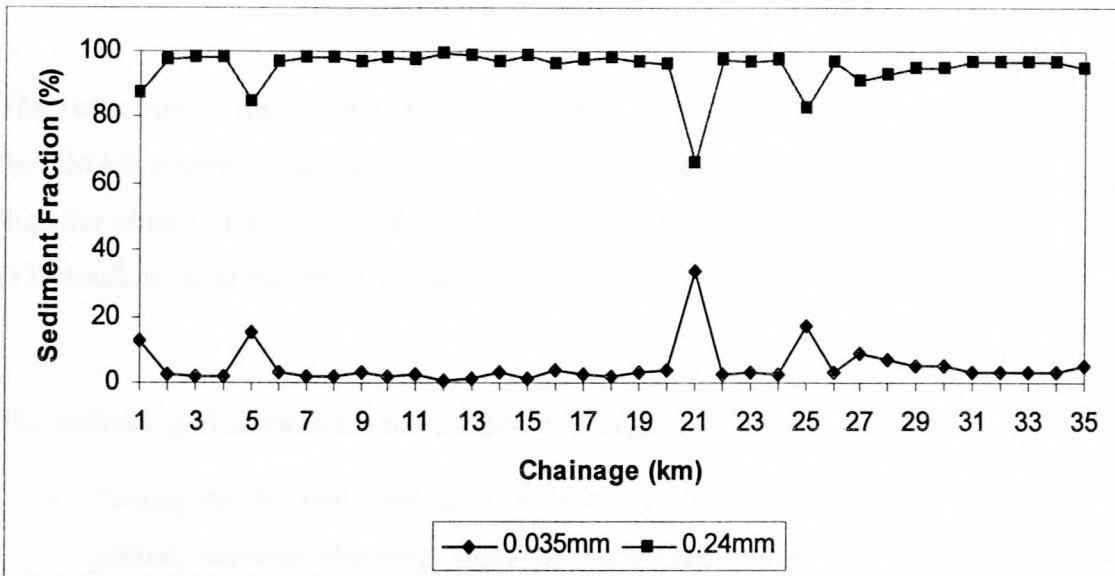


Figure 5.3.4: Simulated sediment fractions – 2MAR60 reservoir

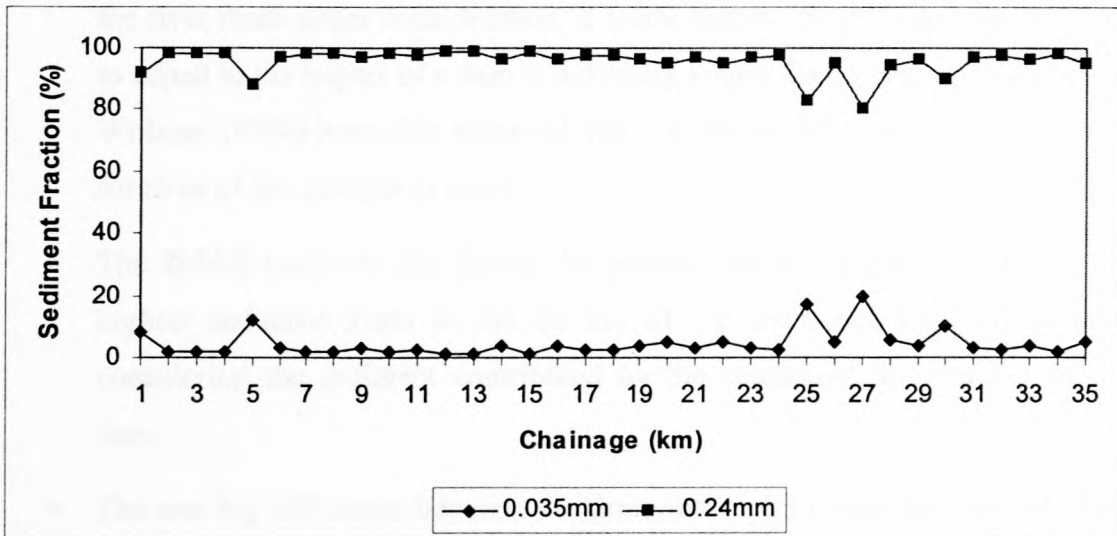


Figure 5.3.5: Simulated sediment fractions – 1MAR45 reservoir

From Figure 5.3.4 and 5.3.5 it can be seen that on average the sediment fractions have changed only slightly in comparison to the natural conditions, decreasing about 3%. This might not seem like much, but as pointed out in Chapter 4, only 7% clay and silt content can already have a considerable influence on the sediment transport behaviour. This means that under natural conditions cohesive sediments may govern the sediment transport, whereas under the influence of a dam there might be not be enough fine material left to influence the sediment transport. Also, as mentioned

before, in some places the fine fraction has increased to as much as 35%, which means that the flows released from both of the two dams were not always competent enough to carry the fine sediment through the whole system.

The reduction of the simulated sediment loads also shows that less erosion than for the 2MAR reservoir has taken place. The simulated sediment yields are still greater than the observed sediment yield (133 ton/km².a) or simulated natural sediment yield (119 ton/km².a) of the effective catchment (680 km²) downstream of the dam.

The following observations can be made with regard to the simulations:

- Seeing that the bed level has continuously changed throughout the simulation period, without showing signs of becoming stable, and the fact that the simulated long-term sediment yields are still greater than the observed sediment yield, could mean that the simulation period has been too short. For the river reach under consideration, it seems that the time it takes for the river to adjust to the impact of a dam is definitely longer than 5 years. Williams and Wolman (1984) have also observed that it generally takes more than 10 years for most of the changes to occur.
- The 2MAR reservoir has shown the greatest impact in that it produces the highest sediment loads in the 40 km of the river, but this was without considering the sediment contributed by the catchment downstream of the dam.
- The one big difference between the three reservoirs is that for the 2MAR60 and 1MAR45 reservoirs most of the smaller flows (< 150 m³/s) have been cut off by the dam, whereas these flows were still released from the 2MAR reservoir (**Figures 5.2.4 to 5.2.6**). This, together with the differences in simulation time, could be a reason for the lower sediment loads determined for the 2MAR60 and 1MAR45 reservoirs. This means that the more frequent floods, as well as durations, are important factors when determining the impacts of dams and also possible remedial measures.

- Without more data it is impossible to determine whether a smaller reservoir, in this case 1MAR, will have a greater or lesser impact than a large reservoir (2MAR).

6.1 Conclusions

The objectives of this thesis were to investigate the effects of dams on river downstream river morphology; by developing methods for predicting the downstream river morphology; by investigating the effect of clay and silt on the sediment transport behaviour of sediments as well as by assessing the changes in downstream river morphology by means of numerical modelling.

The following results have been obtained:

- The impacts of dams on the downstream river morphology depends to a large degree on the operation of the reservoir as well as the reservoir capacity in relation to the MAR, since these two factors determine the magnitude, duration and frequency of all but the largest floods. Some examples of this are presented in Table 6.1:

Table 6.1: Impacts and causes

| Impact | Cause |
|-------------------------------------|--|
| Riverbed degradation | Clear water releases due to sediment trapped in reservoir |
| Coarsening of bed material | Clear water releases |
| Reduced sediment transport capacity | Attenuated flood peaks, heavier bed materials, flatter slopes |
| Riverbed aggradation | Reduced sediment transport capacity, tributary sediment supply |
| Increased riparian vegetation | Long periods of low or no flows |
| Narrowing of river channel | Increased riparian vegetation |
| Widening of river channel | Regular wet and dry periods |

6. Conclusions and Recommendations

6.1 Conclusions

The objectives of this thesis were to investigate the effects of dams on the downstream river morphology: by developing methods for predicting the downstream river morphology; by investigating the effect of clay and silt on the sediment transport behaviour of sediments as well as by assessing the changes in downstream river morphology by means of numerical modelling.

The following results have been obtained:

- The impacts of dams on the downstream river morphology depend to a large degree on the operation of the reservoir as well as the reservoir capacity in relation to the MAR, since these two factors determine the magnitude, duration and frequency of all but the largest floods. Some examples of impacts are presented in **Table 6.1**:

Table 6.1: Impacts and causes

| Impact | Cause |
|-------------------------------------|--|
| Riverbed degradation | Clear water releases due to sediment trapped in reservoir |
| Coarsening of bed material | Clear water releases |
| Reduced sediment transport capacity | Attenuated flood peaks, coarser bed materials, flatter slopes |
| Riverbed aggradation | Reduced sediment transport capacity, tributary sediment supply |
| Increased riparian vegetation | Long periods of low or no flows |
| Narrowing of river channel | Increased riparian vegetation |
| Widening of river channel | Regular wet and dry periods |

- For South African rivers in their natural state the dominant discharge was found to be the 1:10-year flood peak. The same is not true for rivers downstream of dams with a very unnatural release pattern, where a 1:10-year discharge or any other flood peak associated with a particular recurrence interval is meaningless.
- Regime equations describing the average width and depth of a river were developed, based on South African river data. The equations were verified with the aid of international river data, and compared to results obtained from semi-theoretical regime equations developed in the United States. The new regime equations compared favourably to these regime equations.
- The regime equations developed in **Chapter 3**, as well as other international regime equations are not suitable for predicting the channel geometry of rivers downstream of dams with highly unnatural release patterns, mainly as a result of the problems with the determination of the dominant discharge. The use of the correct dominant discharge could change that, since the regime equations appear to be adequate for natural rivers, although they are not very accurate, keeping in mind that both the width and depth of a natural river tend to be variable.
- It has been found, through laboratory experiments, that as little as 7% clay and silt can affect the sediment transport behaviour of sand. When sediments contain more than 23% sand the erosion could be affected by armouring. At higher clay and silt contents (> 7%) almost no bedforms develop.
- A methodology was developed by which the critical conditions for mass erosion of cohesive sediments and cohesive – non-cohesive mixtures can be described in terms of the applied stream power at the bed. The applied stream power at the bed can be related to the percentage clay and silt in the bed material.
- Sediment transport equations in terms of the unit input stream power for cohesive and non-cohesive sediments, as well as mixtures of the two, were developed with data gained from laboratory experiments. The equations were successfully verified against independent flume data, as well as United States river data.

- The results of the mathematical modelling, incorporating the fine sediment transport equation developed during this study, show decreased sediment loads (by about 35%), coarser riverbeds and slightly reduced slopes for the dam scenarios in relation to the simulated natural state.
- The simulations have shown that both low flows and floods work together to form and maintain the river channel with a constant process of aggradation and degradation. Along a 35 km river course under consideration some reaches underwent more scouring than others as a result of sudden changes in cross-section and slope. However, the net effect for the 35 km reach was significant degradation.

6.2 Recommendations for Further Research

The following aspects require further investigation.

- Studies such as those done in the United States (Williams and Wolman, 1984) and China (Chien, 1985) should be done in South Africa to determine the nature and extent of the effects that dams have on rivers, in the form of repeated surveys downstream of dams, and to compare these findings to international experiences.
- In order to improve on the regime equations established in this thesis and to resolve whether these can be applied to impacted rivers, more data is necessary, especially on rivers that have been affected by dams.
- The concept of a dominant discharge value should be investigated further, since the use of a 1:10-year discharge does not seem appropriate for a river that is affected by the releases from a dam that are highly regulated and unnatural. The effect of the duration of certain floods should also be investigated.

- The sediment transport of cohesive – non-cohesive mixtures and fine sediments other than those studied in this thesis should be investigated to obtain more data for describing the critical conditions for mass erosion of sediment mixtures as well as to calibrate the proposed sediment transport equations for a wider range of particle sizes.
- The effect of consolidation and drying of fine sediments on the sediment transport behaviour should be investigated.
- The effects of different magnitudes of floods, as well as durations of flows should be investigated.

7. References

- Ackers, P. (1988). Alluvial Channel Hydraulics. *Journal of Hydrology*, 100, pp. 177-204.
- Ackers, P. and Charlton, F.G. (1970). Meander Geometry arising from varying flows. *Journal of Hydrology*, 11, pp. 230-252.
- Acreman, M. (2000). *Managed Flood Releases from Reservoirs: Issues and Guidance*. Contributing Paper to the World Commission on Dams, Cape Town. www.dams.org
- Andrews, E.D. (1986). Downstream Effects of Flaming Gorge Reservoir on the Green River, Colorado and Utah. *Geological Society of America Bulletin*, 97(8), pp. 177-204.
- Bagnold, R.A. (1966). An Approach to the Sediment Transport Problem from General Physics. *Geological Survey Professional Paper 422-I*, U.S. Government Printing Office, Washington, D.C.
- Basson, G.R. and Rooseboom, A. (1996). *Dealing with Reservoir Sedimentation*. South African Water Research Commission, Report No. TT91/97, South Africa.
- Blench, T. (1957). *Regime Behaviour of Canals and Rivers*. Butterworth Scientific Publications, London.
- Brandt, S.A. (1999). Reservoir Desiltation by Means of Hydraulic Flushing. PhD Thesis, University of Copenhagen, Copenhagen, Denmark.
- Bray, D.I. (1982). Regime Equations for Gravel-Bed Rivers. In: Hey, R.D., Bathurst, J.C., Thorne, C.R. (eds.) *Gravel-bed Rivers*. John Wiley & Sons, Chichester, UK.
- Brierley, G.J. and Fitchett, K. (2000). Channel Planform Adjustments along the Waiau River, 1946-1992: Assessment of the Impacts of Flow Regulation. In: Brizga, S. and Finlayson, B. (eds.) *River Management: the Australasian Experience*. John Wiley & Sons, Chichester, UK, pp. 51 – 71.

- Carling, P.A. (1988). Channel Change and Sediment Transport in Regulated UK Rivers. *Regulated Rivers: Research and Management*, 2, pp. 369-387.
- Chang, H.H. (1979). Minimum Stream Power and River Channel Patterns. *Journal of Hydrology*, 41, pp. 303-327.
- Chang, H.H. (1988). *Fluvial Processes in River Engineering*. John Wiley & Sons, New York.
- Chien, N. (1985). Changes in River Regime after the Construction of Upstream Reservoirs. *Earth Surface Processes and Landforms*, 10, pp. 143 – 159.
- Chitale, S.V. (1966). Cited in Wargadalam.
- Clark, P.B. and Davies, S.M.A. (1988). The Application of Regime Theory to Wadi Channels in Desert Conditions. In: White, W.R. (ed.) *International Conference on River Regime*. John Wiley & Sons, Chichester, UK, pp. 67-82.
- DHI (1992). *MIKE 11: A Microcomputer Based Modelling System for Rivers and Channels, Reference Manual*. Danish Hydraulic Institute Software. Denmark.
- Dollar, E.J.S., Rowntree, K.M., Wadeson, R.A. (2000). *Geomorphological Research for the Conservation and Management of Southern African Rivers, Volume 2*. Draft Report to the Water Research Commission.
- DT (1997). *Road Drainage Manual*. Department of Transport, Chief Directorate Roads. South Africa.
- DWA (1987). *Mathematical Model of the Hydraulics of the Pongolo River Flood Plain – Draft*. Department of Water Affairs. South Africa.
- DWAF (1998). *Hydrological Calculation Files*. Department of Water Affairs and Forestry, South Africa.
- Gilbert, G.K. (1914). The Transportation of Debris by Running Water, Based on Experiments Made with the Assistance of E.C. Murphy. *Geological Survey Professional Paper 86*.
- Guy, H.P., Simons, D.B., Middleton, B.J. (1966). Summary of Alluvial Channel Data

- from Flume Experiments, 1956-61. *Sediment Transport in Alluvial Channels. Geological Survey Professional Paper 462-I*, U.S. Government Printing Office, Washington, D.C.
- Hadley, R.F. and Emmett, W.W. (1998). Channel Changes Downstream of a Dam. *Journal of the American Water Resources Association*, 34(4), pp. 629 –637.
- Harvey, A.M. (1969). Channel Capacity and the Adjustment of Stream to the Hydrologic Regime. *Journal of Hydrology*, 8, pp. 82-98.
- Henderson, F.M. (1963). Cited in Wargadalam.
- Hey, R.D. and Thorne, C.R. (1986). Stable Channels with mobile Gravel Beds. *Journal of Hydraulic Engineering*, 112(8), pp. 671-689.
- Julien, P.Y. and Wargadalam, J. (1995). Alluvial Channel Geometry: Theory and Applications. *Journal of Hydraulic Engineering*, 121(4), pp. 312-325.
- Kamphuis, J.W. and Hall, K.R. (1983). Cohesive Material Erosion by Unidirectional Currents. *Journal of the Hydraulics Division*, 109(1), pp. 49-61.
- Kellerhals, R. (1967). Stable Channels with Gravel-Paved Beds. *Journal of the Waterways and Harbours Division*, 93(WW1), pp. 63-84.
- Kovacs, Z.P, Du Plessis, D.B., Bracher, P.R., Dunn, P. Mallory, G.C.L. (1985). *Documentation of the 1984 Domoina Floods*. Technical Report TR122, Department of Water Affairs, South Africa
- Lacey, G. (1930). Cited in Wargadalam.
- Le Grange, A.duP. (1994). *Techniques for Predicting the Deformation and Hydraulic Resistance of Sand-Bed Rivers*. PhD. Thesis, University of Stellenbosch, Stellenbosch, South Africa.
- Leopold, L.B. and Maddock, T. (1953). Cited in Wargadalam.
- Leopold, L.B. and Wolman, G. (1957). River Channel Patterns: Braided, Meandering and Straight. *Geological Survey Professional Paper 282-B*, U.S. Government Printing Office, Washington, D.C.

- Mehta, A.J., Hayter, E.J., Parker, R., Krone, R.B., Teeter, A.M. (1989). Cohesive Sediment Transport I: Process Description. *Journal of Hydraulic Engineering*, 115(8), pp.1076-1093.
- Midgley, D.C., Pitman, W.V., Middleton, B.J. (1990). *Water Surface Resources of South Africa 1990, Volume VI, Appendices*. South African Water Research Commission, Report No. 298/6.1/94, South Africa.
- Nouh, M. (1988). Regime Channels of an Extremely Arid Zone. In: White, W.R. (ed.) *International Conference on River Regime*. John Wiley & Sons, Chichester, UK, pp. 55-66.
- Osterkamp, W.R. and Hedman, E.R. (1979). Cited in Wharton, G. (1995). Information from Channel Geometry-Discharge Relations. In: Gurnell, A. and Petts, G. (eds.) *Changing River Channels*. John Wiley & Sons. Chichester, UK.
- Panagiotopoulos, I., Voulgaris, G., Collins, M.B. (1997). The Influence of Clay on the Threshold of Movement of Fine Sandy Beds. *Coastal Engineering*, 32, pp. 19-43.
- Parchure, T.M. and Mehta, A.J. (1985). Erosion of Soft Cohesive Sediment Deposits. *Journal of Hydraulic Engineering*, 111(10), pp.1308-1326.
- Partheniades, E. (1971). Erosion and Deposition of Cohesive Materials. In: Shen, H.W. (ed.) *River Mechanics*, Volume II, Fort Collins, Colorado, pp. 25.1 – 25.91.
- Partheniades, E. and Paaswell, R.E. (1970). Erodibility of Channels with Cohesive Boundary. *Journal of the Hydraulics Division*, 96(3), pp. 755-771.
- Rooseboom, A. (1992). *Sediment Transport in Rivers and Reservoirs - a South African Perspective*. South African Water Research Commission, Report No. 297/1/92, South Africa.
- Rowntree, K.M., Du Plessis, A.J.E., McGregor, G.K. (2000). *Geomorphological Research for the Conservation and Management of Southern African Rivers, Volume 1*. Draft Report to the Water Research Commission.
- Rutherford, I. (2000). Some Human Impacts on Australian Stream Channel Morphology. In: Brizga, S. and Finlayson, B. (eds.) *River Management: the*

Australasian Experience. John Wiley & Sons, Chichester, UK, pp. 11-49.

Schumm, S.A. and Galay, V.J. (1994). The River Nile in Egypt. In: Schumm, S.A. and Winkley, B.R (eds.) *The Variability of Large Alluvial Rivers*. ASCE, United States, pp. 75-100.

SI and CESDC – Soils Incorporated (Pty) Ltd and Chalo Environmental and Sustainable Development Consultants (2000). *Kariba Dam Case Study*, prepared as an input to the World Commission on Dams, Cape Town. www.dams.org

Torfs, H., Huygens, M., Tito, L. (1994). Influence of the Cross-section on the Erosion Criteria for Partly Cohesive Sediments. *Water, Science and Technology*, 29, pp. 103-111.

Wargadalam, J. (1993). *Hydraulic Geometry Equations of Alluvial Channels*. PhD. Thesis, Colorado State University, Fort Collins, Colorado.

WCD (2000a). *Dams and Development: A new Framework for Decision-Making*. World Commission on Dams. www.dams.org

WCD (2000b). *Orange River Development Project, South Africa*. Case study prepared as input to the World Commission on Dams, Cape Town. www.dams.org

White, R. (2000). Introduction: World Stock of Reservoirs. In: *Reservoir Sedimentation – One-Day Seminar*. HR Wallingford, UK.

Williams, G.P. (1978), Bankfull Discharge of Rivers. *Water Resources Research*, 14(6), pp. 1141-1154.

Williams, G.P. and Wolman, M.G. (1984). Downstream Effects of Dams on Alluvial Rivers. *Geological Survey Professional Paper 1286*, U.S. Government Printing Office, Washington, D.C.

Wolman, M.G. and Miller, J.P. (1960). Cited in Wharton, G. (1995). Information from Channel Geometry-Discharge Relations. In: Gurnell, A. and Petts, G. (eds.) *Changing River Channels*. John Wiley & Sons. Chichester, UK.

Yang, C.T. (1972). Unit Stream Power and Sediment Transport. *Journal of the Hydraulics Division*, 98(10), pp. 1805-1826.

- Yang, C.T. (1973). Incipient Motion and Sediment Transport. *Journal of the Hydraulics Division*, 99(10), pp. 1679-1704.
- Yang, C.T. and Molinas, A. (1982). Sediment Transport and Unit Stream Power Function. *Journal of the Hydraulics Division*, 108(6), pp. 774-793.
- Yang, C.T., Molinas, A., Wu, B. (1996). Sediment Transport in the Yellow River. *Journal of Hydraulic Engineering*, 122(5), pp. 237-244.
- Zanke, U. (1977). Cited in Basson and Rooseboom.
- Zhou, Z. and Pan, X. (1994). Lower Yellow River. In: Schumm, S.A. and Winkley, B.R (eds.) *The Variability of Large Alluvial Rivers*. ASCE, United States, pp. 363-393.

APPENDIX A

- **A1: SOUTH AFRICAN RIVER DATA**
- **A2: VERIFICATION DATA**
- **A3: CHANNEL PATTERN DATA**
- **A4: REGRESSION RESULTS**

River Information

| River | Basin | Flow (m³/s) | Flow (km³/a) | Flow (km³/a) | Flow (km³/a) |
|------------------|---------------------|-------------|--------------|--------------|--------------|
| 1Aberdein | Highland | 0.00000 | 0.000 | 0.000 | 0.000 |
| 2Aberystwyth | Wales | 0.00000 | 0.000 | 0.000 | 0.000 |
| 3Bospoort | Lesotho | 0.00000 | 0.000 | 0.000 | 0.000 |
| 6Buffelspoort | Wales | 0.00000 | 0.000 | 0.000 | 0.000 |
| 7Buffelspoort | Wales | 0.00000 | 0.000 | 0.000 | 0.000 |
| 8Buffelspoort | Wales | 0.00000 | 0.000 | 0.000 | 0.000 |
| 9Duitsvlei | Oranje | 0.00000 | 0.000 | 0.000 | 0.000 |
| 10Dullstorp | Wes | 0.00000 | 0.000 | 0.000 | 0.000 |
| 11Edmalond | Hoogvlei | 0.00000 | 0.000 | 0.000 | 0.000 |
| 12Oamvliet | Oranje | 0.00000 | 0.000 | 0.000 | 0.000 |
| 13Craigie Burn | Afrykanse | 0.00000 | 0.000 | 0.000 | 0.000 |
| 14Dagema | Witwaters | 0.00000 | 0.000 | 0.000 | 0.000 |
| 15Dunington | Sundays | 0.00000 | 0.000 | 0.000 | 0.000 |
| 16Doomdras | Stek | 0.00000 | 0.000 | 0.000 | 0.000 |
| 17Doringvlei | Doring | 0.00000 | 0.000 | 0.000 | 0.000 |
| 18Duiwenhoks | Dunmaring | 0.00000 | 0.000 | 0.000 | 0.000 |
| 19Ebenezer | Groot Letaba | 0.00000 | 0.000 | 0.000 | 0.000 |
| 20Erfenis | Groot Vlei | 0.00000 | 0.000 | 0.000 | 0.000 |
| 21Gamska | Gamska | 0.00000 | 0.000 | 0.000 | 0.000 |
| 22Gamskepoort | Gamska | 0.00000 | 0.000 | 0.000 | 0.000 |
| 23Gariep | Oranje | 0.00000 | 0.000 | 0.000 | 0.000 |
| 24Glen Alpine | Hoogvlei | 0.00000 | 0.000 | 0.000 | 0.000 |
| 25Groenluis | Groot Brak | 0.00000 | 0.000 | 0.000 | 0.000 |
| 26Gubu | Gubu | 0.00000 | 0.000 | 0.000 | 0.000 |
| 27Hartbeespoort | Crocodile | 0.00000 | 0.000 | 0.000 | 0.000 |
| 28Hesselmans | Molli | 0.00000 | 0.000 | 0.000 | 0.000 |
| 29Huduma | Huduma | 0.00000 | 0.000 | 0.000 | 0.000 |
| 30Kalkfontein | Riet | 0.00000 | 0.000 | 0.000 | 0.000 |
| 31Kammarsale | Kammarsale | 0.00000 | 0.000 | 0.000 | 0.000 |
| 32Kater | Kat | 0.00000 | 0.000 | 0.000 | 0.000 |
| 33Klein Maricoop | Nieu Marica | 0.00000 | 0.000 | 0.000 | 0.000 |
| 34Kloppers | Kroon | 0.00000 | 0.000 | 0.000 | 0.000 |
| 35Kloppoor | Pieters (Grootvlei) | 0.00000 | 0.000 | 0.000 | 0.000 |
| 36Kommeridrif | Tarka | 0.00000 | 0.000 | 0.000 | 0.000 |
| 37Koster | Koster | 0.00000 | 0.000 | 0.000 | 0.000 |
| 38Kouga | Kouga | 0.00000 | 0.000 | 0.000 | 0.000 |
| 39Krugersdrif | Modder | 0.00000 | 0.000 | 0.000 | 0.000 |
| 40Lindleypoort | Flende | 0.00000 | 0.000 | 0.000 | 0.000 |
| 41Loerle | Loerlepoort | 0.00000 | 0.000 | 0.000 | 0.000 |
| 42Lonsmans | Wit | 0.00000 | 0.000 | 0.000 | 0.000 |
| 43Loskop | Oranje | 0.00000 | 0.000 | 0.000 | 0.000 |
| 44Lugobaskoof | Poitsie | 0.00000 | 0.000 | 0.000 | 0.000 |
| 45Medner | Mperi | 0.00000 | 0.000 | 0.000 | 0.000 |
| 46Nolgedacht | Komati | 0.00000 | 0.000 | 0.000 | 0.000 |
| 47Pietersfontein | Pietersfontein | 0.00000 | 0.000 | 0.000 | 0.000 |

APPENDIX A1: SOUTH AFRICAN RIVER DATA

River Information

| No. | Dam | River | S ₀ | A (km ²) | w (m/s) | d ₅₀ (mm) |
|-----|-------------------|---------------------|----------------|----------------------|---------|----------------------|
| 1 | Albertfalls | Mgeni | 0.00015 | 905 | 0.052 | 0.241 |
| 2 | Allemankraal | Sand | 0.00109 | 2925 | 0.002 | 0.043 |
| 3 | Armenia | Leeu | 0.00140 | 734 | 0.000 | 0.009 |
| 4 | Boskop | Mooi | 0.00278 | 2098 | 0.130 | 0.381 |
| 5 | Bospoort | Hex | 0.00233 | 555 | 0.002 | 0.050 |
| 6 | Buffeljags | Buffeljags | 0.00363 | 550 | 0.051 | 0.239 |
| 7 | Buffelskloof | Waterval | 0.01112 | 289 | 0.002 | 0.049 |
| 8 | Buffelspoort | Strekstroom | 0.00603 | 123 | 0.002 | 0.050 |
| 9 | Bulshoek | Olifants | 0.00612 | 736 | 0.224 | 0.500 |
| 10 | Calitzdorp | Nels | 0.00664 | 218 | 0.002 | 0.050 |
| 11 | Chelmsford | Ngagane | 0.00100 | 920 | 0.001 | 0.040 |
| 12 | Clanwilliam | Olifants | 0.00055 | 1942 | 0.167 | 0.432 |
| 13 | Craigie Burn | Mnyamvubu | 0.00300 | 182 | 0.224 | 0.500 |
| 14 | Dagama | White Waters | 0.00347 | 212 | 0.002 | 0.050 |
| 15 | Darlington | Sundays | 0.00051 | 13066 | 0.000 | 0.022 |
| 16 | Doorndraai | Sterk | 0.00448 | 564 | 0.002 | 0.050 |
| 17 | Doringrivier | Doring | 0.00056 | 269 | 0.002 | 0.052 |
| 18 | Duiwenhoks | Duiwenhoks | 0.07198 | 123 | 0.224 | 0.500 |
| 19 | Ebenezer | Groot Letaba | 0.00345 | 73 | 0.000 | 0.005 |
| 20 | Erfenis | Groot Vet | 0.00094 | 4364 | 0.001 | 0.028 |
| 21 | Gamka | Gamka | 0.03233 | 428 | 0.000 | 0.005 |
| 22 | Gamkapoort | Gamka | 0.00463 | 14275 | 0.000 | 0.009 |
| 23 | Gariep | Oranje | 0.00074 | 68885 | 0.001 | 0.025 |
| 24 | Glen Alpine | Mogalakwena | 0.00115 | 10689 | 0.002 | 0.041 |
| 25 | Grassridge | Groot Brak | 0.00125 | 3937 | 0.000 | 0.005 |
| 26 | Gubu | Gubu | 0.01464 | 93 | 0.000 | 0.006 |
| 27 | Hartebeespoort | Crocodile | 0.00685 | 3838 | 0.035 | 0.198 |
| 28 | Hazelmere | Mdloti | 0.00585 | 340 | 0.000 | 0.012 |
| 29 | Hluhluwe | Hluhluwe | 0.00235 | 688 | 0.000 | 0.018 |
| 30 | Kalkfontein | Riet | 0.00137 | 8346 | 0.001 | 0.028 |
| 31 | Kammanassie | Kammanassie | 0.00288 | 1600 | 0.078 | 0.295 |
| 32 | Katrivier | Kat | 0.01001 | 79 | 0.000 | 0.009 |
| 33 | Klein Maricopoort | Klein Marico | 0.00304 | 940 | 0.002 | 0.050 |
| 34 | Klipberg | Konings | 0.01346 | 228 | 0.163 | 0.426 |
| 35 | Klipvoor | Pienaars (Moretele) | 0.00399 | 5051 | 0.002 | 0.050 |
| 36 | Kommandodrift | Tarka | 0.00274 | 857 | 0.000 | 0.005 |
| 37 | Koster | Koster | 0.00335 | 266 | 0.002 | 0.050 |
| 38 | Kouga | Kouga | 0.00294 | 2706 | 0.214 | 0.490 |
| 39 | Krugersdrift | Modder | 0.00056 | 4258 | 0.004 | 0.064 |
| 40 | Lindleyspoort | Elands | 0.00606 | 729 | 0.002 | 0.050 |
| 41 | Loerie | Loeriespruit | 0.00940 | 154 | 0.012 | 0.114 |
| 42 | Longmere | Wit | 0.00079 | 77 | 0.002 | 0.050 |
| 43 | Loskop | Olifants | 0.00200 | 5774 | 0.157 | 0.418 |
| 44 | Magoebaskloof | Politsie | 0.01718 | 79 | 0.000 | 0.005 |
| 45 | Midmar | Mgeni | 0.00046 | 789 | 0.004 | 0.067 |
| 46 | Nooitgedacht | Komati | 0.00308 | 1734 | 0.207 | 0.481 |
| 47 | Pietersfontein | Pietersfontein | 0.01118 | 82 | 0.007 | 0.088 |

| No. | Dam | River | S_0 | A (km ²) | w (m/s) | d_{50} (mm) |
|-----|-----------------|---------------------|---------|----------------------|---------|---------------|
| 48 | Pongolapoort | Pongolo | 0.00147 | 7834 | 0.010 | 0.108 |
| 49 | Poortjieskloof | Groot | 0.00607 | 645 | 0.032 | 0.190 |
| 50 | Primkop | Wit | 0.00735 | 63 | 0.002 | 0.050 |
| 51 | Roode-Elsberg | Sanddrif | 0.01836 | 124 | 0.220 | 0.496 |
| 52 | Roodeplaat | Pienaars (Moretele) | 0.01310 | 888 | 0.008 | 0.097 |
| 53 | Rust de Winter | Elands | 0.00287 | 1104 | 0.023 | 0.016 |
| 54 | Rustfontein | Modder | 0.00152 | 748 | 0.002 | 0.050 |
| 55 | Van Ryneveldpas | Sundays | 0.00197 | 3308 | 0.000 | 0.005 |
| 56 | Wagendrift | Boesmans | 0.00211 | 682 | 0.014 | 0.126 |
| 57 | Waterdown | Klipplaat | 0.00250 | 633 | 0.000 | 0.023 |
| 58 | Westoe | Usutu | 0.00132 | 600 | 0.221 | 0.497 |
| 59 | Xonxa | White Kei | 0.00236 | 1440 | 0.000 | 0.005 |

| | | | | |
|----------|--------|------|--------|------|
| 0.001240 | 114.24 | 1.23 | 113.01 | 0.23 |
| 0.001300 | 122.24 | 1.23 | 120.99 | 0.24 |
| 0.001360 | 130.24 | 1.23 | 128.97 | 0.25 |
| 0.001420 | 138.24 | 1.23 | 136.95 | 0.26 |
| 0.001480 | 146.24 | 1.23 | 144.93 | 0.27 |
| 0.001540 | 154.24 | 1.23 | 152.91 | 0.28 |
| 0.001600 | 162.24 | 1.23 | 160.89 | 0.29 |
| 0.001660 | 170.24 | 1.23 | 168.87 | 0.30 |
| 0.001720 | 178.24 | 1.23 | 176.85 | 0.31 |
| 0.001780 | 186.24 | 1.23 | 184.83 | 0.32 |
| 0.001840 | 194.24 | 1.23 | 192.81 | 0.33 |
| 0.001900 | 202.24 | 1.23 | 200.79 | 0.34 |
| 0.001960 | 210.24 | 1.23 | 208.77 | 0.35 |
| 0.002020 | 218.24 | 1.23 | 216.75 | 0.36 |
| 0.002080 | 226.24 | 1.23 | 224.73 | 0.37 |
| 0.002140 | 234.24 | 1.23 | 232.71 | 0.38 |
| 0.002200 | 242.24 | 1.23 | 240.69 | 0.39 |
| 0.002260 | 250.24 | 1.23 | 248.67 | 0.40 |
| 0.002320 | 258.24 | 1.23 | 256.65 | 0.41 |
| 0.002380 | 266.24 | 1.23 | 264.63 | 0.42 |
| 0.002440 | 274.24 | 1.23 | 272.61 | 0.43 |
| 0.002500 | 282.24 | 1.23 | 280.59 | 0.44 |
| 0.002560 | 290.24 | 1.23 | 288.57 | 0.45 |
| 0.002620 | 298.24 | 1.23 | 296.55 | 0.46 |
| 0.002680 | 306.24 | 1.23 | 304.53 | 0.47 |
| 0.002740 | 314.24 | 1.23 | 312.51 | 0.48 |
| 0.002800 | 322.24 | 1.23 | 320.49 | 0.49 |
| 0.002860 | 330.24 | 1.23 | 328.47 | 0.50 |
| 0.002920 | 338.24 | 1.23 | 336.45 | 0.51 |
| 0.002980 | 346.24 | 1.23 | 344.43 | 0.52 |
| 0.003040 | 354.24 | 1.23 | 352.41 | 0.53 |
| 0.003100 | 362.24 | 1.23 | 360.39 | 0.54 |
| 0.003160 | 370.24 | 1.23 | 368.37 | 0.55 |
| 0.003220 | 378.24 | 1.23 | 376.35 | 0.56 |
| 0.003280 | 386.24 | 1.23 | 384.33 | 0.57 |
| 0.003340 | 394.24 | 1.23 | 392.31 | 0.58 |
| 0.003400 | 402.24 | 1.23 | 400.29 | 0.59 |
| 0.003460 | 410.24 | 1.23 | 408.27 | 0.60 |
| 0.003520 | 418.24 | 1.23 | 416.25 | 0.61 |
| 0.003580 | 426.24 | 1.23 | 424.23 | 0.62 |
| 0.003640 | 434.24 | 1.23 | 432.21 | 0.63 |
| 0.003700 | 442.24 | 1.23 | 440.19 | 0.64 |
| 0.003760 | 450.24 | 1.23 | 448.17 | 0.65 |
| 0.003820 | 458.24 | 1.23 | 456.15 | 0.66 |
| 0.003880 | 466.24 | 1.23 | 464.13 | 0.67 |
| 0.003940 | 474.24 | 1.23 | 472.11 | 0.68 |
| 0.004000 | 482.24 | 1.23 | 480.09 | 0.69 |
| 0.004060 | 490.24 | 1.23 | 488.07 | 0.70 |
| 0.004120 | 498.24 | 1.23 | 496.05 | 0.71 |
| 0.004180 | 506.24 | 1.23 | 504.03 | 0.72 |
| 0.004240 | 514.24 | 1.23 | 512.01 | 0.73 |
| 0.004300 | 522.24 | 1.23 | 520.00 | 0.74 |
| 0.004360 | 530.24 | 1.23 | 528.00 | 0.75 |
| 0.004420 | 538.24 | 1.23 | 536.00 | 0.76 |
| 0.004480 | 546.24 | 1.23 | 544.00 | 0.77 |
| 0.004540 | 554.24 | 1.23 | 552.00 | 0.78 |
| 0.004600 | 562.24 | 1.23 | 560.00 | 0.79 |
| 0.004660 | 570.24 | 1.23 | 568.00 | 0.80 |
| 0.004720 | 578.24 | 1.23 | 576.00 | 0.81 |
| 0.004780 | 586.24 | 1.23 | 584.00 | 0.82 |
| 0.004840 | 594.24 | 1.23 | 592.00 | 0.83 |
| 0.004900 | 602.24 | 1.23 | 600.00 | 0.84 |
| 0.004960 | 610.24 | 1.23 | 608.00 | 0.85 |
| 0.005020 | 618.24 | 1.23 | 616.00 | 0.86 |
| 0.005080 | 626.24 | 1.23 | 624.00 | 0.87 |
| 0.005140 | 634.24 | 1.23 | 632.00 | 0.88 |
| 0.005200 | 642.24 | 1.23 | 640.00 | 0.89 |
| 0.005260 | 650.24 | 1.23 | 648.00 | 0.90 |
| 0.005320 | 658.24 | 1.23 | 656.00 | 0.91 |
| 0.005380 | 666.24 | 1.23 | 664.00 | 0.92 |
| 0.005440 | 674.24 | 1.23 | 672.00 | 0.93 |
| 0.005500 | 682.24 | 1.23 | 680.00 | 0.94 |
| 0.005560 | 690.24 | 1.23 | 688.00 | 0.95 |
| 0.005620 | 698.24 | 1.23 | 696.00 | 0.96 |
| 0.005680 | 706.24 | 1.23 | 704.00 | 0.97 |
| 0.005740 | 714.24 | 1.23 | 712.00 | 0.98 |
| 0.005800 | 722.24 | 1.23 | 720.00 | 0.99 |
| 0.005860 | 730.24 | 1.23 | 728.00 | 1.00 |

APPENDIX A2: VERIFICATION

DATA

Verification Data

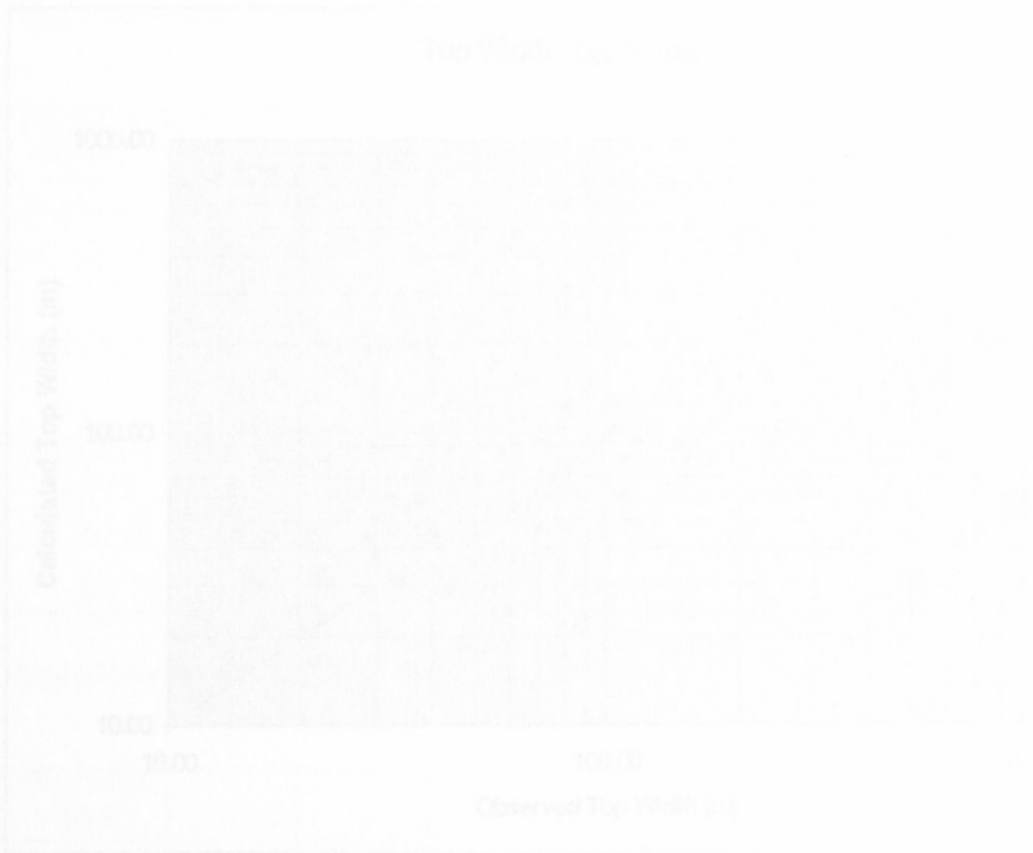
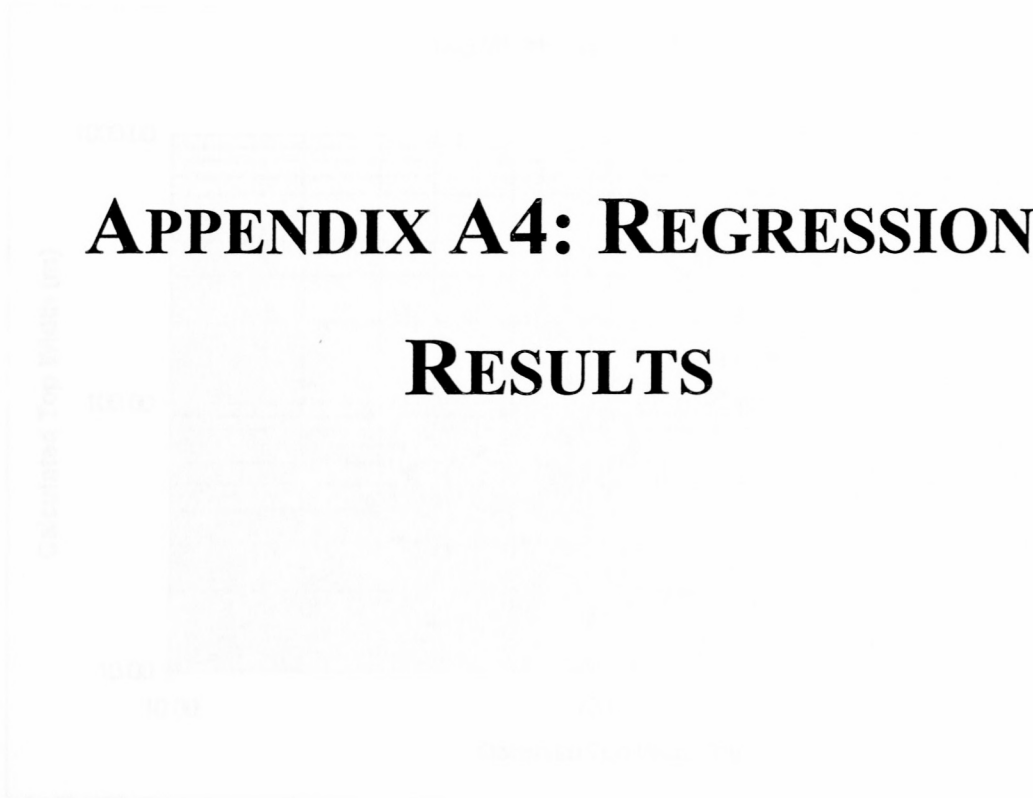
| S (m/m) | B (m) | D (m) | Q (m ³ /s) | d ₅₀ (mm) |
|----------|---------|-------|-----------------------|----------------------|
| 0.001140 | 193.55 | 5.55 | 3143.08 | 0.610 |
| 0.000400 | 142.95 | 5.21 | 1812.22 | 0.400 |
| 0.000800 | 83.21 | 1.46 | 285.99 | 0.315 |
| 0.001705 | 21.64 | 0.49 | 11.81 | 0.212 |
| 0.000230 | 295.00 | 3.01 | 1310.00 | 0.500 |
| 0.000460 | 195.00 | 2.18 | 475.00 | 1.080 |
| 0.000480 | 610.00 | 3.94 | 2710.00 | 1.050 |
| 0.000360 | 785.00 | 2.80 | 2630.00 | 0.405 |
| 0.000130 | 400.00 | 4.62 | 2720.00 | 0.920 |
| 0.000200 | 454.00 | 5.29 | 3080.00 | 0.375 |
| 0.000450 | 280.00 | 2.88 | 652.00 | 0.265 |
| 0.000110 | 605.00 | 3.08 | 2085.00 | 0.320 |
| 0.000160 | 410.00 | 6.57 | 2858.00 | 0.310 |
| 0.000062 | 582.00 | 13.28 | 10200.00 | 0.210 |
| 0.001920 | 4.33 | 0.44 | 1.48 | 0.899 |
| 0.002750 | 3.92 | 0.15 | 0.65 | 0.286 |
| 0.000144 | 214.70 | 4.28 | 1523.45 | 0.227 |
| 0.001155 | 43.89 | 0.34 | 10.78 | 0.368 |
| 0.001480 | 8.00 | 0.65 | 4.85 | 1.440 |
| 0.001660 | 8.00 | 0.20 | 2.24 | 1.330 |
| 0.000140 | 253.10 | 2.30 | 403.57 | 0.310 |
| 0.000187 | 117.03 | 2.83 | 362.46 | 0.300 |
| 0.000134 | 162.43 | 3.59 | 443.16 | 0.195 |
| 0.000193 | 113.09 | 2.90 | 310.61 | 0.350 |
| 0.000207 | 149.09 | 3.08 | 387.66 | 0.280 |
| 0.000389 | 136.11 | 1.45 | 132.24 | 0.315 |
| 0.000044 | 451.10 | 13.23 | 10222.07 | 0.188 |
| 0.000035 | 1097.28 | 15.67 | 26560.40 | 0.342 |

Channel Patterns

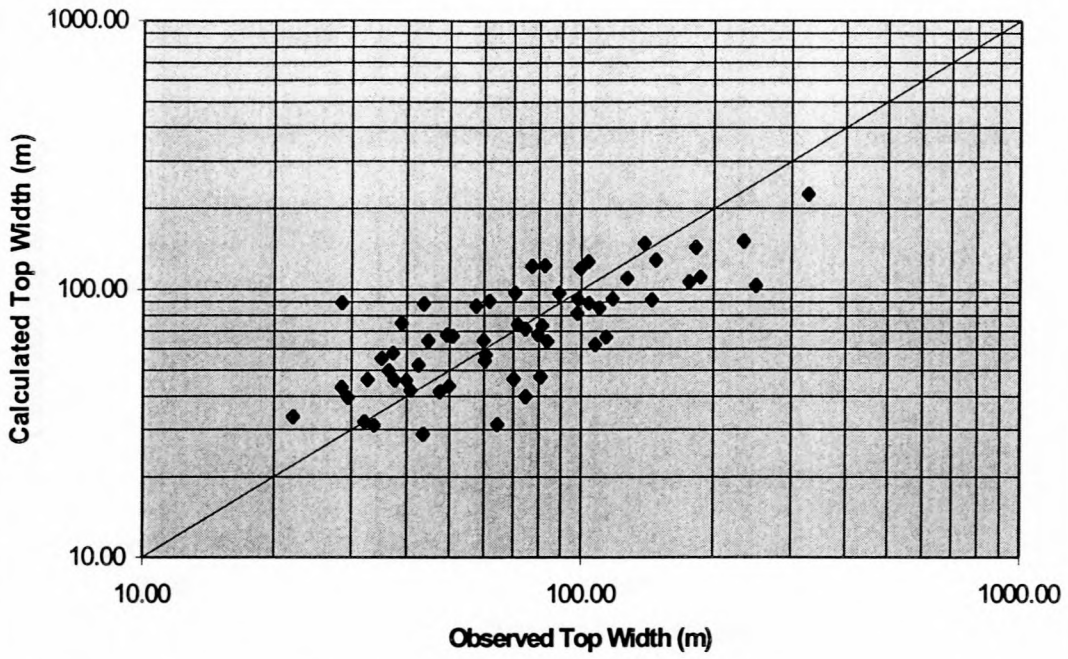
| River | Dam | Q ₁₀ (m ³ /s) | Slope (m/m) | Sinuosity |
|---------------------|-------------------|-------------------------------------|-------------|-----------|
| Mgeni | Albertfalls | 245 | 0.00015 | 1.42 |
| Sand | Allemanskraal | 795 | 0.00109 | 1.19 |
| Leeu | Armenia | 165 | 0.0014 | 1.13 |
| Brak | Bellair | 168 | 0.00253 | 1.04 |
| Mooi | Boskop | 71 | 0.00278 | 1.03 |
| Hex | Bospoort | 310 | 0.00233 | 1.09 |
| Bronkhorstspruit | Bronkhorstspruit | 340 | 0.00058 | 1.16 |
| Buffeljags | Buffeljags | 330 | 0.00363 | 1.09 |
| Waterval | Buffelskloof | 160 | 0.01112 | 1.44 |
| Strekstroom | Buffelspoort | 190 | 0.00603 | 1.09 |
| Olifants | Bulshoek | 451 | 0.00612 | 1.08 |
| Nels | Calitzdorp | 170 | 0.00664 | 1.19 |
| Ngagane | Chelmsford | 440 | 0.001 | 1.55 |
| Olifants | Clanwilliam | 824 | 0.00055 | 1.07 |
| Mnyamvubu | Craigie Burn | 255 | 0.003 | 1.38 |
| White Waters | Dagama | 115 | 0.00347 | 1.09 |
| Sundays | Darlington | 1473 | 0.00051 | 1.63 |
| Sterk | Doorndraai | 150 | 0.00448 | 1.01 |
| Doring | Doringrivier | 302 | 0.00056 | 1.30 |
| Duiwenhoks | Duiwenhoks | 170 | 0.07198 | 1.13 |
| Groot Letaba | Ebenezer | 190 | 0.00345 | 1.06 |
| Groot Vet | Erfenis | 1070 | 0.00094 | 1.15 |
| Buffels | Floriskraal | 647 | 0.00084 | 1.25 |
| Gamka | Gamka | 200 | 0.03233 | 1.10 |
| Gamka | Gamkapoort | 1760 | 0.00463 | 1.02 |
| Oranje | Gariep | 5200 | 0.00074 | 1.22 |
| Mogalakwena | Glen Alpine | 810 | 0.00115 | 1.12 |
| Groot Brak | Grassridge | 670 | 0.00125 | 1.11 |
| Gubu | Gubu | 81 | 0.01464 | 1.02 |
| Crocodile | Hartebeespoort | 1234 | 0.00685 | 1.29 |
| Mdloti | Hazelmere | 380 | 0.00585 | 1.43 |
| Hluhluwe | Hluhluwe | 1046 | 0.00235 | 1.50 |
| Riet | Kalkfontein | 1200 | 0.00137 | 1.36 |
| Kammanassie | Kammanassie | 641 | 0.00288 | 1.09 |
| Kat | Katrivier | 242 | 0.01001 | 1.70 |
| Klein Marico | Klein Maricopoort | 297 | 0.00304 | 1.11 |
| Mooi | Klerkskraal | 75 | 0.00041 | 1.04 |
| Konings | Klipberg | 68 | 0.01346 | 1.07 |
| Loopspruit | Klipdrift | 338 | 0.0003 | 1.09 |
| Pienaars (Moretele) | Klipvoor | 449 | 0.00399 | 1.11 |
| Tarka | Kommandodrift | 851 | 0.00274 | 1.59 |
| Koster | Koster | 283 | 0.00335 | 1.11 |
| Kouga | Kouga | 1379 | 0.00294 | 1.47 |
| Klein Marico | Kromellenboog | 369 | 0.00391 | 1.08 |
| Modder | Krugersdrift | 797 | 0.00056 | 1.48 |
| Tarka | Lake Arthur | 745 | 0.004 | 1.40 |
| Leeu | Leeu Gamka | 446 | 0.00345 | 1.09 |

| River | Dam | Q ₁₀ (m ³ /s) | Slope (m/m) | Sinuosity |
|---------------------|---------------------|-------------------------------------|-------------|-----------|
| Elands | Lindleyspoort | 268 | 0.00606 | 1.14 |
| Loeriespruit | Loerie | 588 | 0.0094 | 1.29 |
| Wit | Longmere | 119 | 0.00079 | 1.24 |
| Olifants | Loskop | 1560 | 0.002 | 2.02 |
| Politsie | Magoebaskloof | 259 | 0.01718 | 1.07 |
| Groot Marico | Marico Bosveld | 346 | 0.00106 | 1.21 |
| Mgeni | Midmar | 430 | 0.00046 | 1.54 |
| Komati | Nooitgedacht | 470 | 0.00308 | 1.35 |
| Hex | Olifantsnek | 510 | 0.0046 | 1.18 |
| Pietersfontein | Pietersfontein | 75 | 0.01118 | 1.13 |
| Pongolo | Pongolapoort | 1979 | 0.00147 | 1.60 |
| Groot | Poortjieskloof | 96 | 0.00607 | 1.20 |
| Wit | Primkop | 219 | 0.00735 | 1.03 |
| Sanddrif | Roode-Elsberg | 211 | 0.01836 | 1.18 |
| Pienaars (Moretele) | Roodeplaat | 315 | 0.0131 | 1.08 |
| Leeuspruit | Roodepoort-Cornelia | 69 | 0.00048 | 1.13 |
| Elands | Rust de Winter | 332 | 0.00287 | 1.17 |
| Modder | Rustfontein | 492 | 0.00152 | 1.11 |
| Olifants | Stompdrift | 520 | 0.00032 | 1.04 |
| Kaffer | Tierpoort | 230 | 0.00089 | 1.30 |
| Sundays | Van Ryneveldpas | 790 | 0.00197 | 1.41 |
| Boesmans | Wagendrift | 486 | 0.00211 | 1.53 |
| Klipplaat | Waterdown | 325 | 0.0025 | 1.72 |
| Caledon | Welbedacht | 1500 | 0.00225 | 1.63 |
| Usutu | Westoe | 221 | 0.00132 | 1.34 |
| White Kei | Xonxa | 460 | 0.00236 | 1.44 |

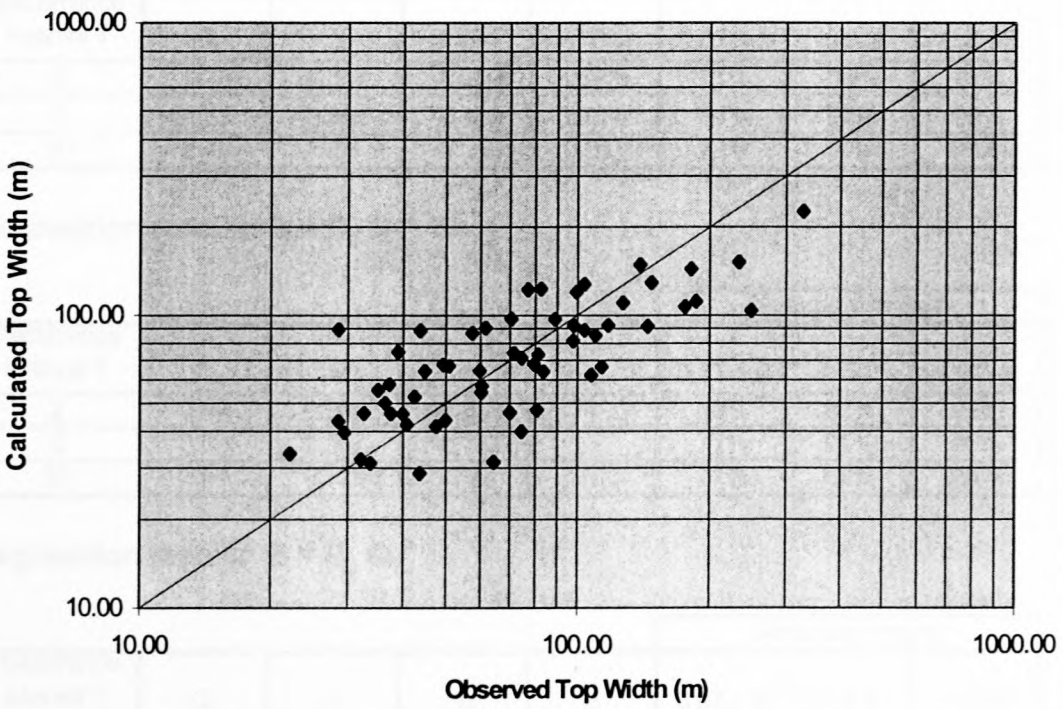
APPENDIX A4: REGRESSION RESULTS

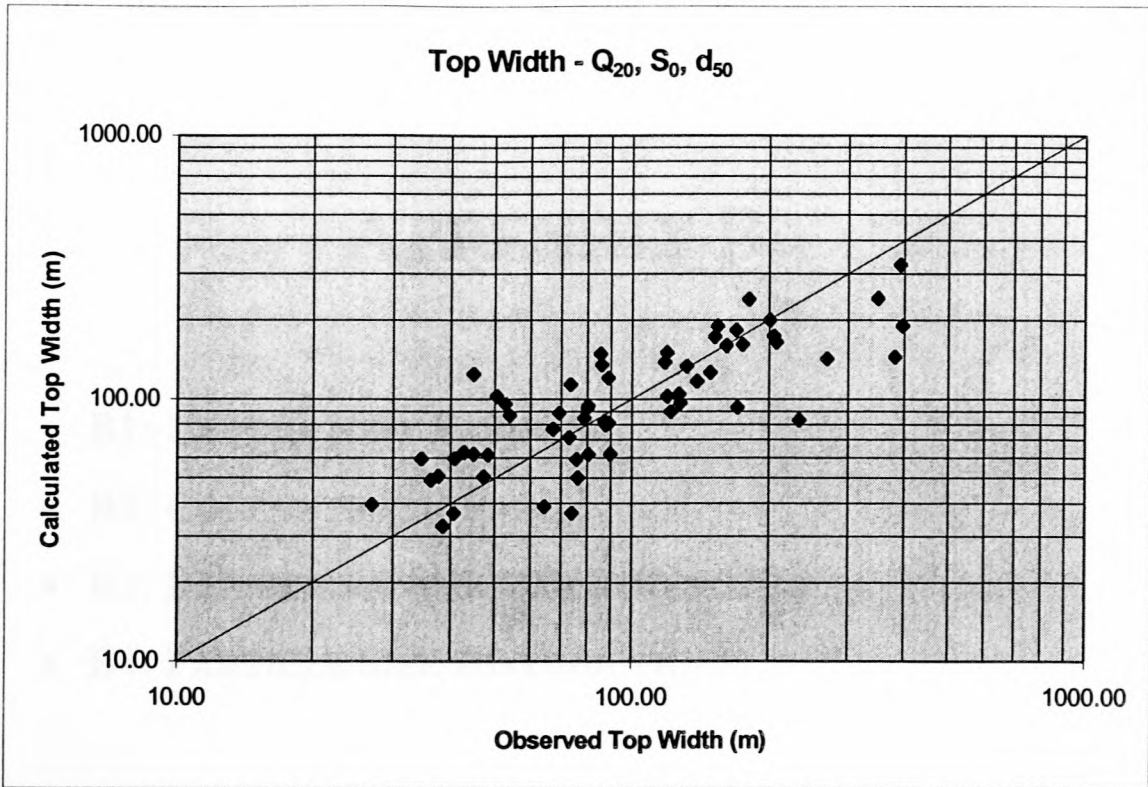


Top Width - Q_2 , S_0 , d_{50}



Top Width - Q_5 , S_0 , d_{50}





Regression results: $B = C_b Q_T^a S^b d_{50}^c$

| Recurrence interval T | C_b | a | b | c | Accuracy ranges | | | r^2 |
|-----------------------|-------|-------|--------|-------|-----------------|-------|--------|-------|
| | | | | | 0.67-1.5 | 0.5-2 | 0.33-3 | |
| 2 | 5.75 | 0.368 | -0.209 | 0.085 | 51% | 86% | 97% | 0.4 |
| 5 | 4.63 | 0.361 | -0.182 | 0.036 | 61% | 93% | 98% | 0.58 |
| 20 | 2.79 | 0.33 | -0.269 | 0.011 | 73% | 90% | 100% | 0.63 |

Regression results: $B = C_b Q_T^a S^b$

| Recurrence interval T | C_b | a | b | c | Accuracy ranges | | | r^2 |
|-----------------------|-------|-------|--------|---|-----------------|-------|--------|-------|
| | | | | | 0.67-1.5 | 0.5-2 | 0.33-3 | |
| 2 | 2.49 | 0.369 | -0.208 | - | 53% | 83% | 95% | 0.38 |
| 5 | 3.33 | 0.357 | -0.183 | - | 71% | 92% | 98% | 0.57 |
| 20 | 2.54 | 0.329 | -0.27 | - | 71% | 92% | 100% | 0.63 |

Regression results: $B = C_b Q_T^a$

| Recurrence interval T | C_b | a | b | c | Accuracy ranges | | | r^2 |
|-----------------------|-------|-------|---|---|-----------------|-------|--------|-------|
| | | | | | 0.67-1.5 | 0.5-2 | 0.33-3 | |
| 2 | 4.94 | 0.475 | - | - | 47% | 83% | 97% | 0.31 |
| 5 | 5.47 | 0.458 | - | - | 64% | 92% | 98% | 0.48 |
| 20 | 4.89 | 0.473 | - | - | 63% | 85% | 98% | 0.45 |

APPENDIX B

- **B1: LABORATORY RESULTS**
- **B2: CONCENTRATIONS**
- **B3: DENSITIES AND SHEAR STRENGTHS**
- **B4: PARTICLE SIZE DISTRIBUTIONS**

APPENDIX B1: LABORATORY RESULTS

Flume Experiments: Sand

| Run | Water Depth (cm) | Flow Rate (l/s) | Channel Width (cm) | Channel Length (cm) | Flow Velocity (cm/s) | Water Surface Slope | Bed Slope | Friction Factor | Reynolds Number | Flow Regime |
|-----|------------------|-----------------|--------------------|---------------------|----------------------|---------------------|-----------|-----------------|-----------------|-------------|
| 1 | 0.012 | 0.001 | 0.010 | 0.175 | 0.041 | 0.001 | 0.001 | 0.112 | 0.00001 | 0.18 |
| 2 | 0.015 | 0.008 | 0.012 | 0.180 | 0.064 | 0.001 | 0.001 | 0.118 | 0.00003 | 0.12 |
| 3 | 0.018 | 0.020 | 0.015 | 0.187 | 0.075 | 0.001 | 0.001 | 0.127 | 0.00007 | 0.19 |
| 4 | 0.023 | 0.038 | 0.021 | 0.193 | 0.179 | 0.001 | 0.001 | 0.134 | 0.00015 | 0.12 |
| 5 | 0.028 | 0.055 | 0.025 | 0.198 | 0.212 | 0.001 | 0.001 | 0.139 | 0.00022 | 0.12 |
| 6 | 0.034 | 0.072 | 0.030 | 0.204 | 0.240 | 0.001 | 0.001 | 0.145 | 0.00028 | 0.12 |
| 7 | 0.040 | 0.090 | 0.035 | 0.210 | 0.257 | 0.001 | 0.001 | 0.151 | 0.00035 | 0.12 |

Flume Experiments: Clay (6% Fine)

| Run | Water Depth (cm) | Flow Rate (l/s) | Channel Width (cm) | Channel Length (cm) | Flow Velocity (cm/s) | Water Surface Slope | Bed Slope | Friction Factor | Reynolds Number | Flow Regime |
|-----|------------------|-----------------|--------------------|---------------------|----------------------|---------------------|-----------|-----------------|-----------------|-------------|
| 1 | 0.012 | 0.001 | 0.010 | 0.224 | 0.041 | 0.001 | 0.001 | 0.112 | 0.00001 | 0.18 |
| 2 | 0.015 | 0.008 | 0.012 | 0.229 | 0.064 | 0.001 | 0.001 | 0.118 | 0.00003 | 0.12 |
| 3 | 0.018 | 0.020 | 0.015 | 0.234 | 0.075 | 0.001 | 0.001 | 0.127 | 0.00007 | 0.19 |
| 4 | 0.023 | 0.038 | 0.021 | 0.239 | 0.179 | 0.001 | 0.001 | 0.134 | 0.00015 | 0.12 |
| 5 | 0.028 | 0.055 | 0.025 | 0.244 | 0.212 | 0.001 | 0.001 | 0.139 | 0.00022 | 0.12 |
| 6 | 0.034 | 0.072 | 0.030 | 0.249 | 0.240 | 0.001 | 0.001 | 0.145 | 0.00028 | 0.12 |
| 7 | 0.040 | 0.090 | 0.035 | 0.254 | 0.257 | 0.001 | 0.001 | 0.151 | 0.00035 | 0.12 |
| 8 | 0.046 | 0.108 | 0.040 | 0.259 | 0.270 | 0.001 | 0.001 | 0.157 | 0.00042 | 0.12 |
| 9 | 0.052 | 0.126 | 0.045 | 0.264 | 0.280 | 0.001 | 0.001 | 0.163 | 0.00049 | 0.12 |

Flume Experiments: Sand

| Run | Water Surface Slope | Bed Slope | Average Slope | Depth (m) | Discharge (m ³ /s) | Velocity (m/s) | Froude No. | Hydraulic Radius (m) | k _s (m) | d ₅₀ (mm) | C (mg/l) | T (°C) | Bedform |
|-----|---------------------|-----------|---------------|-----------|-------------------------------|----------------|------------|----------------------|--------------------|----------------------|----------|--------|------------|
| 1 | 0.0012 | 0.0007 | 0.0010 | 0.179 | 0.051 | 0.478 | 0.361 | 0.112 | 0.00357 | 0.12 | 566 | 24.5 | Ripples |
| 2 | 0.0015 | 0.0008 | 0.0012 | 0.187 | 0.061 | 0.544 | 0.401 | 0.115 | 0.00330 | 0.12 | 500 | 30.5 | Dunes |
| 8 | 0.0013 | 0.0009 | 0.0011 | 0.167 | 0.052 | 0.521 | 0.407 | 0.107 | 0.00280 | 0.12 | 553 | 29.0 | Dunes |
| 3 | 0.0023 | 0.0019 | 0.0021 | 0.138 | 0.070 | 0.850 | 0.732 | 0.094 | 0.00050 | 0.12 | 1552 | 27.0 | Transition |
| 4 | 0.0024 | 0.0019 | 0.0022 | 0.136 | 0.073 | 0.891 | 0.772 | 0.094 | 0.00036 | 0.12 | 1500 | 29.0 | Transition |
| 5 | 0.0026 | 0.0023 | 0.0025 | 0.132 | 0.078 | 0.986 | 0.867 | 0.092 | 0.00024 | 0.12 | 1616 | 32.0 | Transition |
| 6 | 0.0041 | 0.0052 | 0.0047 | 0.119 | 0.079 | 1.112 | 1.031 | 0.085 | 0.00080 | 0.12 | 2668 | 28.0 | Antidunes |
| 7 | 0.0080 | 0.0070 | 0.0075 | 0.086 | 0.052 | 1.011 | 1.101 | 0.067 | 0.00249 | 0.12 | 35745 | 28.5 | Antidunes |

Flume Experiments: Clay (88% Fines)

| Run | Water Surface Slope | Bed Slope | Energy Slope | Depth (m) | Discharge (m ³ /s) | Velocity (m/s) | Froude No. | Hydraulic Radius (m) | k _s (m) | τ (Pa) | d ₅₀ (mm) | C (mg/l) | T (°C) |
|-----|---------------------|-----------|--------------|-----------|-------------------------------|----------------|------------|----------------------|--------------------|--------|----------------------|----------|--------|
| 1 | 0.00035 | 0.0051 | 0.00044 | 0.225 | 0.0078 | 0.057 | 0.039 | 0.129 | 0.5831 | 0.973 | 0.001 | 458 | 17.5 |
| 2 | 0.0004 | 0.0048 | 0.00037 | 0.223 | 0.0101 | 0.076 | 0.051 | 0.128 | 0.3755 | 0.808 | 0.001 | 444 | 19.5 |
| 3 | 0.00035 | 0.0049 | 0.00024 | 0.221 | 0.0131 | 0.099 | 0.067 | 0.127 | 0.1535 | 0.520 | 0.001 | 606 | 21 |
| 4 | 0.00035 | 0.005 | 0.00035 | 0.219 | 0.0159 | 0.121 | 0.082 | 0.127 | 0.1489 | 0.752 | 0.001 | 600 | 22.5 |
| 5 | 0.0003 | 0.0051 | 0.00041 | 0.213 | 0.0200 | 0.156 | 0.108 | 0.124 | 0.0906 | 0.856 | 0.001 | 630 | 18.5 |
| 6 | 0.00035 | 0.0051 | 0.0003 | 0.210 | 0.0250 | 0.199 | 0.138 | 0.124 | 0.0228 | 0.618 | 0.001 | 800 | 21 |
| 7 | 0.00035 | 0.0051 | 0.00038 | 0.205 | 0.0301 | 0.244 | 0.172 | 0.122 | 0.0148 | 0.765 | 0.001 | 2030 | 24 |
| 8 | 0.0003 | 0.0005 | 0.00034 | 0.199 | 0.0350 | 0.294 | 0.211 | 0.120 | 0.0039 | 0.663 | 0.001 | 2400 | 19 |
| 9 | 0.00035 | 0.0049 | 0.00044 | 0.197 | 0.0399 | 0.338 | 0.243 | 0.119 | 0.0036 | 0.850 | 0.001 | 3180 | 21 |
| 10 | 0.00055 | 0.0046 | 0.00065 | 0.196 | 0.0500 | 0.424 | 0.305 | 0.119 | 0.0030 | 1.253 | 0.001 | 7530 | 23 |

Flume Experiments: Mixture 1 (77% Fines)

| Run ¹ | Water Surface Slope | Bed Slope | Energy Slope | Depth (m) | Discharge (m ³ /s) | Velocity (m/s) | Froude No. | Hydraulic Radius (m) | k _s (m) | τ (Pa) | d ₅₀ (mm) | C (mg/l) | T (°C) |
|------------------|---------------------|-----------|--------------|-----------|-------------------------------|----------------|------------|----------------------|--------------------|--------|----------------------|----------|--------|
| 1 | 0.00043 | 0.0011 | 0.00036 | 0.194 | 0.0079 | 0.068 | 0.049 | 0.118 | 0.3735 | 0.685 | 0.001 | 430 | 15.5 |
| 2 | 0.00038 | 0.0011 | 0.00036 | 0.193 | 0.0101 | 0.087 | 0.063 | 0.117 | 0.2528 | 0.682 | 0.001 | 475 | 18 |
| 3 | 0.00033 | 0.00092 | 0.00042 | 0.192 | 0.0136 | 0.118 | 0.086 | 0.117 | 0.1631 | 0.790 | 0.001 | 585 | 19.5 |
| 4 | 0.00028 | 0.00098 | 0.00036 | 0.194 | 0.0155 | 0.134 | 0.097 | 0.118 | 0.1027 | 0.685 | 0.001 | 645 | 16 |
| 5 | 0.00031 | 0.00099 | 0.00029 | 0.193 | 0.0200 | 0.173 | 0.126 | 0.117 | 0.0318 | 0.548 | 0.001 | 900 | 18.5 |
| 6 | 0.00032 | 0.00099 | 0.00035 | 0.191 | 0.0250 | 0.219 | 0.160 | 0.117 | 0.0176 | 0.655 | 0.001 | 1465 | 21.5 |
| 7 | 0.00037 | 0.00101 | 0.00041 | 0.183 | 0.0292 | 0.265 | 0.198 | 0.114 | 0.0095 | 0.737 | 0.001 | 1830 | 15.5 |
| 8 | 0.00031 | 0.00102 | 0.00022 | 0.181 | 0.0328 | 0.302 | 0.227 | 0.113 | 0.0006 | 0.391 | 0.001 | 2595 | 18 |
| 9 | 0.00047 | 0.00118 | 0.00053 | 0.178 | 0.0383 | 0.359 | 0.272 | 0.112 | 0.0034 | 0.924 | 0.001 | 3545 | 19.5 |
| 10 | 0.0006 | 0.00101 | 0.00063 | 0.172 | 0.0460 | 0.444 | 0.342 | 0.110 | 0.0014 | 1.066 | 0.001 | 6470 | 21.5 |

Flume Experiments: Mixture 2 (54% Fines)

| Run ¹ | Water Surface Slope | Bed Slope | Energy Slope | Depth (m) | Discharge (m ³ /s) | Velocity (m/s) | Froude No. | Hydraulic Radius (m) | k _s (m) | τ (Pa) | d ₅₀ (mm) | C (mg/l) | T (°C) |
|------------------|---------------------|-----------|--------------|-----------|-------------------------------|----------------|------------|----------------------|--------------------|--------|----------------------|----------|--------|
| 1 | 0.00036 | 0.00087 | 0.00055 | 0.191 | 0.0083 | 0.072 | 0.053 | 0.117 | 0.4418 | 1.029 | 0.017 | 1555 | 14 |
| 2 | 0.0003 | 0.00086 | 0.00061 | 0.192 | 0.0101 | 0.088 | 0.064 | 0.117 | 0.3694 | 1.146 | 0.017 | 1550 | 18 |
| 3 | 0.00036 | 0.00069 | 0.0004 | 0.191 | 0.0136 | 0.118 | 0.087 | 0.117 | 0.1353 | 0.675 | 0.017 | 1575 | 20 |
| 4 | 0.00024 | 0.00078 | 0.00006 | 0.189 | 0.0161 | 0.143 | 0.105 | 0.116 | 0.0011 | 0.444 | 0.017 | 1425 | 21 |
| 5 | 0.00032 | 0.00095 | 0.00025 | 0.185 | 0.0200 | 0.180 | 0.133 | 0.115 | 0.0180 | 0.446 | 0.017 | 1770 | 16.5 |
| 6 | 0.00027 | 0.00083 | 0.0003 | 0.185 | 0.0244 | 0.221 | 0.164 | 0.114 | 0.0085 | 0.489 | 0.017 | 1800 | 18 |
| 7 | 0.00028 | 0.00087 | 0.00016 | 0.184 | 0.0291 | 0.264 | 0.197 | 0.114 | 0.0005 | 0.285 | 0.017 | 2170 | 21 |
| 8 | 0.00039 | 0.00091 | 0.00032 | 0.181 | 0.0326 | 0.300 | 0.225 | 0.113 | 0.0022 | 0.559 | 0.017 | 2455 | 18 |
| 9 | 0.00050 | 0.00092 | 0.00039 | 0.174 | 0.0380 | 0.364 | 0.278 | 0.110 | 0.0011 | 0.662 | 0.017 | 4195 | 24 |
| 10 | 0.00079 | 0.00096 | 0.00088 | 0.168 | 0.0457 | 0.452 | 0.352 | 0.108 | 0.0035 | 1.461 | 0.017 | 5095 | 25 |
| 11 | 0.00102 | 0.00096 | 0.00107 | 0.163 | 0.0540 | 0.552 | 0.437 | 0.106 | 0.0016 | 1.710 | 0.017 | 7095 | 26 |
| 12 | 0.00135 | 0.00127 | 0.00157 | 0.160 | 0.0638 | 0.667 | 0.533 | 0.104 | 0.0016 | 2.457 | 0.017 | 11235 | 26 |

Flume Experiments: Mixture 3 (20% Fines)²

| Run ¹ | Water Surface Slope | Bed Slope | Energy Slope | Depth (m) | Discharge (m ³ /s) | Velocity (m/s) | Froude No. | Hydraulic Radius (m) | k _s (m) | τ (Pa) | d ₅₀ (mm) | C (mg/l) | T (°C) | Remarks |
|------------------|---------------------|-----------|--------------|-----------|-------------------------------|----------------|------------|----------------------|--------------------|--------|----------------------|----------|--------|--------------|
| 4 | 0.00026 | 0.00195 | 0.00033 | 0.186 | 0.0160 | 0.143 | 0.106 | 0.115 | 0.0696 | 0.601 | 0.105 | 3550 | 17 | |
| 6 | 0.00032 | 0.00198 | 0.00031 | 0.183 | 0.0250 | 0.228 | 0.170 | 0.114 | 0.0101 | 0.556 | 0.105 | 3593 | 21 | |
| 7 | 0.00023 | 0.00182 | 0.0002 | 0.184 | 0.0289 | 0.262 | 0.195 | 0.114 | 0.0012 | 0.415 | 0.105 | 3958 | 18 | |
| 8 | 0.00034 | 0.00192 | 0.00044 | 0.172 | 0.0330 | 0.320 | 0.246 | 0.109 | 0.0036 | 0.574 | 0.105 | 4333 | 21 | |
| 9 | 0.00044 | 0.00185 | 0.00057 | 0.170 | 0.0380 | 0.372 | 0.288 | 0.108 | 0.0030 | 0.950 | 0.105 | 5163 | 22 | |
| 10 | 0.00064 | 0.0021 | 0.00084 | 0.165 | 0.0450 | 0.455 | 0.358 | 0.106 | 0.0027 | 1.034 | 0.105 | 6575 | 16 | Sand Ripples |
| 11 | 0.00087 | 0.00193 | 0.00106 | 0.163 | 0.0529 | 0.540 | 0.426 | 0.106 | 0.0019 | 1.700 | 0.105 | 8925 | 19 | Sand Ripples |
| 12 | 0.0013 | 0.00168 | 0.00147 | 0.160 | 0.0640 | 0.667 | 0.533 | 0.104 | 0.0013 | 2.306 | 0.105 | 13655 | 20 | Sand Ripples |

Flume Experiments: Mixture 4 (7% Fines)²

| Run ¹ | Water Surface Slope | Bed Slope | Energy Slope | Depth (m) | Discharge (m ³ /s) | Velocity (m/s) | Froude No. | Hydraulic Radius (m) | k _s (m) | τ (Pa) | d ₅₀ (mm) | C (mg/l) | T (°C) | Remarks |
|------------------|---------------------|-----------|--------------|-----------|-------------------------------|----------------|------------|----------------------|--------------------|--------|----------------------|----------|--------|--------------|
| 4 | 0.00043 | 0.00296 | 0.00057 | 0.186 | 0.0160 | 0.143 | 0.106 | 0.115 | 0.1429 | 1.039 | 0.11 | 2300 | 12 | |
| 7 | 0.00026 | 0.00244 | 0.00046 | 0.185 | 0.0289 | 0.261 | 0.193 | 0.114 | 0.0139 | 0.835 | 0.11 | 3080 | 20 | Dunes (+6mm) |
| 9 | 0.00074 | 0.00308 | 0.0007 | 0.174 | 0.0380 | 0.364 | 0.279 | 0.110 | 0.0066 | 1.262 | 0.11 | 6760 | 23 | Dunes |
| 10 | 0.00097 | 0.00306 | 0.00119 | 0.169 | 0.0450 | 0.445 | 0.346 | 0.108 | 0.0086 | 1.605 | 0.11 | 9500 | 22 | Dunes |
| 11 | 0.00126 | 0.00312 | 0.00141 | 0.162 | 0.0529 | 0.544 | 0.431 | 0.105 | 0.0042 | 2.242 | 0.11 | 14840 | 22 | Dunes |
| 12 | 0.00152 | 0.00113 | 0.00134 | 0.156 | 0.0638 | 0.683 | 0.552 | 0.103 | 0.0007 | 2.324 | 0.11 | 12020 | 19 | Dunes+Flat |
| 13 | 0.00183 | 0.00089 | 0.00142 | 0.147 | 0.0738 | 0.839 | 0.700 | 0.098 | 0.0001 | 2.043 | 0.11 | 10420 | 23 | Transition |

¹: Runs with the same numbers indicate that they were done at similar discharges and flow depths

²: Mixtures 3 and 4 were started at higher flow rates because of the larger amounts of sand

| Sediment | Run | Duration (h) | C (mg/l) | Sediment | Run | Duration (h) | C (mg/l) | Sediment | Run | Duration (h) | C (mg/l) |
|-------------------|-----|--------------|----------|-------------------------------|-----|--------------|----------|------------------------------------|------|--------------|----------|
| Sand ¹ | 1 | 11.75 | 566 | Clay (88% Fines) ² | 1 | | 656 | Mixture 1 (77% Fines) ² | 1 | | 493 |
| | 2 | 18 | 1682 | | | 0.5 | 458 | | | 2.8 | 430 |
| | 3 | 16.5 | 1552 | | 2 | | 486 | | 2 | | 435 |
| | 4 | 9.3 | 513 | | | 2 | 444 | | | 1.5 | 475 |
| | 5 | 5.5 | 1616 | | 3 | | 530 | | 3 | | 550 |
| | 6 | 3.8 | 2668 | | | 1 | 606 | | | 2 | 585 |
| | 7 | 2 | 35745 | | 4 | | 600 | | 4 | | 570 |
| | 8 | 26.1 | 553 | | | 1.8 | 630 | | | 2 | 645 |
| | | | | | 5 | | 555 | | 5 | | 655 |
| | | | | | | 1 | 600 | | | 2 | 900 |
| | | | | 6 | | 620 | 6 | | 940 | | |
| | | | | | 2 | 800 | | 3 | 1465 | | |
| | | | | 7 | | 840 | 7 | | 1380 | | |
| | | | | | 3.5 | 2030 | | 1.5 | 1830 | | |
| | | | | 8 | | 1495 | 8 | | 1885 | | |
| | | | | | 1.3 | 2400 | | 2 | 2595 | | |
| | | | | 9 | | 2570 | 9 | | 2660 | | |
| | | | | | 1.8 | 3180 | | 2 | 3545 | | |
| | | | | 10 | | 3400 | 10 | | 4100 | | |
| | | | | | 2 | 7530 | | 2 | 6470 | | |

¹ Concentrations taken at the end of each run

² Concentrations taken at the start and end of each run

| Sediment | Run | Duration (h) | C (mg/l) | Sediment | Run | Duration (h) | C (mg/l) | Sediment | Run | Duration (h) | C (mg/l) | |
|------------------------------------|------|--------------|----------|------------------------------------|------|--------------|----------|-----------------------------------|-------|--------------|----------|-------|
| Mixture 2 (54% Fines) ² | 1 | | 1985 | Mixture 3 (20% Fines) ² | 4 | | 3873 | Mixture 4 (7% Fines) ² | 4 | | 2340 | |
| | | 1.7 | 1555 | | | 5 | 3550 | | | 1.3 | 2300 | |
| | 2 | | - | | | 6 | 3373 | | | 7 | 2440 | |
| | | 2.5 | 1550 | | | | 5 | | 3593 | | 6.3 | 3080 |
| | 3 | | 1535 | | | 7 | 2975 | | | 9 | 3800 | |
| | | 2.3 | 1575 | | | | 4.3 | | 3958 | | 1.5 | 6760 |
| | 4 | | 1600 | | | 8 | 3953 | | | 10 | 6840 | |
| | | 1.8 | 1425 | | | | 2.7 | | 4333 | | 9.5 | 9500 |
| | 5 | | 1745 | | | 9 | 4378 | | | 11 | 7680 | |
| | | 2.5 | 1770 | | | | 2.3 | | 5163 | | 14.8 | 14840 |
| | 6 | | 1760 | | | 10 | 4855 | | | 12 | 11120 | |
| | | 2.4 | 1800 | | | | 2 | | 6575 | | 23.3 | 12020 |
| 7 | | 1875 | | 11 | 6457 | | 13 | | 10680 | | | |
| | 2.3 | 2170 | | | 2.8 | 8925 | | 4.8 | 10420 | | | |
| 8 | | 2220 | | 12 | 8910 | | | | | | | |
| | 3.2 | 2455 | | | 24.3 | 13655 | | | | | | |
| 9 | | 2480 | | | | | | | | | | |
| | 20.8 | 4195 | | | | | | | | | | |
| 10 | | 3695 | | | | | | | | | | |
| | 5.6 | 5095 | | | | | | | | | | |
| 11 | | 5250 | | | | | | | | | | |
| | 3.3 | 7095 | | | | | | | | | | |
| 12 | | 2755 | | | | | | | | | | |
| | 2.5 | 11235 | | | | | | | | | | |

² Concentrations taken at the start and end of each run

Densities and shear strengths of the bed measured after 100 days

| Bed Sediment | Wet density (kg/m ³) | Dry density (kg/m ³) | Wet shear strength (kPa) | Dry shear strength (kPa) |
|--------------|-------------------------------------|-------------------------------------|-----------------------------|-----------------------------|
| Clay | 1850 | 1450 | 10 | 10 |
| Mixture 1 | 1850 | 1450 | 10 | 10 |
| Mixture 2 | 1850 | 1450 | 10 | 10 |
| Mixture 3 | 1850 | 1450 | 10 | 10 |
| Mixture 4 | 1850 | 1450 | 10 | 10 |

APPENDIX B3: DENSITIES AND SHEAR STRENGTHS

Densities and shear strengths of the bed measured after each experiment

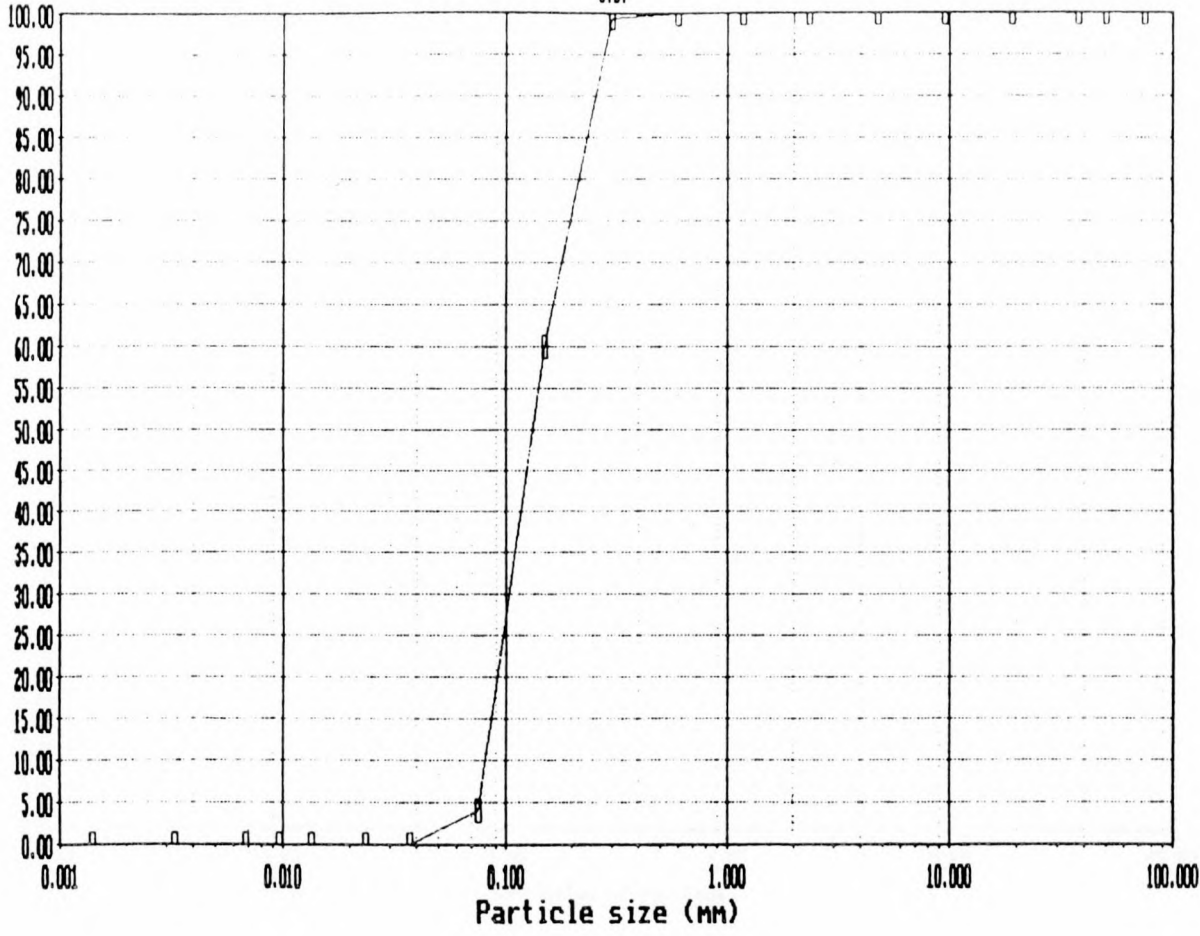
| Bed Sediment | Wet density (kg/m ³) | Dry density (kg/m ³) | Moisture content (%) | Shear Strength (kPa) |
|--------------|----------------------------------|----------------------------------|----------------------|----------------------|
| Sand | 1971 | 1602 | 23 | 1.4 |
| Clay | 1169 | 310 | 298 | 0.7 |
| Mixture 1 | 1890 | 1131 | 67 | 0.4 |
| Mixture 2 | 1693 | 1273 | 34 | 0.68 |
| Mixture 3 | 2139 | 1865 | 16 | 0.93 |
| Mixture 4 | 1747 | 1460 | 20 | 0.58 |

Particle size distributions

| | | d (mm) | 0.002 | 0.02 - 0.002 | 0.05 - 0.02 | 0.106 - 0.05 | 0.25 - 0.106 | 0.5 - 0.25 | 2 - 0.5 |
|-----------------|---|-----------------------|----------|--------------|-------------|--------------|--------------|------------|---------|
| | | d _{ave} (mm) | 0.0014 | 0.0063 | 0.032 | 0.073 | 0.163 | 0.354 | 1 |
| | | w (m/s) | 1.76E-06 | 3.57E-05 | 0.00092 | 0.00479 | 0.0187 | 0.0525 | 0.1176 |
| S0 | Sand - bed material before tests | % in Category | 0 | 0 | 2 | 29 | 61 | 8 | 0 |
| C0 | Sand - bed material after tests | % in Category | 73 | 9 | 11 | 7 | 0 | 0 | 0 |
| SSUR | Clay (88% fines)- bed material before tests | % in Category | 0 | 0 | 1 | 24 | 67 | 7 | 0 |
| CS1 | Clay (88% fines) - bed material after tests | % in Category | 79 | 10 | 7 | 4 | 0 | 0 | 0 |
| M0 | Mixture 1 (77% fines) - bed material before tests | % in Category | 64 | 9 | 8 | 9 | 9 | 1 | 0 |
| M21 | Mixture 1 (77% fines) - bed material after tests | % in Category | 74 | 8 | 9 | 6 | 3 | 0 | 0 |
| S4C6-1.1 | Mixture 2 (54% fines) - bed material before tests | % in Category | 44 | 7 | 6 | 15 | 24 | 4 | 0 |
| S4C6-12.3 | Mixture 2 (54% fines) - bed material after tests | % in Category | 27 | 9 | 20 | 38 | 6 | 0 | 0 |
| S4C6-Monsters | Mixture 2 (54% fines) - suspended sediments | % in Category | 57 | 25 | 8 | 10 | 0 | 0 | 0 |
| S6C4-4-1 | Mixture 3 (20% fines) - bed material before tests | % in Category | 16 | 3 | 5 | 22 | 48 | 6 | 1 |
| S6C4-12.3 | Mixture 3 (20% fines) - bed material after tests | % in Category | 2 | 1 | 2 | 22 | 62 | 10 | 1 |
| S6C4-Monsters | Mixture 3 (20% fines) - suspended sediments | % in Category | 63 | 18 | 7 | 12 | 0 | 0 | 0 |
| S8C2-1.1 | Mixture 4 (7% fines) - bed material before tests | % in Category | 6 | 0 | 2 | 26 | 58 | 7 | 1 |
| S8C2-13.3 | Mixture 4 (7% fines) - bed material after tests | % in Category | 0 | 1 | 2 | 29 | 60 | 7 | 1 |
| S8C2-Kombinasie | Mixture 4 (7% fines) - suspended sediments | % in Category | 43 | 9 | 13 | 20 | 13 | 2 | 0 |

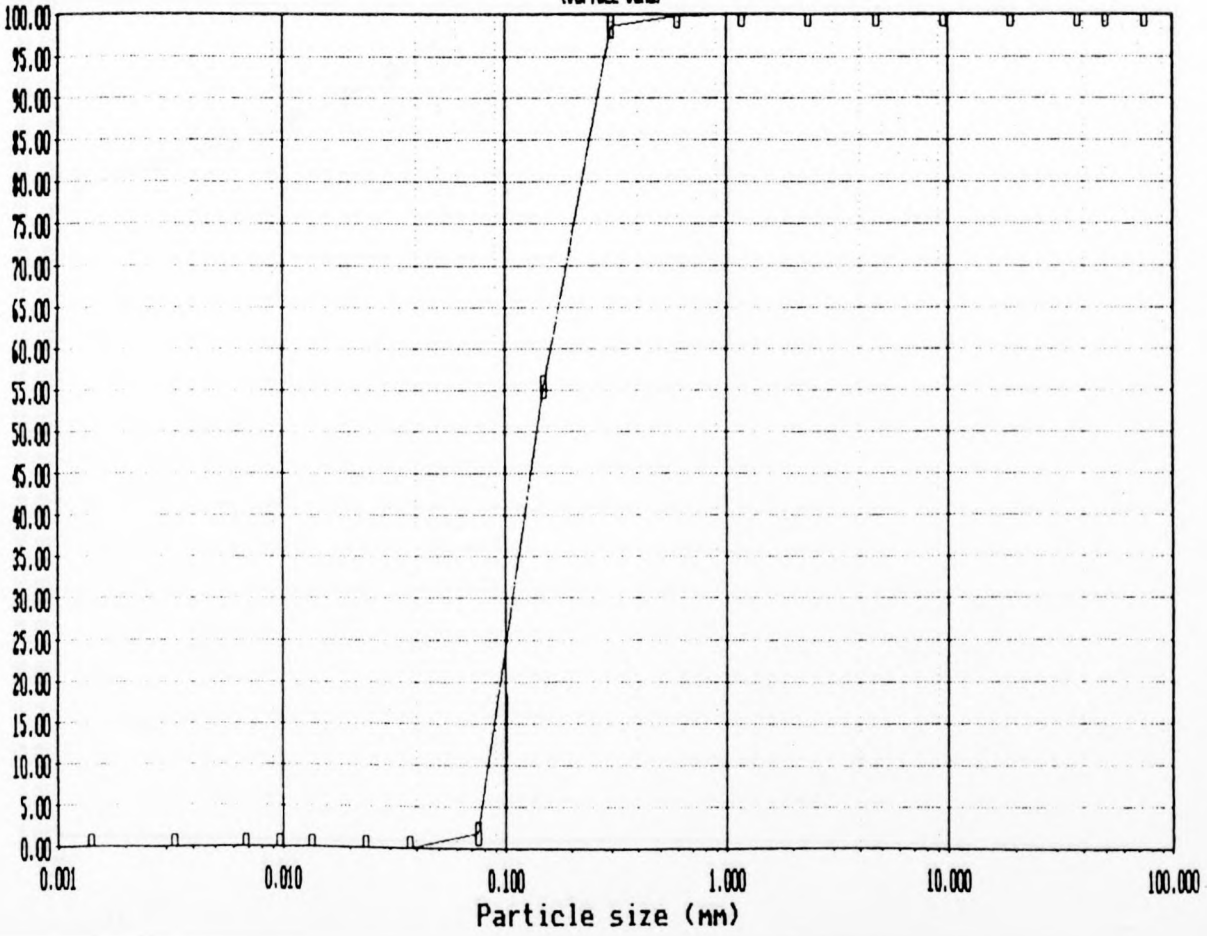
Cumulative percentage passing

SØ
J.B.



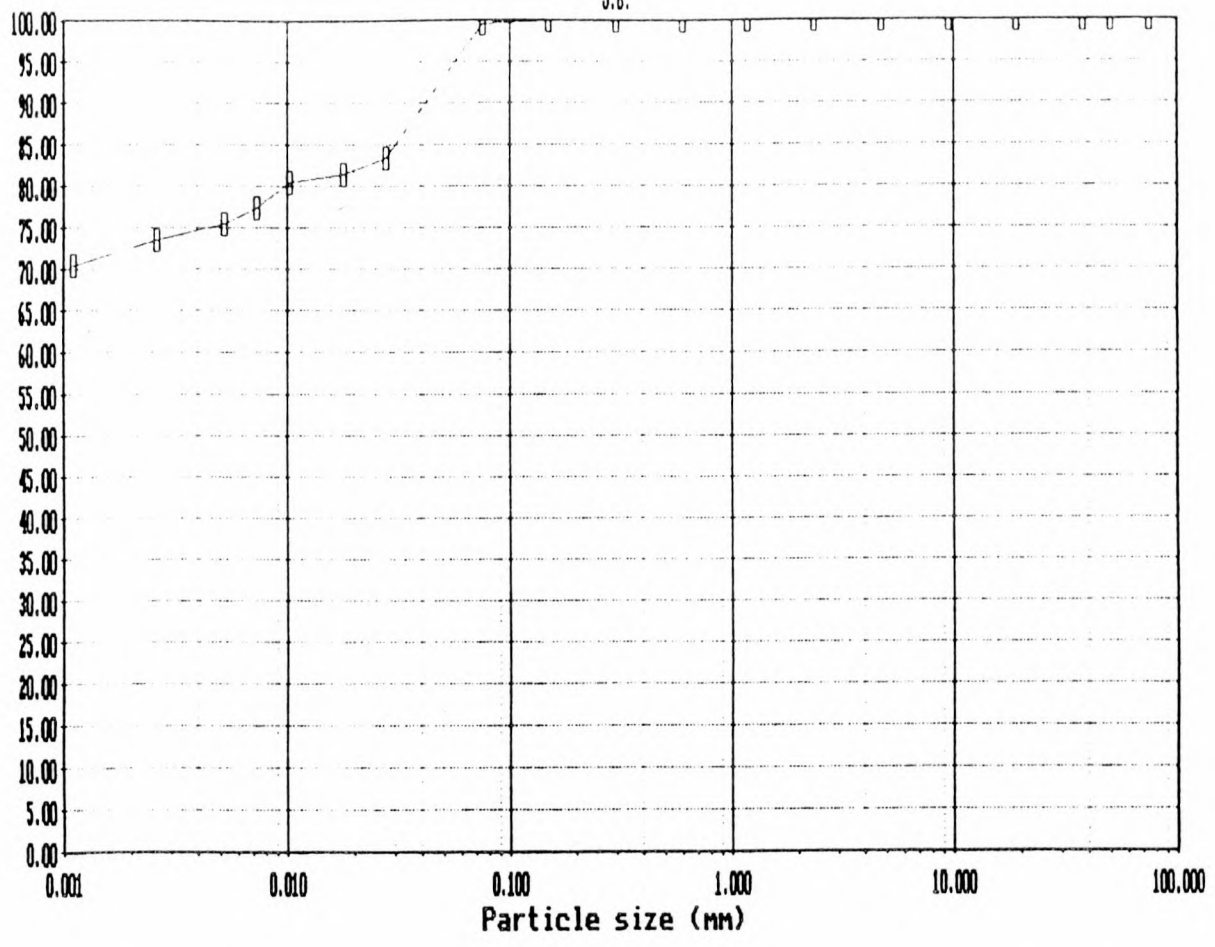
SSUR
(Surface Sand)

Cumulative percentage passing



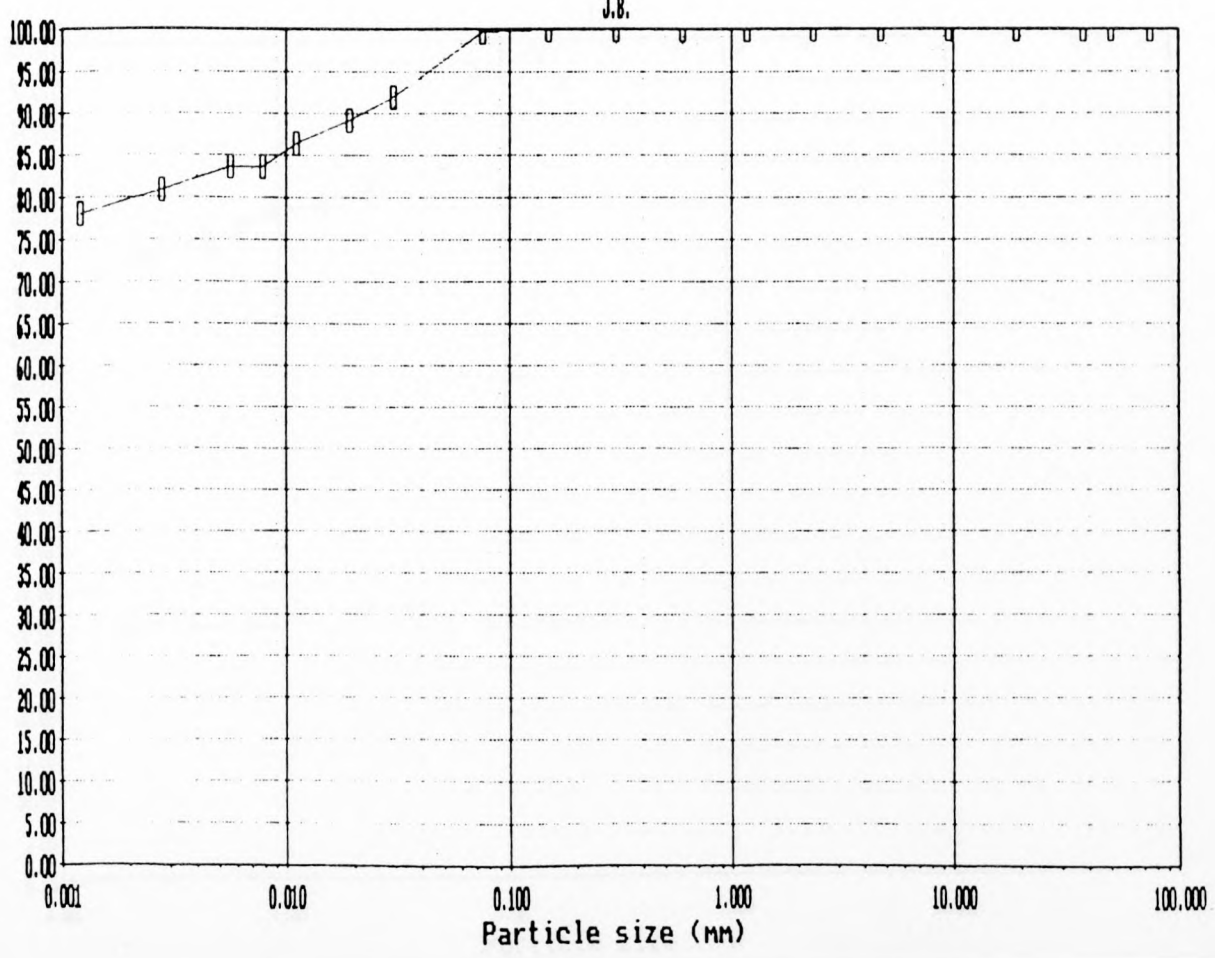
Cumulative percentage passing

C8
J.B.

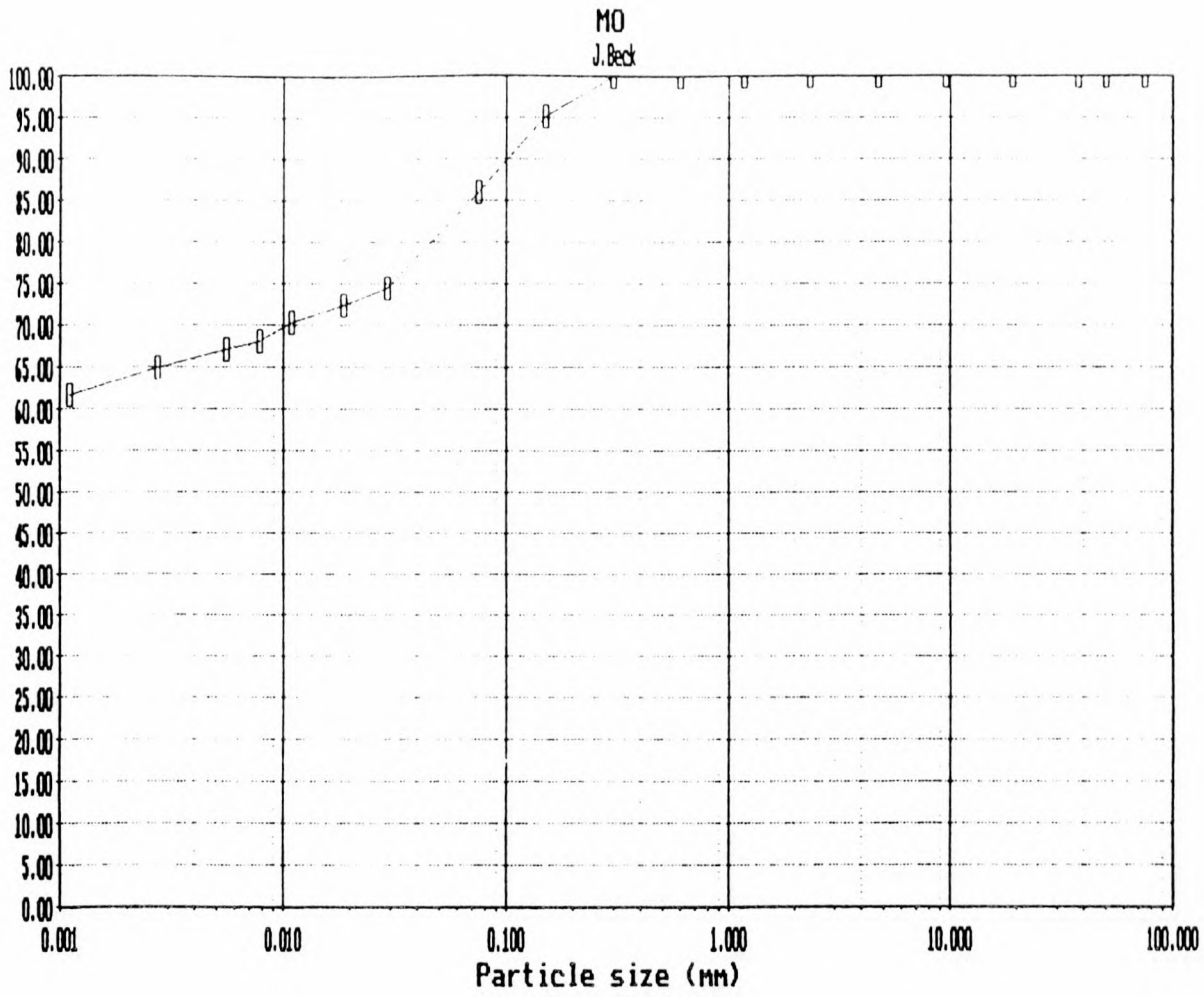


Cumulative percentage passing

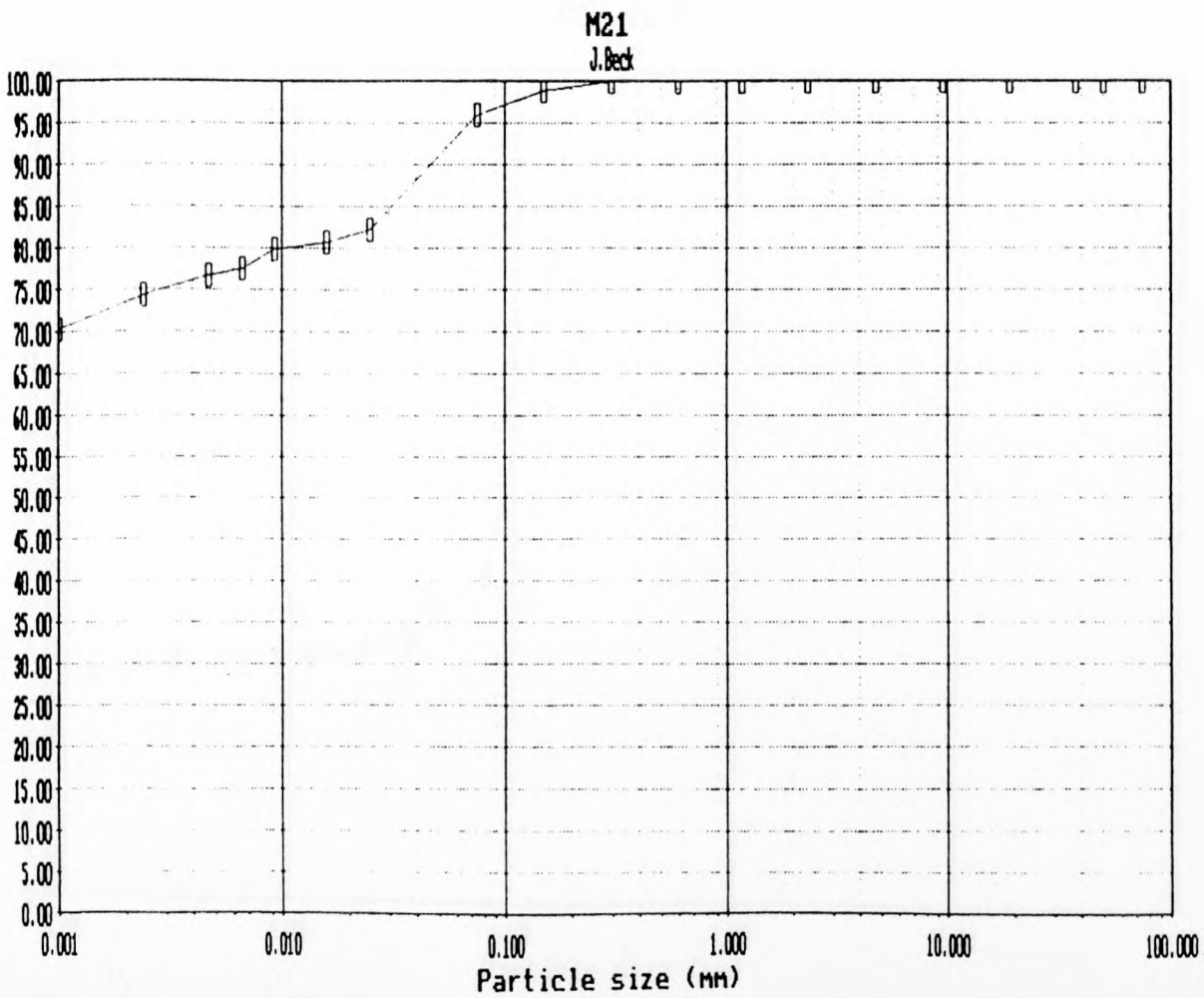
CS1
J.B.



Cumulative percentage passing



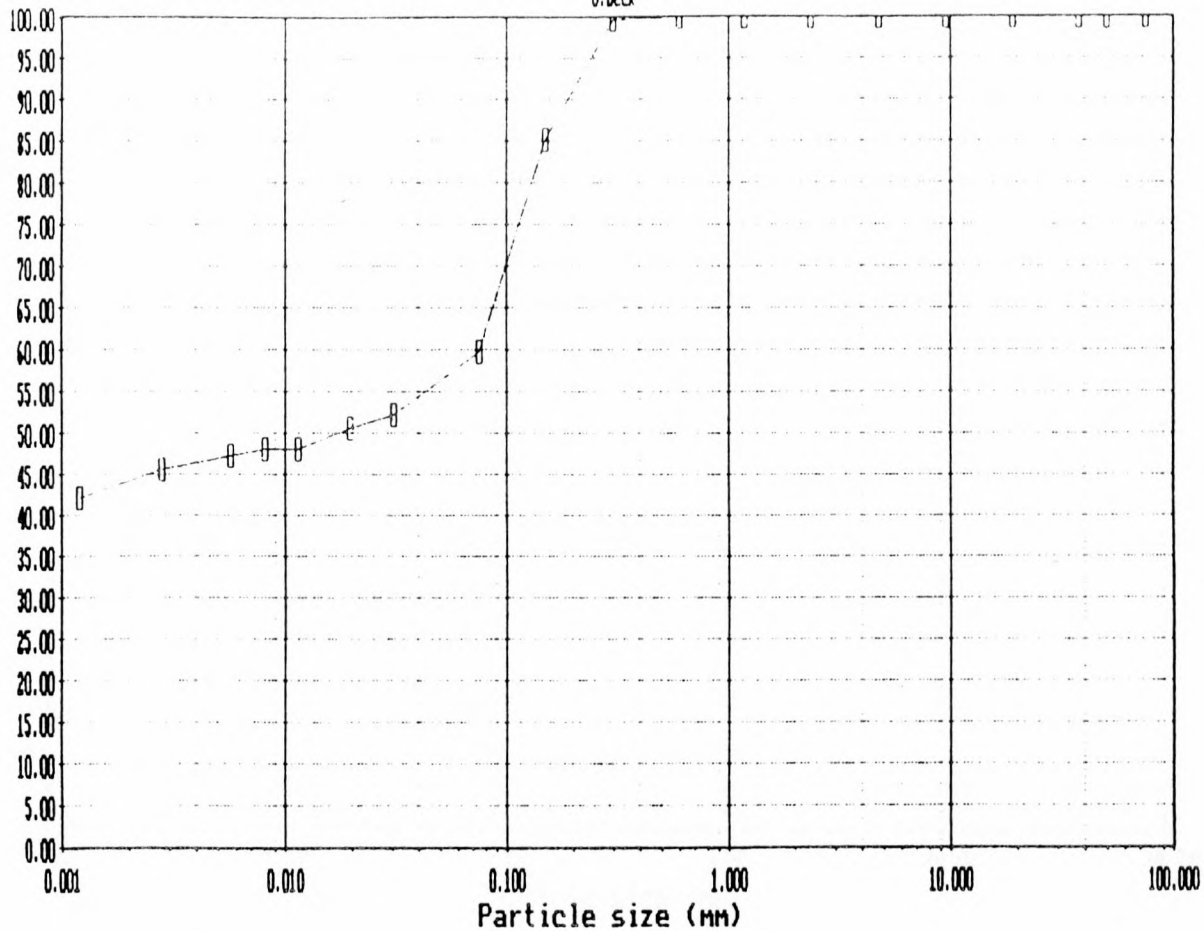
Cumulative percentage passing



S4C6-1.1

J. Beck

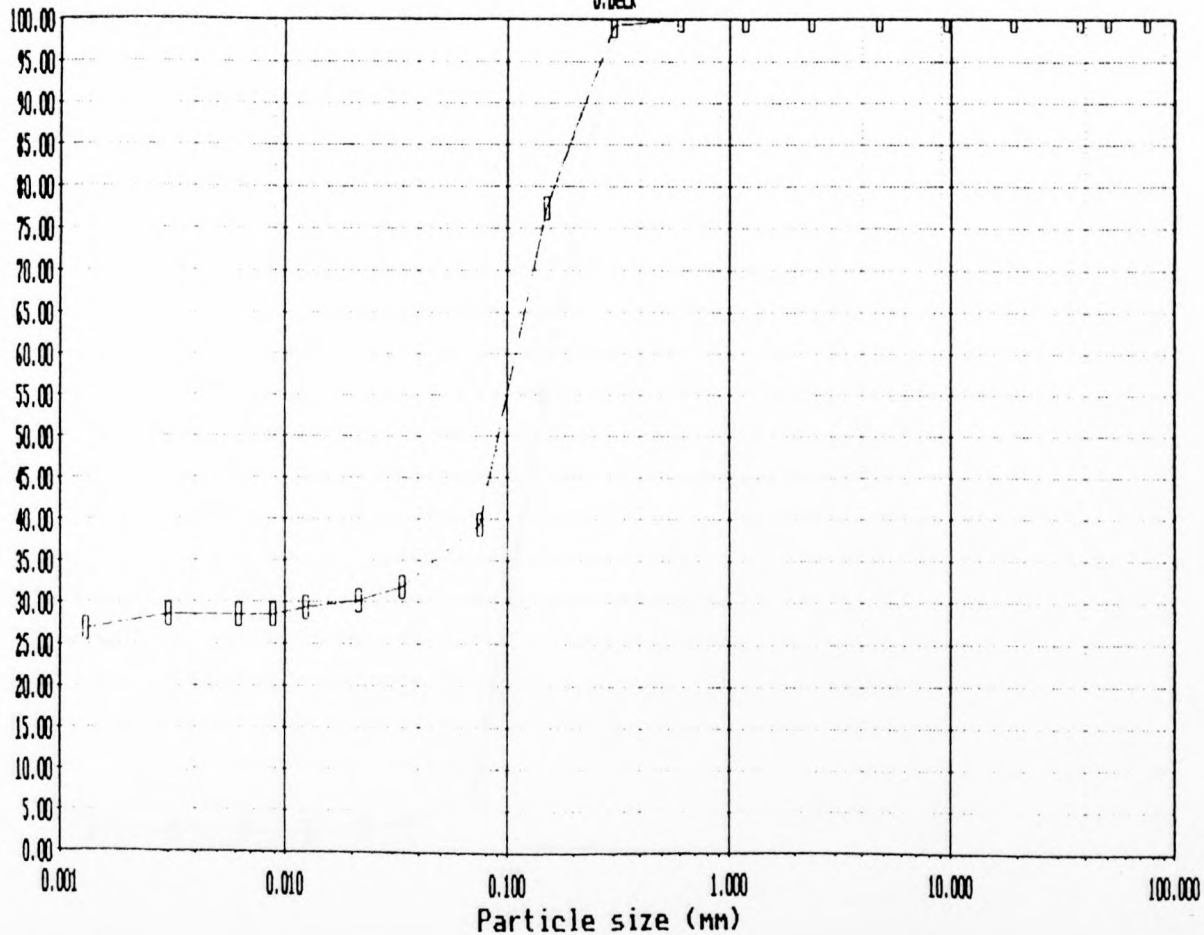
Cumulative percentage passing



S4C6-12.3

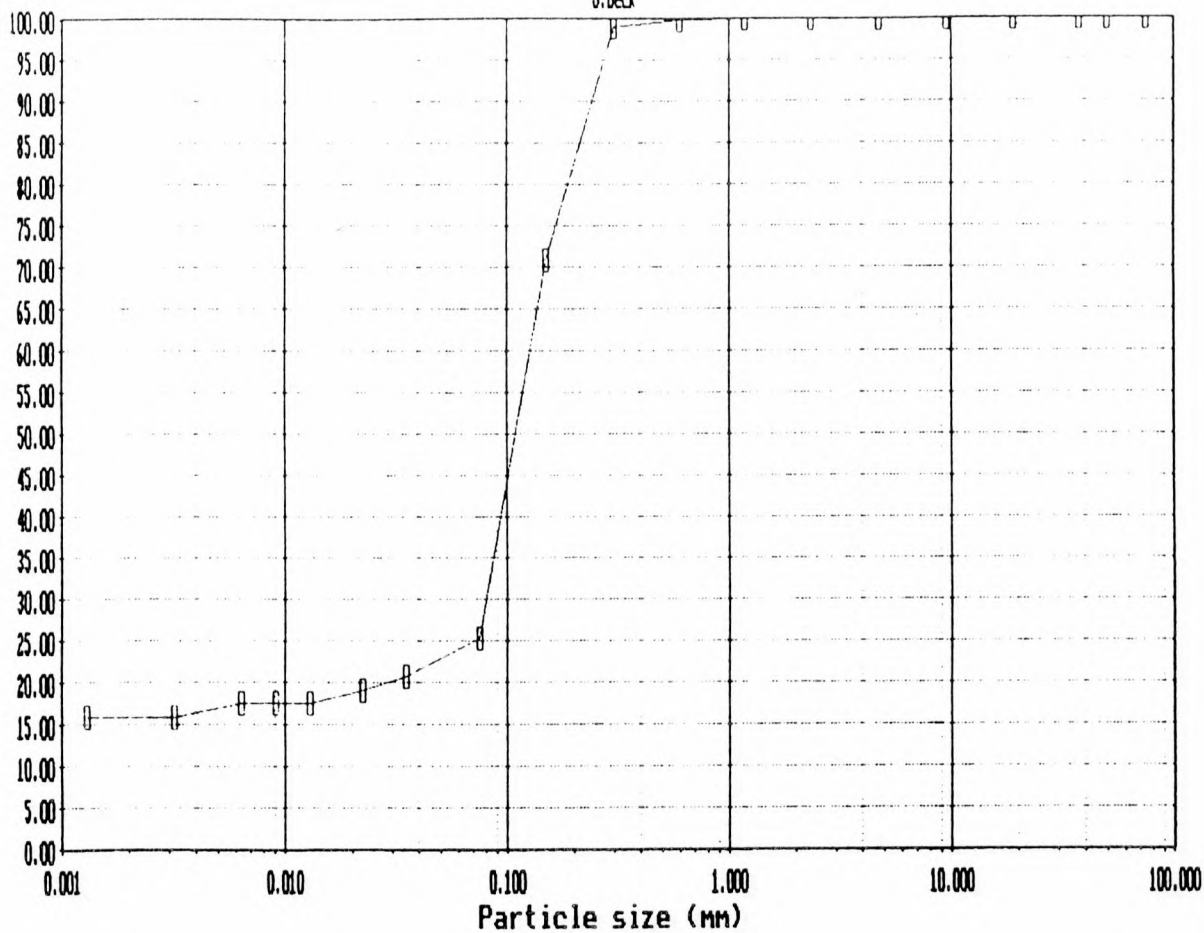
J. Beck

Cumulative percentage passing



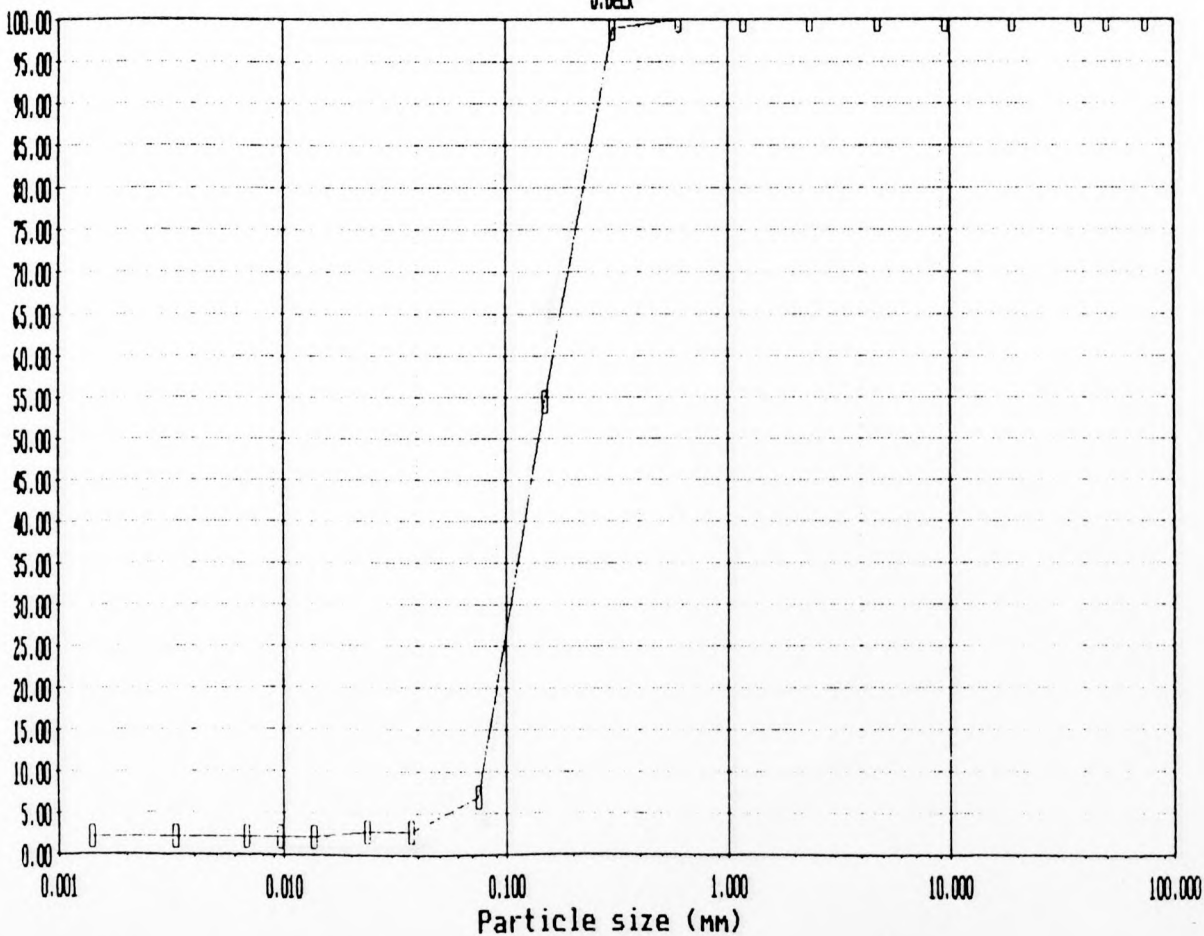
S6C4-4.1

J.Beck



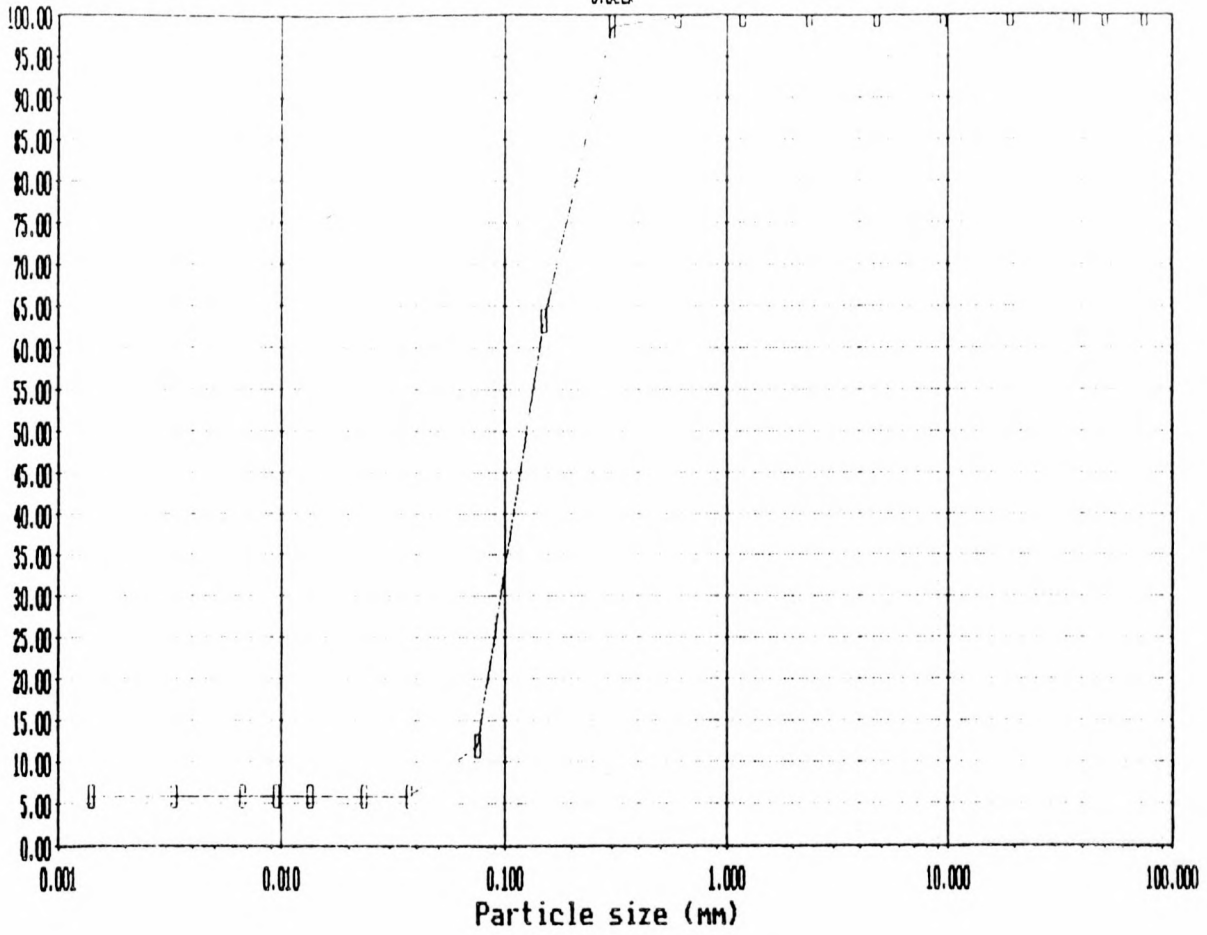
S6C4-12.3

J.Beck



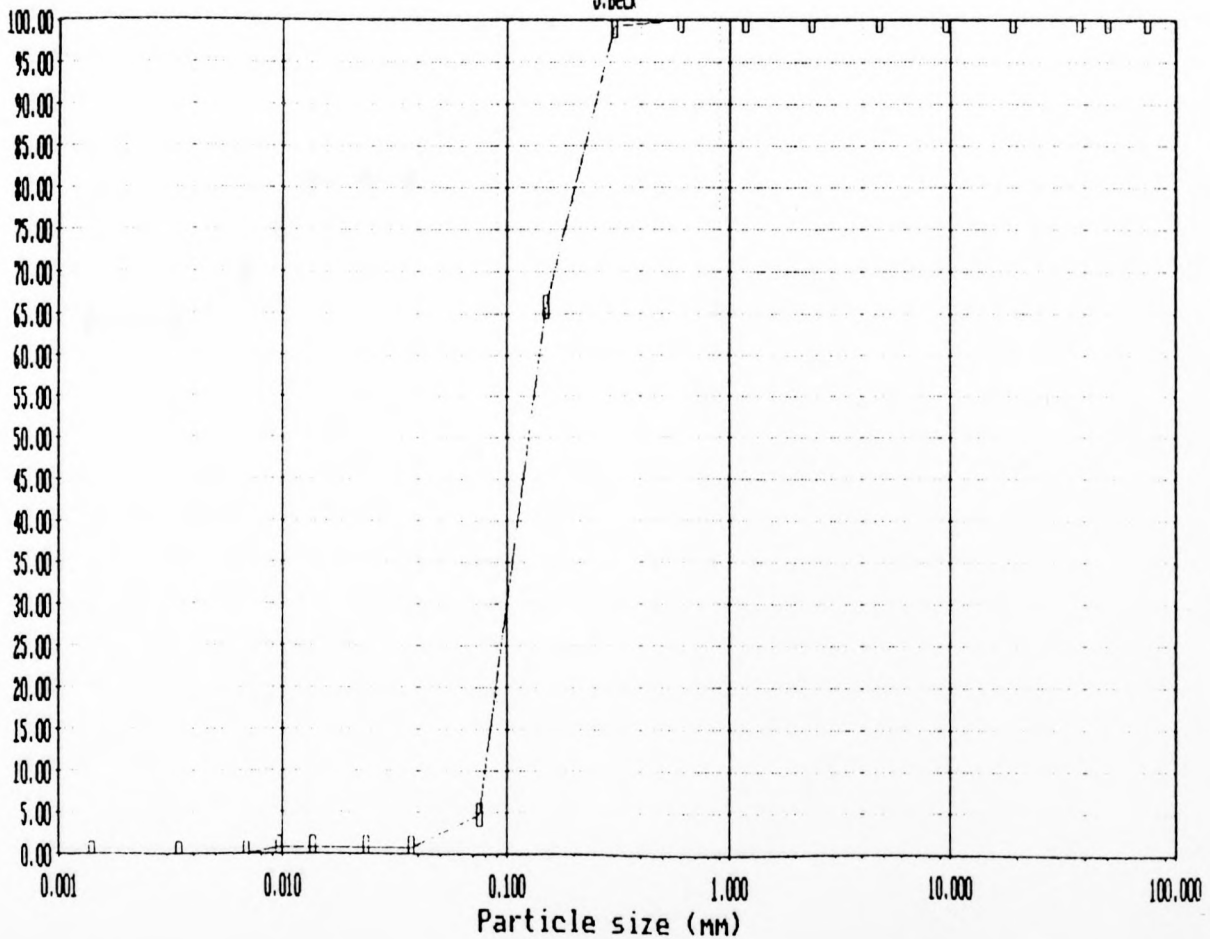
S8C2-1.1

J. Beck



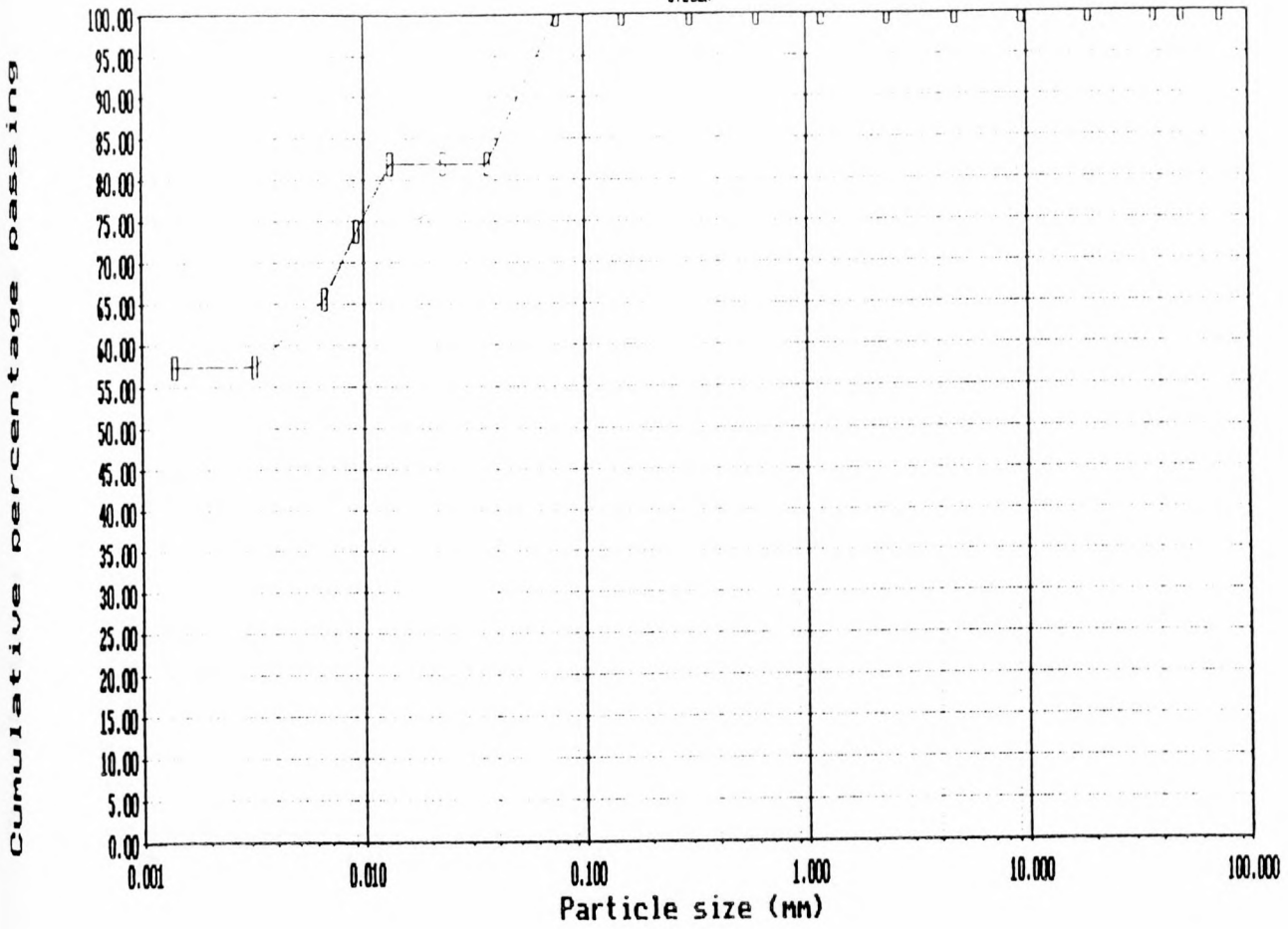
S8C2 13.3

J. Beck



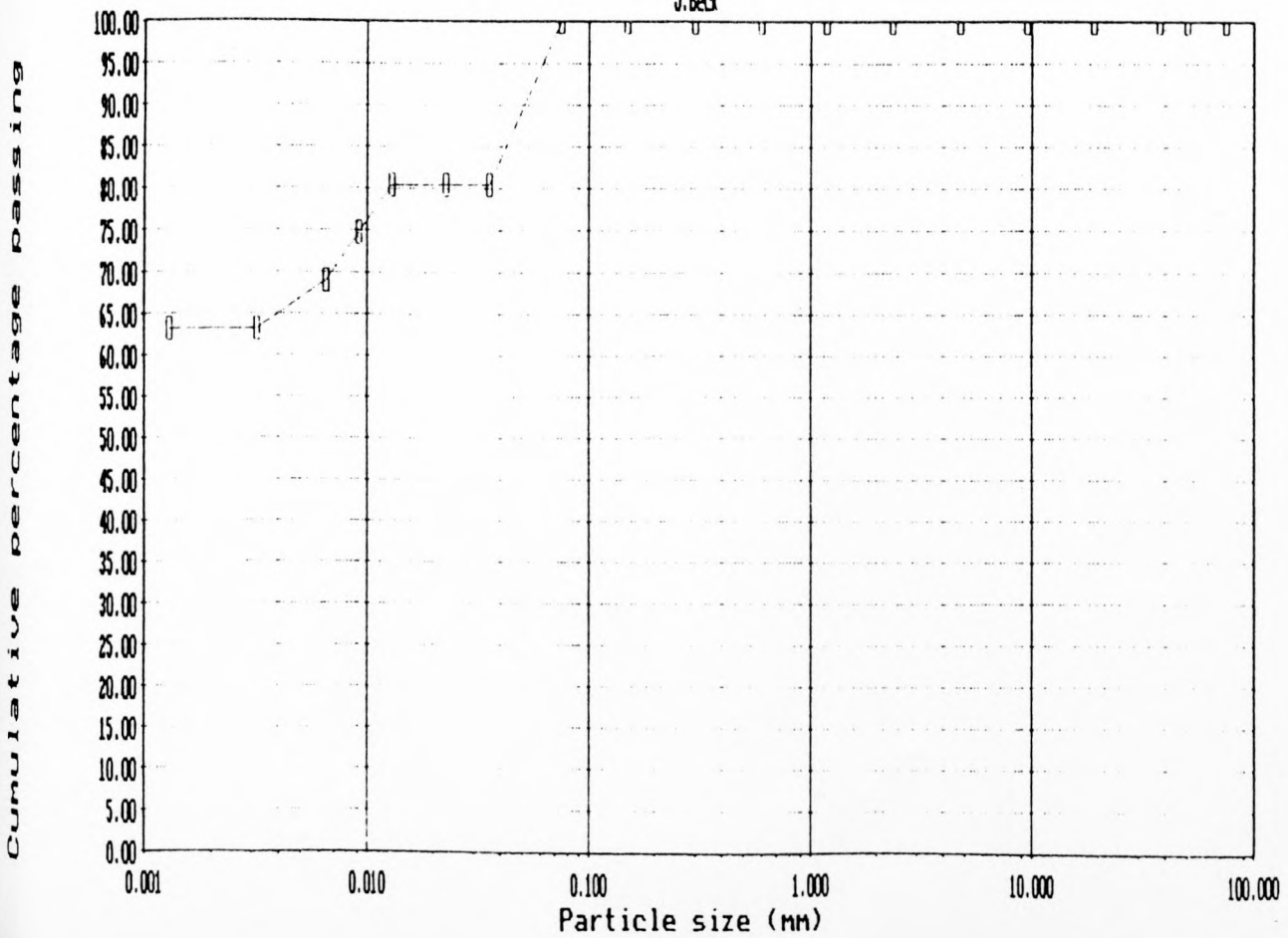
MONSTERS S4C6

J. Beck



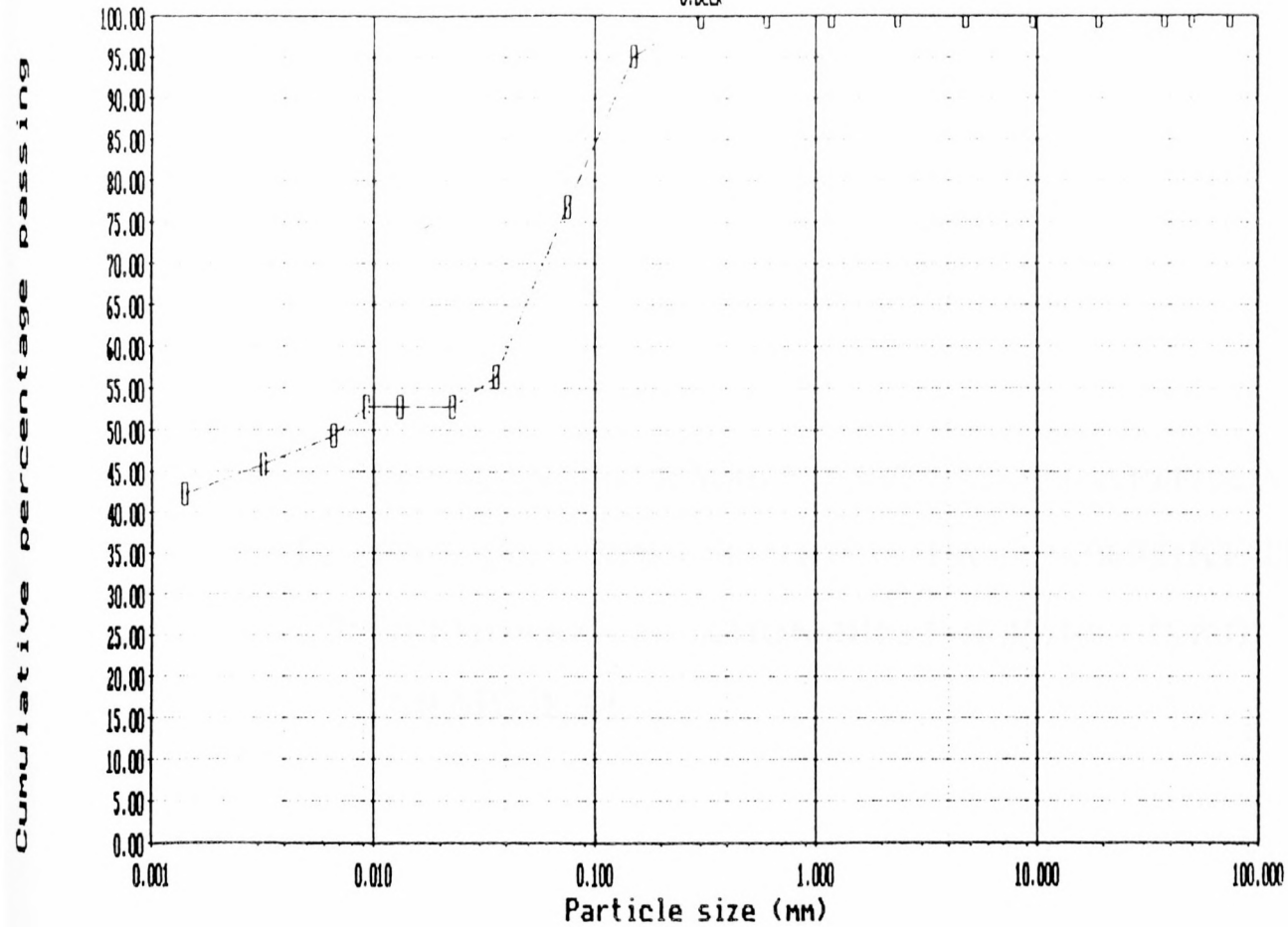
MONSTERS S6C4

J. Beck



S8C2 KOMBINASIE

J. Beck



APPENDIX C

WIDTHS BEFORE AND AFTER DAM

- **C1: PONGOLA RIVER WIDTHS BEFORE AND AFTER DAM**
- **C2: PONGOLA CROSS-SECTIONS – INPUT FOR MIKE 11**
- **C3: DEPTH-AREA RELATIONSHIPS FOR PANS – INPUT FOR MIKE 11**

APPENDIX C1: PONGOLA RIVER WIDTHS BEFORE AND AFTER DAM

| Station | Width before dam (m) | Width after dam (m) | Change (m) |
|---------|----------------------|---------------------|------------|
| 10 | 4.40 | 170.0 | 165.6 |
| 11 | 5.32 | 170.0 | 164.7 |
| 12 | 1.38 | 170.0 | 168.6 |
| 13 | 8.13 | 170.0 | 161.9 |
| 14 | 8.22 | 170.0 | 161.8 |
| 15 | 7.48 | 170.0 | 162.5 |
| 16 | 7.88 | 170.0 | 162.1 |
| 17 | 8.99 | 170.0 | 161.0 |
| 18 | 2.48 | 170.0 | 167.5 |
| 19 | 2.10 | 170.0 | 167.9 |
| 20 | 2.88 | 170.0 | 167.1 |
| 21 | 10.85 | 170.0 | 159.2 |
| 22 | 10.73 | 170.0 | 159.3 |
| 23 | 11.01 | 170.0 | 159.0 |
| 24 | 11.48 | 170.0 | 158.5 |
| 25 | 11.87 | 170.0 | 158.1 |
| 26 | 10.48 | 170.0 | 159.5 |
| 27 | 12.35 | 170.0 | 157.7 |
| 28 | 12.53 | 170.0 | 157.5 |
| 29 | 14.04 | 170.0 | 156.0 |
| 30 | 14.52 | 170.0 | 155.5 |
| 31 | 15.00 | 170.0 | 155.0 |
| 32 | 15.48 | 170.0 | 154.5 |
| 33 | 15.96 | 170.0 | 154.0 |
| 34 | 16.43 | 170.0 | 153.6 |
| 35 | 16.90 | 170.0 | 153.1 |
| 36 | 17.45 | 170.0 | 152.6 |
| 37 | 17.92 | 170.0 | 152.1 |
| 38 | 18.40 | 170.0 | 151.6 |
| 39 | 18.88 | 170.0 | 151.1 |
| 40 | 19.36 | 170.0 | 150.6 |
| 41 | 19.82 | 170.0 | 150.2 |
| 42 | 20.30 | 170.0 | 149.7 |
| 43 | 20.78 | 170.0 | 149.2 |
| 44 | 21.27 | 170.0 | 148.7 |
| 45 | 21.77 | 170.0 | 148.2 |
| 46 | 22.26 | 170.0 | 147.7 |
| 47 | 22.72 | 170.0 | 147.3 |
| 48 | 23.19 | 170.0 | 146.8 |

Pongola River widths before and after Pongolapoort Dam

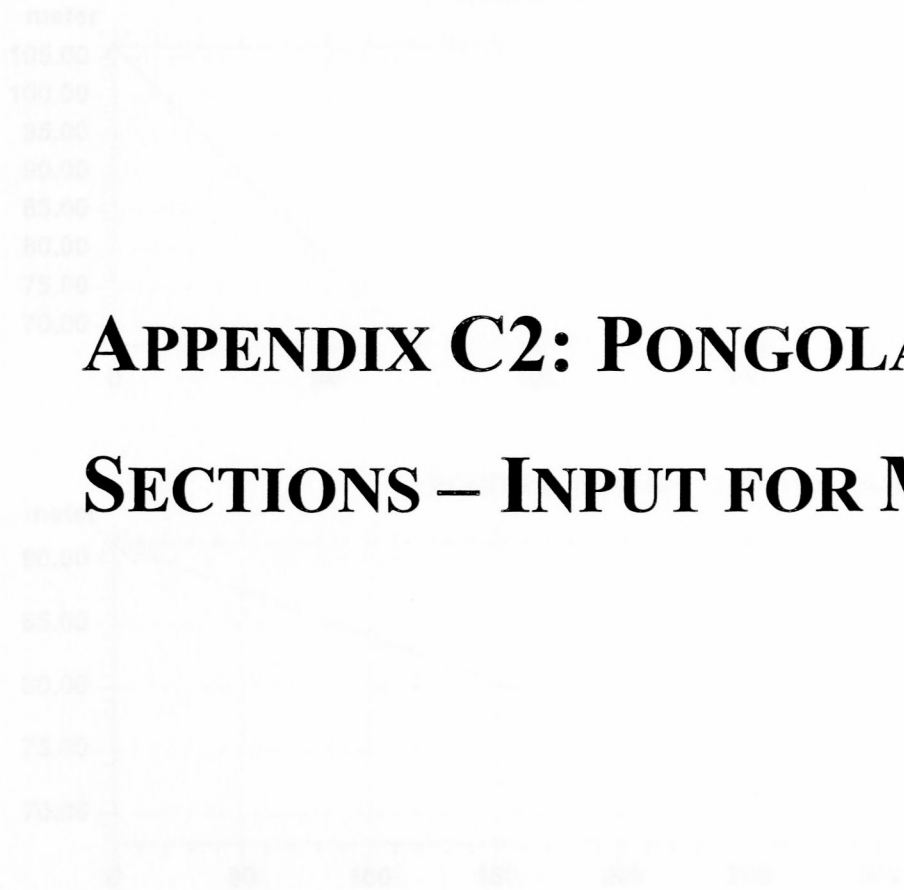
| Section | Chainage (km) | Width (m) | |
|---------|---------------|-----------|-------|
| | | 1956 | 1996 |
| 1 | 0.46 | 82.7 | 90.5 |
| 2 | 0.95 | 183.1 | 135.7 |
| 3 | 1.43 | 224.5 | 60.3 |
| 4 | 1.91 | 177.2 | 60.3 |
| 5 | 2.39 | 141.8 | 62.1 |
| 6 | 2.87 | 159.5 | 62.1 |
| 7 | 3.36 | 189.0 | 62.1 |
| 8 | 3.86 | 153.6 | 54.3 |
| 9 | 4.33 | 153.6 | 46.6 |
| 10 | 4.81 | 82.7 | 46.6 |
| 11 | 5.32 | 88.6 | 38.8 |
| 12 | 5.58 | 130.0 | 46.6 |
| 13 | 6.13 | 82.7 | 46.6 |
| 14 | 6.62 | 130.0 | 62.1 |
| 15 | 7.09 | 118.1 | 62.1 |
| 16 | 7.58 | 153.6 | 77.6 |
| 17 | 8.07 | 124.0 | 62.1 |
| 18 | 8.58 | 206.7 | 62.1 |
| 19 | 9.10 | 153.6 | 54.3 |
| 20 | 9.52 | 342.6 | 77.6 |
| 21 | 10.05 | 153.6 | 69.8 |
| 22 | 10.53 | 135.9 | 62.1 |
| 23 | 11.01 | 112.2 | 62.1 |
| 24 | 11.48 | 194.9 | 69.8 |
| 25 | 11.97 | 177.2 | 77.6 |
| 26 | 12.49 | 147.7 | 66.7 |
| 27 | 12.99 | 200.8 | 58.3 |
| 28 | 13.53 | 177.2 | 116.7 |
| 29 | 14.04 | 124.0 | 50.0 |
| 30 | 14.52 | 147.7 | 66.7 |
| 31 | 15.00 | 130.0 | 75.0 |
| 32 | 15.48 | 147.7 | 83.3 |
| 33 | 15.96 | 106.3 | 75.0 |
| 34 | 16.43 | 183.1 | 91.7 |
| 35 | 16.96 | 200.8 | 108.3 |
| 36 | 17.45 | 159.5 | 100.0 |
| 37 | 17.92 | 135.9 | 75.0 |
| 38 | 18.40 | 141.8 | 75.0 |
| 39 | 18.86 | 130.0 | 100.0 |
| 40 | 19.36 | 130.0 | 83.3 |
| 41 | 19.82 | 141.8 | 83.3 |
| 42 | 20.30 | 112.2 | 75.0 |
| 43 | 20.78 | 106.3 | 91.7 |
| 44 | 21.27 | 141.8 | 100.0 |
| 45 | 21.77 | 76.8 | 56.5 |
| 46 | 22.26 | 135.9 | 96.8 |
| 47 | 22.72 | 130.0 | 80.7 |
| 48 | 23.19 | 118.1 | 80.7 |

| Section | Chainage (km) | Width (m) | |
|---------|---------------|-----------|------|
| | | 1956 | 1996 |
| 49 | 23.72 | 118.1 | 64.5 |
| 50 | 24.24 | 94.5 | 63.3 |
| 51 | 24.69 | 118.1 | 71.2 |
| 52 | 25.29 | 135.9 | 79.1 |
| 53 | 25.86 | 82.7 | 63.3 |
| 54 | 26.29 | 230.4 | 79.1 |
| 55 | 26.75 | 130.0 | 94.9 |
| 56 | 27.24 | 159.5 | 79.1 |
| 57 | 27.79 | 88.6 | 79.1 |
| 58 | 28.29 | 100.4 | 63.3 |
| 59 | 28.76 | 82.7 | 47.4 |
| 60 | 29.24 | 112.2 | 55.3 |
| 61 | 29.73 | 70.9 | 56.6 |
| 62 | 30.21 | 65.0 | 56.6 |
| 63 | 30.68 | 112.2 | 48.5 |
| 64 | 31.15 | 65.0 | 48.5 |
| 65 | 31.67 | 70.9 | 48.5 |
| 66 | 32.15 | 53.2 | 48.5 |
| 67 | 32.63 | 76.8 | 56.6 |
| 68 | 33.11 | 82.7 | 48.5 |
| 69 | 33.58 | 76.8 | 48.5 |
| 70 | 34.05 | 147.7 | 48.5 |
| 71 | 34.53 | 88.6 | 48.5 |
| 72 | 35.01 | 76.8 | 56.6 |
| 73 | 35.48 | 130.0 | 48.5 |
| 74 | 35.97 | 230.4 | 73.2 |
| 75 | 36.44 | 53.2 | 40.7 |
| 76 | 36.92 | 29.5 | 40.7 |
| 77 | 37.41 | 35.4 | 48.8 |
| 78 | 37.91 | 47.3 | 48.8 |
| 79 | 38.40 | 70.9 | 40.7 |
| 80 | 38.89 | 106.3 | 48.8 |
| 81 | 39.44 | 76.8 | 56.9 |
| 82 | 40.20 | 59.1 | 32.5 |
| 83 | 40.79 | 59.1 | 32.5 |
| 84 | 41.38 | 47.3 | 32.5 |
| 85 | 41.87 | 53.2 | 65.1 |
| 86 | 42.44 | 70.9 | 40.5 |
| 87 | 42.92 | 59.1 | 24.3 |
| 88 | 43.42 | 53.2 | 16.2 |
| 89 | 43.95 | 48.0 | 40.5 |
| 90 | 44.51 | 53.3 | 32.4 |
| 91 | 45.37 | 21.3 | 24.3 |
| 92 | 45.79 | 42.6 | 24.3 |
| 93 | 46.29 | 21.3 | 32.4 |
| 94 | 46.83 | 48.0 | 32.4 |
| 95 | 47.34 | 26.6 | 40.5 |
| 96 | 47.83 | 53.3 | 24.3 |
| 97 | 48.36 | 32.0 | 32.4 |
| 98 | 48.79 | 26.6 | 32.5 |

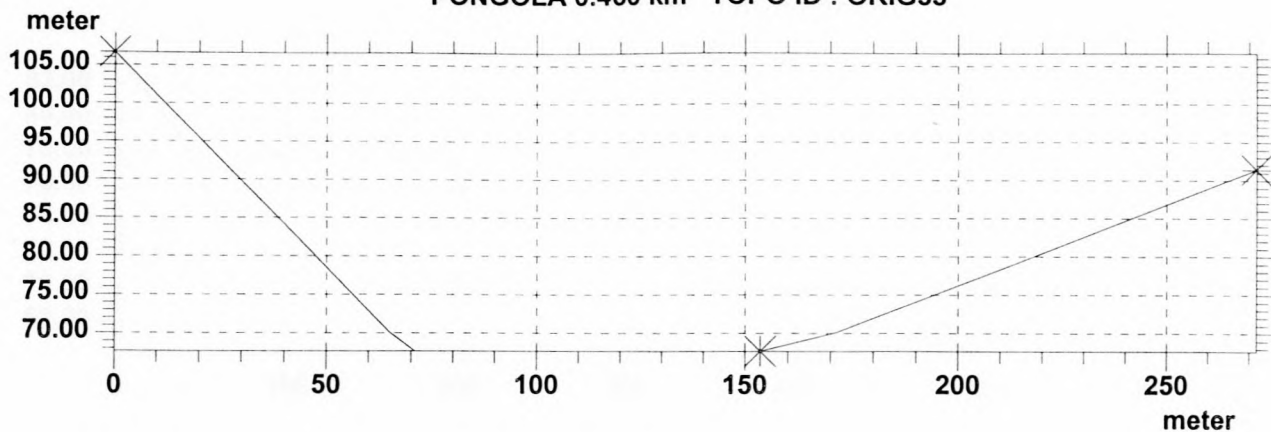
| Section | Chainage (km) | Width (m) | |
|---------|---------------|-----------|------|
| | | 1956 | 1996 |
| 99 | 49.27 | 10.7 | 32.5 |
| 100 | 49.77 | 53.3 | 40.6 |
| 101 | 50.24 | 59.7 | 32.5 |
| 102 | 50.75 | 35.8 | 48.7 |
| 103 | 51.26 | 74.6 | 40.6 |
| 104 | 51.76 | 47.8 | 40.6 |
| 105 | 52.26 | 41.8 | 32.5 |
| 106 | 52.76 | 41.8 | 48.7 |
| 107 | 53.26 | 65.7 | 32.5 |
| 108 | 53.77 | 53.3 | 40.6 |
| 109 | 54.27 | 42.6 | 24.4 |
| 110 | 54.76 | 42.6 | 32.5 |
| 111 | 55.28 | 42.6 | 24.4 |
| 112 | 55.70 | 42.6 | 16.2 |
| 113 | 56.18 | 37.3 | 24.4 |
| 114 | 56.67 | 32.0 | 33.0 |
| 115 | 57.17 | 37.3 | 33.0 |
| 116 | 57.65 | 37.3 | 24.8 |
| 117 | 58.16 | 32.0 | 16.5 |
| 118 | 58.64 | 32.0 | 33.0 |
| 119 | 59.17 | 64.0 | 16.5 |
| 120 | 60.21 | 37.3 | 24.8 |
| 121 | 60.71 | 48.0 | 24.8 |
| 122 | 61.21 | 53.3 | 24.8 |
| 123 | 61.71 | 48.0 | 16.5 |
| 124 | 62.17 | 42.6 | 16.5 |
| 125 | 62.67 | 53.3 | 16.5 |
| 126 | 63.17 | 37.3 | 24.8 |
| 127 | 63.67 | 42.6 | 16.5 |
| 128 | 64.16 | 48.0 | 25.0 |
| 129 | 64.66 | 53.3 | 16.7 |
| 130 | 65.14 | 48.0 | 16.7 |
| 131 | 65.63 | 53.3 | 16.7 |
| 132 | 66.11 | 42.6 | 16.7 |
| 133 | 66.59 | 42.6 | 25.0 |
| 134 | 67.09 | 42.6 | 16.7 |
| 135 | 67.59 | 42.6 | 16.7 |
| 136 | 68.10 | 41.8 | 25.0 |
| 137 | 68.62 | 38.8 | 25.0 |
| 138 | 69.13 | 47.8 | 25.0 |
| 139 | 69.63 | 35.8 | 16.7 |
| 140 | 70.11 | 35.8 | 25.0 |
| 141 | 70.61 | 35.8 | 16.7 |
| 142 | 71.09 | 44.8 | 25.0 |
| 143 | 71.61 | 38.8 | 32.8 |
| 144 | 72.12 | 44.8 | 32.8 |
| 145 | 72.63 | 59.7 | 32.8 |
| 146 | 73.14 | 47.8 | 32.8 |
| 147 | 73.65 | 59.7 | 41.1 |
| 148 | 74.16 | 47.8 | 32.8 |

| Section | Chainage (km) | Width (m) | |
|---------|---------------|-----------|------|
| | | 1956 | 1996 |
| 149 | 74.67 | 41.8 | 16.4 |
| 150 | 75.18 | 44.8 | 24.6 |
| 151 | 75.68 | 47.8 | 32.8 |
| 152 | 76.19 | 42.6 | 16.4 |
| 153 | 76.70 | 48.0 | 24.6 |
| 154 | 77.22 | 53.3 | 24.6 |
| 155 | 77.74 | 42.6 | 24.6 |
| 156 | 78.28 | 64.0 | 49.3 |

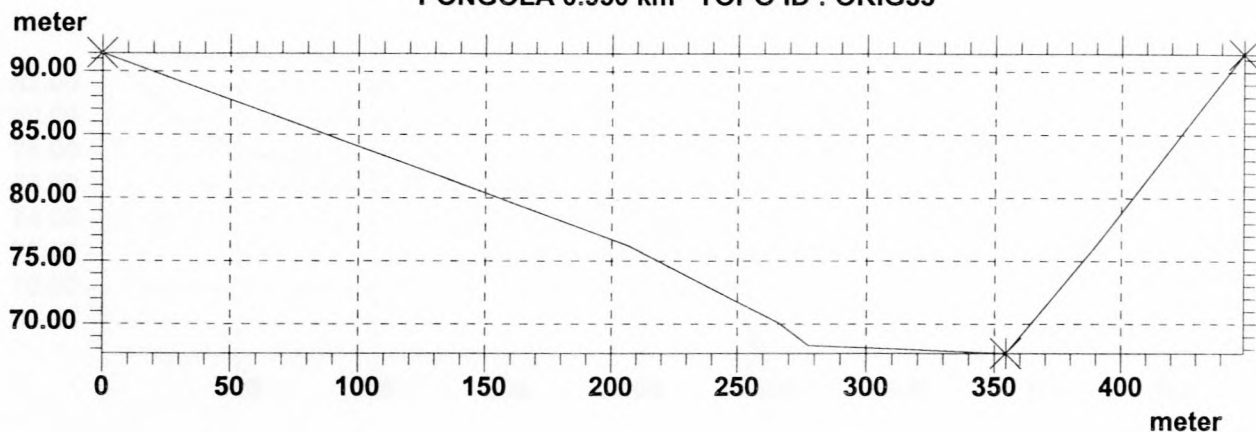
APPENDIX C2: PONGOLA CROSS-SECTIONS – INPUT FOR MIKE 11



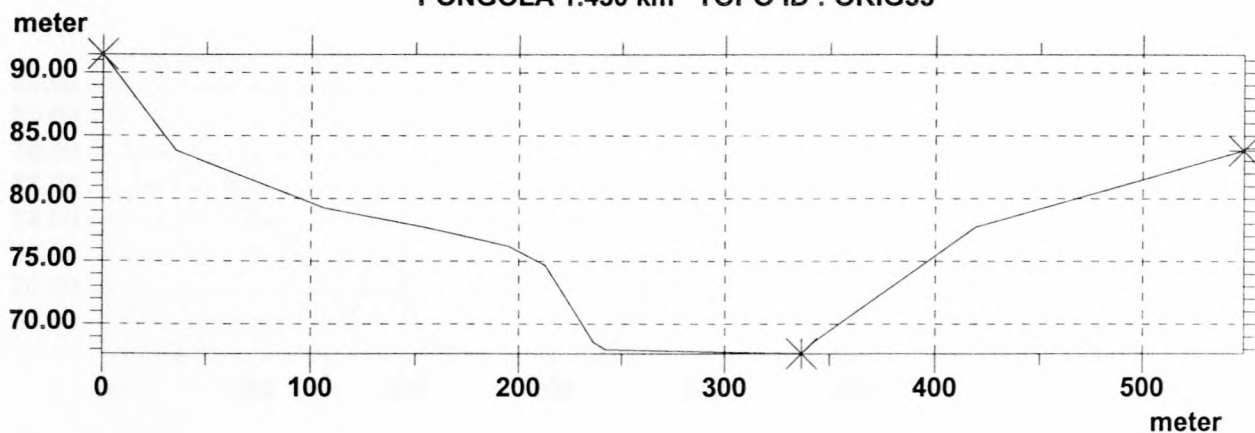
PONGOLA 0.460 km TOPO ID : ORIG33



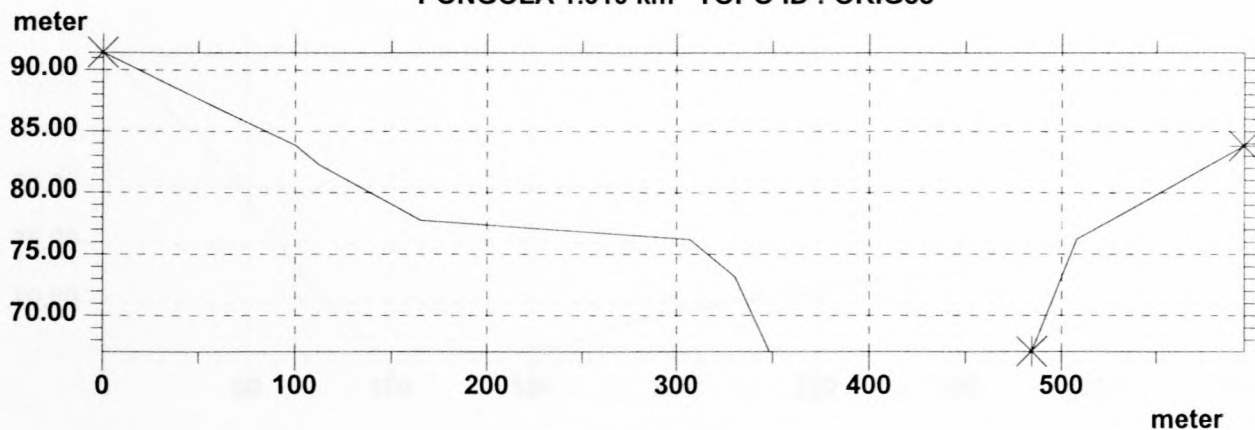
PONGOLA 0.950 km TOPO ID : ORIG33



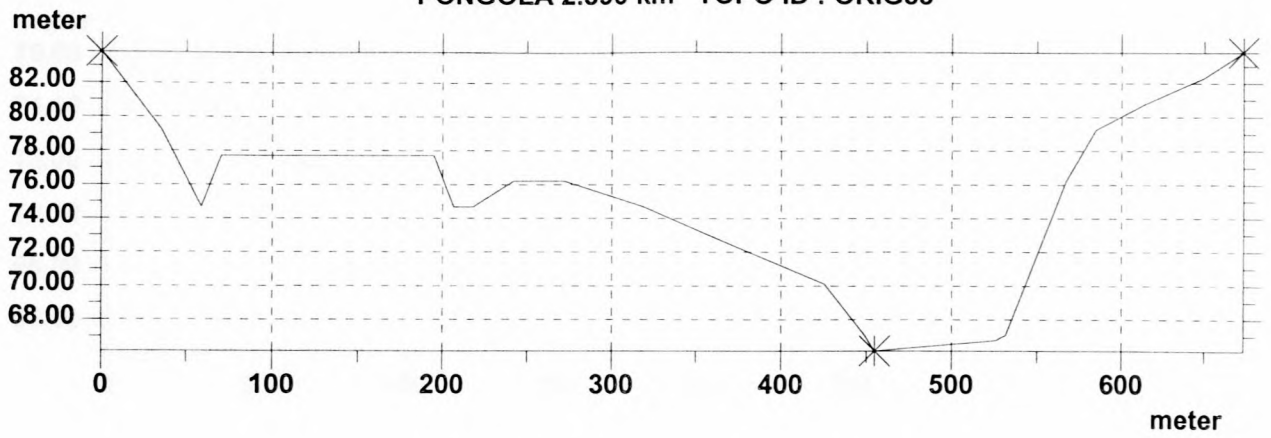
PONGOLA 1.430 km TOPO ID : ORIG33



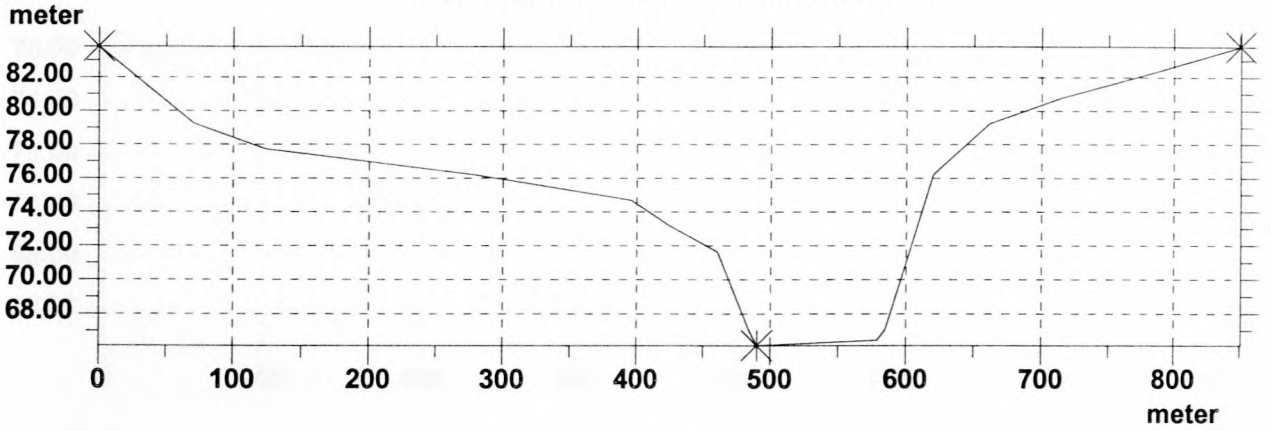
PONGOLA 1.910 km TOPO ID : ORIG33



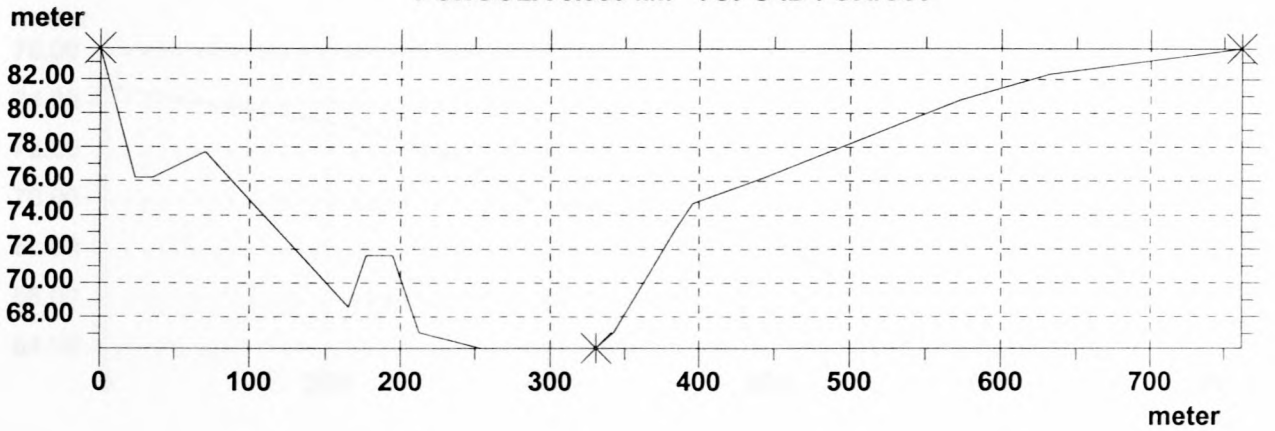
PONGOLA 2.390 km TOPO ID : ORIG33



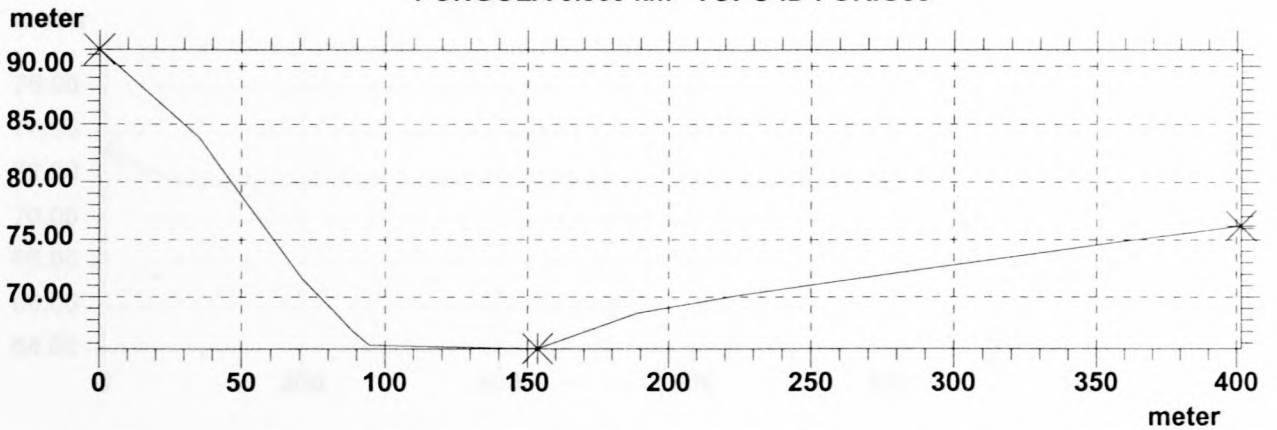
PONGOLA 2.870 km TOPO ID : ORIG33



PONGOLA 3.360 km TOPO ID : ORIG33

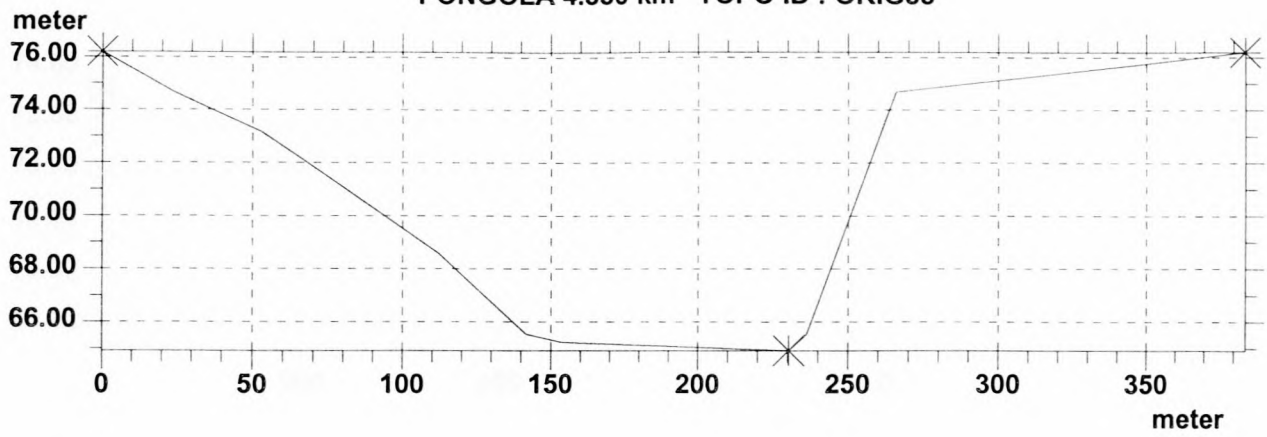


PONGOLA 3.860 km TOPO ID : ORIG33

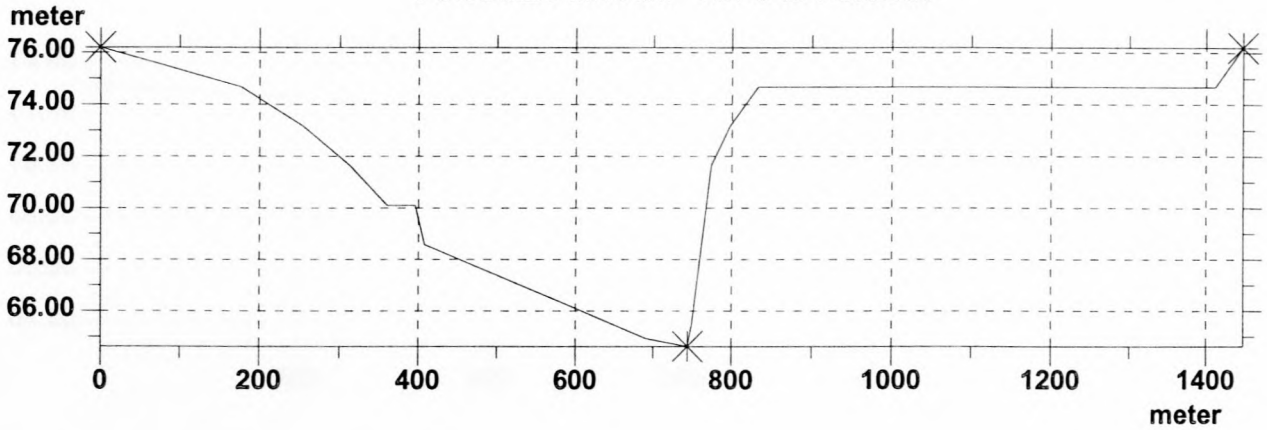


| | | |
|-------------------|--|---------|
| | | |
| DATA BASE : TEST2 | | MIKE 11 |

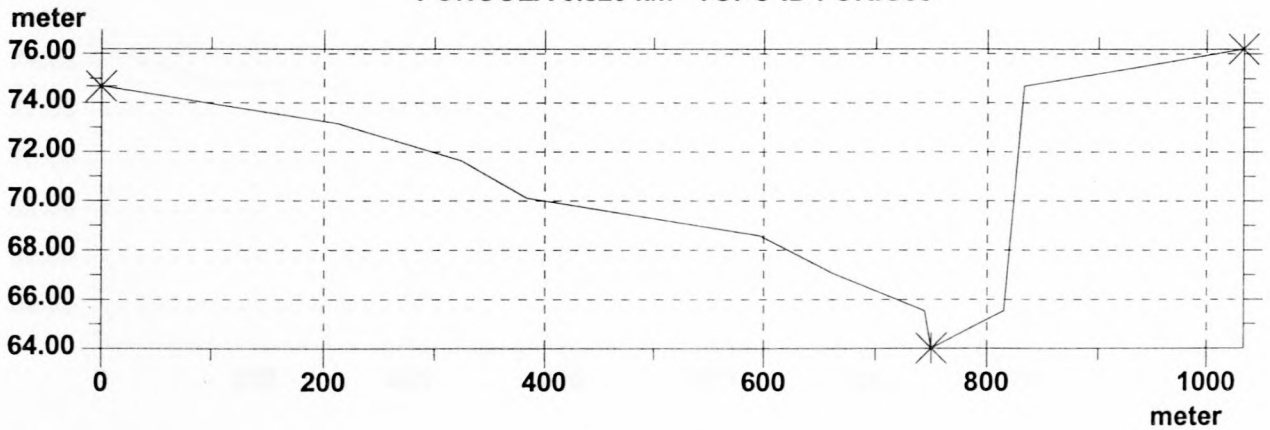
PONGOLA 4.330 km TOPO ID : ORIG33



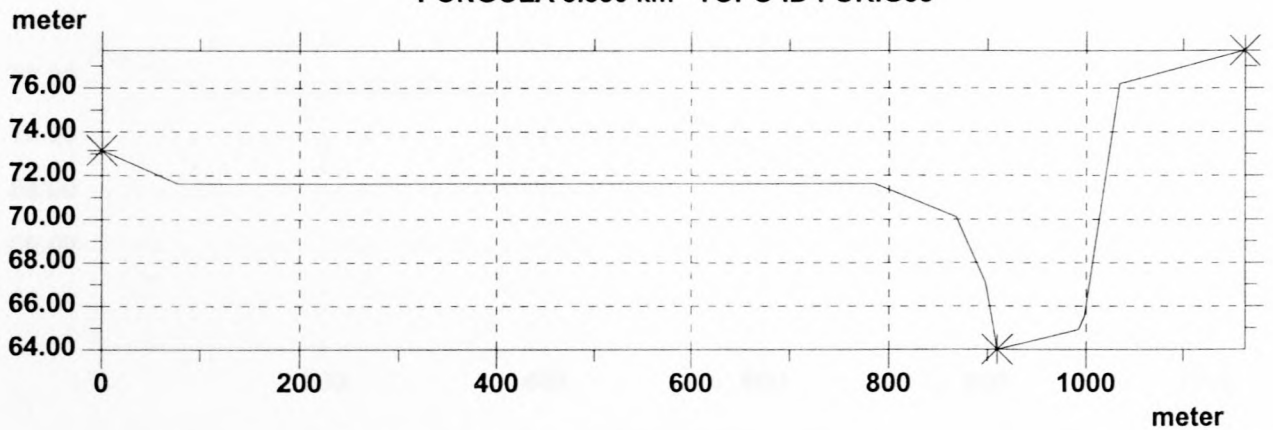
PONGOLA 4.810 km TOPO ID : ORIG33



PONGOLA 5.320 km TOPO ID : ORIG33

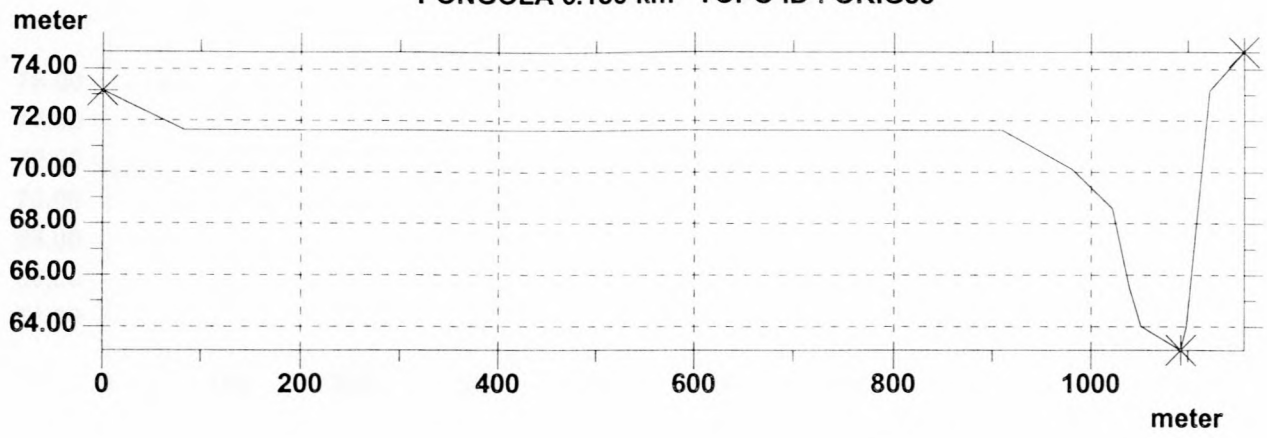


PONGOLA 5.580 km TOPO ID : ORIG33

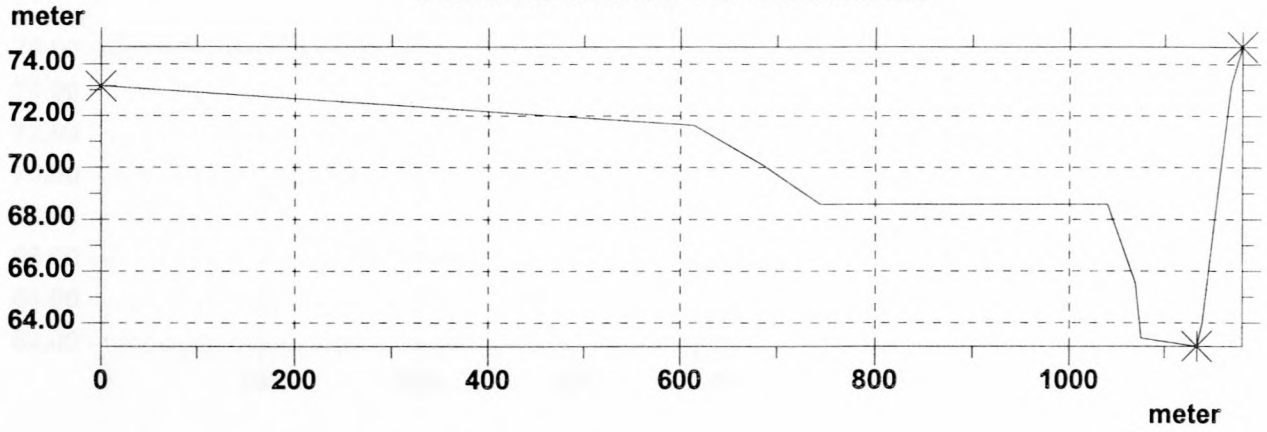


| | |
|-------------------|---------|
| | |
| DATA BASE : TEST2 | MIKE 11 |

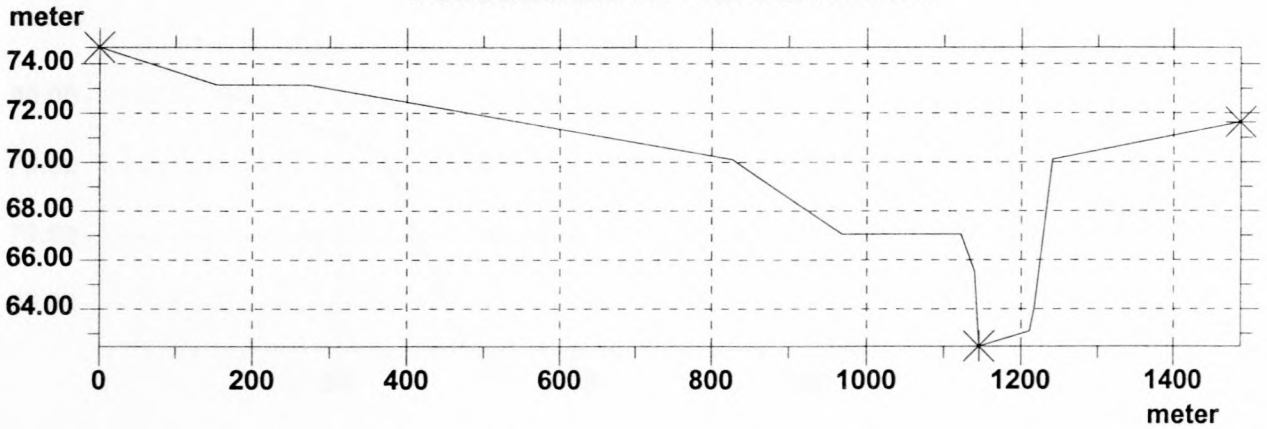
PONGOLA 6.130 km TOPO ID : ORIG33



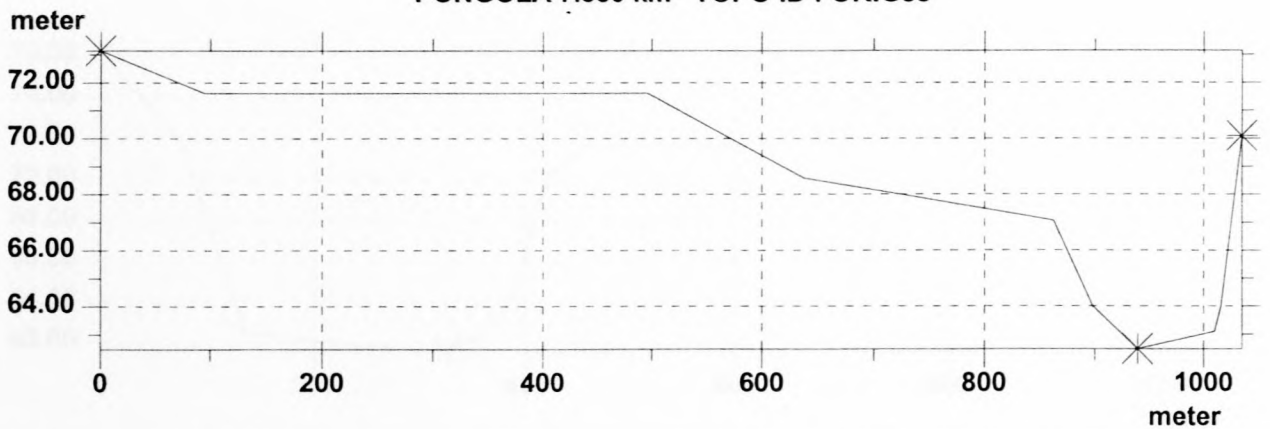
PONGOLA 6.620 km TOPO ID : ORIG33



PONGOLA 7.090 km TOPO ID : ORIG33

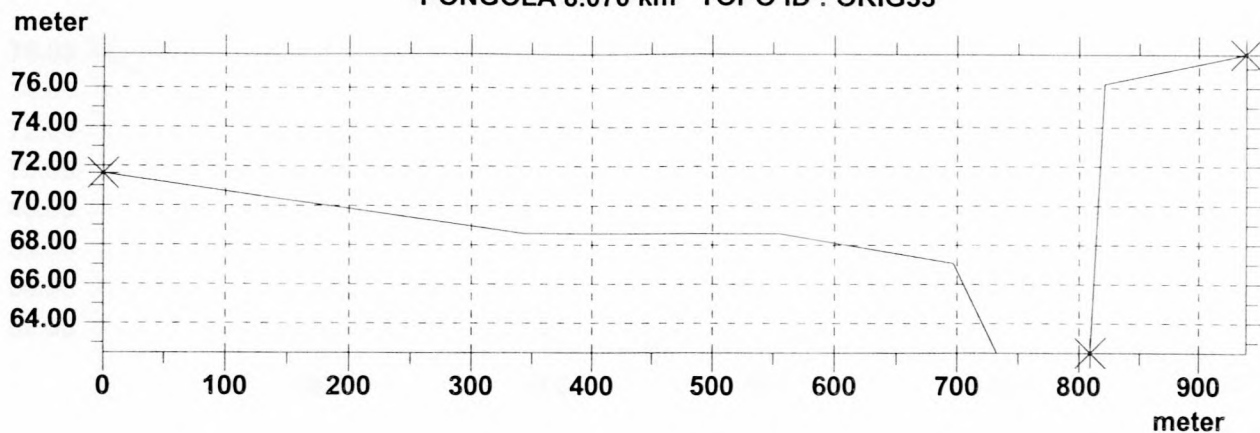


PONGOLA 7.580 km TOPO ID : ORIG33

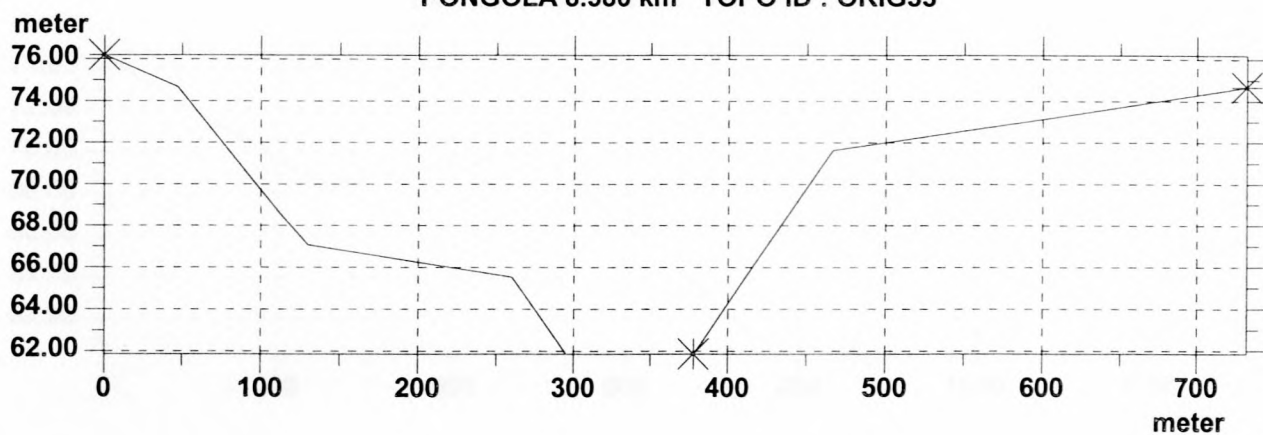


| | | |
|--------------------------|--|----------------|
| | | |
| | | MIKE 11 |
| DATA BASE : TEST2 | | |

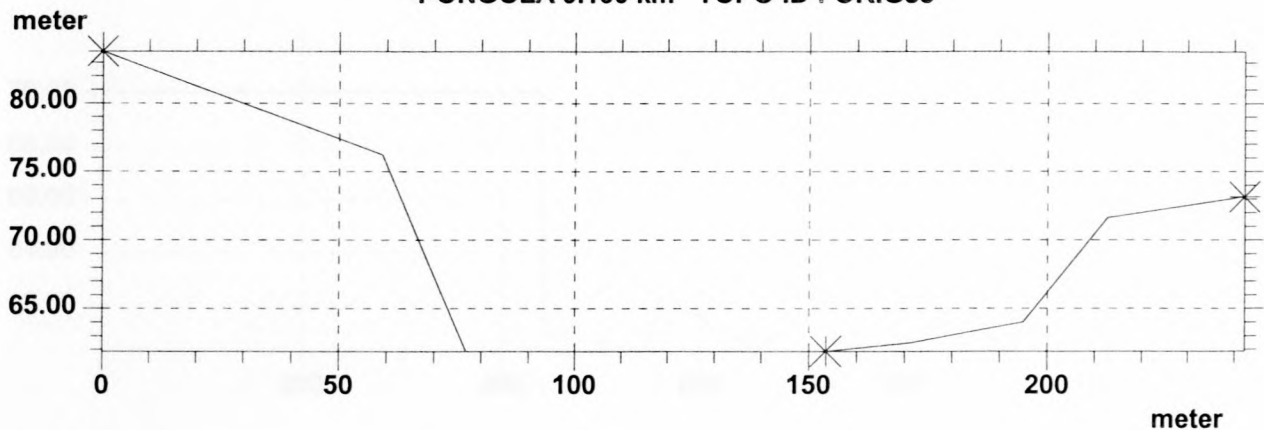
PONGOLA 8.070 km TOPO ID : ORIG33



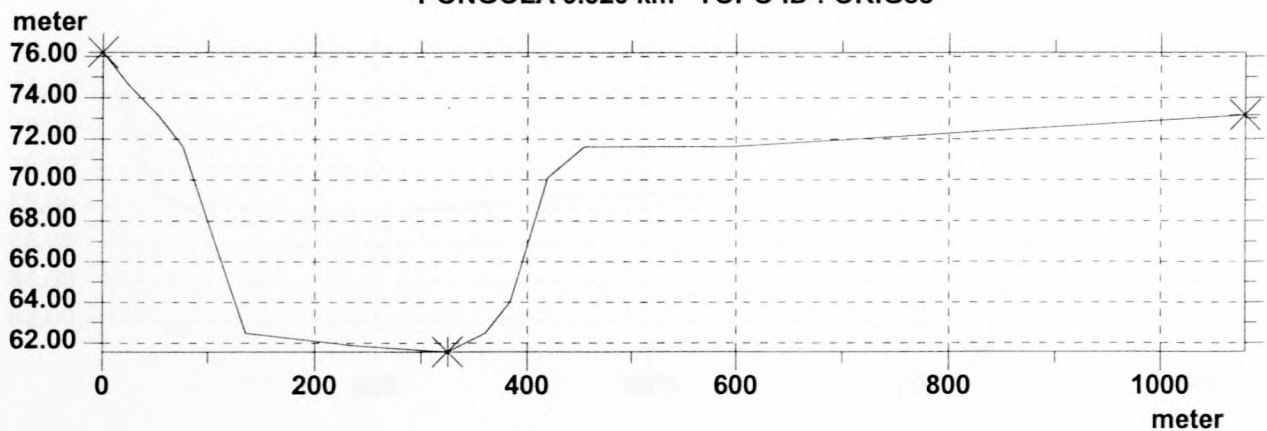
PONGOLA 8.580 km TOPO ID : ORIG33



PONGOLA 9.100 km TOPO ID : ORIG33

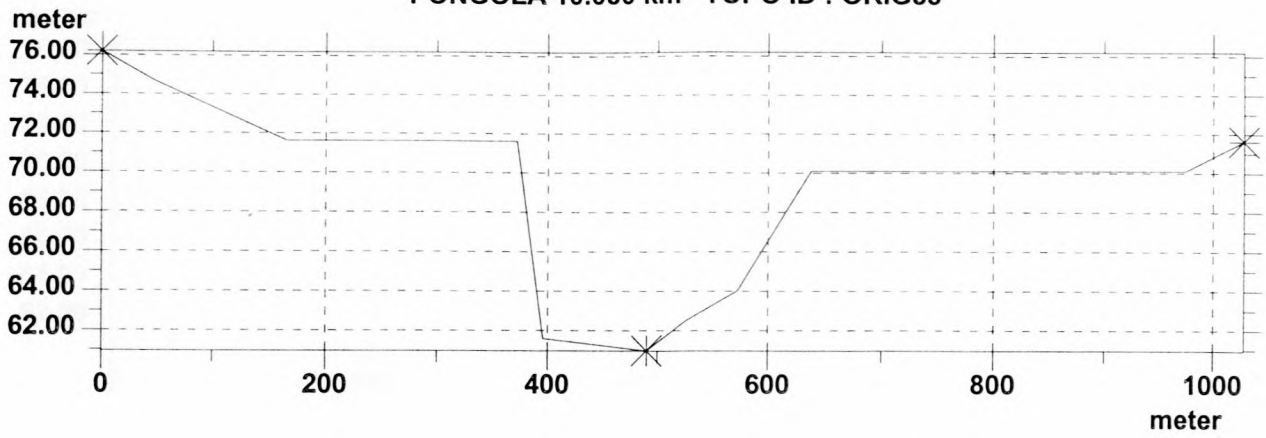


PONGOLA 9.520 km TOPO ID : ORIG33

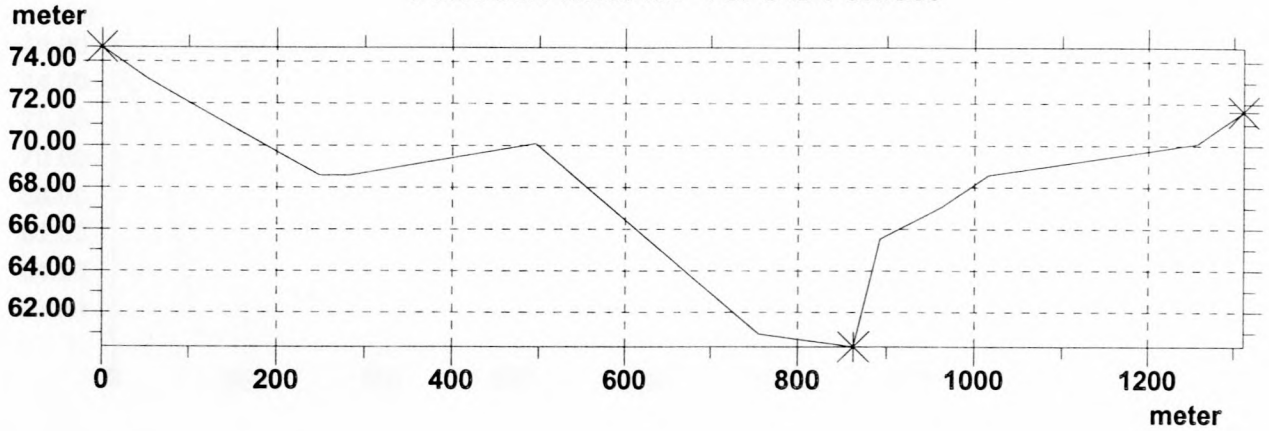


| | | |
|--------------------------|--|----------------|
| | | |
| | | MIKE 11 |
| DATA BASE : TEST2 | | |

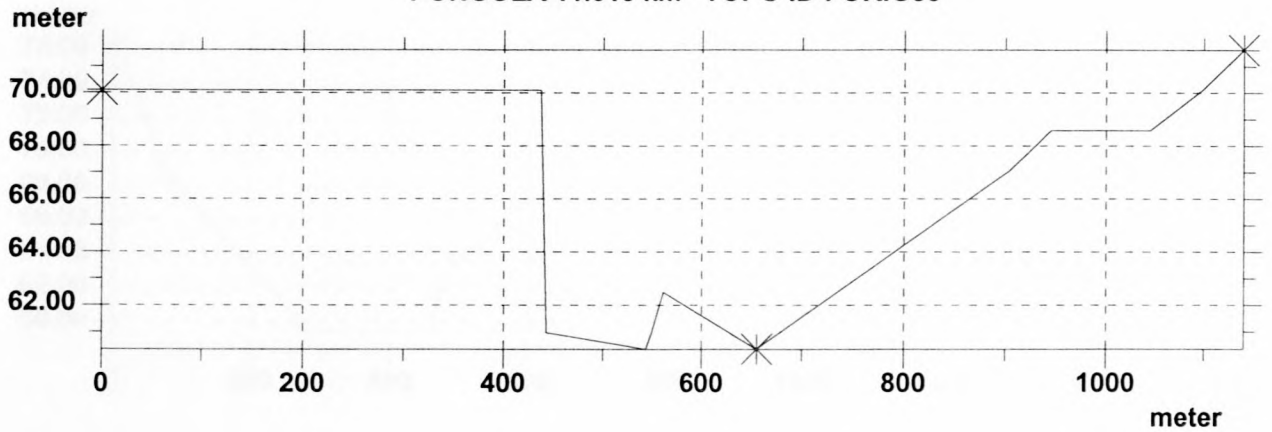
PONGOLA 10.050 km TOPO ID : ORIG33



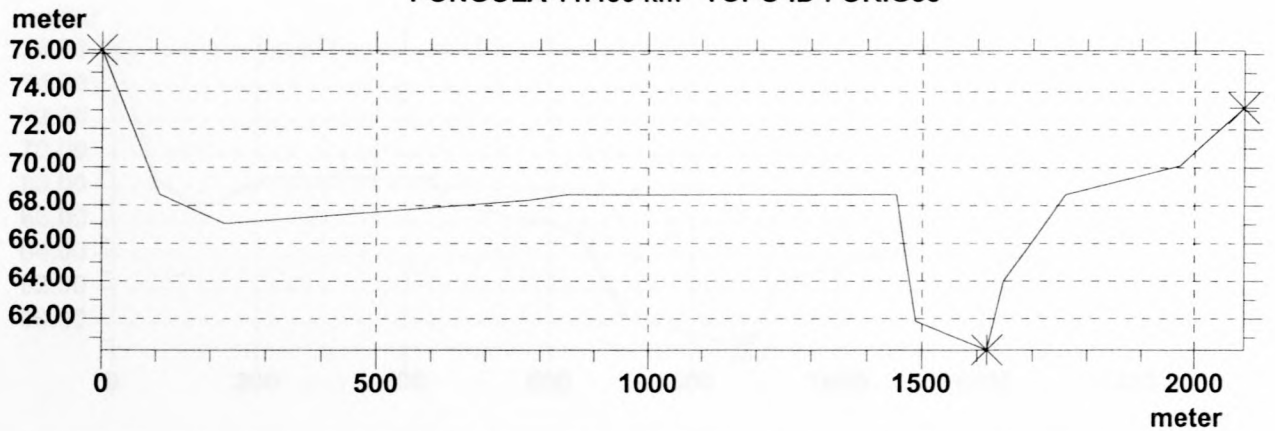
PONGOLA 10.530 km TOPO ID : ORIG33



PONGOLA 11.010 km TOPO ID : ORIG33

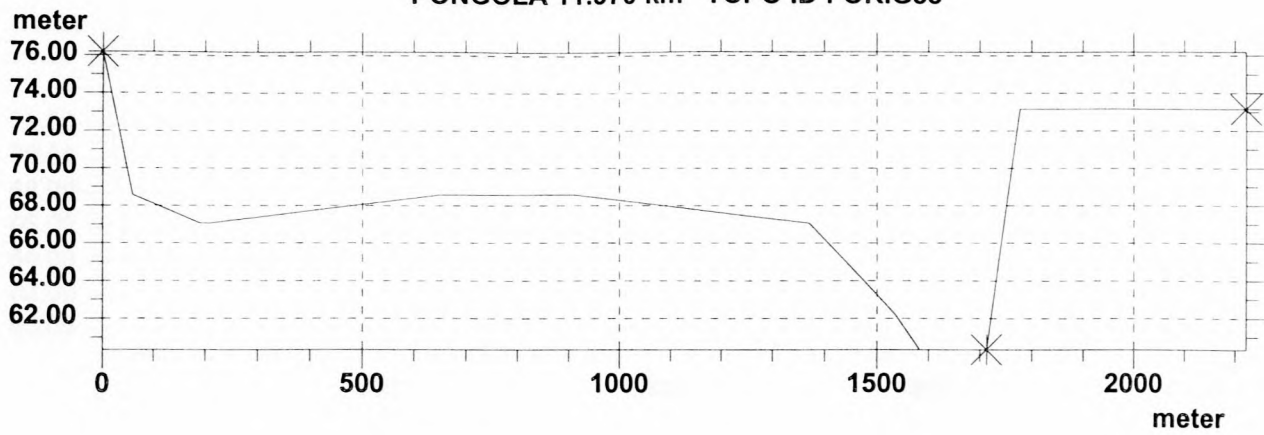


PONGOLA 11.480 km TOPO ID : ORIG33

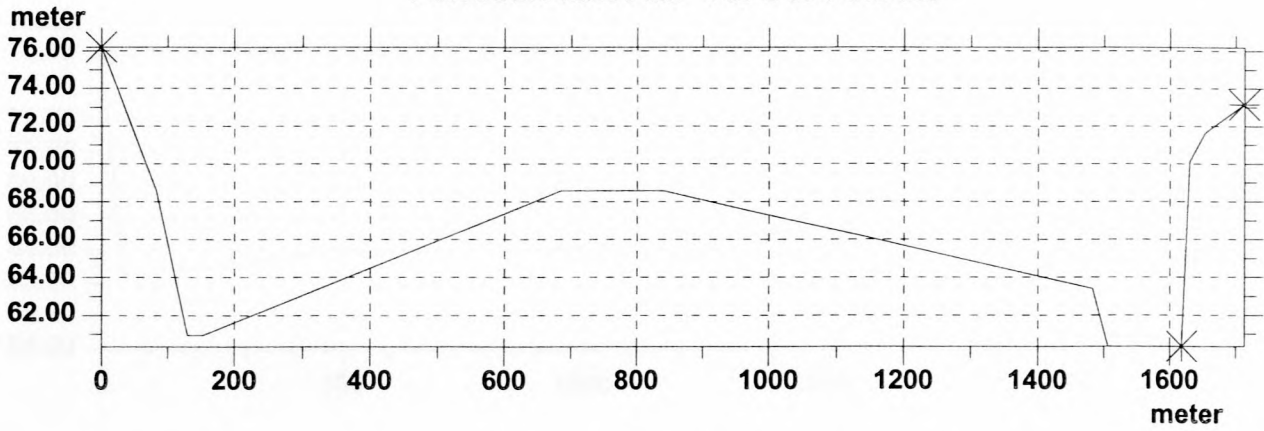


| | |
|-------------------|---------|
| | |
| DATA BASE : TEST2 | MIKE 11 |

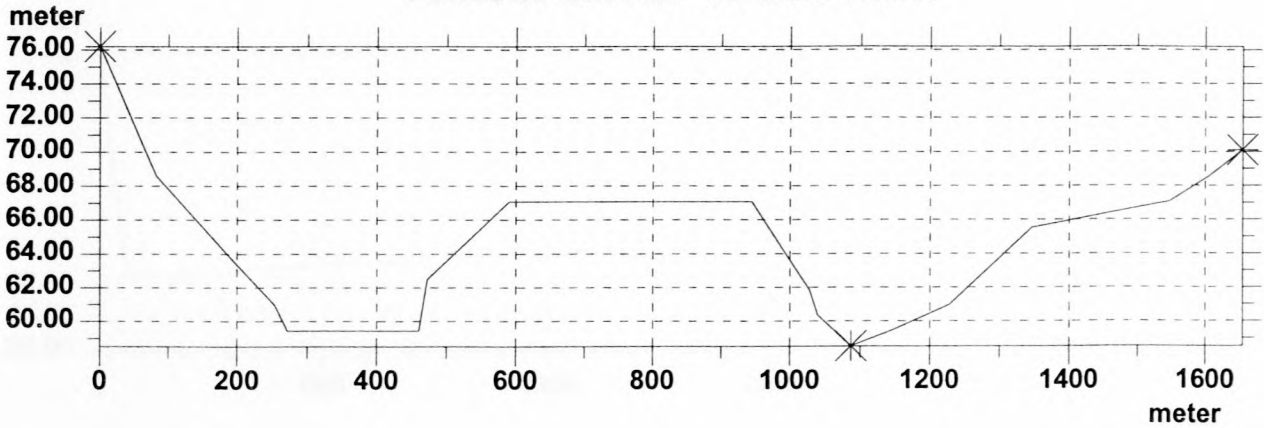
PONGOLA 11.970 km TOPO ID : ORIG33



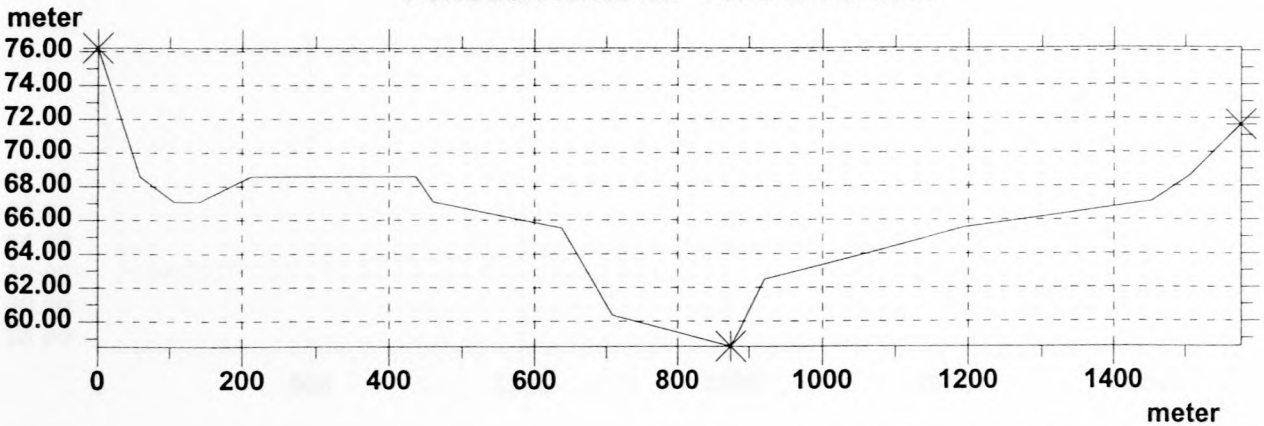
PONGOLA 12.490 km TOPO ID : ORIG33



PONGOLA 12.990 km TOPO ID : ORIG33

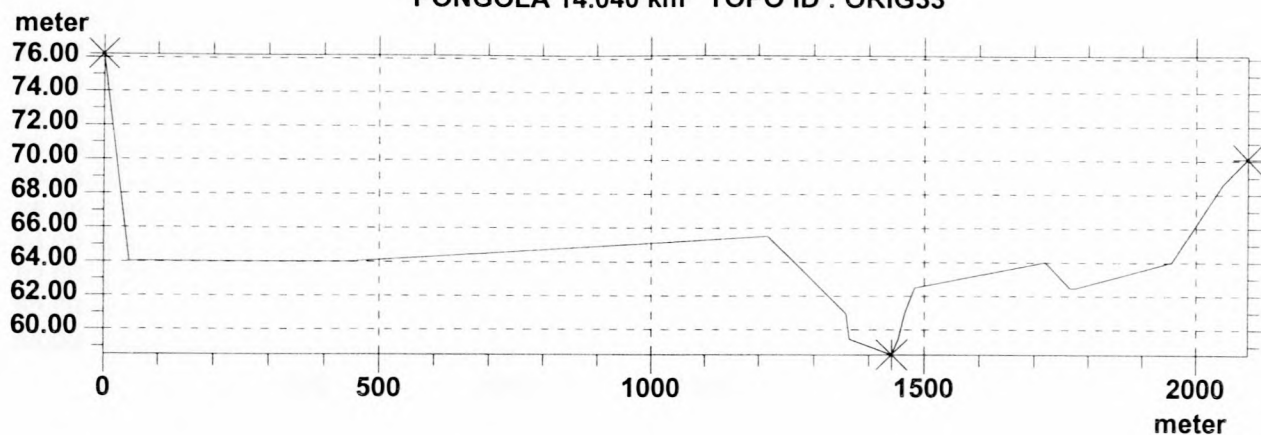


PONGOLA 13.530 km TOPO ID : ORIG33

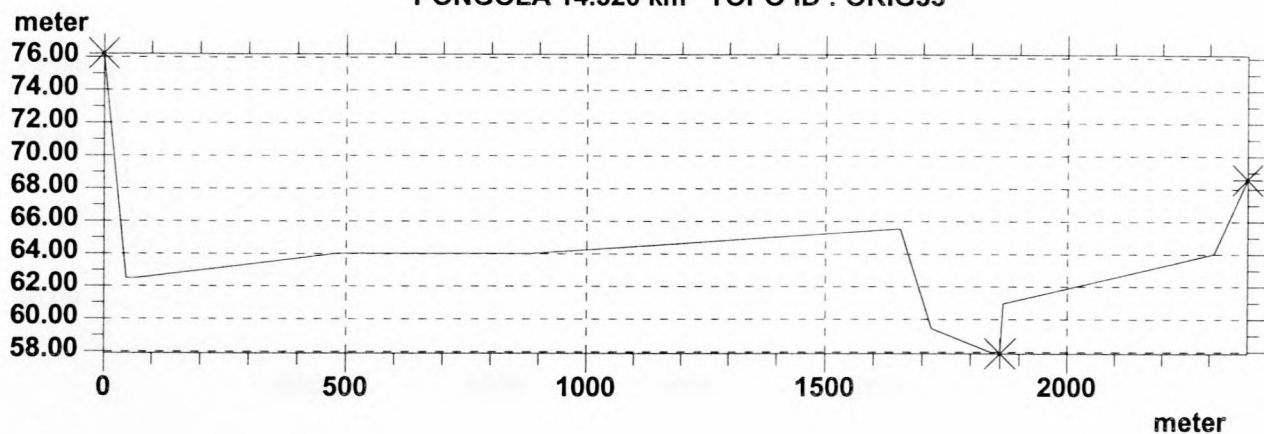


| | | | |
|--------------------------|--|----------------|--|
| | | | |
| | | MIKE 11 | |
| DATA BASE : TEST2 | | | |

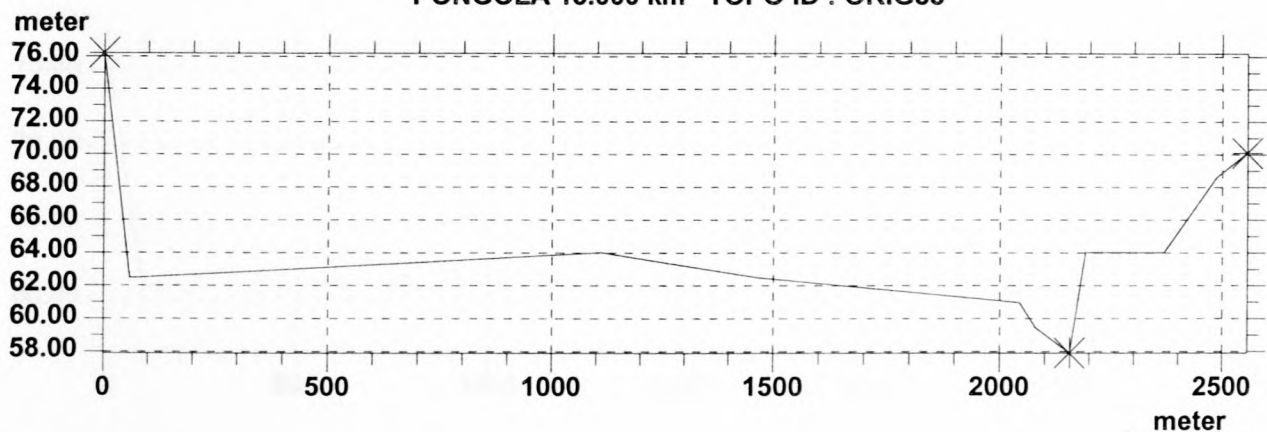
PONGOLA 14.040 km TOPO ID : ORIG33



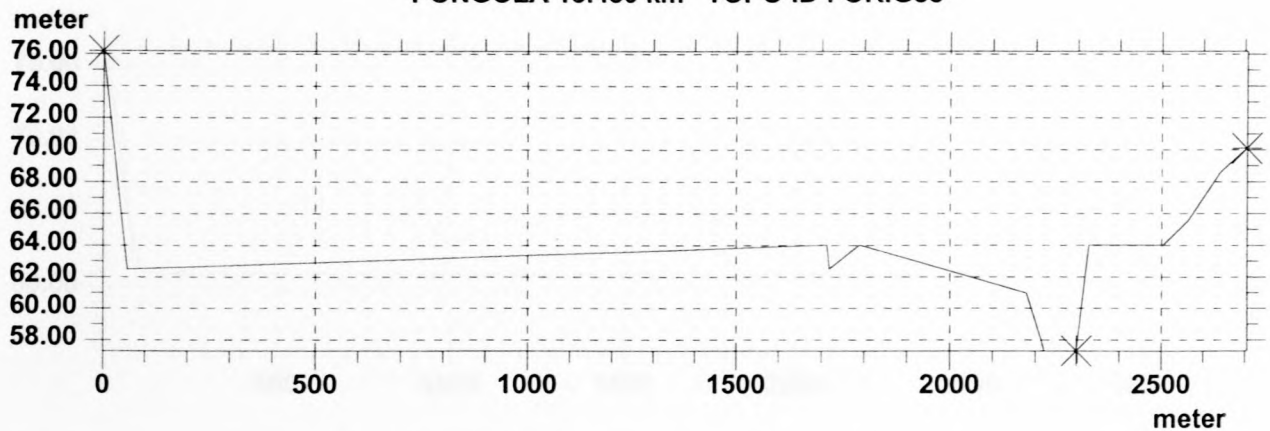
PONGOLA 14.520 km TOPO ID : ORIG33



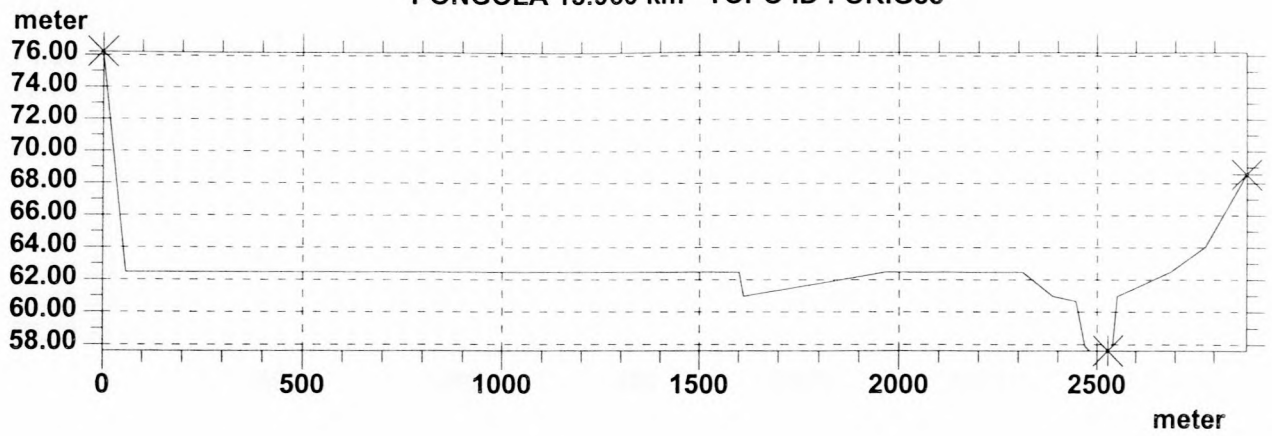
PONGOLA 15.000 km TOPO ID : ORIG33



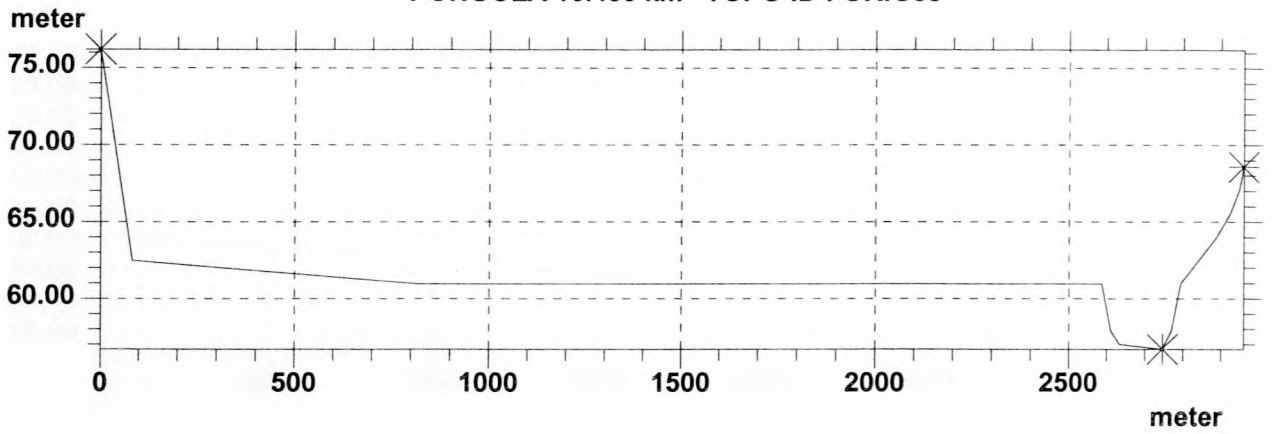
PONGOLA 15.480 km TOPO ID : ORIG33



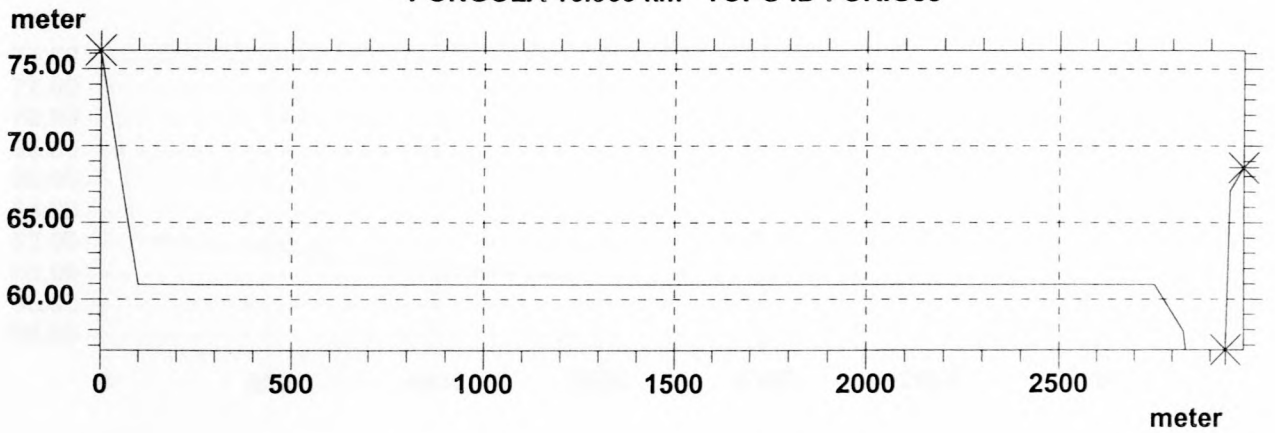
PONGOLA 15.960 km TOPO ID : ORIG33



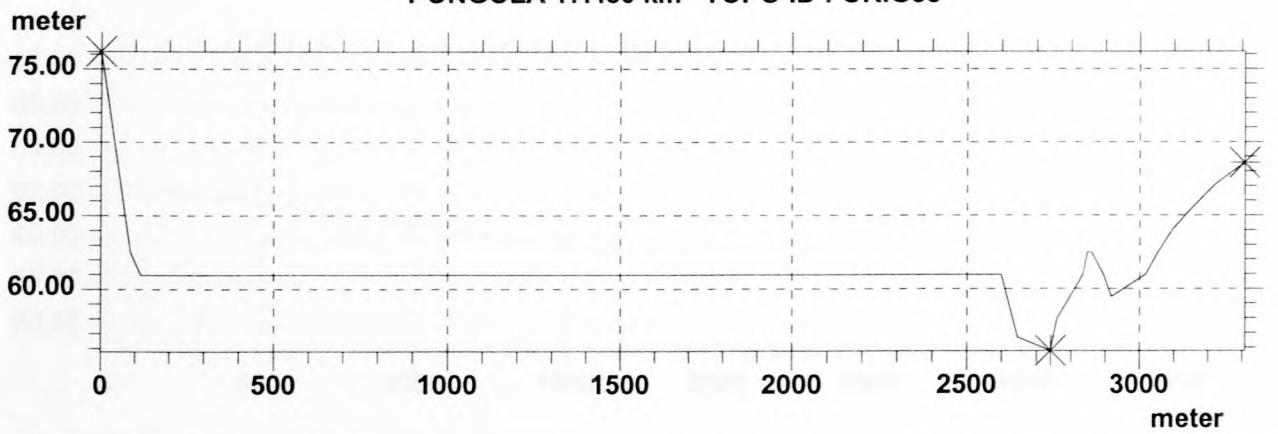
PONGOLA 16.430 km TOPO ID : ORIG33



PONGOLA 16.960 km TOPO ID : ORIG33

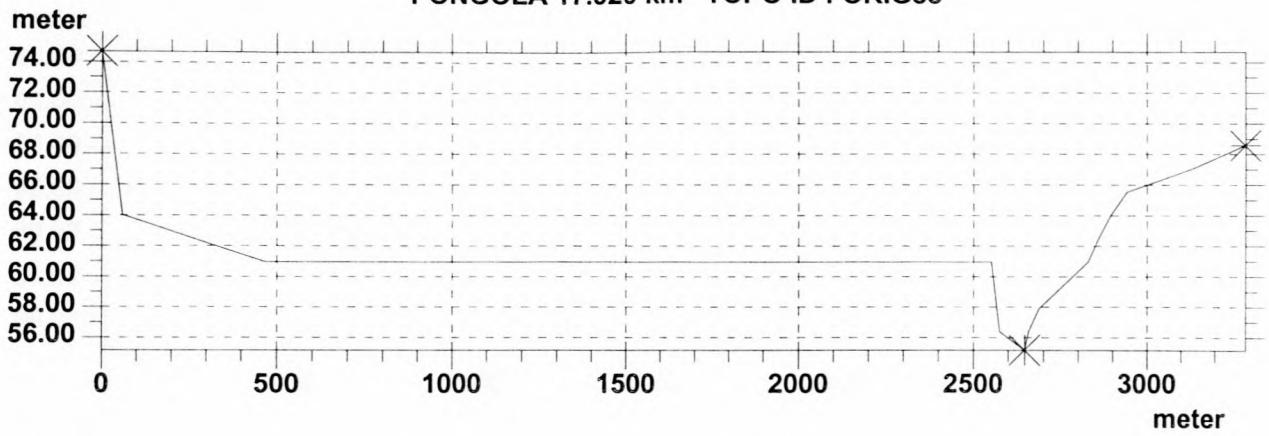


PONGOLA 17.450 km TOPO ID : ORIG33

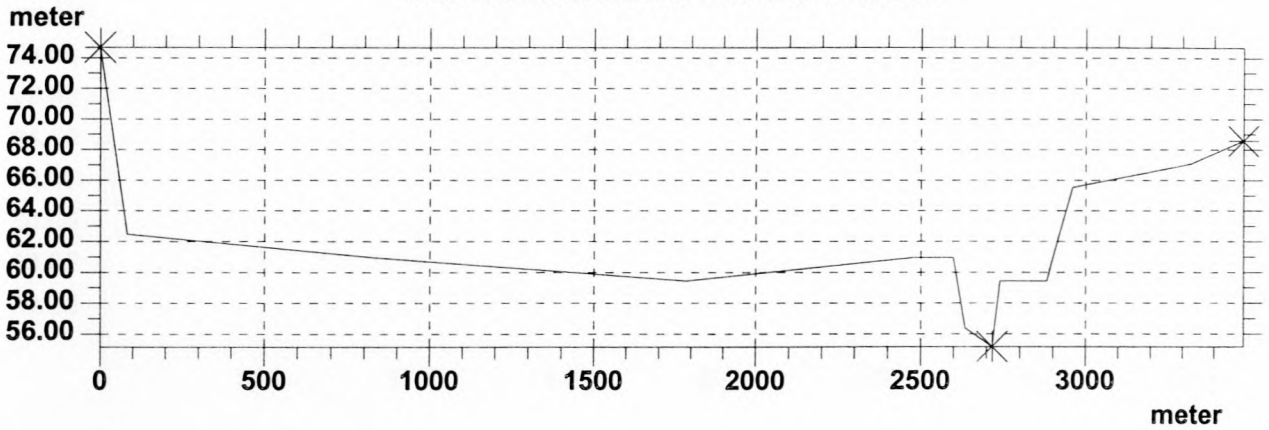


| | | |
|--------------------------|--|----------------|
| | | |
| | | MIKE 11 |
| DATA BASE : TEST2 | | |

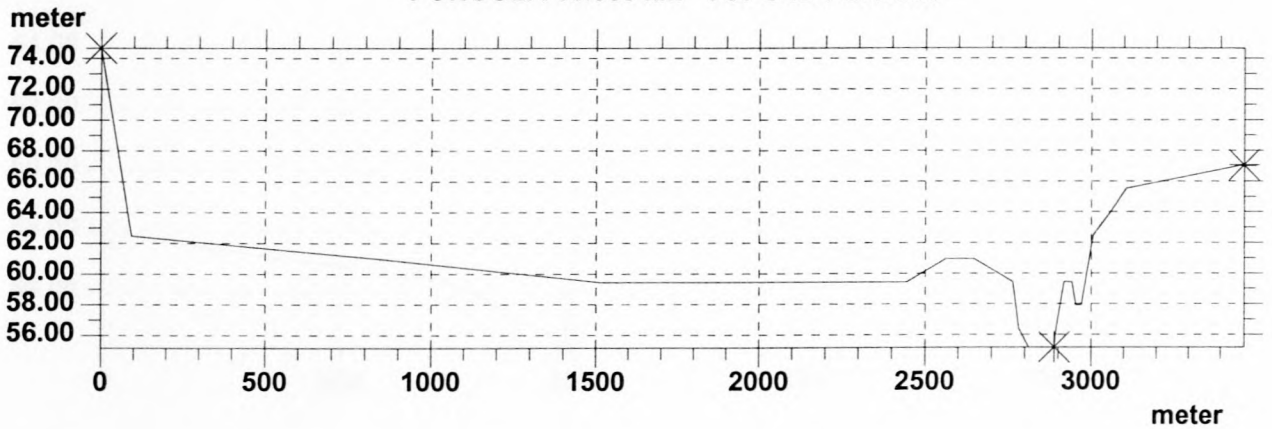
PONGOLA 17.920 km TOPO ID : ORIG33



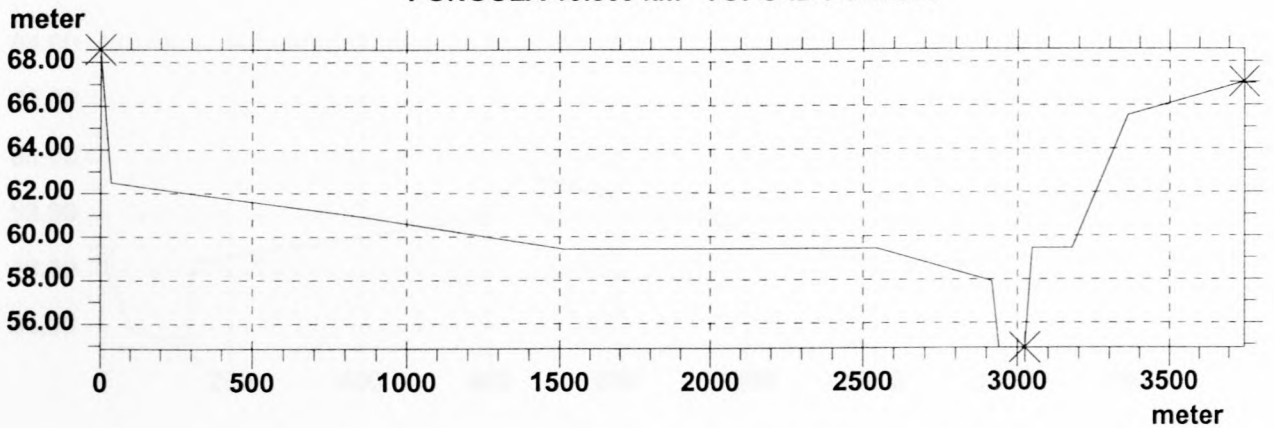
PONGOLA 18.400 km TOPO ID : ORIG33



PONGOLA 18.860 km TOPO ID : ORIG33

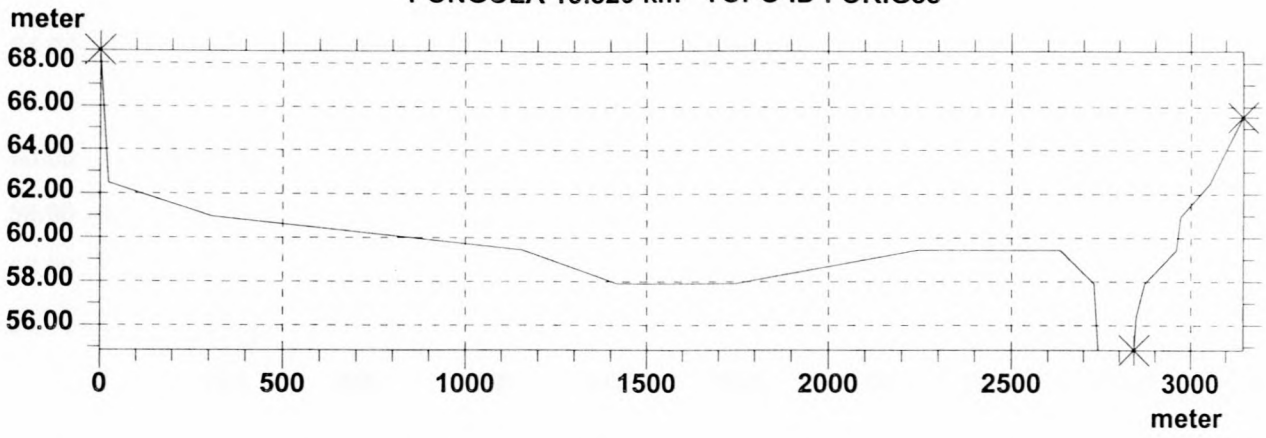


PONGOLA 19.360 km TOPO ID : ORIG33

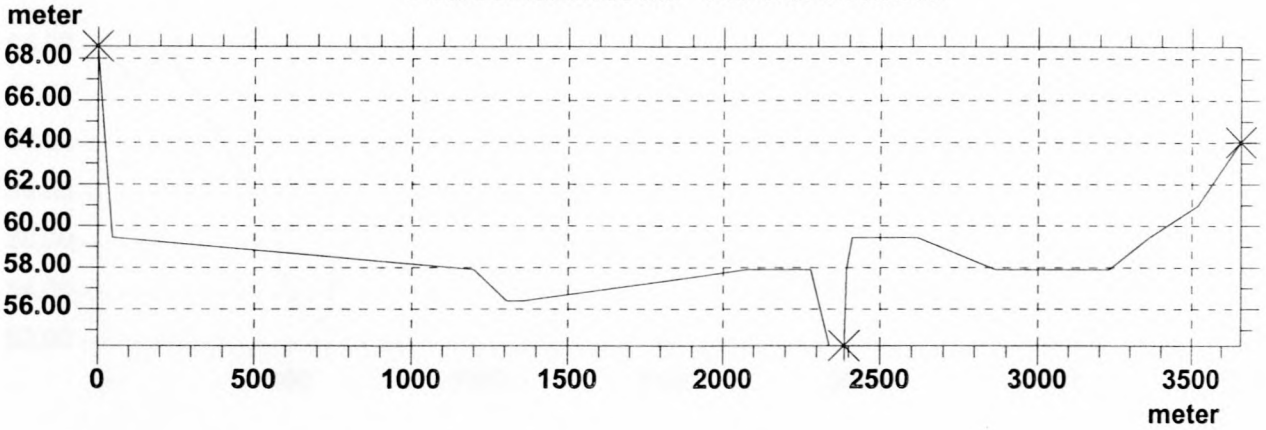


| | |
|-------------------|---------|
| | |
| DATA BASE : TEST2 | MIKE 11 |

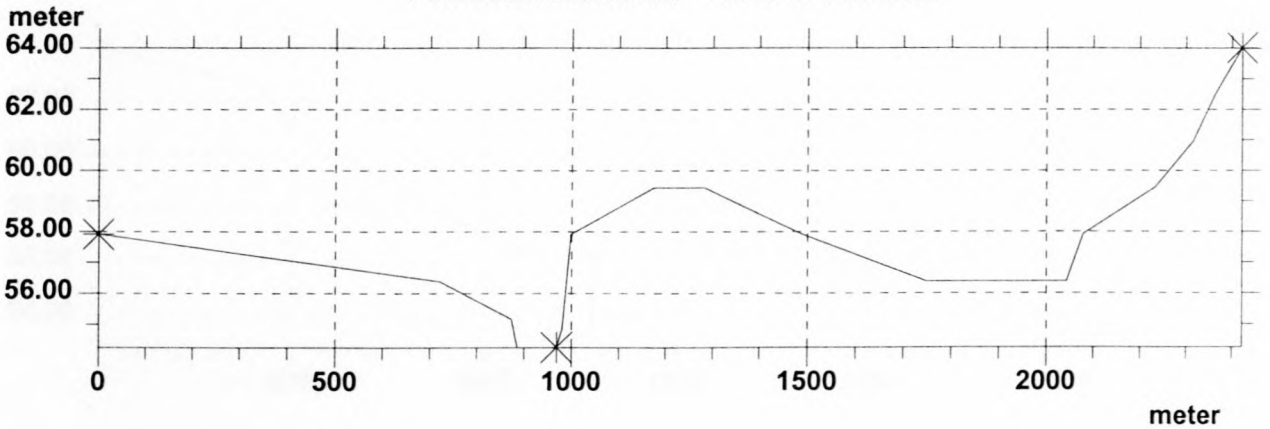
PONGOLA 19.820 km TOPO ID : ORIG33



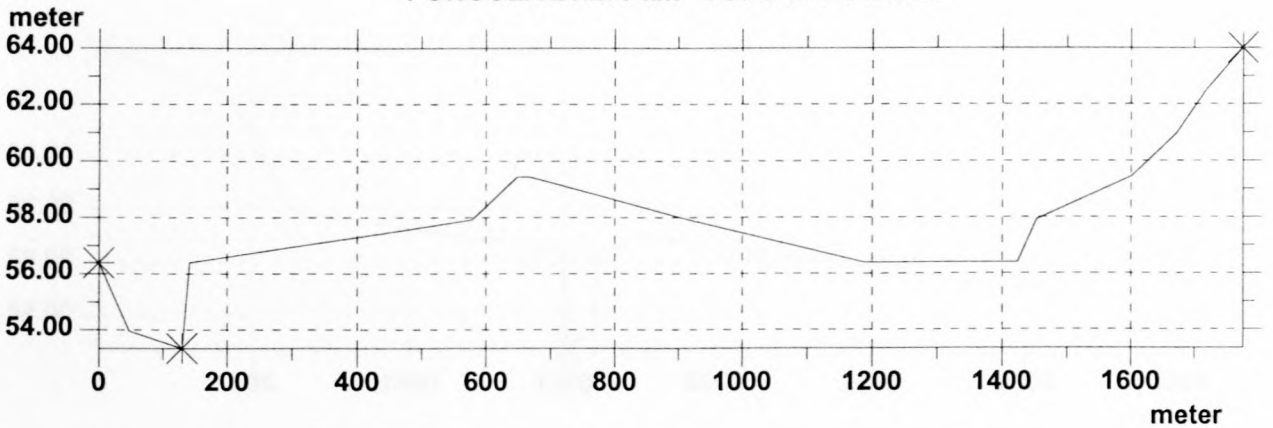
PONGOLA 20.300 km TOPO ID : ORIG33



PONGOLA 20.780 km TOPO ID : ORIG33

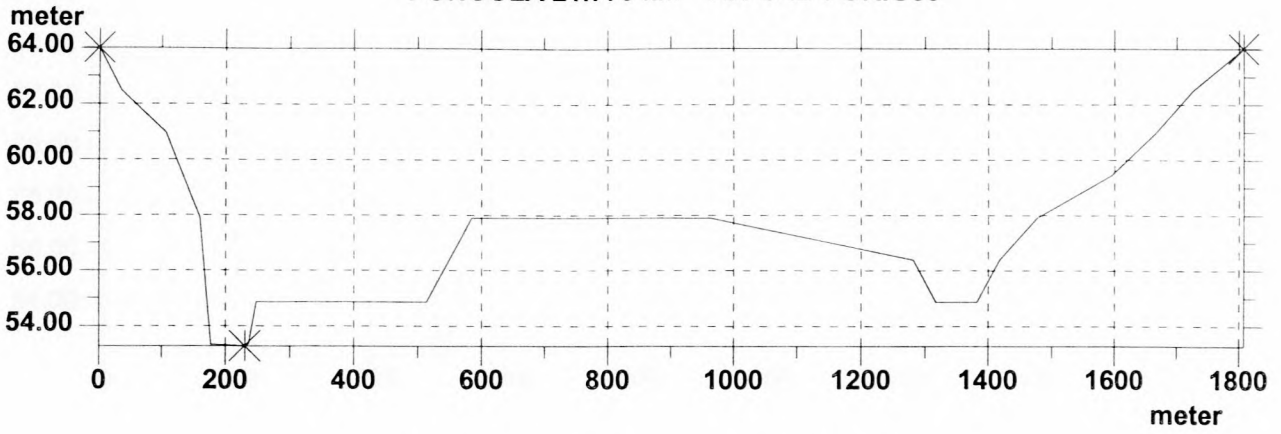


PONGOLA 21.270 km TOPO ID : ORIG33

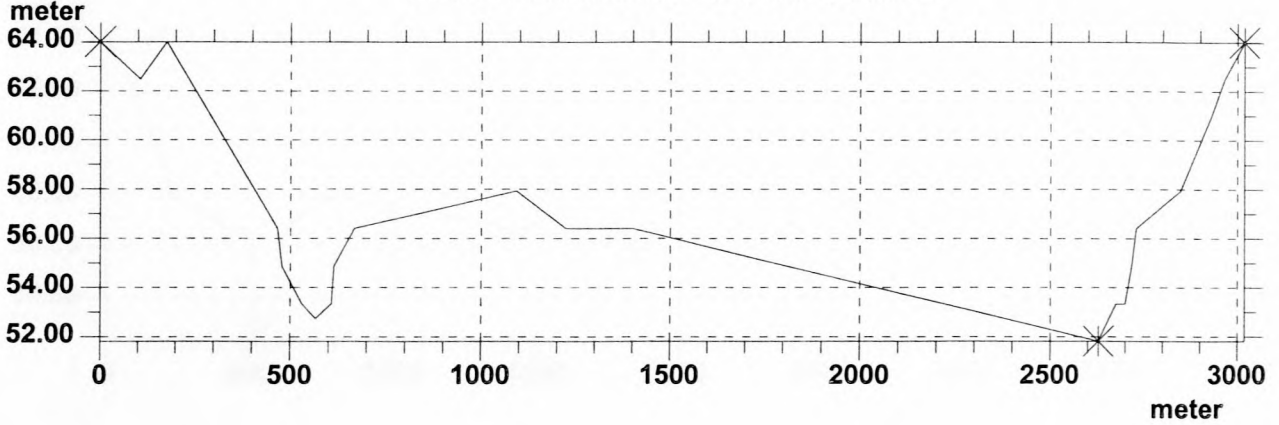


| | |
|-------------------|---------|
| | |
| DATA BASE : TEST2 | MIKE 11 |

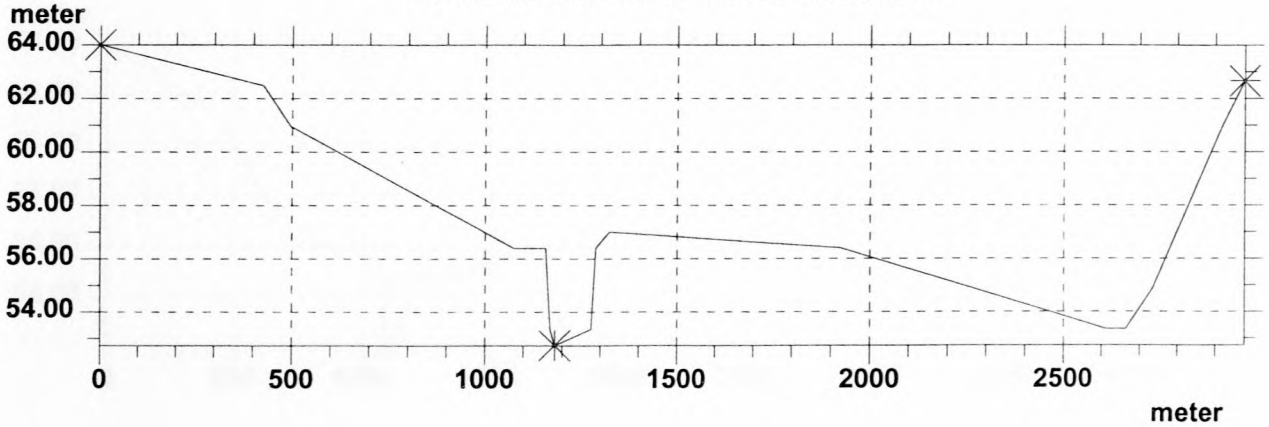
PONGOLA 21.770 km TOPO ID : ORIG33



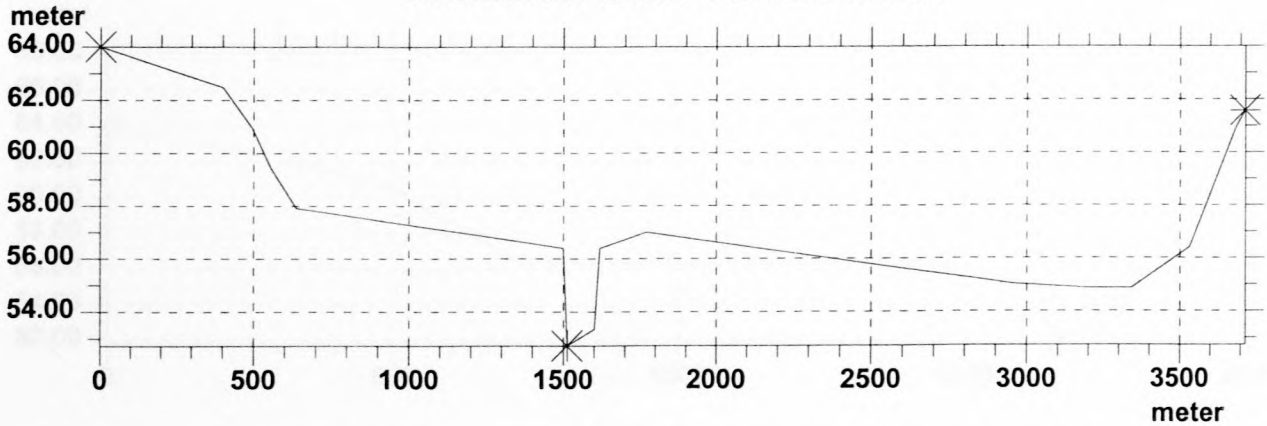
PONGOLA 22.260 km TOPO ID : ORIG33



PONGOLA 22.720 km TOPO ID : ORIG33

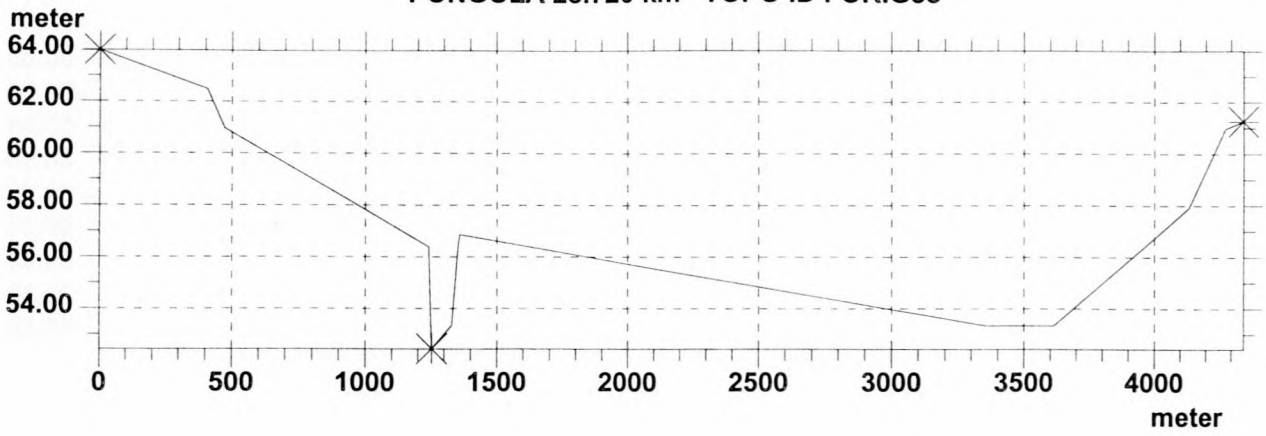


PONGOLA 23.190 km TOPO ID : ORIG33

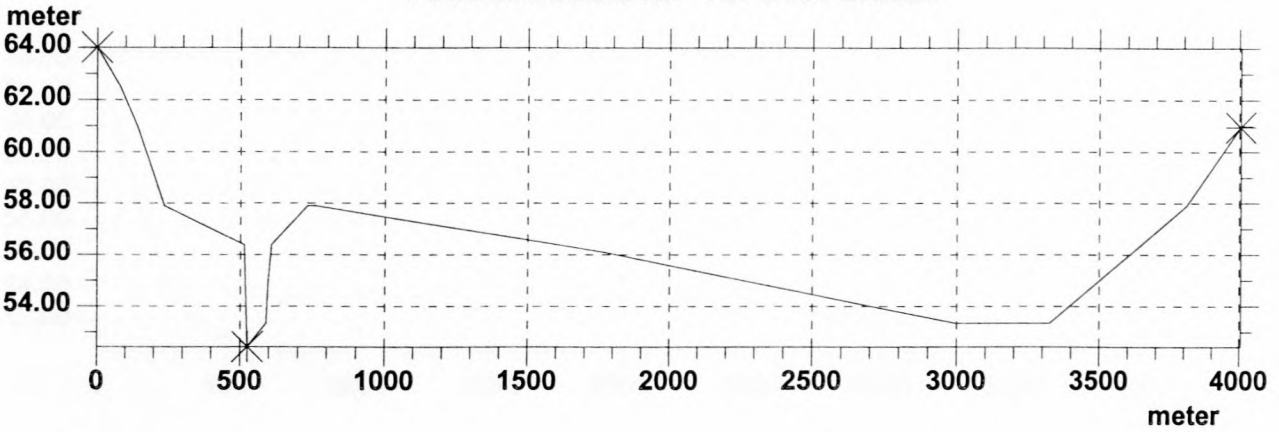


| | | |
|--------------------------|--|----------------|
| | | |
| | | MIKE 11 |
| DATA BASE : TEST2 | | |

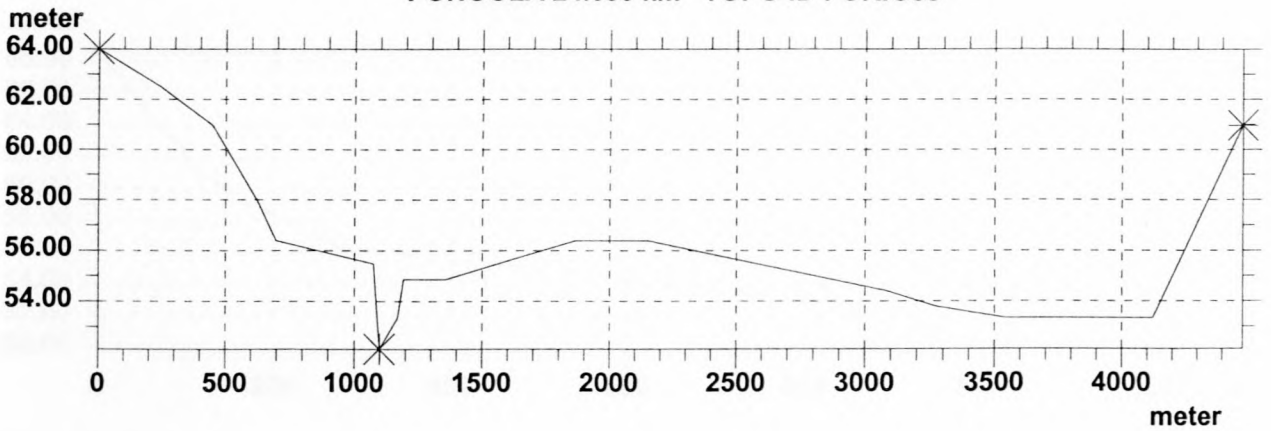
PONGOLA 23.720 km TOPO ID : ORIG33



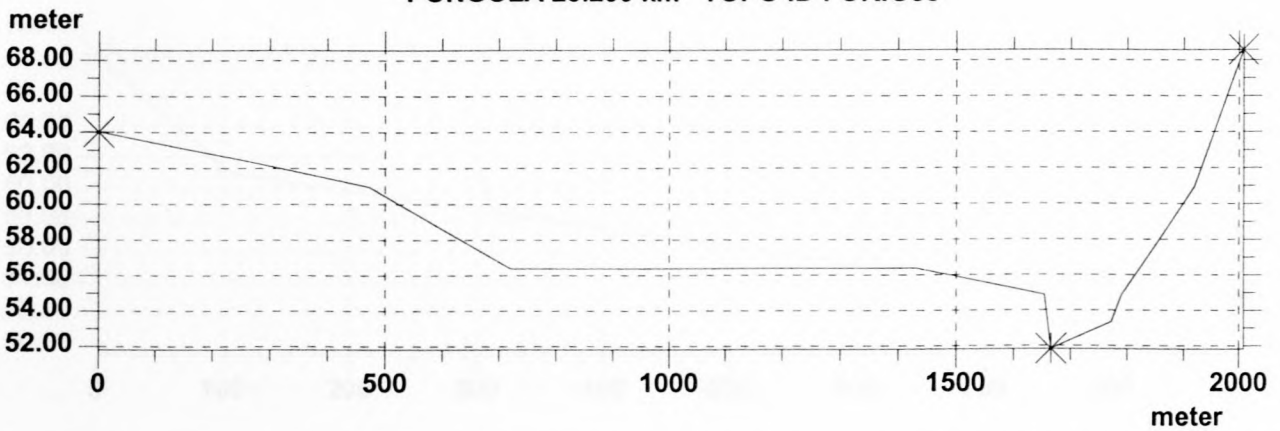
PONGOLA 24.240 km TOPO ID : ORIG33



PONGOLA 24.690 km TOPO ID : ORIG33

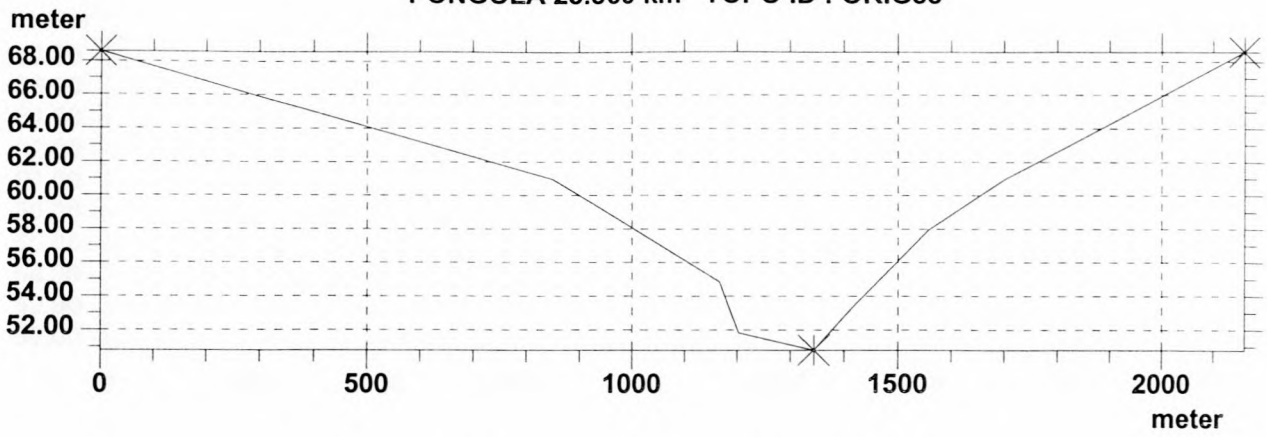


PONGOLA 25.290 km TOPO ID : ORIG33

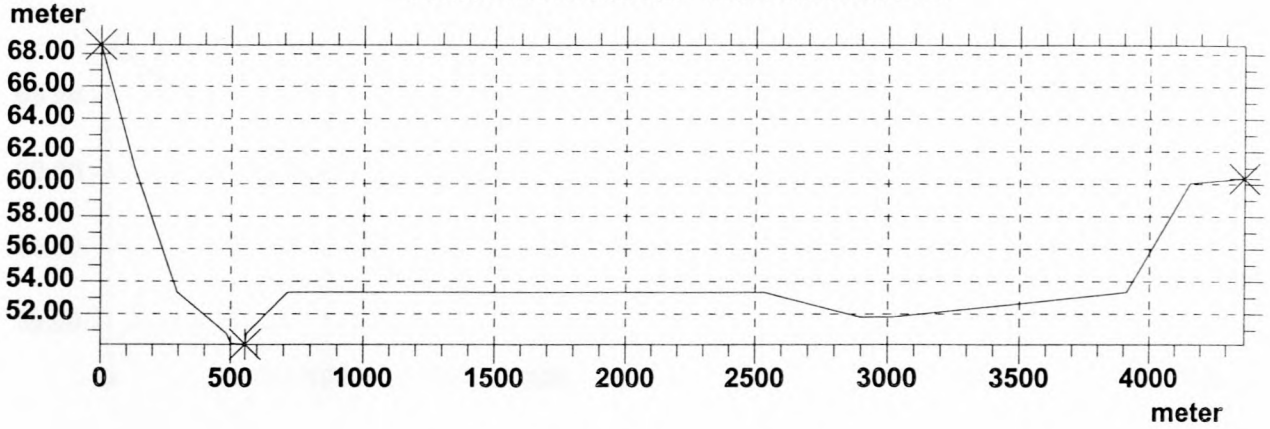


| | |
|-------------------|---------|
| | |
| DATA BASE : TEST2 | MIKE 11 |

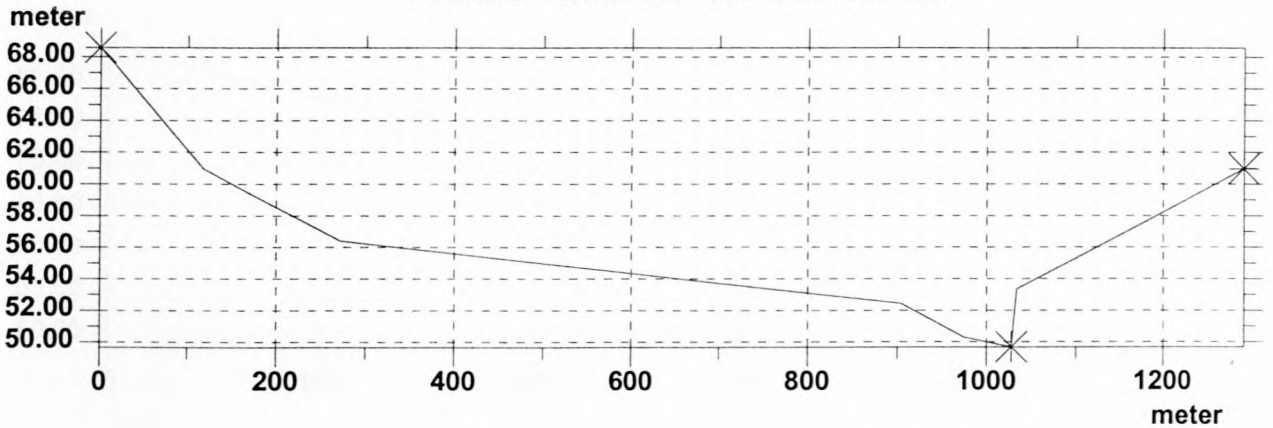
PONGOLA 25.860 km TOPO ID : ORIG33



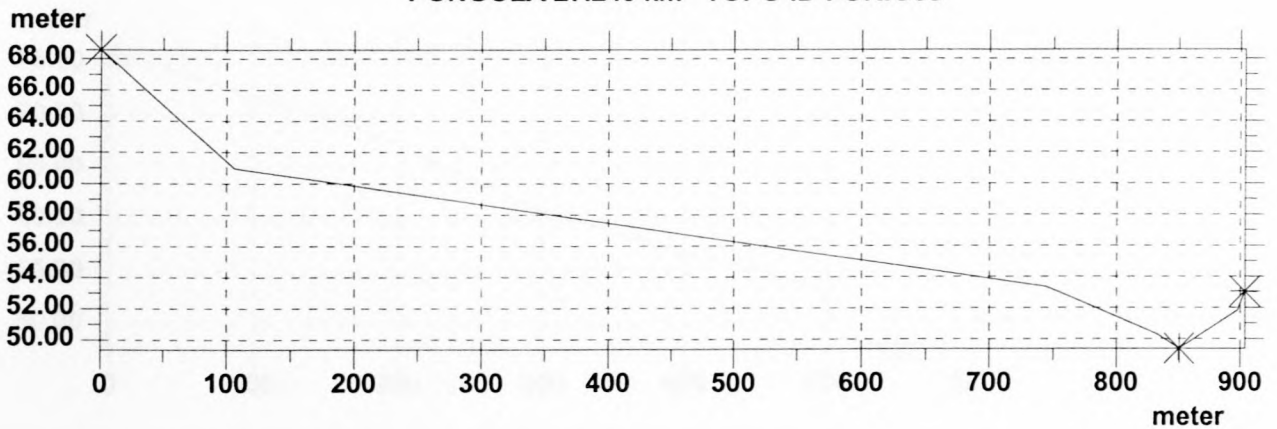
PONGOLA 26.290 km TOPO ID : ORIG33



PONGOLA 26.750 km TOPO ID : ORIG33

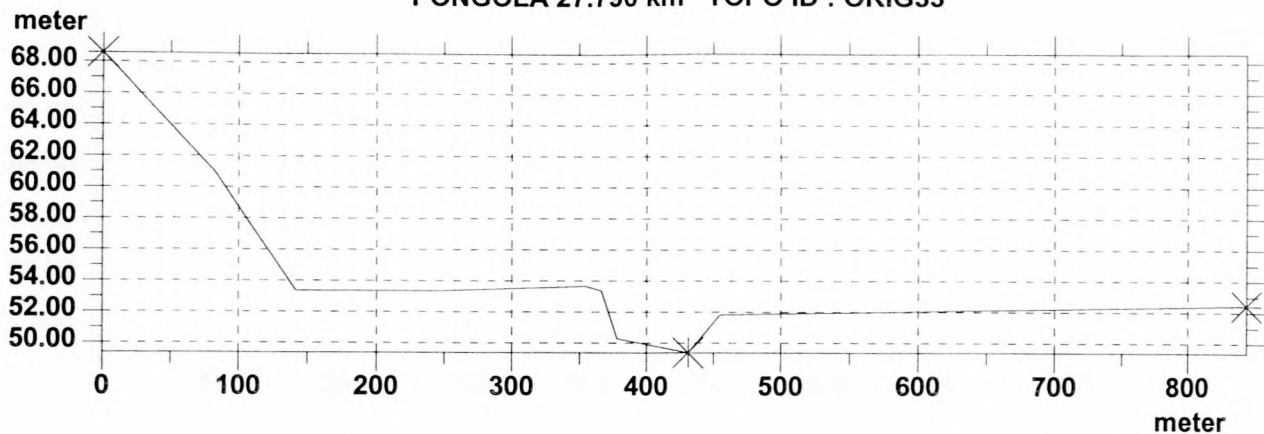


PONGOLA 27.240 km TOPO ID : ORIG33

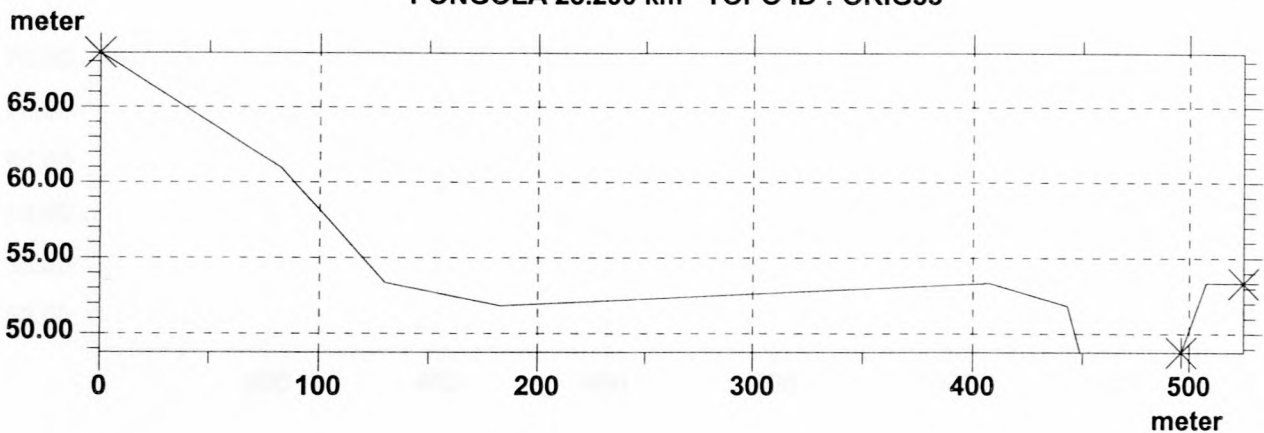


| | | |
|--------------------------|--|----------------|
| | | |
| | | MIKE 11 |
| DATA BASE : TEST2 | | |

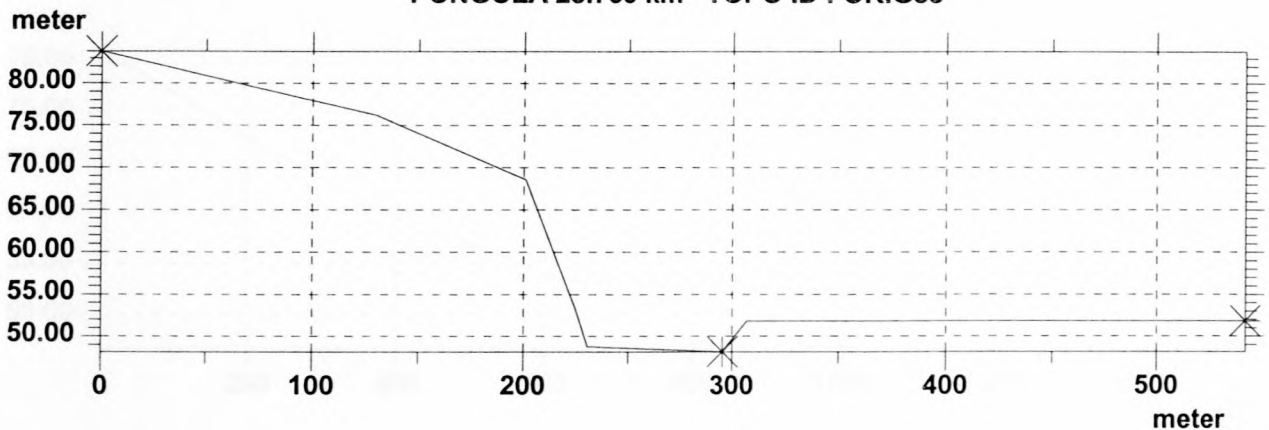
PONGOLA 27.790 km TOPO ID : ORIG33



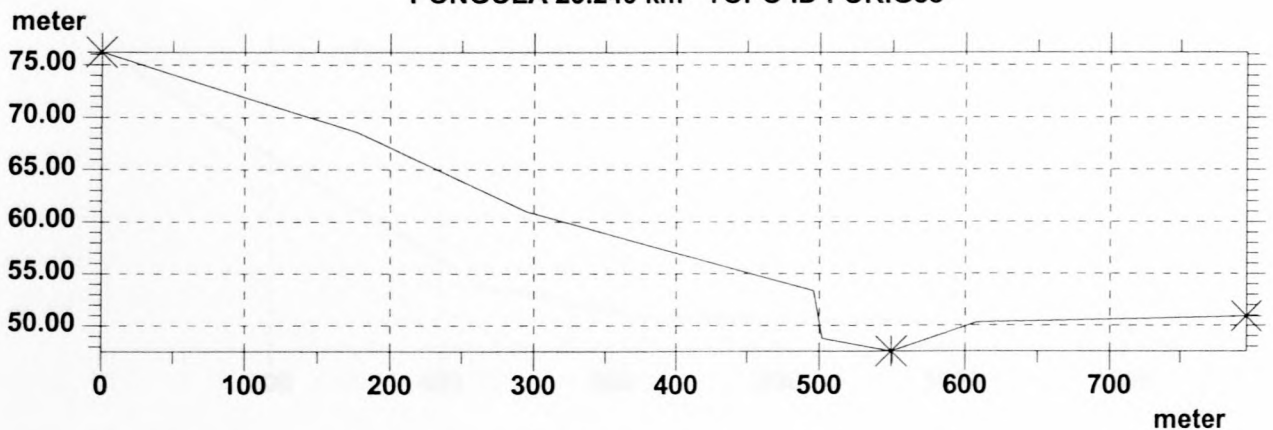
PONGOLA 28.290 km TOPO ID : ORIG33



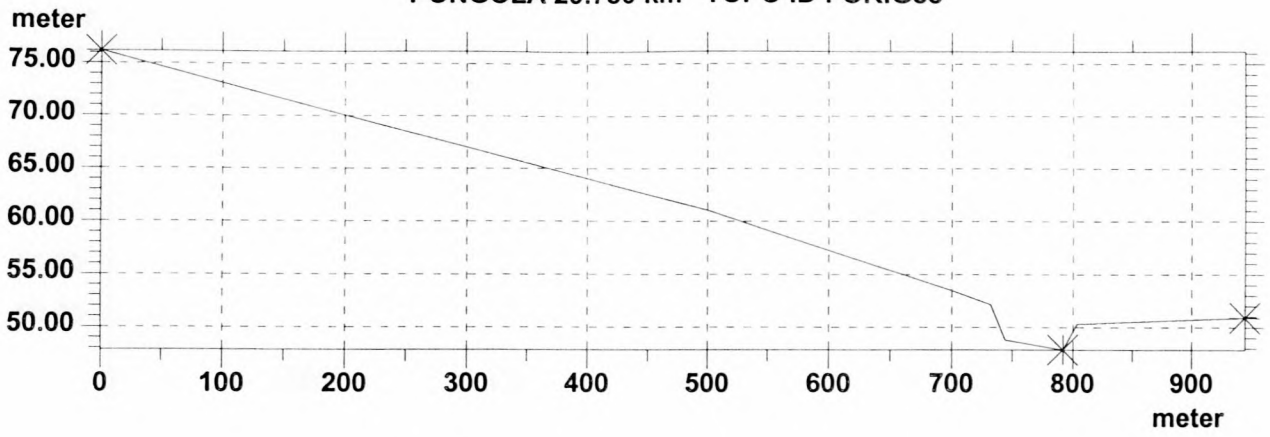
PONGOLA 28.760 km TOPO ID : ORIG33



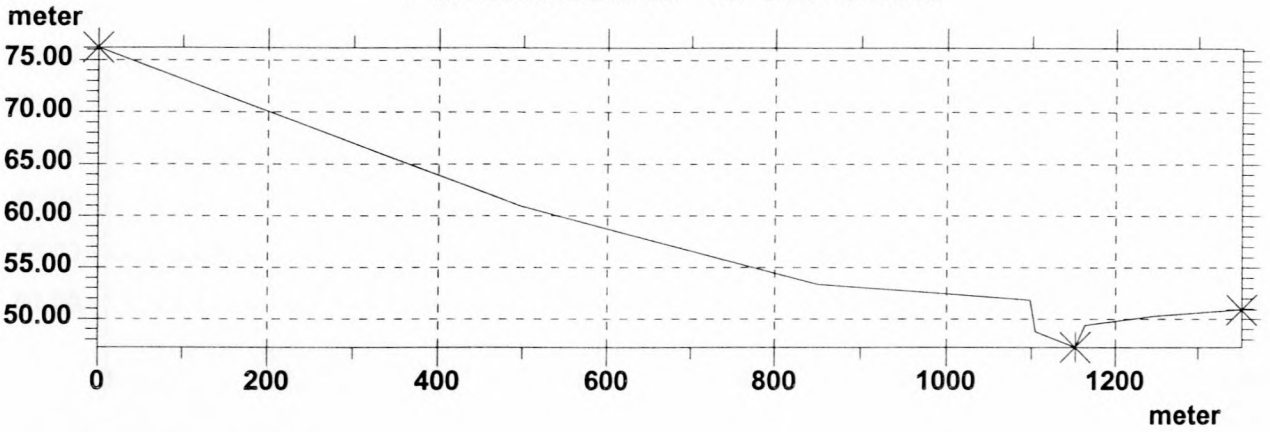
PONGOLA 29.240 km TOPO ID : ORIG33



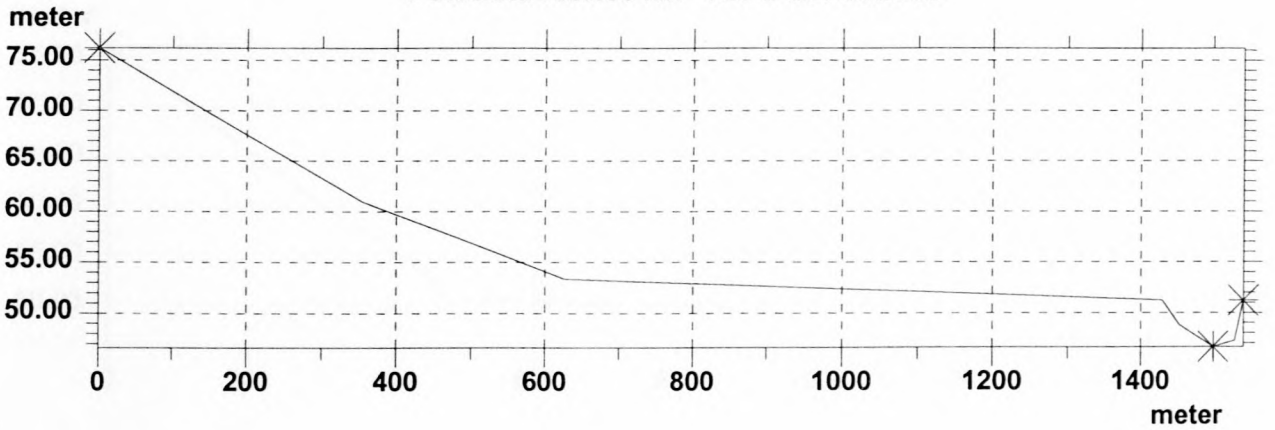
PONGOLA 29.730 km TOPO ID : ORIG33



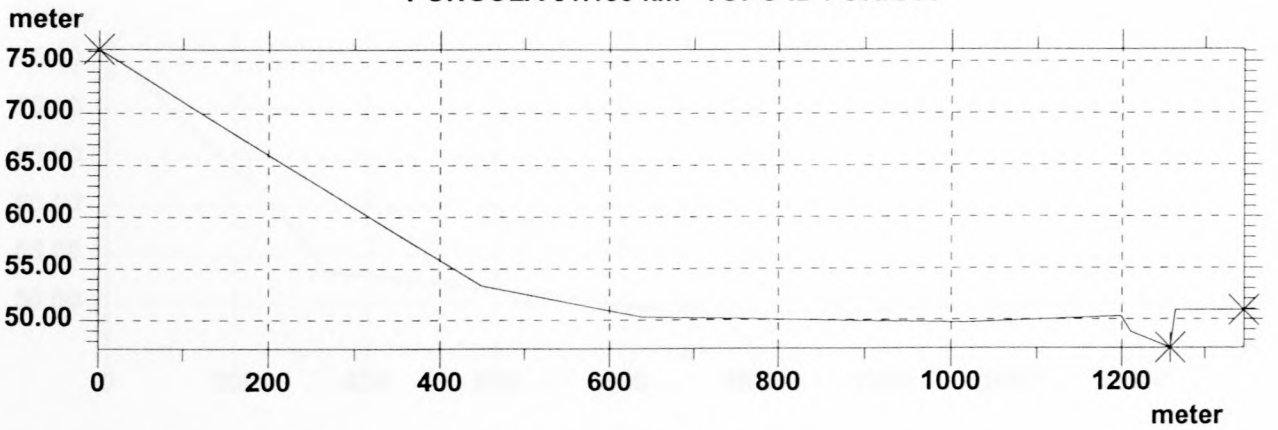
PONGOLA 30.210 km TOPO ID : ORIG33



PONGOLA 30.680 km TOPO ID : ORIG33

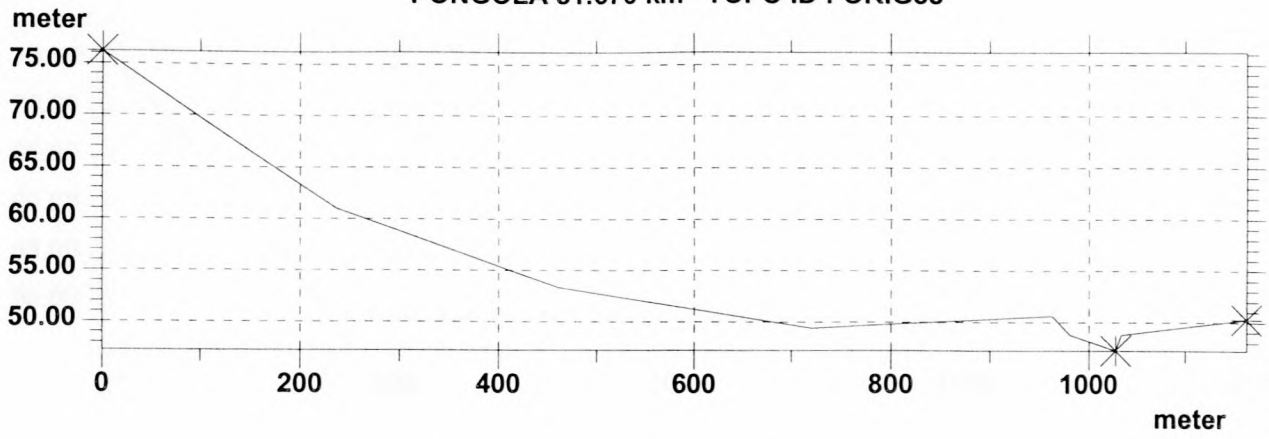


PONGOLA 31.150 km TOPO ID : ORIG33

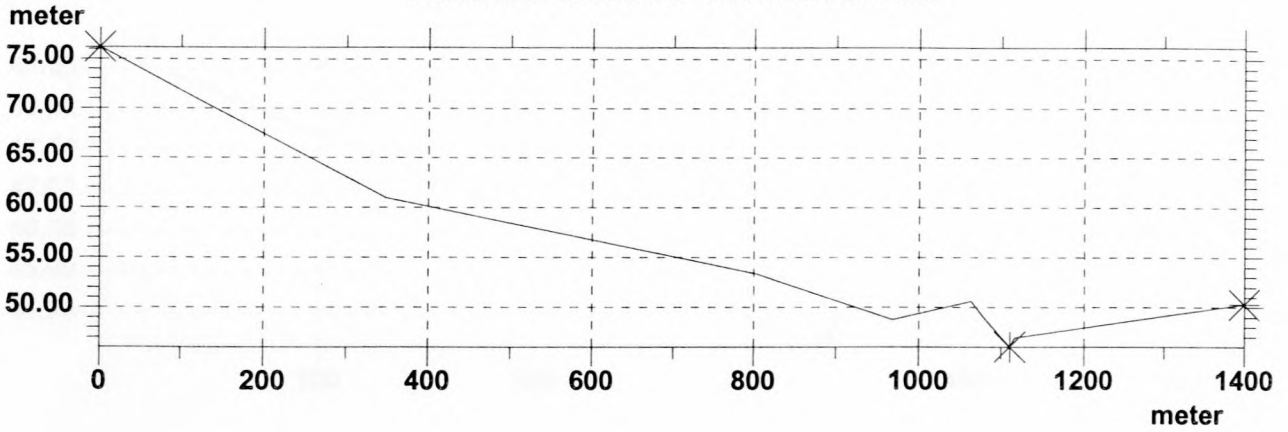


| | | |
|--------------------------|--|----------------|
| | | |
| | | MIKE 11 |
| DATA BASE : TEST2 | | |

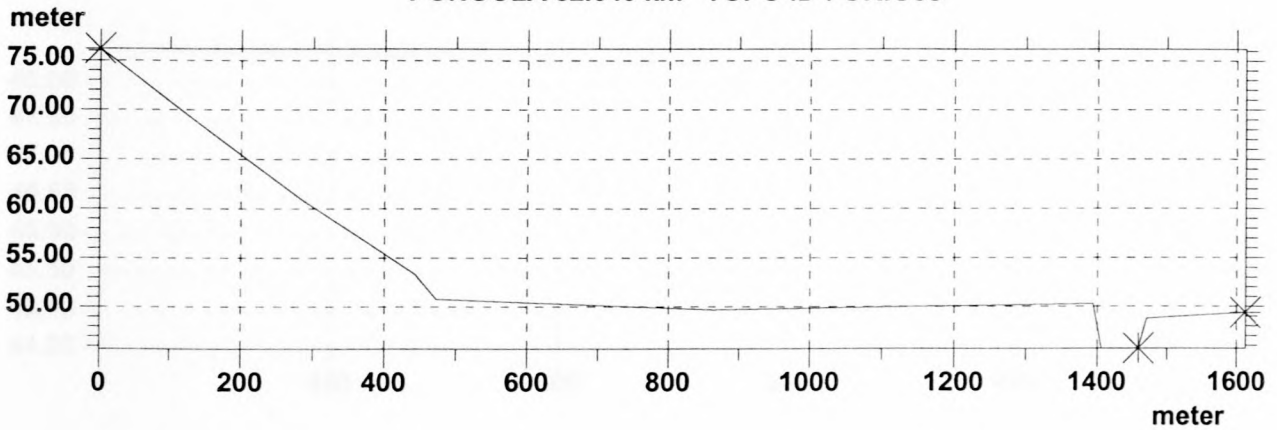
PONGOLA 31.670 km TOPO ID : ORIG33



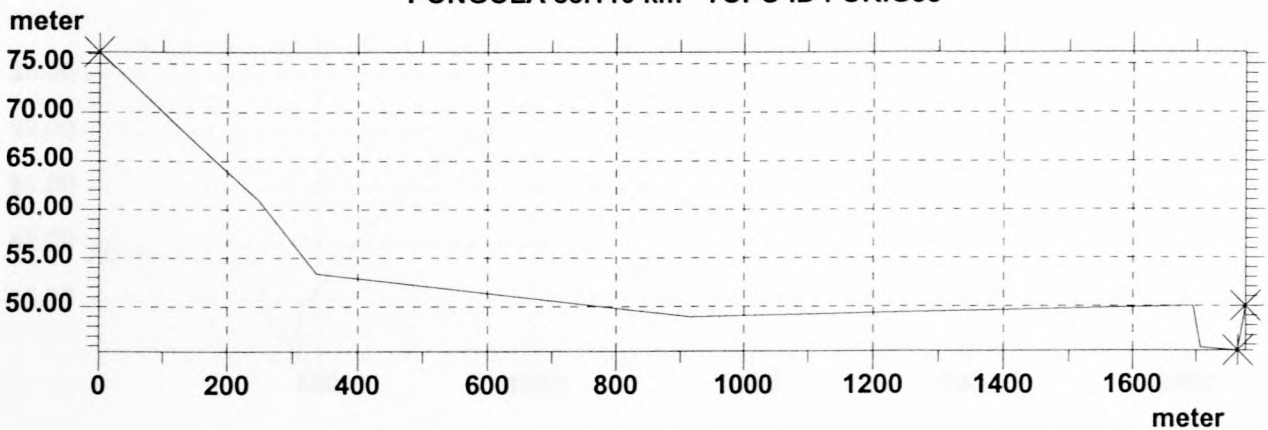
PONGOLA 32.150 km TOPO ID : ORIG33



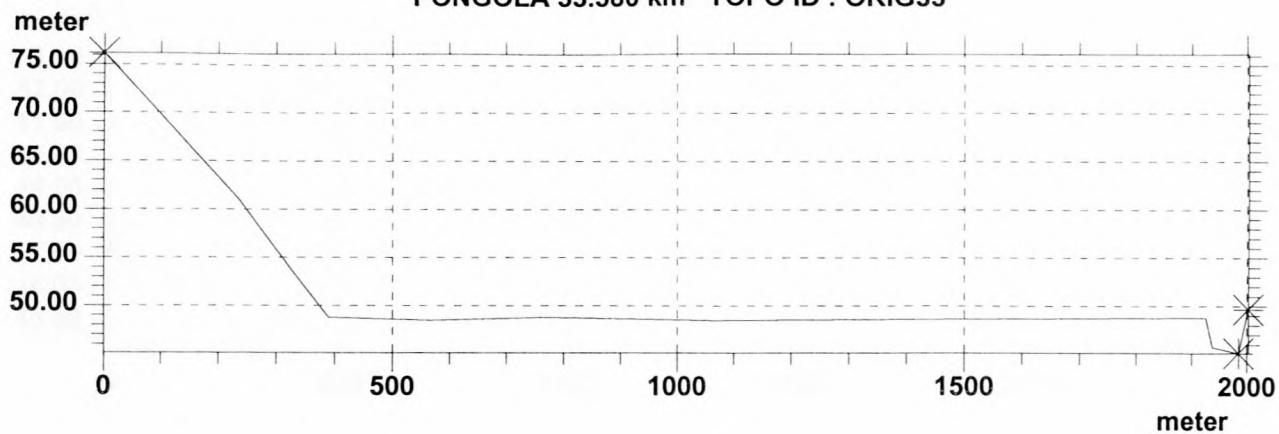
PONGOLA 32.640 km TOPO ID : ORIG33



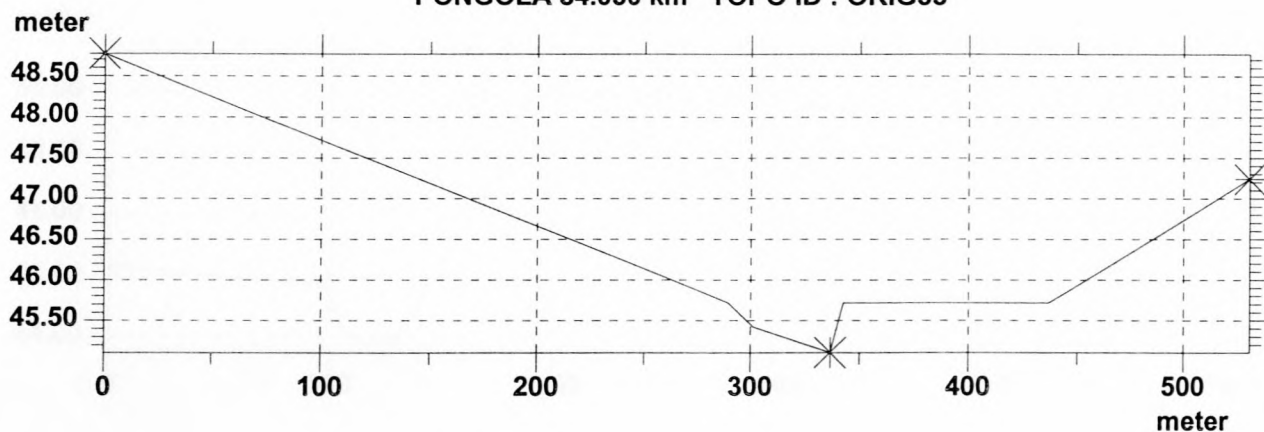
PONGOLA 33.110 km TOPO ID : ORIG33



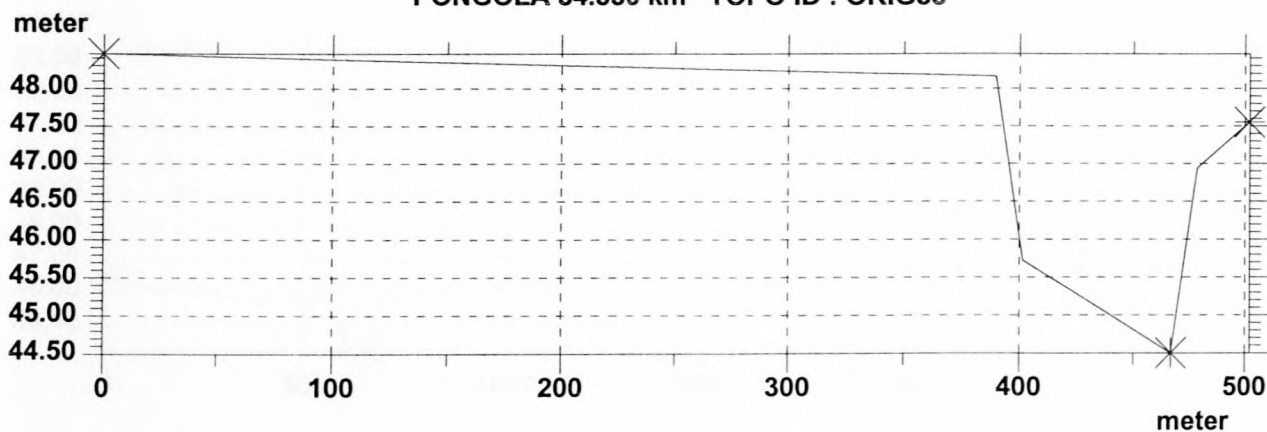
PONGOLA 33.580 km TOPO ID : ORIG33



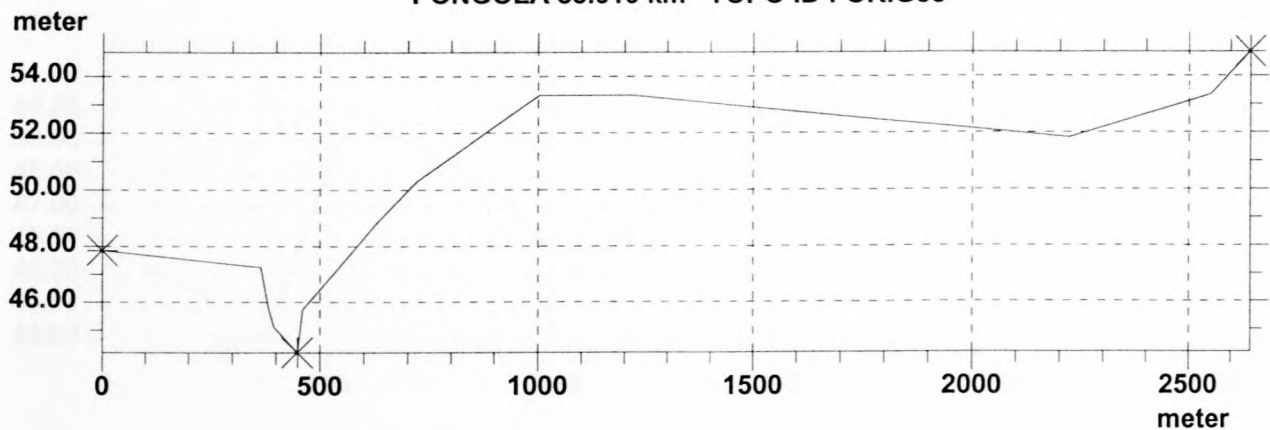
PONGOLA 34.050 km TOPO ID : ORIG33



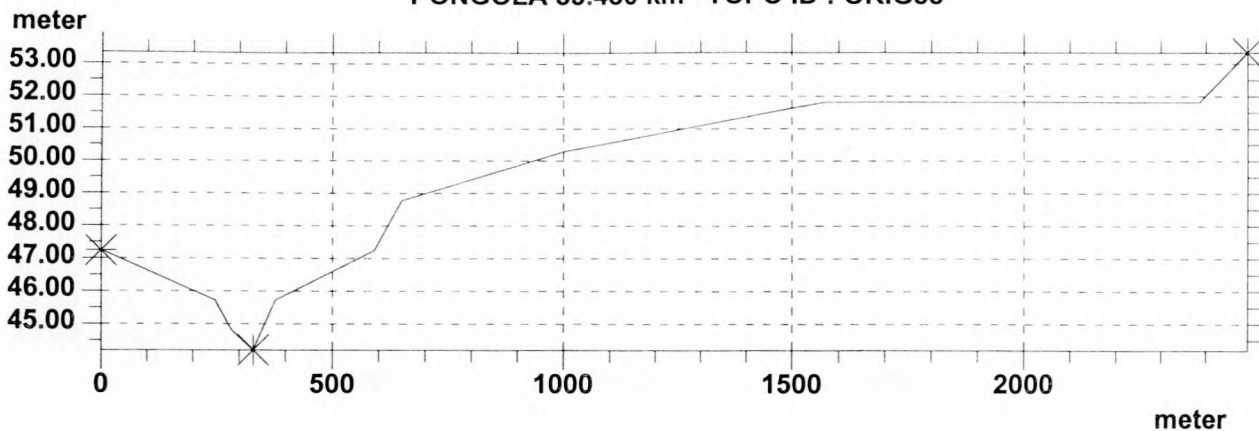
PONGOLA 34.530 km TOPO ID : ORIG33



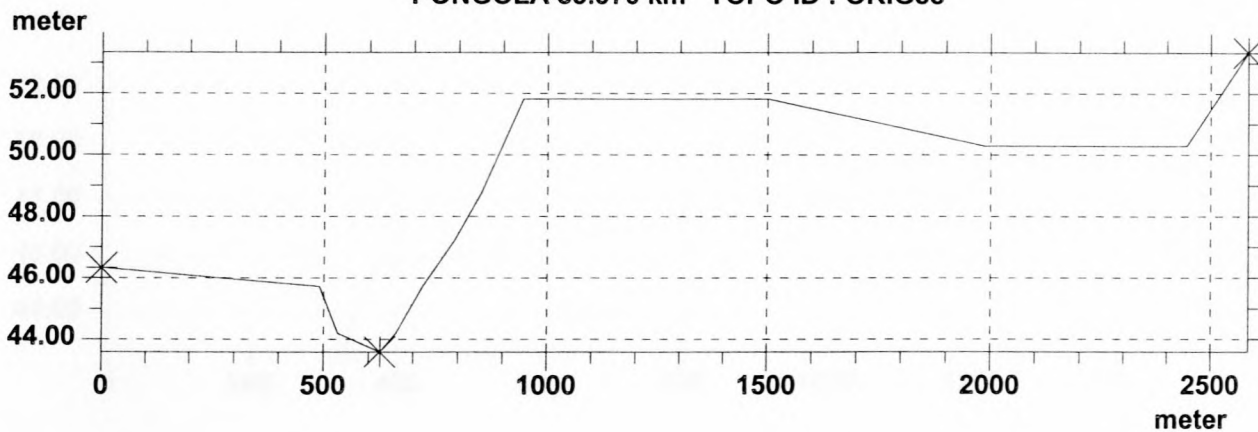
PONGOLA 35.010 km TOPO ID : ORIG33



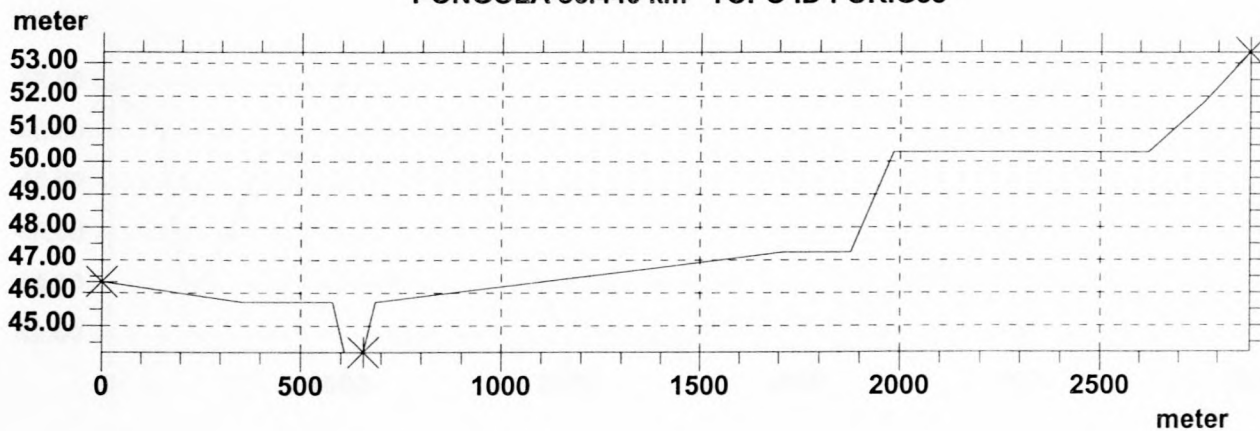
PONGOLA 35.480 km TOPO ID : ORIG33



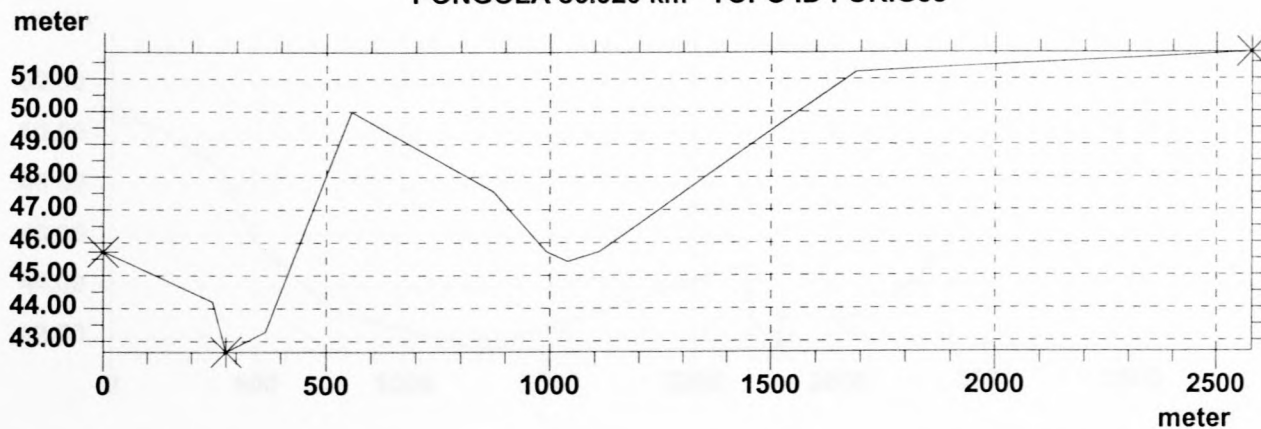
PONGOLA 35.970 km TOPO ID : ORIG33



PONGOLA 36.440 km TOPO ID : ORIG33

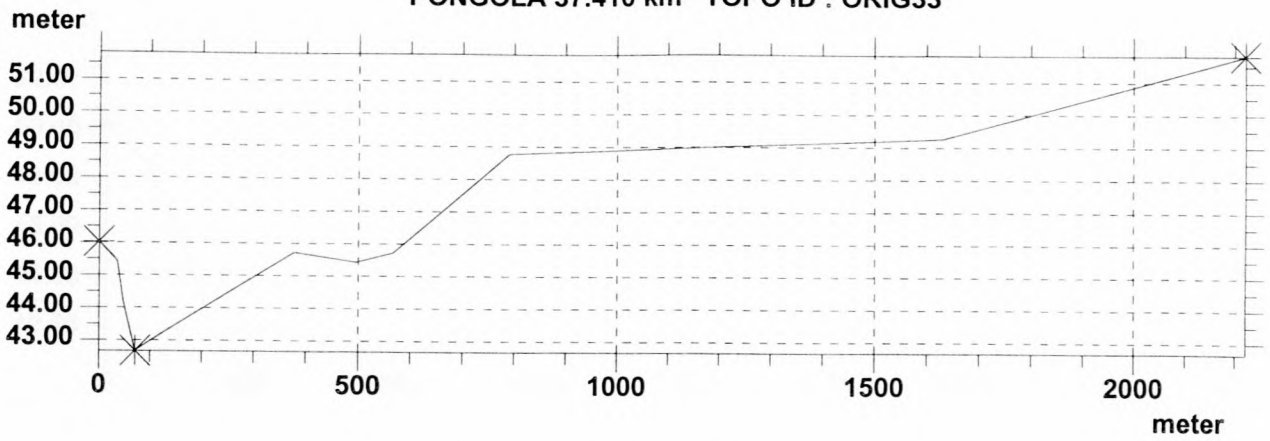


PONGOLA 36.920 km TOPO ID : ORIG33

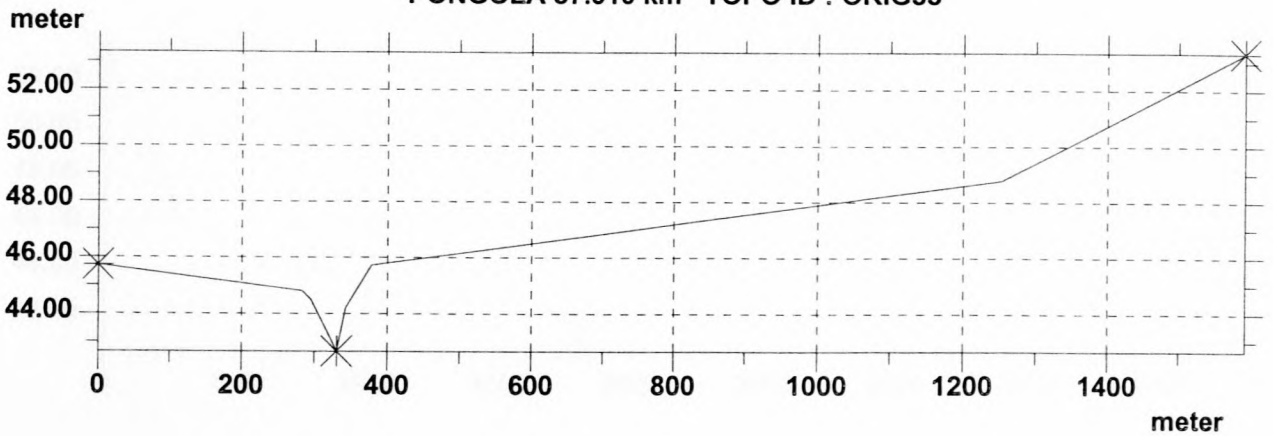


| | |
|-------------------|---------|
| | |
| DATA BASE : TEST2 | MIKE 11 |

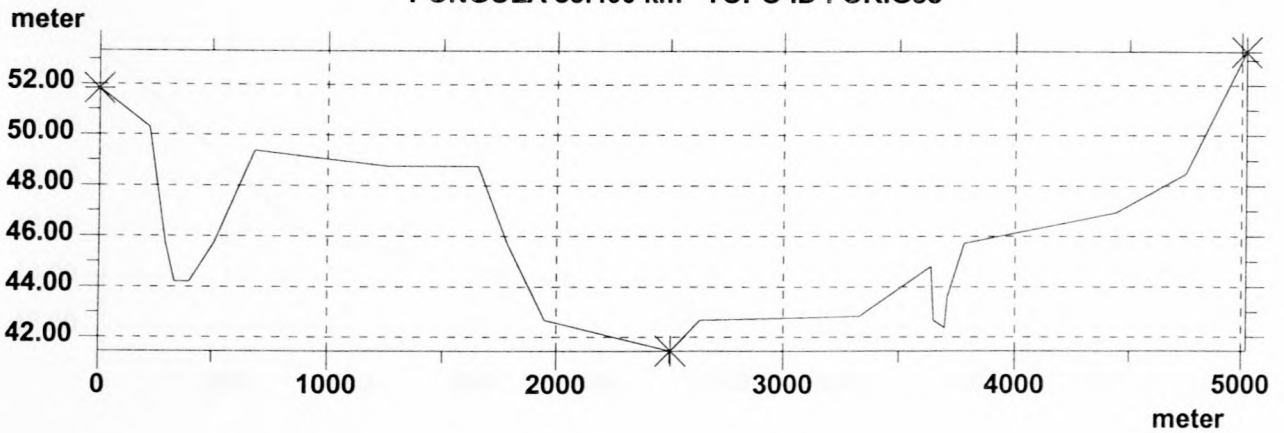
PONGOLA 37.410 km TOPO ID : ORIG33



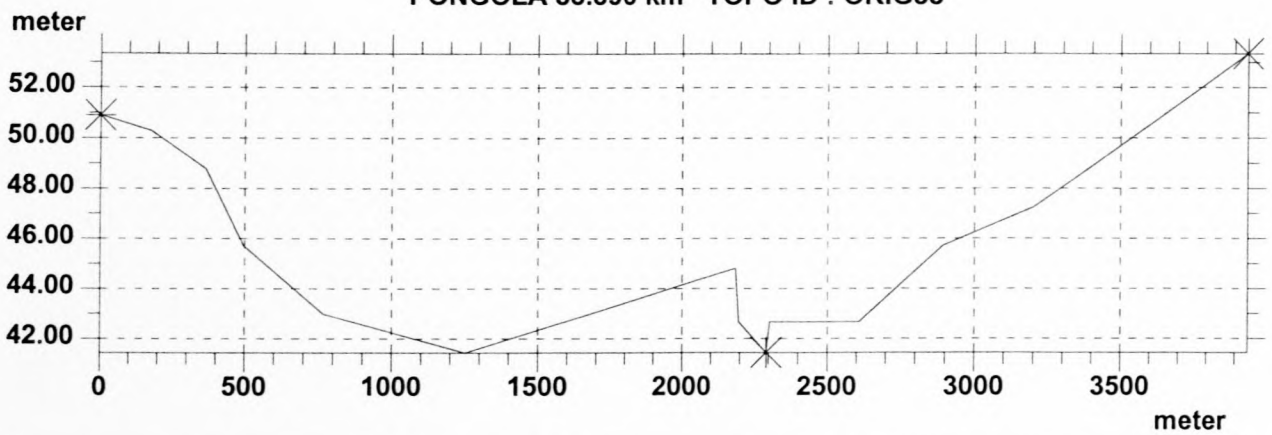
PONGOLA 37.910 km TOPO ID : ORIG33



PONGOLA 38.400 km TOPO ID : ORIG33

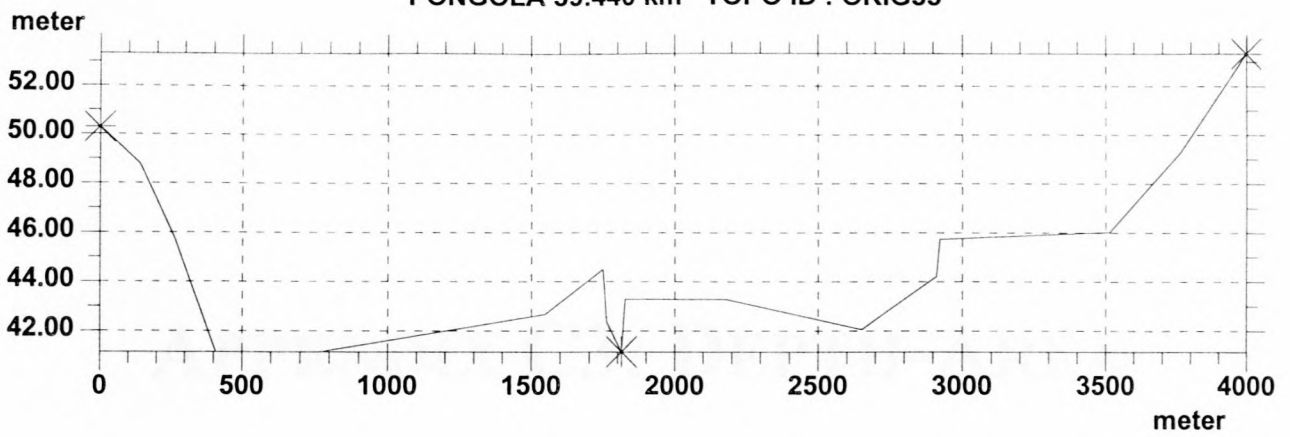


PONGOLA 38.890 km TOPO ID : ORIG33

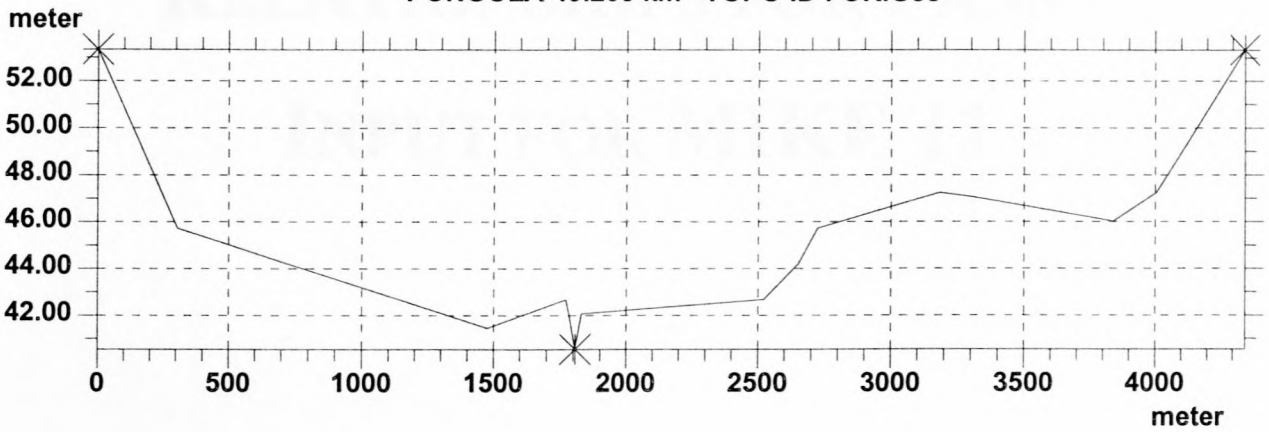


| | | |
|--------------------------|--|----------------|
| | | |
| | | MIKE 11 |
| DATA BASE : TEST2 | | |

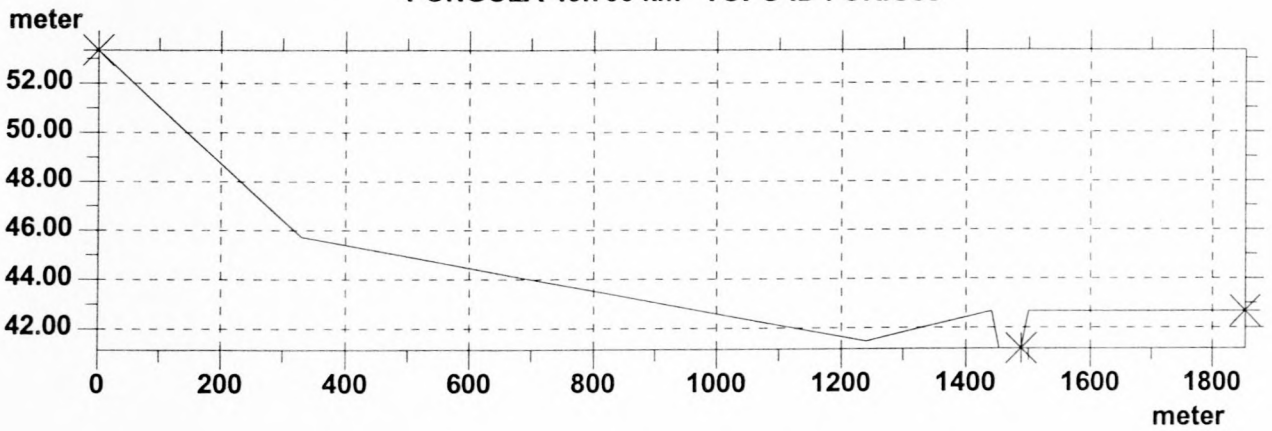
PONGOLA 39.440 km TOPO ID : ORIG33



PONGOLA 40.200 km TOPO ID : ORIG33

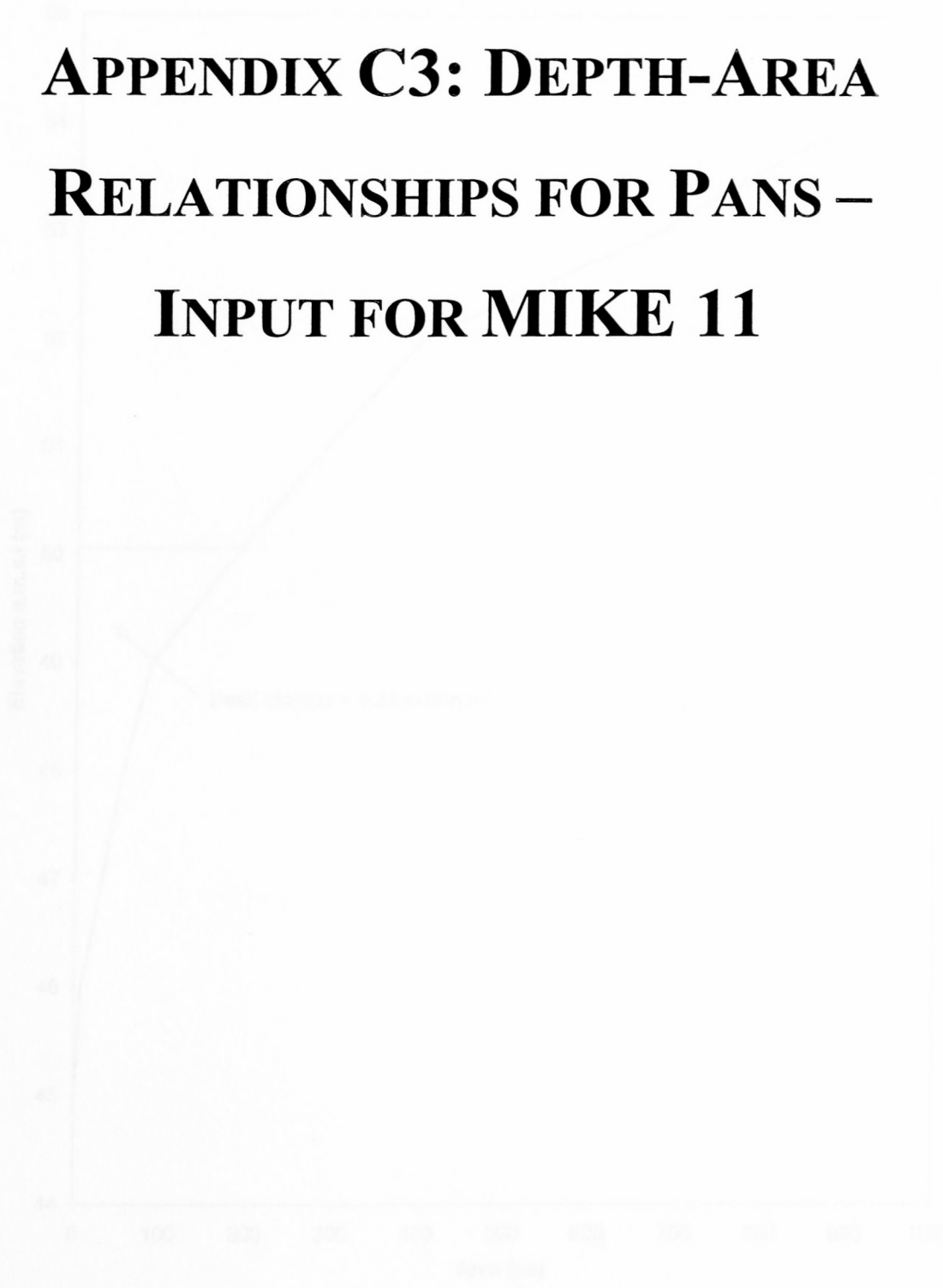


PONGOLA 40.790 km TOPO ID : ORIG33

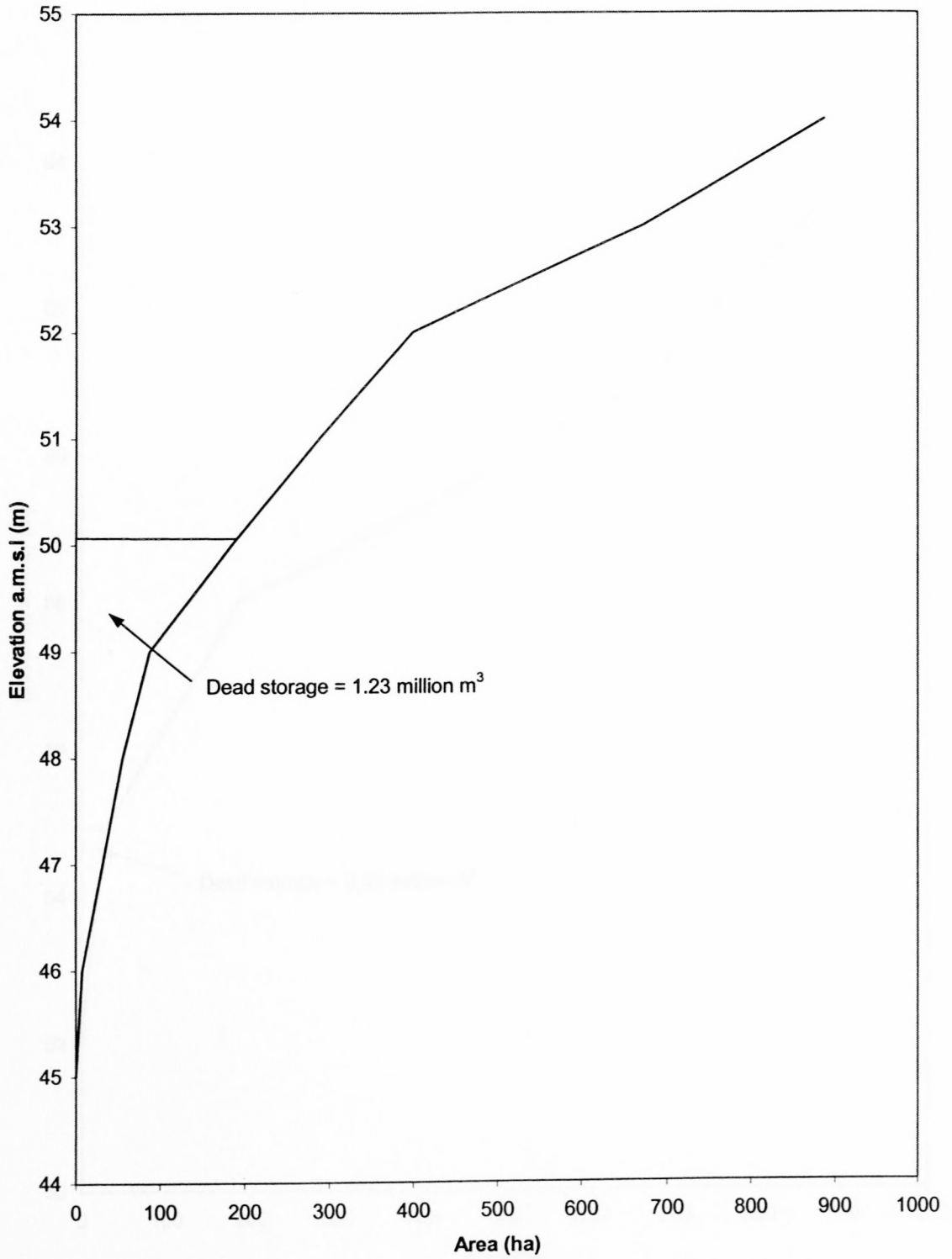


| | |
|-------------------|---------|
| | |
| DATA BASE : TEST2 | MIKE 11 |

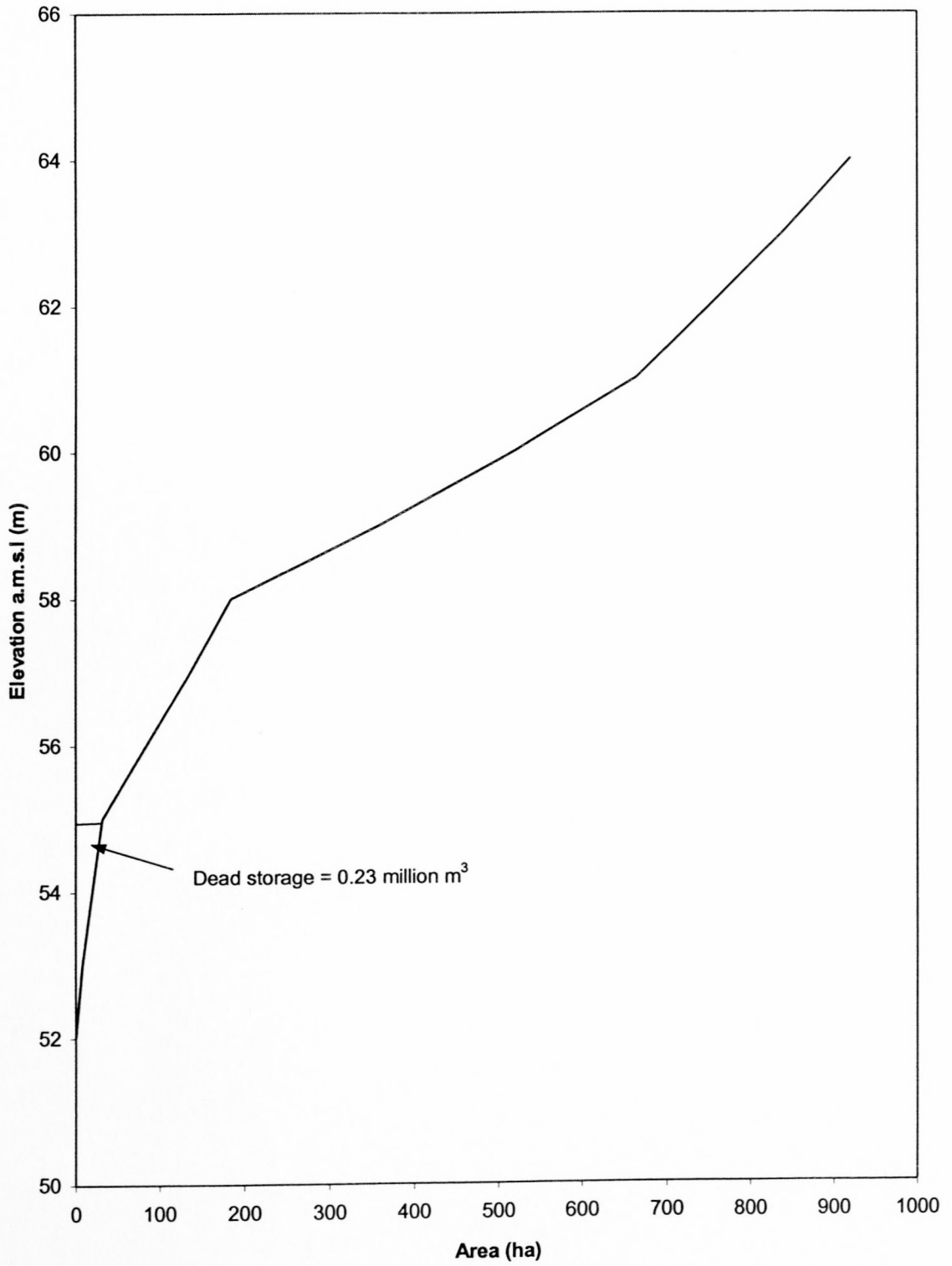
APPENDIX C3: DEPTH-AREA RELATIONSHIPS FOR PANS – INPUT FOR MIKE 11



Depth-area relationship: Nhlanjane pan



Depth-area relationship: Mfongozi pan





beck_downstream_2001

